Impact ionisation by hot electrons and luminescence in ZnS and other wide band-gap semiconductors.

A thesis presented by **Timothy David Thompson** B.Sc. to the University of St.Andrews in application for the degree of Doctor of Philosophy.

Declaration.

I hereby certify that this thesis has been composed by me, and is a record of work done by me, and has not previously been presented for a higher degree.

The research was carried out in the Wolfson Institute of Luminescence, within the School of Physical Sciences in the University of St.Andrews, under the supervision of Professor J.W. Allen.

Timothy D. Thompson

Certificate

I certify that Timothy David Thompson has spent nine terms at research work in the Wolfson Institute of Luminescence within the School of Physical Sciences in the University of St. Andrews under my direction, that he has fulfilled the conditions of the Resolution of the University Court, 1967, No. 1, and that he is qualified to submit the accompanying thesis in application for the Degree of Doctor of Philosophy.

Professor J. W. Allen

(Research Supervisor.)

Career

I first matriculated in the University of St.Andrews in October 1980. I studied Biological Sciences until 1982 when I abandoned this course in favour of a Physics degree. In 1986 I obtained the degree of Bachelor of Science in Physics and Electronics with First Class Honours and the first E.E.V. Lincoln prize.

In October 1986, following the award of a S.E.R.C. Scholarship, I enrolled as a research student under the Resolution of the University Court, 1967, No.1, as a candidate for the degree of Doctor of Philosophy.

Acknowledgements

Firstly I would like to thank my supervisor, Professor J.W.Allen. His knowledge and experience have been invaluable throughout this research.

I would also like to thank Dr H. Allen for her help in the production of the evaporated thin film samples.

Financial support for the research was provided by the S.E.R.C.

Abstract.

We have designed, constructed and demonstrated the feasibility of a temperature sensor based on phosphor luminescence decay time analysis in the frequency domain.

We have shown that in insulating GaAs:Cr optical ionisation of the chromium centres leads to carrier hopping between such sites and consequently dispersive sample conductivity. A similar effect was found in ZnSe.

The band-to-band impact ionisation threshold field has been determined for ZnS, and is ~1.5 x $10^6 Vcm^{-1}$. The breakdown can be fitted to Shockley`s lucky electron initiation model and the resulting ionisation parameter "b" has a value of 1.3 x $10^7 Vcm^{-1}$. A two stage impurity impact ionisation mechanism has been found to lead to carrier multiplication in some preparations of ZnS. We have studied the variation of this mechanism with electric field and by comparison to luminescence quantum efficiencies have been able to derive information about the hot electron distribution in ZnS. We discuss the implications of this to electroluminescence in ZnS.

We have proposed a design for a ZnS based MIS LED and constructed prototypes. Experiments on these prototypes have led us to believe that ultimately such devices could produce efficient blue or violet emission.

The photoluminescence emissions of ZnS:Te have been studied. We have produced evidence which suggests that the blue emission in heavily doped material which some workers believe to be due to tellurium doublets may in fact simply be due to the self-activated centre. We also discuss this in relation to some of the available literature on this material. The photoluminescence emission from our ZnS samples takes several seconds to build up to full intensity, we have investigated this and proposed a model to explain our observations.

The chapters.

Contents.

(1) "An introduction."

(2) "Band-to-band impact ionisation in ZnS."

(3) "Hot electron effects in ZnS."

(5) "The origin and time dependence of the photoluminescence emissions of ZnS:Te."

(6) " A frequency domain phosphor decay time thermometer."

(7) "Optically induced deep level electron hoping in GaAs:Cr and ZnSe."

(8) "Conclusion."

The References.

Chapter 1

An introduction.

(1) The origins of electroluminescence.

Before beginning a detailed discussion of the physics of solid state electroluminescence, it is perhaps interesting to digress a little, and consider the origins of, and justifications for such work.

(1.1) The quest for a source of light.

A combination of the daily rotation of the earth about its axis and cave dwelling resulted in primitive man being repeatedly plunged into darkness. To an animal whose principal sense is vision, this was no doubt a source of considerable annoyance. The earliest solution to this problem was to simply "set fire to something". This idea was employed with considerable enthusiasm for many millennia, any advances in technology simply being the discovery of a better material to "set fire to". One significant advance which was made towards the end of this period was the use of the flame to heat an incandescent material, which in turn emitted light. The technology of flame lighting culminated in such inventions as Drummond's "lime light" of 1826. It is interesting to note that one of the first uses of electricity for lighting was by Nollet, who suggested that electric current could be used to decompose water to provide the oxygen/hydrogen flame for such a lime light. In 1857 Holmes produced the first practical all electric lamp which operated by striking an arc between carbon electrodes. However the origins of domestic electric lighting lie with Swan and his prototype carbon filament lamp of 1878. Edison was so impressed by this design that in 1881 he patented it and has since taken much of the credit for the idea. Between the 1880's and the

present day, the principle of filament lighting remained essentially unchanged, although advances in materials technology have of course been considerable. (For further reading see[1].)

In the 1930's lamps were developed which used electrical discharges in tubes to excite phosphors. These were, even at the time, very much more efficient than filament lamps and consequently have been developed intensively into modern fluorescent lamps. It was during 1936 that Destriau first reported light emission by the direct electrical excitation of a phosphor[2]. The emission was feeble and the apparatus cumbersome and consequently this discovery attracted little interest from industrialists.

A casual observer might be tempted to ask, why, when filament and fluorescent lighting have reached such advanced states, do we still pursue the pioneering work of Destriau on solid state electroluminescent devices?

(1.2) The role of modern electroluminescent devices.

As the technology of electronics has developed a demand for advanced display devices has arisen. Conventional lamps have failed to meet this demand for several reasons. Firstly, a large panel of tungsten lights tends to get hot. Such lamps also consume large amounts of power and have short life times, as anyone who possesses a Christmas tree will know. Fluorescent lamps are impractical to miniaturise and so a problem arose. The development of the p-n junction light emitting diode was an excellent solution. These devices might be considered a landmark in electroluminescence, since they were for the first time superior in their efficiency and durability to the conventional lamps that they aimed to

replace. As technology has progressed further and light generation has become an integral part of modern communications systems, the fast switching times of the latest solid state light emitters has once again more than justified their development. The LED in its present state has not, however, solved all the problems associated with display lighting. Blue emitting diodes are very expensive and inefficient, whilst violet LED's are non-existent. The materials used for current LED's are also intrinsically expensive and so large area displays of this type are not commercially viable. Recently interest has turned towards ZnS as a possible solution to both these problems. The 3.7eV band gap at room temperature means that, in principle at least, devices can be constructed which emit throughout the visible range. ZnS is also comparatively cheap, so that large area displays are feasible. Indeed thin film "Sharp" devices based on ZnS:Mn are currently used in some compact computer display units. Perhaps one of the most exciting possibilities for the future of ZnS electroluminescent devices is flat screen colour television, where large area and blue emission are essential.

(2) The contributions of this work.

A great deal of work has been done on ZnS electroluminescent devices, although unfortunately much of this has had a "suck it and see" philosophy. In this thesis we have studied some of the processes which relate to electroluminescence in ZnS in order to better understand the physics involved. It is hoped that this will add to the existing knowledge in this field and ultimately lead to better device design.

Most of the main high field electroluminescent processes in ZnS can be illustrated by considering the operation of an Inoguchi[3] type luminescent panel, such as is shown in section in the diagram below.

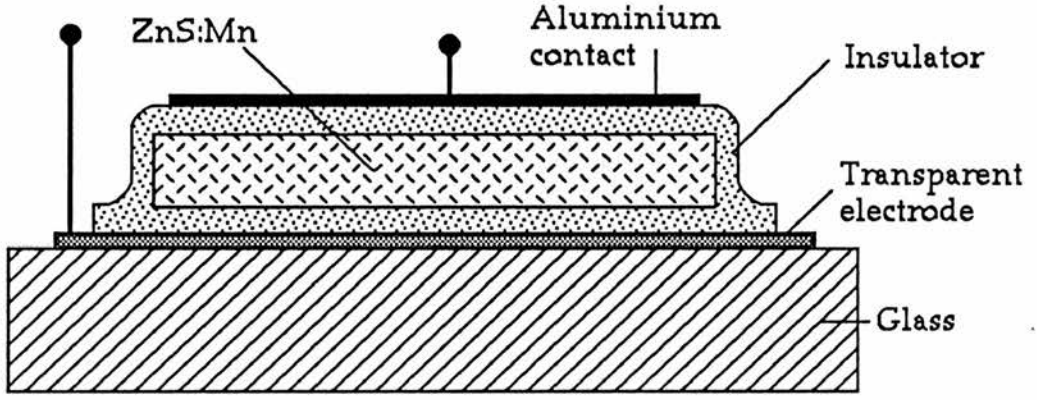

The active element is the ZnS:Mn layer. The insulator serves to ensure against catastrophic failure of the device. (This was one of the principal difficulties with earlier devices). The device operates AC so that the energy can be coupled into the active layer capacitively. The physical processes involved are however very much faster than the operating period, and so no special account need be taken of this. The device is viewed through the

glass substrate.

When the electric field is applied a small number of electrons are generated. The precise source of these electrons has been a topic of considerable controversy, but it is commonly believed that they are the result of surface processes (Smith[4]). These electrons accelerate in the applied field and gain energy. It has been speculated that the electrons become so energetic that they can impact ionise a valence electron across the energy gap and thus create an avalanche process (Mach & Müller[5]). This would lead to considerable current flow. We have been able to more preciously define the fields at which band-to-band ionisation occurs in ZnS. From this we are able to say that at the operating fields of Inoguchi[3] type devices, band-to-band impact ionisation will occur. This is an end to much speculation. Prior to 1987 no quantitative work had been done on impact ionisation rates in ZnS, largely as a result of the experimental difficulties this material presents. In the work presented here (see also Thompson & Allen[6]), we have, by measuring the photocurrent in a reverse biased single crystal ZnS Schottky diode, been able to study the band-to-band impact ionisation process. We have measured the ionisation parameter "b" and shown that this fits into a general empirical trend for all the tetrahedral semiconductors that was originally proposed by Livingstone & Allen[7]. During the ionisation experiments we have also detected a large change in the carrier number at lower fields which we believe to correspond to a two stage impact ionisation process involving a deep centre. A brief photocapacitance study has revealed that there is a

neutral level ~2eV below the conduction band which we believe to be responsible for the impurity based multiplication.

Returning to our description of the operation of an Inoguchi type device, the hot electrons must ultimately impact excite a luminescent centre if light emission is to occur. If one is expecting visible light from the device via such an impact excitation process the electron energy must be of the order of a couple of electron volts. Such an electron is very hot by the standards of studies on other materials (see for example GaAs[8]), and as such occupies states high above the conduction band minima. Some workers have used parabolic band models to describe the behaviour of these electrons (see for example Mach & Müller[5]). However, if one looks at the general form of the band structure that has been calculated for ZnS (page22 of this thesis, after Wang & Klein[9]), one can see that beyond ~1eV above the Γ_1 valley minima the conduction band is far from parabolic. This results in hot electron energy distributions which are far from Maxwellian. The nature of the electron distribution is of vital importance to electroluminescent processes. Hot electron transition luminescence has been studied by Rigby & Allen[10], and from this, qualitative information about the energy distribution of hot electrons has been obtained. Rigby and Allen believe that at high fields (~$10^6 V cm^{-1}$) electrons leave the Γ_1 minima and populate the upper valleys of the conduction band. Our studies of impurity impact ionisation processes have enabled us to substantiate these ideas. As a result of studies on ZnS:RE, Bryant[11] has

proposed a model of the hot electron distribution in ZnS that is different to that of Rigby and Allen. We have shown that, providing that the two stage impact ionisation process is also present in Bryant's samples, an alternative explanation of his results is possible, that does not contradict the findings of Rigby & Allen.

Electron processes in ZnS have been discussed extensively in the literature whilst the role of free holes is often ignored. This is probably largely because it is not at present possible to produce low resistivity p-type ZnS. If however, a two stage impact ionisation process operates, free holes can be generated at considerably lower fields then those of band-to-band impact ionisation. Photocapacitance studies performed by Zheng[12], have shown that holes are not always trapped in ZnS under a high electric field and thus thus are able to move when the field is applied. As a result of this, we have been able to propose a design for an LED based on impact ionisation. Holes generated in an impact ionisation process in an insulating surface layer are injected into n-type ZnS, where they radiatively recombine with conduction electrons. This might potentially offer highly efficient blue light emission. Experiments performed on prototypes have enabled us to refine the design.

We have performed photoluminescence experiments on ZnS:Te, to investigate the suitability of this material as a substrate for our LED's. In lightly doped material tellurium acts as an isoelectronic hole trap and a violet photoluminescence emission results from radiative recombination of a bound exciton on such a centre. In heavily doped material the violet

emission disappears and is replaced by a blue emission peak. It has been speculated that this blue peak is due to tellurium doublet centres[13]. As a result of our work and a survey of the available literature, we have found evidence which casts doubt upon this interpretation.

During our photoluminescence study of ZnS:Te, it was noticed that the luminescence took a considerable time to build up. An investigation of this has led us to believe that a mechanism involving electron trapping centres is responsible.

The time decay characteristics of ZnS phosphor emissions are often strongly temperature dependent. There are at present commercially available temperature sensors which are based on time domain analysis of the decay of such phosphors. We have designed, constructed and tested a system which performs the same operation in the frequency domain, and offers considerable advantages over existing designs.

Because of the large band gap of ZnS and ZnSe, these materials naturally contain comparatively high concentrations of defects. Such defects and defect related centres often produce energy levels deep within the energy gap. If these levels are only partially occupied, and their concentration is high enough, it is possible for an electron to hop from one such centre to another when an electric field is applied. We have used capacitance techniques to study this effect in ZnSe. We have also dedicated a sizable portion of this study to GaAs:Cr, because the nature of the energy levels are better understood in this material. Previous work in this field, although extensive, has concentrated on shallow levels at low

temperature.

To summarise, we have studied hot electron ionisation and luminescence processes in ZnS. We have been able to determine the fields at which various effects occur within the same sample and from this obtain information about hot electron behaviour. Such knowledge is applicable to many ZnS devices. We have proposed a new type of ZnS LED, and constructed prototypes. During the course of this work we have investigated the photoluminescence emissions of ZnS:Te. We have as a result of this assembled considerable evidence against some existing ideas about this system and proposed a new and simpler explanation of the results. We have used a ZnS phosphor as the basis of a temperature sensor, and demonstrated the viability of a novel frequency domain approach. Finally we have studied optically induced deep level electron hopping in ZnSe and GaAs:Cr. This process is important in oxide layer MIS devices.

Chapter 2

Band-to-band impact ionisation in ZnS.

(1) Introduction.

In a semiconductor under an electric field electrons and holes gain energy as they move along the direction of the field. This gain is balanced by loss via various scattering mechanisms. The movement of the electrons through the lattice at very low fields can be described by the familiar mobility relation $\underline{v} = \mu |\underline{E}|$. At very high fields (typically $>10^5 V cm^{-1}$ depending on the material) interaction with optical and acoustic phonons fails to remove energy from the electrons at the same rate as they gain energy from the field. Such electrons may typically accumulate energies of several eV. This energy may be lost by ionisation of a valence electron into the conduction band. Such a collision may be visualised in real space as ionisation of an electron from one of the host lattice atoms. This ionised electron can also accelerate in the field and gain sufficient energy to ionise a further electron across the gap. In this way an avalanche breakdown can build up. This is analogous to a Townsend breakdown in a gas discharge tube. A coefficient α is defined as the number of pairs an electron produces in traversing a given distance.

In the diagram overleaf the process is shown only for electrons, however, to sustain a discharge it is necessary to have some mechanism for regeneration of electrons at the cathode. In the Townsend gas this mechanism is ion bombardment of the cathode, the ions being too large and immobile to produce ionisation themselves. In a semiconductor however the holes are small and mobile so that the discharge can be

sustained by "hole ionisation" producing new electrons near the cathode. A hole coefficient β is defined in the same way as α for electrons.

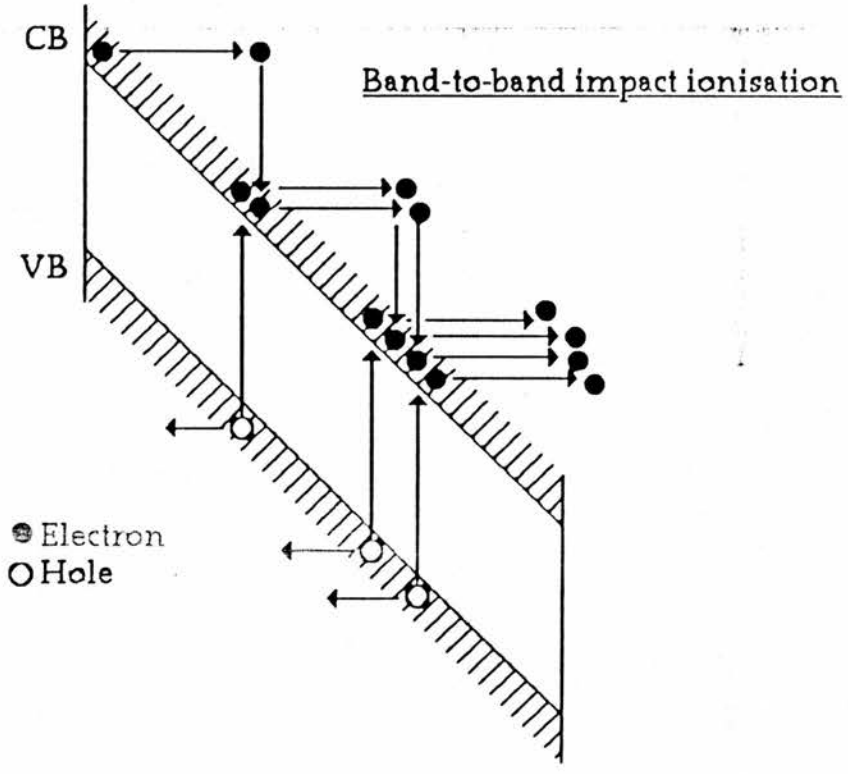

It is important to note that we are dealing with very energetic carriers so that the velocity is governed largely by band structure effects and that the smaller magnitude of the hole mobility is of little consequence in this field regime. If one were able to inject a constant number of electrons into a high field region and count the number that leave a curve like the one below would result.

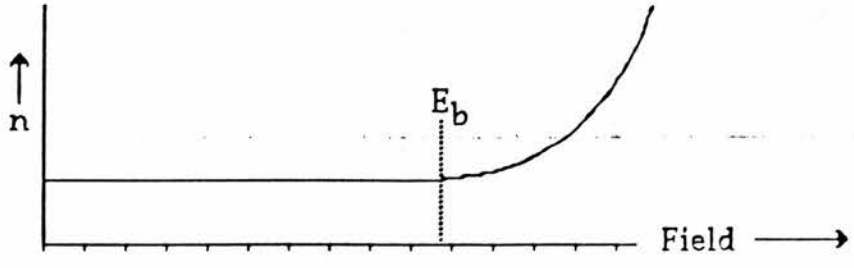

In a direct small gap semiconductor a few electrons with energies of the order of Eg above the conduction band minima may be easily obtained without the majority of the electrons deviating far from the minima. However in wide gap materials with complex band structure such as ZnS this is not the case.

In the following "background theory" section it will be shown that the coefficient α is expected to vary with field according to,

$$\alpha = \alpha_0 \exp(-b/E)$$

The ionisation parameter "b" is constant for a given material and has been determined for a variety of comparatively small gap semiconductors. In 1970 Livingstone and Allen[7] pointed out that there is a correlation between the ionisation parameter b and the energy gap of the tetrahedral semiconductors. This is reproduced below.

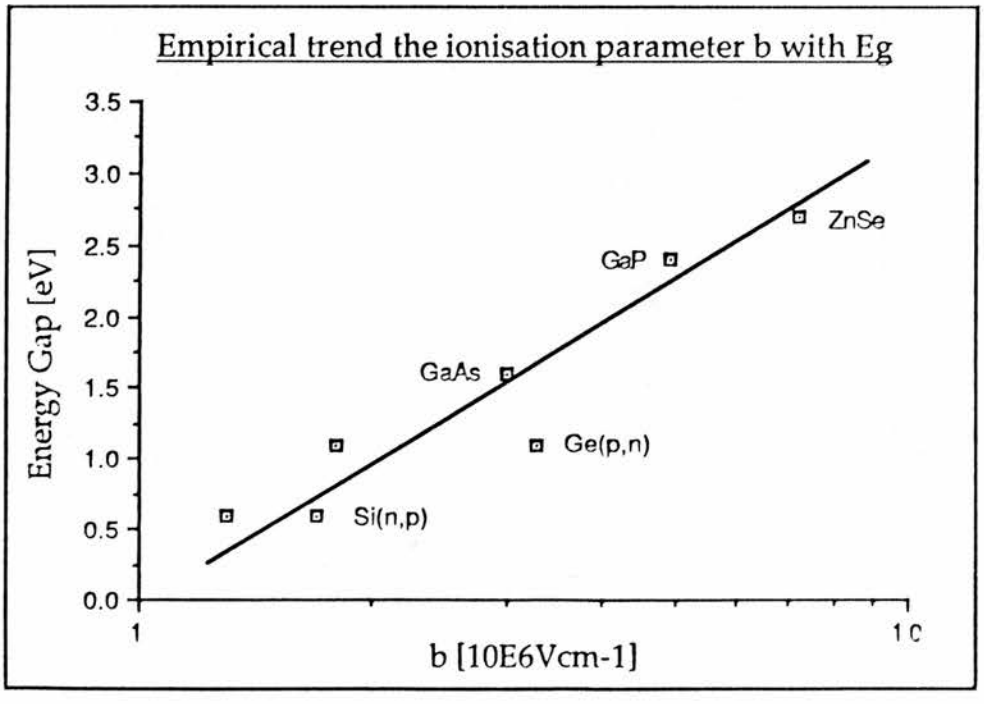

Our aim in this work was to quantitatively investigate avalanche breakdown in ZnS, to determine the nature of the process, and if it is of the form,

$$\alpha = \alpha_0 \exp(-b/E) ,$$

to determine "b" to see if this conforms to the empirical trend. From this we might be able to determine the nature of breakdown in the larger gap materials and whether or not it is qualitatively different to that in the small gap semiconductors. Beyond this important theoretical question there is a very real practical interest in this process.

There is considerable interest in ZnS at the moment as a material for large area electroluminescent displays, because within its large bandgap (3.7eV at 300K) it can accommodate a whole range of impurity levels. This means that in principle it is possible to have light emission over the entire visible range.

Many current thin-film electroluminescent devices are believed to operate at fields where avalanche breakdown occurs[5][14]. Thus, a better understanding of the process will help to move towards a more scientific rather than empirical device design.

(2) Experimental principles.

In order to determine the multiplication factor M and consequently $\alpha(\underline{E})$, we require to know the ratio of the number of carriers entering the high field region to that leaving at various fields. No method which simply involves measuring current-voltage characteristics is valid because of the carrier velocity dependence. Since

$$\underline{j} = ne\underline{v}$$

and $\underline{v}$ is a complex function of field in itself then $\underline{j}$ is no true measure of n.

To get around this problem we chose to measure photocurrent. In this case a fixed photon flux produces a constant number of carriers in unit time. The current dQ/dt is thus completely independent of carrier velocity, providing recombination during transit can be neglected. There is however one difficulty associated with this method. Whatever choice of structure we make our measurements on, there is likely to be a finite dark current which may to some extent be a function of carrier velocity. To distinguish between this and the photocurrent one can use chopped light. This brings the additional advantage of facilitating the use of phase sensitive detection, and consequent improvement in signal to noise ratio.

(2.1) Choice of structure.

(2.1a). A thin film.

This at first would seem the obvious choice since one only needs a small voltage to generate a high field. However if grown by evaporation or sputtering the material is not single crystal. This inhomogeneity means

that the field distribution is not well defined, and thus such structures can only provide a qualitative picture of the ionisation process.

(2.1b). A simple slab.

Here we have single crystal and consequently a well defined field, but if the slab is of manageable thickness the voltage required to achieve the fields under which ionisation may take place would be unreasonably large. For example 10kV would be needed to achieve $10^6 Vcm^{-1}$ with a slab 100μm thick.

(2.1c). A diode.

Since it is not at present technologically possible to make low resistance p type ZnS this must be a Schottky diode. The manufacture of n type ZnS from insulating ZnS is possible using a special zinc treatment. The diodes are made of single crystal material. The narrow depletion region at the junction means the voltages required to reach high fields are comparatively small.

The diode thus seems the most sensible structure to use in the ionisation measurements.

(3) Background theory.

The theoretical treatment of the band-to-band ionisation process is discussed by Moll[15]. The theory that is relevant to this work is outlined below.

It is only necessary to follow one sign of carrier. Choose electrons.

Assume,

(1). No recombination loss

(2). α_i is a function only of field.

(3). Interaction between conduction electrons is small.

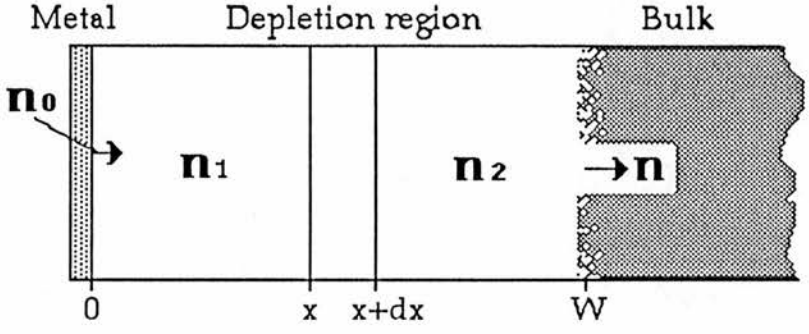

Define,

n_1 as the number of pairs produced by an electron between 0 and x.

n_2 as the number of pairs produced by an electron between x and W.

α_i as the number of pairs generated in unit length by an electron.

β_i as the number of pairs produced in unit length by a hole.

The number of pairs generated between x and x+dx, (dn_i) is thus,

$$dn_1 = (n_0 + n_1)\,\alpha_i\,dx + n_2\beta_i dx$$

It is generally assumed for simplicity that $\alpha_i = \beta_i$ thus,

$$dn_1 = (n_0 + n_1)\,\alpha_i\,dx + n_2\,\alpha_i\,dx$$

By continuity we have,

$$n = n_1 + n_2 + n_0$$

Thus,

$$dn_1 = n\,\alpha_i\,dx$$

Consider the limits before integration, $n_1=0$ at $x=0$ and $n_1=n-n_0$ at $x=W$

Integrate over the whole region.

$$\int_0^{n-n_o} dn_1 = \int_0^W n\,\alpha_i\,dx$$

$$[n_1]_0^{n-n_o} = n\int_0^W \alpha_i\,dx$$

Now rearrange to get,

$$1-(n0/n) = \int_0^W \alpha_i\,dx$$

and define,

$$M = (n/n_0)\ .$$

Thus we have,

$$[1-1/M] = \int_0^W \alpha_i \, dx \qquad \{1\}$$

The form of α has to be known before this integral can be evaluated. Wolff[16], by solving the Boltzmann equation for high field strengths, and assuming that electrons gain more energy from the field between collisions than they lose in the subsequent emission of an optical phonon, showed that α is expected to have the form,

$$\alpha = \alpha_o \exp(-E_o^2/E^2)$$

where E_o is the impact ionisation parameter and α_o is a constant. This treatment is designed for a system where the electrons in the Maxwellian tail of the main distribution initiate the ionisation process.

Shockley[17] assumed that the electrons which attain sufficient energy to cause ionisation are those which escape the collisions which randomise the motions, the so called "lucky electrons". By considering only these electrons he showed the form of α to be

$$\alpha = \alpha_o \exp(-b/E) \qquad \{2\}$$

where b is the ionisation parameter. This expression would be applicable

to a system where ionisation is initiated by lucky electrons beyond the main distribution. Baraff[18] showed that these two expressions are limiting cases of the same general solution. The essential difference between the two approximations lies in the relationship of mean electron energy to ionisation energy E_i. If the mean energy is less than the threshold energy α has the E^{-1} form, and the E^{-2} form holds when the mean energy is greater than that required for ionisation. E_i can reasonably be expected to assume any value greater than E_g. Thus in the case of band-to-band excitation the threshold for ionisation is well above the thermal energy of the lattice and equation (2) can be expected to hold.

It is interesting to consider the electron distribution in ZnS at high fields. In simple direct small gap materials the electron distribution is believed to be essentially Maxwellian with a "lucky electron tail" where electrons have unusually high energies. Thus Shockleys`s analysis would indeed be applicable. However it has been shown by Rigby & Allen[10] that at high fields (around $10^6 Vcm^{-1}$) in ZnS many of the electrons occupy the X_1 & X_3 valleys in the conduction band. The approximate shape of the distribution at various fields might be expected to be as is shown in the sketch overleaf. A sketch of the band structure of ZnS is also shown.

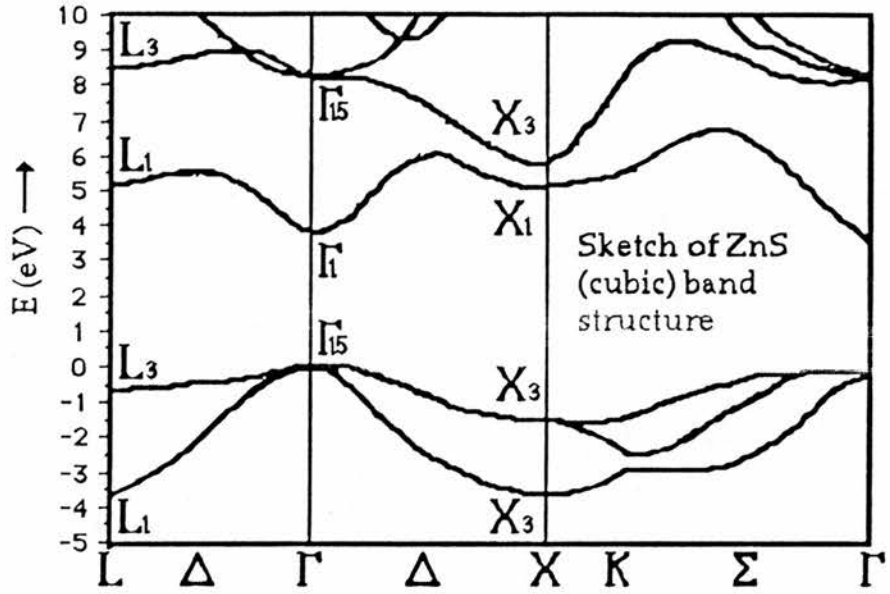

Sketch of the electron distribution in ZnS at various fields

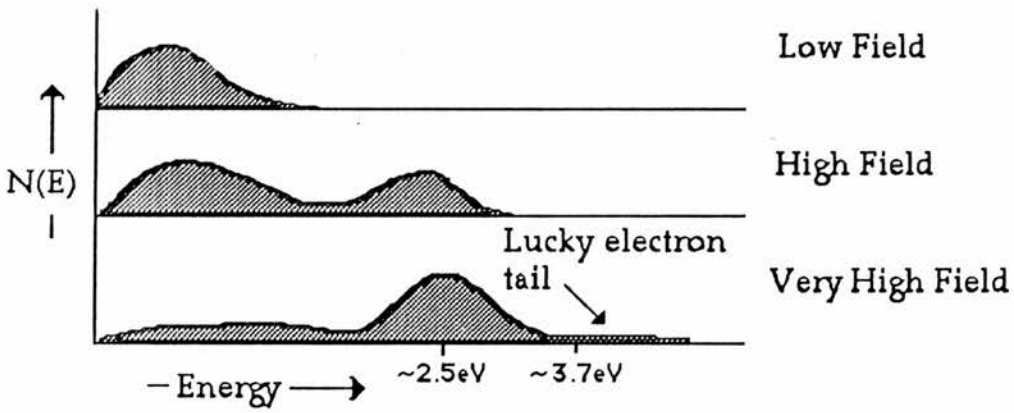

The electron distribution is far from Maxwellian but the X valley accumulations might still be expected to possess a lucky electron tail. Unfortunately at present there is little known about the electron distribution in ZnS beyond the X_1 & X_3 valleys. If one pursues the analysis for a lucky electron initiation process then using {2}, {1} can be reduced to,

$$[1\text{-}1/M] = \alpha(E_m)\, W_{(eff.)} \qquad \{3\}$$

where E_m is the maximum junction field and $W_{(eff)}$ is an effective

width. This is tabulated by Moll[15] as a function of E_m for various values of the ionisation parameter.

Returning to {1}, we have

$$[1-1/M] = \int_0^W \alpha_i \, dx \qquad \{1\}$$

We now consider some properties of Schottky junctions.

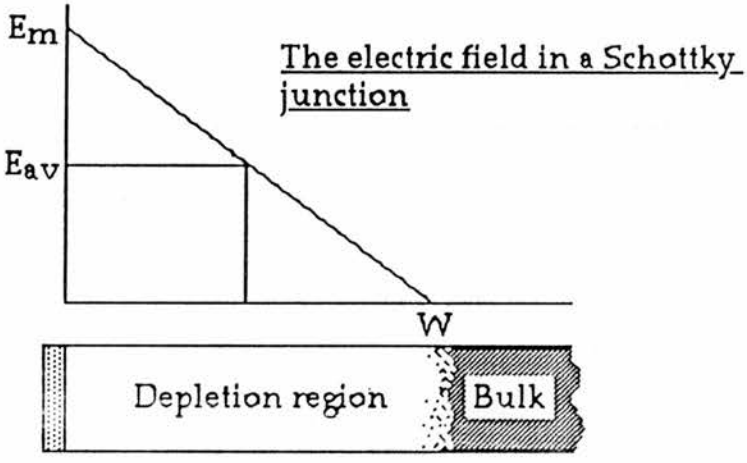

(a). $E = E_m(1 - x/W)$

(b). $E_m = 2V/W$

(c). $W = W_1/(V^{1/2})$

W1 is a width constant defined by, $W_1 = (2\varepsilon_o\varepsilon_r/EN_d)$

However we require α as a function of field. Using the above properties it is possible to change the variable in {1} to E.

Using (a),

$$(1 - 1/M) = (W/E_m) \int_0^{E_m} \alpha_i \, dE$$

Using (c) and (b),

$$(1 - 1/M) = (W_i^2/2) \int_0^{E_m} \alpha_i(E) \, dE .$$

Differentiation yields,

$$\alpha_i (E_m) = 2/W_1^2 \, d(1 - 1/M)/dE_m - 4/W_1^3 (1 - 1/M) dW_1/dE_m .$$

This equation shows that there are two possibilities for measuring α_i experimentally.

(1) Measure E_m at breakdown for various diodes (M = infinity at E_b)

$$\alpha_i (E_m) = -4/W_1^3 \, dW_1/ dE_b .$$

This is very difficult because defining just where total breakdown occurs in a noisy junction is imprecise. E_b can be determined by measurements of M at

$E < E_b$ and extrapolation but this in principle amounts to method 2.

(2) use the same diode, thus W_1 is constant and $dW_1/dE_m = 0$

$$\alpha_i (E_m) = [2/W_1^2] \, d(1 - 1/M)/dE_m .$$

Thus $\alpha(E)$ is found from M(E) measured at various fields.This seems the most sensible practical approach.

(4) Experimental methods.

(4.1)Sample preparation.

Starting material of three types from two sources was used.

(1)Nominally undoped vapour transport grown ZnS from this laboratory.

(2)Melt grown ZnS:Mn (0.05%Mn) from Eagle Picher.

(3)Melt grown ZnS:Mn (0.5%Mn) from Eagle Picher.

The process of melt growing ZnS is difficult because ZnS has no liquid state at atmospheric pressure. The melt must thus be kept at very high temperature and many atmospheres pressure in order to draw a crystal.

The original ingots were of the order 1cmx1cmx1cm in size. They were cut with a water-cooled diamond saw at a feed rate of around 0.1mm per minute. This was kept deliberately slow to avoid stress fractures in the slices. A finished sample would typically have dimensions 5x5x2mm. Before entering the conductivity process the samples were polished with silicon carbide followed by cerium oxide powder to remove any saw marks or deep surface damage. They were then chemically cleaned by etching in 50% caustic soda at 70C for 10 minutes followed by 10% hydrochloric acid at 70C for 30 minutes. The conductivity process took place in a graphite boat like the one shown on the next page. The samples were loaded in the bottom chamber and a zinc-aluminium mixture into the top. The zinc was 99.9998% pure in the form of pellets (from Koch Light laboratories) and

was only handled in clean glass. The aluminium was in the form of 99.99% purity wire. This was cut into 0.5cm pieces using a glass blade. (Use of metal might result in material transfer and the contamination of the mixture). After cutting, the sections of wire were etched for 1 minute in 50% caustic soda at 70C followed by a deionised water rinse. This etch was to remove surface dirt and oxide. The mixture of zinc and aluminium was prepared by weight. The whole loading procedure was performed in a dust-excluding clean cupboard. It must be very much emphasised to any one wishing to duplicate this process that absolute cleanliness is vital for success. (If one is aiming for 10^{16} cm^{-3} donors and using a 10 gramme zinc mixture with a 1 gramme sample, 0.01 milligrammes of dirt or impurity will equal this concentration.) The graphite boat was then sealed in a silica tube which was evacuated to $<10^{-3}$Torr. Silica is used to withstand the high furnace temperatures and evacuation prevents explosive reaction of the zinc with residual oxygen.

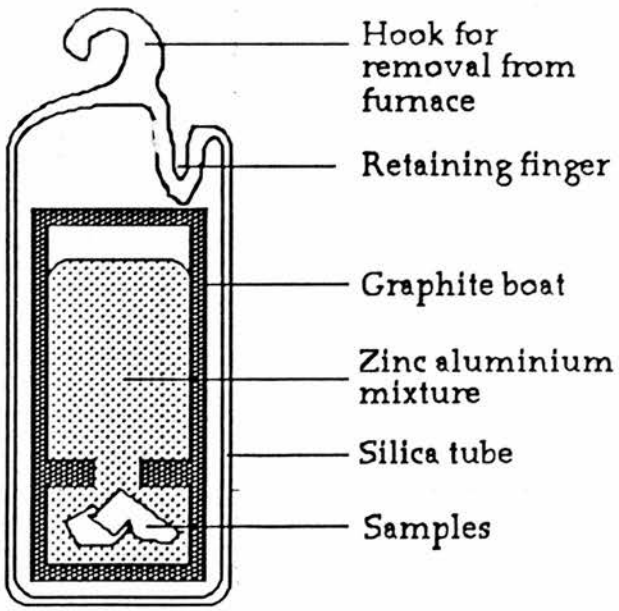

The retaining finger prevented the boat from simply floating on the top of any zinc which leaked out. After several trials the best recipe was found to be Zn/10%Al mixture at 1222K for 170 hours. Other workers propose small variations on this (eg.[19]).

When the samples are removed from the furnace the surfaces are coated with white powdery aluminiumsulphide from the reaction

$$3\,ZnS + 2\,Al \rightarrow Al_2S_3 + 3\,Zn\,.$$

This was removed by grinding with silicon carbide followed by cerium oxide. This resulted in pale yellow transparent crystals with good optical surfaces. Surface oxidation in ZnS is always a large problem, but can be reduced to quite acceptable levels by etching. The best etch was found to be 20 minutes in 50% caustic soda at 50C, then a rinse in deionised water followed by 30 minutes in 10% hydrochloric acid at 50C again followed by a rinse in deionised water.

Electrolytic Schottky contacts were tried using hydrochloric acid and these produced diodes with excellent I-V characteristics. However even the smallest current flow produces electrolysis and consequently gas bubbles. These bubbles cause random fluctuation in the effective contact area. If allowed to go too far electrolysis destroys the sample surface. Consequently acid contacts are of little use at higher voltages and were abandoned for the band to band measurements at an early stage. However the results were very useful for the low field work in later chapters.

For the band-to-band ionisation measurements metal Schottky contacts

were used, and aluminium was chosen rather than gold because previous workers in this laboratory found it to be more durable and of similar electrical quality. Ohmic contacts were made on one side by alloying indium dots to the surface at 520K under an atmosphere of 90%$N_2$10%H_2. Many dots were used so that they could operate in parallel providing minimum resistance. These gave reasonable ohmic behaviour but still had considerable series resistance (1-10kΩ). Although of little consequence when reverse bias is applied due to the large depletion region resistance this spoils the capacitance measurements used to determine N_d because it alters the equivalent circuit. To get around this a layer of Al was evaporated over the whole back face. This formed a second depletion region with a large capacitance so that at the 1MHz used for the capacitance measurements it was in effect a short circuit. This layer also served to connect all the indium dots in parallel thus ensuring minimum DC resistance. The front Schottky contact must of course have a smaller area and thus a smaller capacitance than the rear contact so that it is this capacitance which dominates the capacitance-voltage measurement. The front contact must also be semi-transparent so that light used to produce the photocurrent can pass through. This condition is satisfied by using a very thin Al front contact. A 50% transmission can easily be achieved whilst maintaining satisfactory mechanical strength. A finished diode is shown in the diagrams over the page.

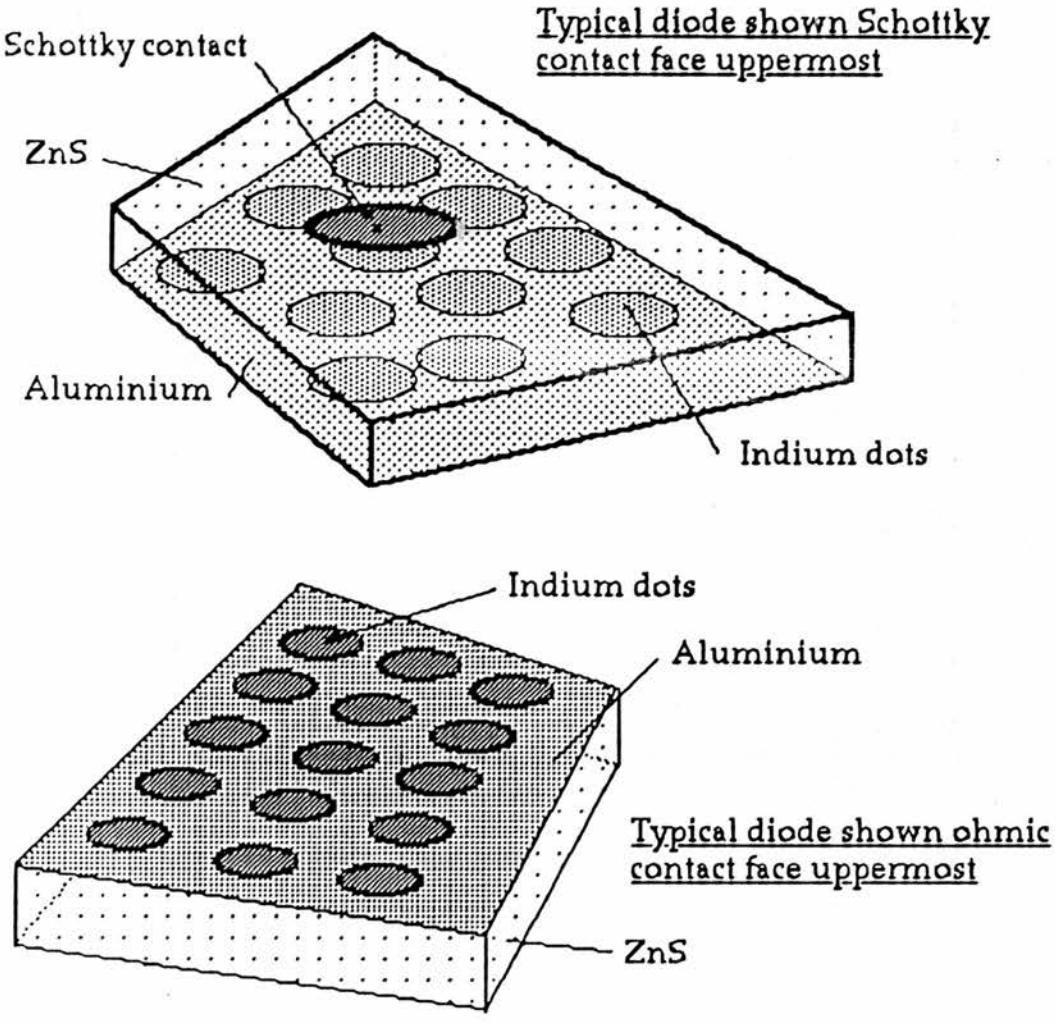

During the course of this work many diodes were made from the three starting materials and a suitable labelling system was required. Rather than simply labelling them 1,2,3 etc. a descriptive system was employed. (This system is maintained throughout this thesis.)

A typical sample name might be.

$$\underbrace{\text{Ep1}}_{\text{(a)}}\ \underbrace{\text{Tr4}}_{\text{(b)}}\ \underbrace{\text{S2}}_{\text{(c)}}$$

(a) Source material,

Ep1 - Eagle Picher 0.05% Mn.

Ep2 - Eagle Picher 0.5% Mn,

Ew1 - Vapour grown.

(b) Treatment number.

Starting with the first satisfactory result of the process being called 1. Any two samples with the same Tr number were in the same conductivity treatment, (and from the same source material as these were not mixed during treatment).

(c) Sample number.

Random allocation to distinguish between different samples from the same conductivity treatment.

(4.2)Capacitance measurements.

It is necessary to know the field in the depletion region of the diode at any applied bias so that M(E) may be determined. The usual approach to this when dealing with well-defined junctions is to determine the donor density N_d and using this to deduce $\underline{E}$ from the applied and barrier voltages. The simplest and often most accurate way to measure N_d is to measure junction capacitance as a function of applied voltage. N_d may then be deduced from the standard expression

$$N_d = 2 / (b \, e \, \varepsilon_0 \varepsilon_r A^2)$$

where b is the gradient of the $1/C^2$-V graph and the other symbols have their usual meanings.

The average junction field is

$$[\, V_{(app)} + V_{(bi)} \,] / W$$

where W is the depletion region width as defined by,

$$W = (2 \varepsilon_o \varepsilon_r / N_d e)^{1/2} (V_{(app)} + V_{(bi)})^{1/2} .$$

Here $V_{(bi)}$ is the built in barrier potential and $V_{(app)}$ is the applied voltage. This method offers the additional advantage that the donor density measurements may be performed on the same contact as the ionisation measurements.

ZnS is a difficult material to work on because of its large band gap (3.7eV at 300K) and its tendency to form surface oxide layers.

Although some of the capacitance-voltage measurements behaved in the expected manner (see below) many were more difficult to interpret.

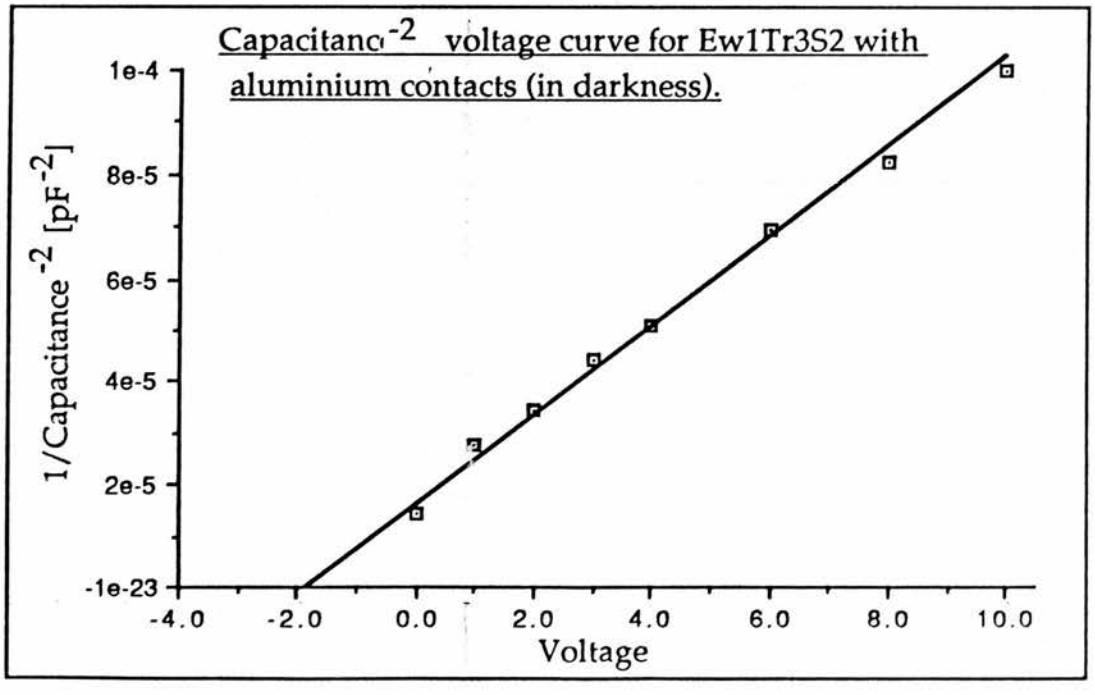

The V against $1/C^2$ plots were always straight lines but the intercept on the voltage axis (which is equal to the built-in junction voltage) was often larger than expected. Furthermore if the contacts were replaced and the run repeated N_d would remain the same but the intercept might be very different.

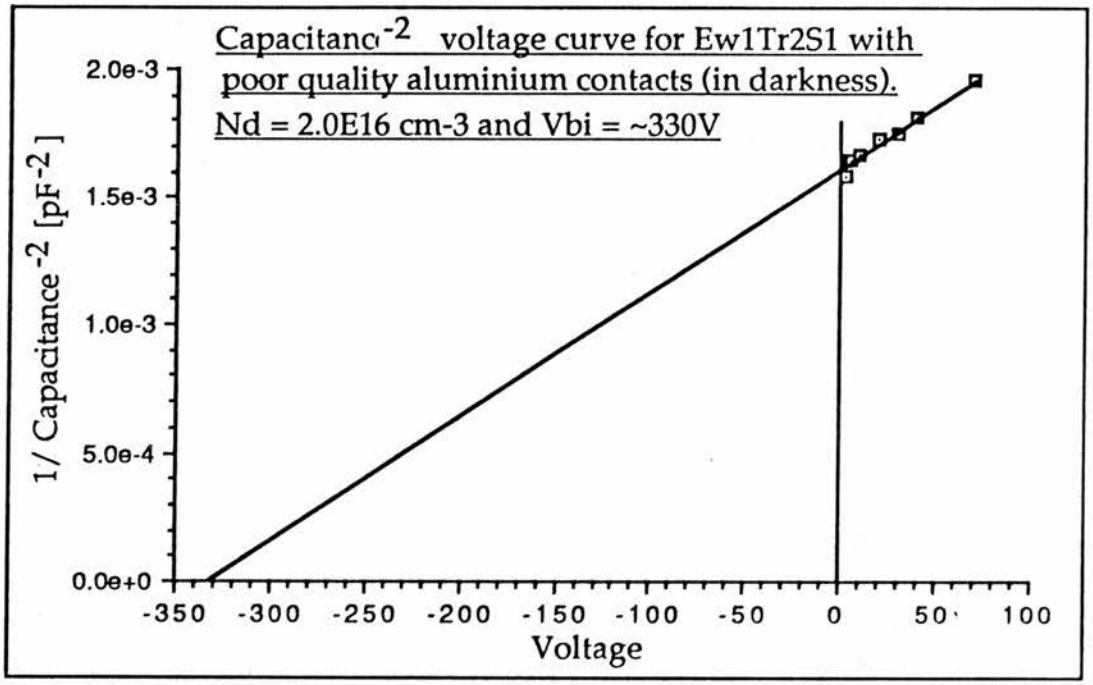

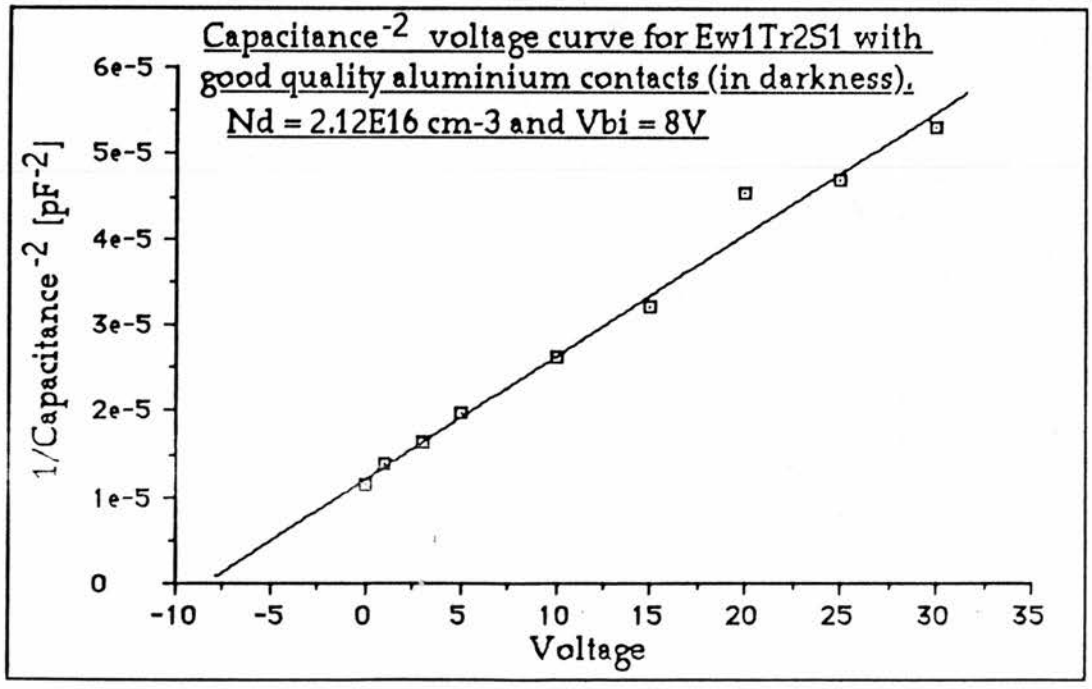

This can be seen in the results on the previous page, N_d from the two runs was 2.0 and 2.1x $10^{16}cm^{-3}$ whereas the intercepts were 8 and 330V.

There are three possible explanations for such large intercepts

(1) Presence of very large numbers of deep levels which ionise at the junction as the bands bend. See for example[23]. This introduces a large additional component to the space charge and thus alters the intercept. In the case of a large negative value the implication is that the centres are acceptors. If this mechanism were responsible for our large intercepts, one would not expect the intercept value to vary wildly when different contacts of the same metal were used on the same sample.

(2) Loss of voltage across the rear contact. The making of good ohmic contacts onto ZnS is extremely difficult, contact resistances remaining of the order of several kΩ. Some voltage is thus inevitably lost across such a contact in the diode. In order to investigate this a diode was made with an ohmic probe contact as illustrated below.

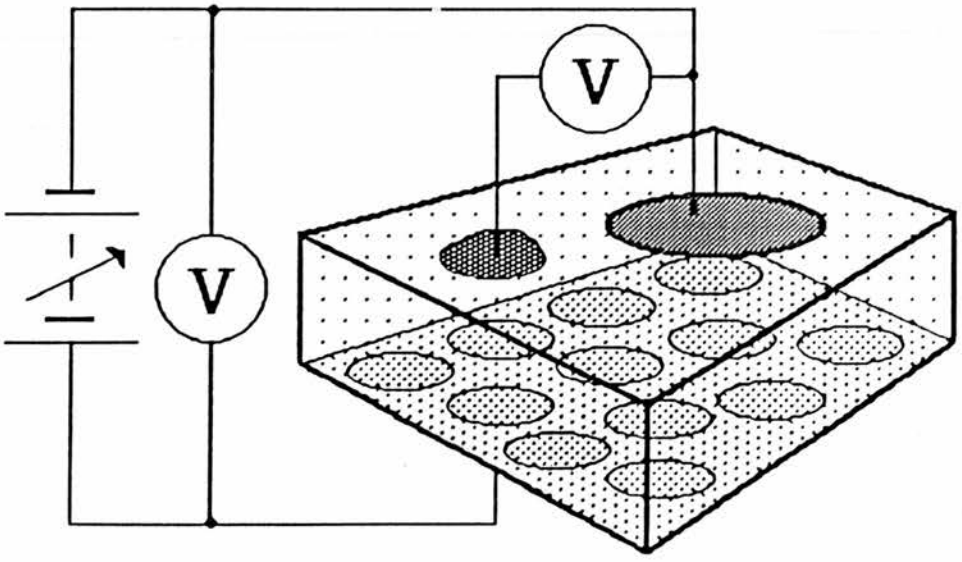

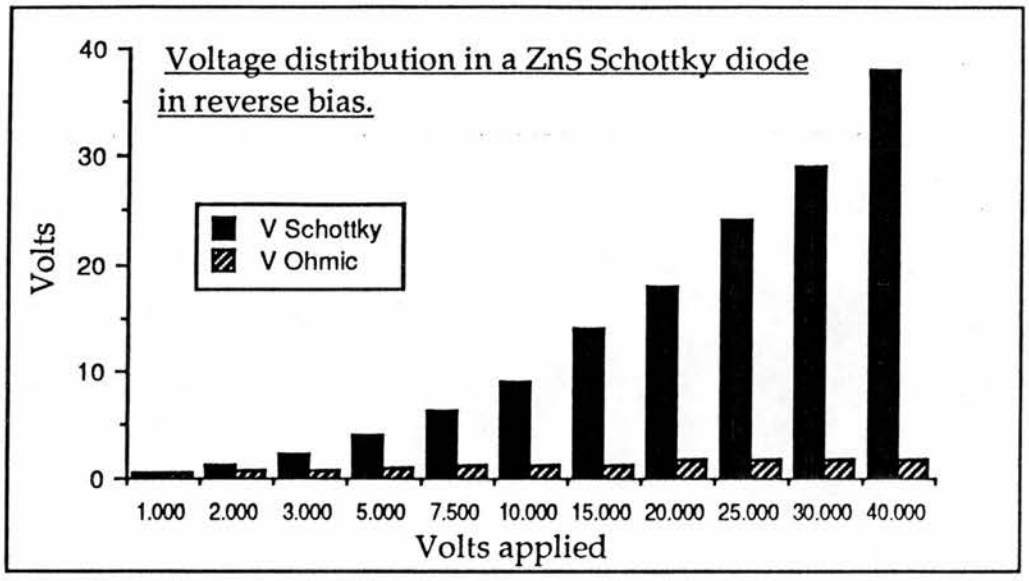

The drop across the rear contact was found not to exceed 1 or 2 volts in most diodes. Whilst this might explain the intercepts that deviated from the expected value by a small amount it does not provide explanation for the >300V intercepts that were observed in some diodes.

It should be stressed that if 1 volt is lost across the rear contact this is of little consequence to the ionisation measurements since the voltages applied to bias a diode into band-to-band ionisation are typically in the range 80 - 120V. Such a small resultant error in the field (~1%) is smaller than other limitations determining the exact field such as sample inhomogeneity.

(3) The remaining possibility is that a layer of oxide is present on the sample surface even after etching. Is has been shown by Cowley[21], with reference to the extensive work of Goodman[22], that capacitance-voltage

runs on MOS structures yield true values for N_d but have larger than expected intercepts. This is consistent with our observations. As better etching techniques were developed the value of the intercepts came down to typically 2 to 10V as compared to the ~1.5V that might be expected for an ideal Al/ZnS junction. Although a layer of partially conducting oxide does not strongly affect the determination of the electric field, it does present two problems when present in large quantities. Firstly, the values of measured capacitance are small (typically 10-30Pf) compared to a diode of similar N_d with very little oxide (typically 200-500Pf). This means the determination of N_d is less accurate and thus the field is not known with such precision. Secondly, some voltage is inevitably dropped across this oxide even though it is of lower resistivity than the depletion region. If the thickness is very large this voltage drop will be considerable and can become a problem. For these reasons the ionisation measurements were made only on the better diodes with intercepts in the range 2-10V. Discussion of diodes with large intercepts is presented only as a cautionary note for future workers.

The donor density of a diode was measured at various capacitance bridge drive frequencies in order to ensure that no dispersion anomalies existed. The result is shown over the page. For most of the capacitance voltage work, a frequency of 1MHz was chosen as the Wayne Kerr B601 bridge is most sensitive at this frequency.

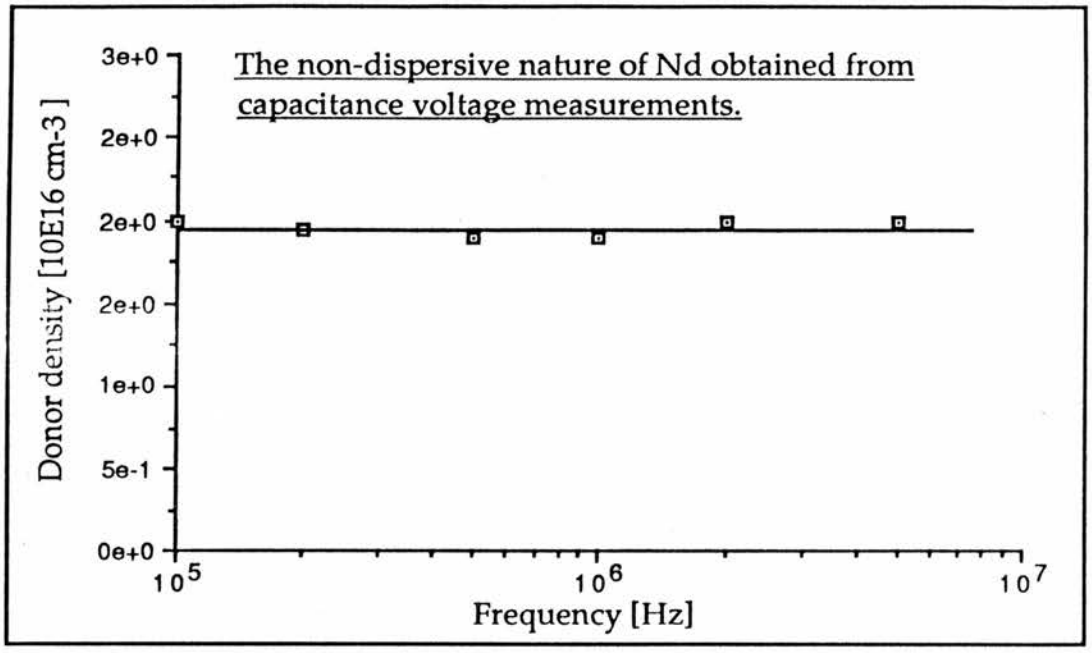

One further complication exists in the determination of the junction field. The capacitance of our ZnS Schottky diodes was very light-sensitive. The zero bias capacitance change when illuminated with moderately bright light (such as a 100W tungsten lamp focused to a 5mm spot) is typically 100 to 500%. This implies that there are a large number of deep centres present some of which are ionised by the light. This is discussed in considerable detail in a later chapter along with the reasons why these deep centres do not affect the capacitance-voltage intercept. Their only importance to this work is that if the excitation light used in the photocurrent measurements contains visible components the depletion region width changes. Such changes in width are of course mirrored by changes in the field of similar magnitude. It is of vital importance therefore to make the capacitance-voltage measurements under identical

illumination conditions as the photocurrent ones.

Schottky contact on n type semiconductor
with a deep level

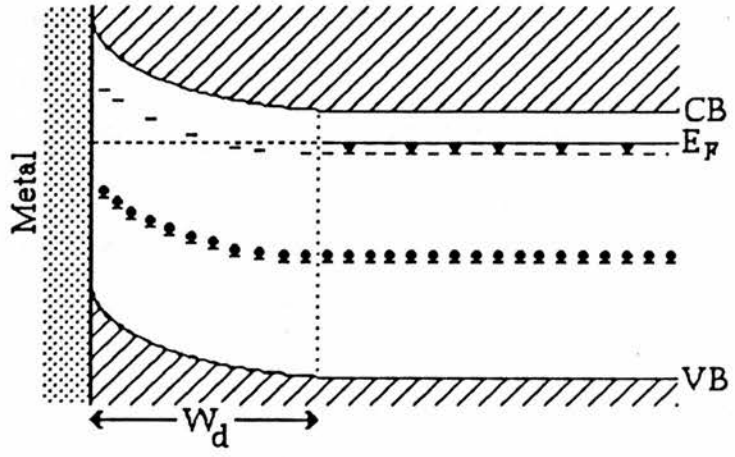

Schottky contact on n type semiconductor
with a deep level when illuminated with hυ>Et

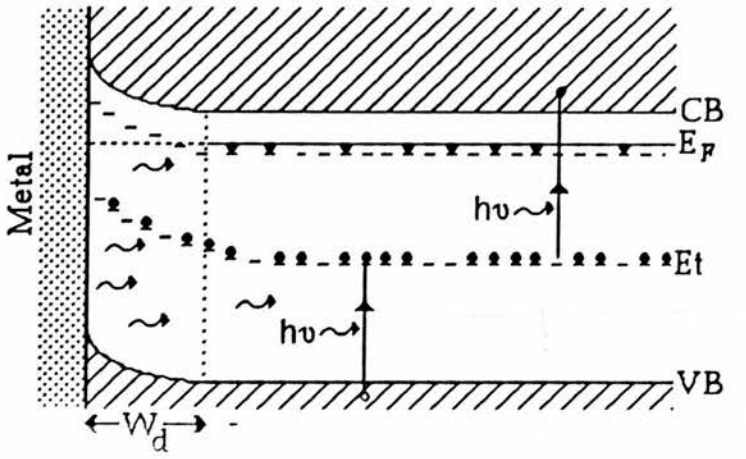

This means that each time one makes a photocurrent measurement it must be accompanied by a capacitance-voltage run on the same contact. (This is because $N_{d(effective)}$ is a function of light intensity and so contact transmission must be constant as well as experimental geometry.)

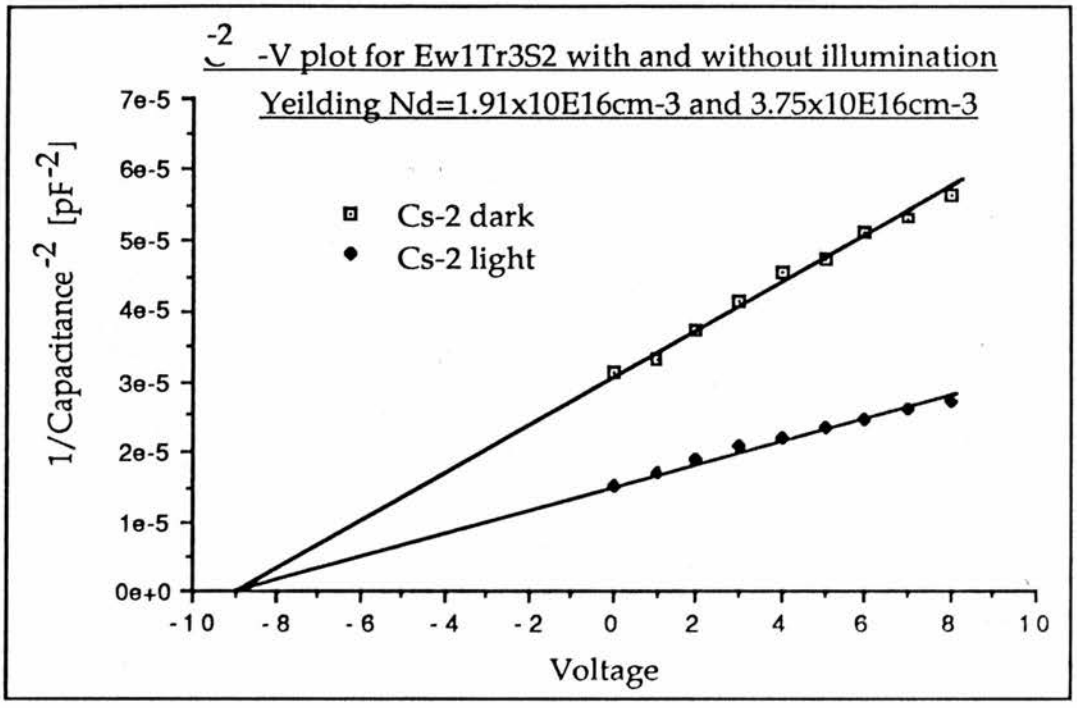

The two lines correspond to the sample in darkness and when illuminated with comparatively weak light (100W tungsten lamp unfocussed at ~ 30cm). This new value of donor density is referred to as N_d(effective) and is a function of light intensity. If N_d(effective) > N_d less volts need to be applied to achieve the same field in the light than the dark. It is important to check that as the light is chopped the depletion width remains constant if the photocurrent measurements are to be accurate. In other words the time constant for the capacitance change must be much larger than the chopping period. This was measured and the decay time constant was found to exceed 150 seconds. This is easily big enough to satisfy the condition since a chopping frequency of ~400Hz (period ~1.2ms) was used for the photocurrent measurements.

An accurate determination of the field in ZnS diodes is by no means as

simple as with many smaller gap materials and great care must be exercised to avoid large error.

(4.3)Ionisation measurements.

The diodes were mounted in a sample holder like the one shown below.

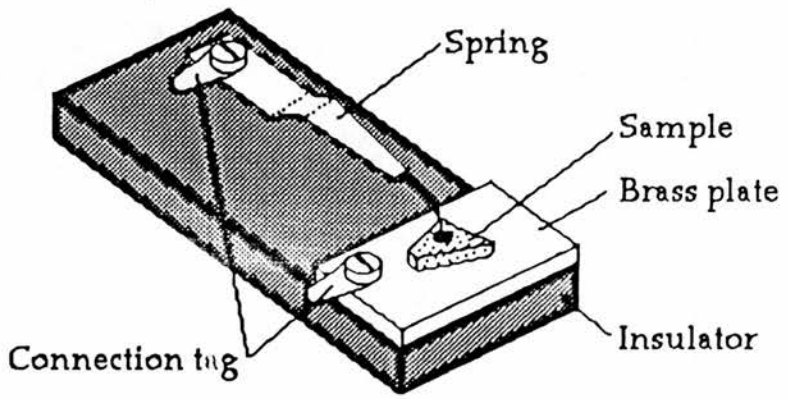

The sample holder was then placed in the experiment. A full diagram of the experimental arrangement is shown on the next page.

In essence the technique simply involves setting the diode in a circuit like the one shown below and measuring the AC photocurrent with a PSD as the diode bias is changed.

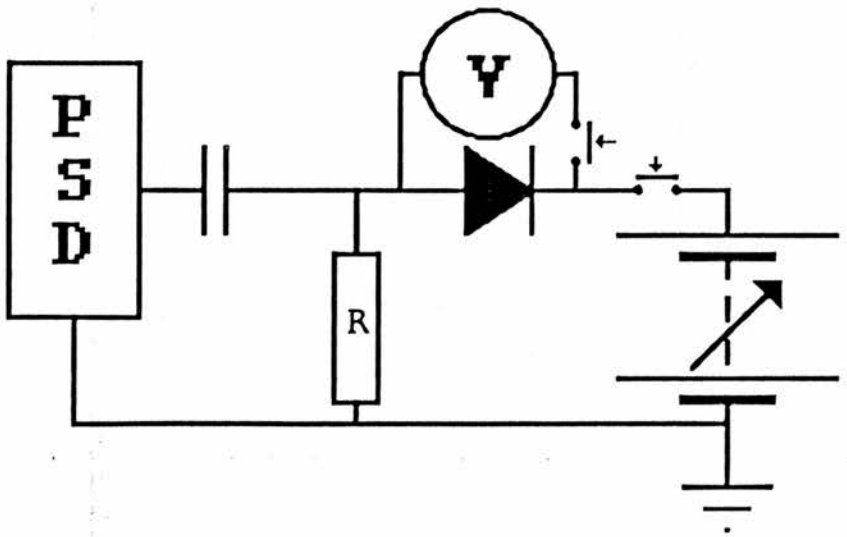

However, there are many technical difficulties in doing this (such difficulties have in the past prevented this work being done). ZnS has a large band gap (3.7eV at room temperature.) Thus to generate electron hole pairs requires quite hard ultra-violet light. This was produced by a Hanovia UV100 ultraviolet gun, which is based around a 100W mercury discharge lamp. Focusing is provided by an integral silica lens, a spot of <0.5mm diameter being typically possible. With such a good focus comparatively large intensities and consequently easily measurable photocurrents could be produced. The light was mechanically chopped using a Bentham 218 chopper with built-in reference generator. A chopping frequency of between 200 and 500Hz was used. The photocurrent was detected by a PSD. The sampling resistor R was kept reasonably small to avoid affecting the system. For a Schottky diode 10 to 500Ω was used producing a signal of around 1mV. The Al contacts on ZnS although more durable than both acid and gold are by no means stable. If subjected to current flow for prolonged periods hotspots burn out reducing the effective area dramatically. This can easily be observed by measuring the capacitance against time under a large DC bias. When large currents flow (>10mA) the capacitance falls and never recovers its original value. To minimise this effect the voltage was only switched on for short periods whilst a single measurement was made. During the setting of the bias voltage the diode was disconnected. A hysteresis check of the photocurrent-voltage curve ensured that no significant contact damage had occurred during data collection. At such high voltages that the

hysteresis check failed the data had to be discarded.

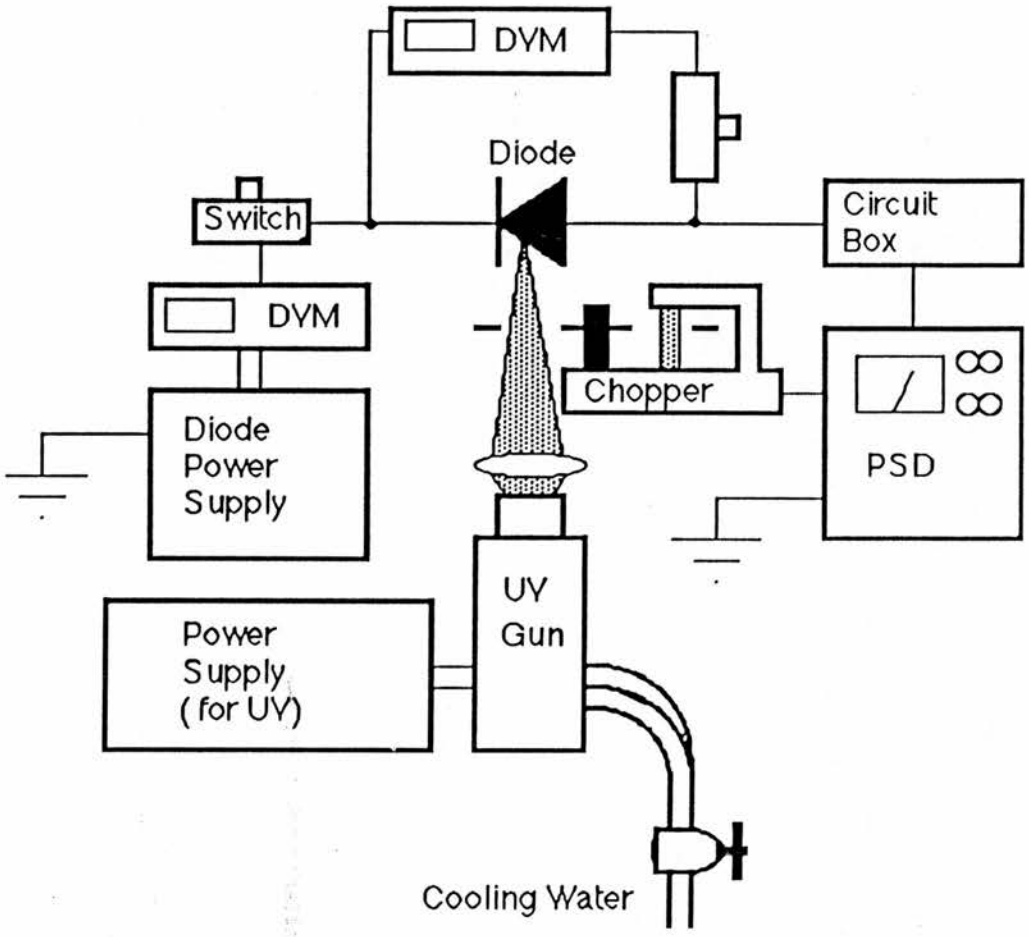

(The circuit box contains a sampling circuit such as was shown at the bottom of page 39).

(5) Results.

The photocurrent measuring system was tested using a yellow light emitting diode. These are weakly photoconductive in reverse bias and are made of pure materials with quite high dielectric strength. It was thus expected that the photocurrent-voltage curve for such a diode would be essentially flat. This provided a check against system anomalies producing multiplication-like features. The result is shown below on a similar scale to that of the ionisation results which appear later.

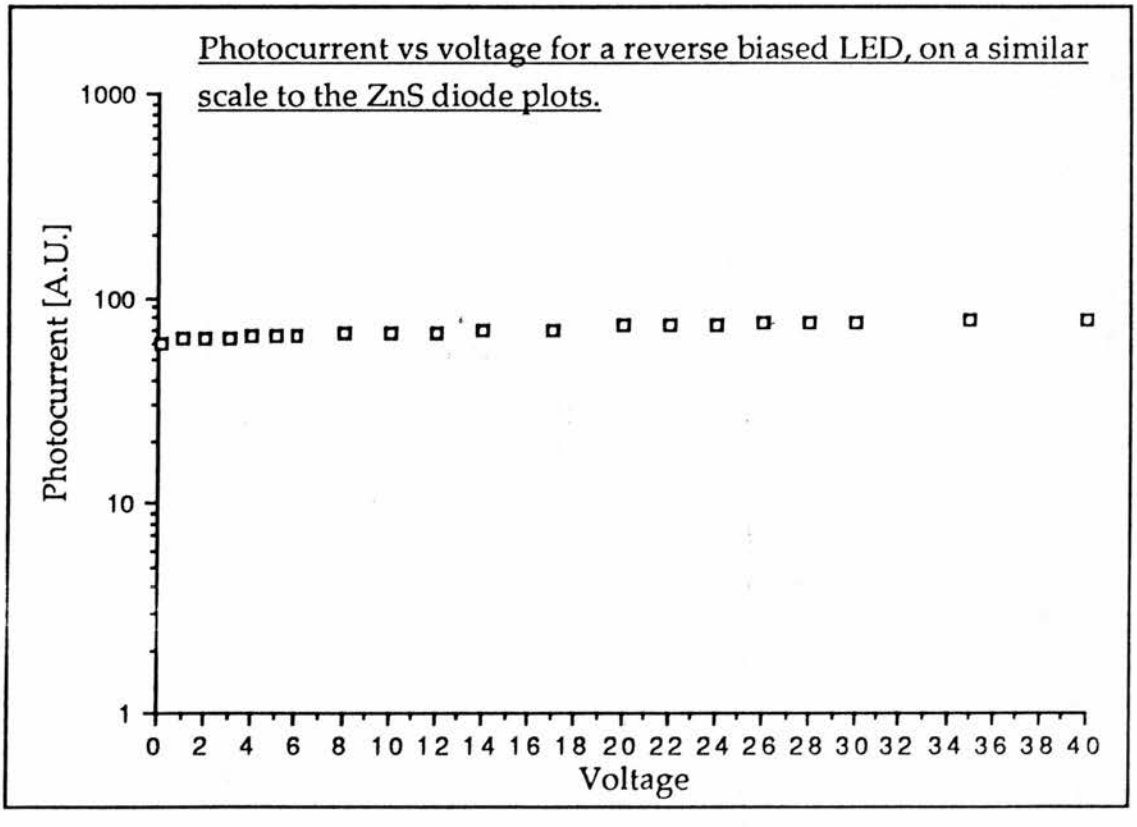

The variation of photocurrent with maximum junction field for diodes from two source materials is shown in the graph below. Breakdown noise often causes problems at these high fields, this coupled with the contact deterioration as current flows makes obtaining such curves difficult. The curves shown below are of typical shape but have better than average noise levels. The validity of the high field data was tested by going back to a field in the plateau region after each higher voltage measurement to check the photocurrent was the same. The last data point shown represents a contact deterioration of less than 5% as measured by this method. Complete contact destruction usually occurs at fields above $2.3 \times 10^6 Vcm^{-1}$, due to the large current flow.

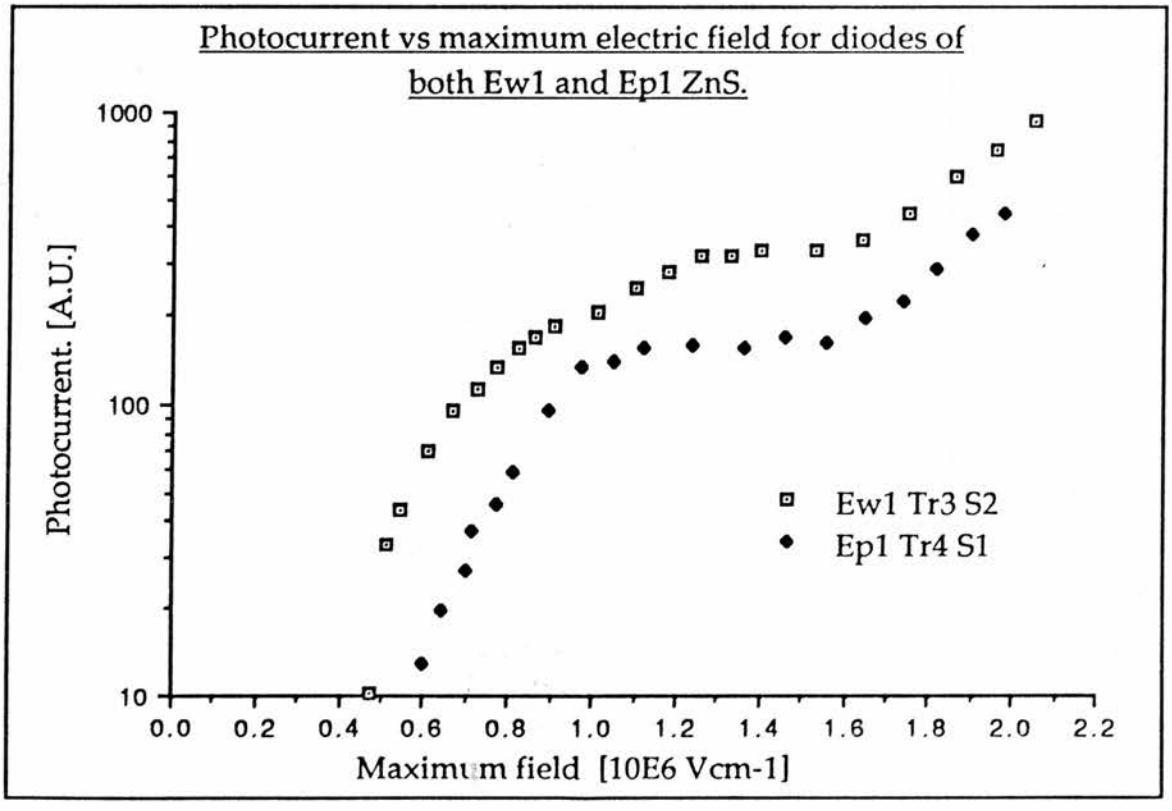

One of the diodes that was produced had a sufficiently high donor density to enable us to reach band-to-band ionisation fields without using visible light to raise $N_{d(effective)}$. This was used to test whether the shape of the curve is affected by the visible components. The UV gun was focused into a monochromator set at 300nm (10nm bandwidth) to isolate the 298nm mercury line. The change in capacitance when this light was shone on the diode was less than 10% compared to 200-500% with the unfiltered light. The only problem with this method was the reduction in signal level. At very high fields hot spots form in the junction and produce a large amount of noise. If the photocurrent is smaller the signal to noise ratio is much worse. The extent of the jitter present on the signal is indicated by the error bars.

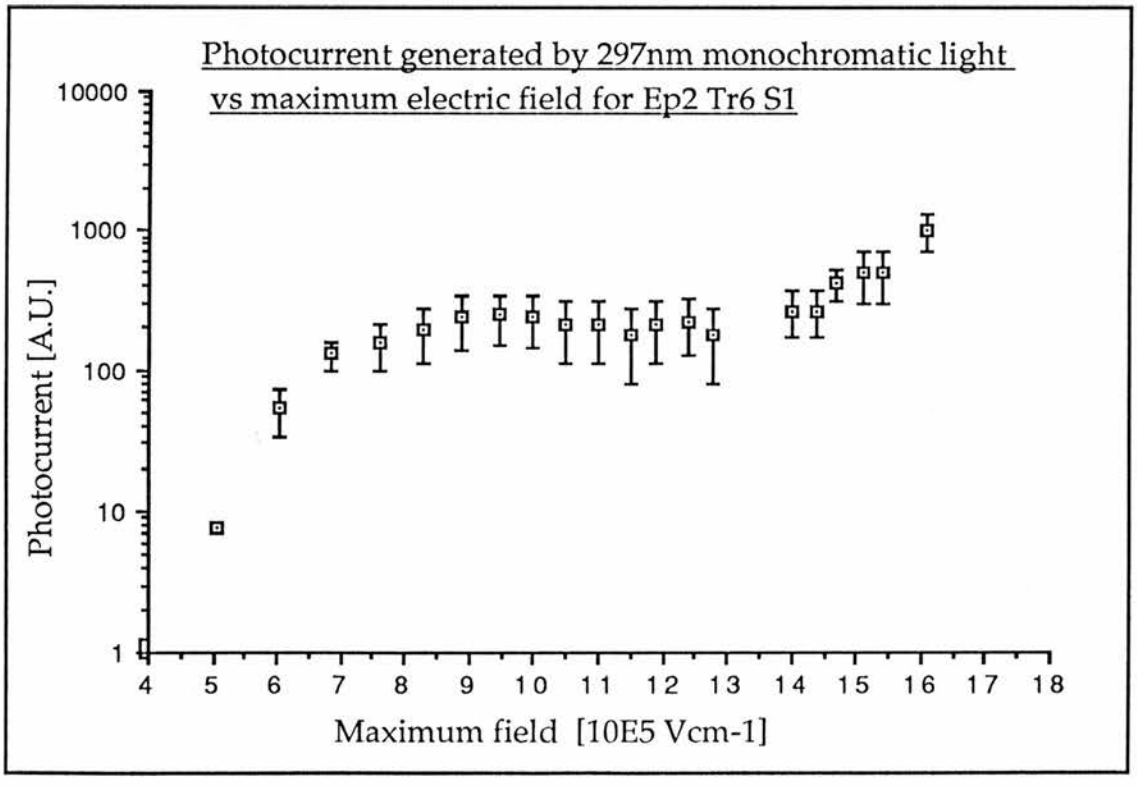

Some high field multiplication results are shown below on a linear scale again for diodes of different source material.

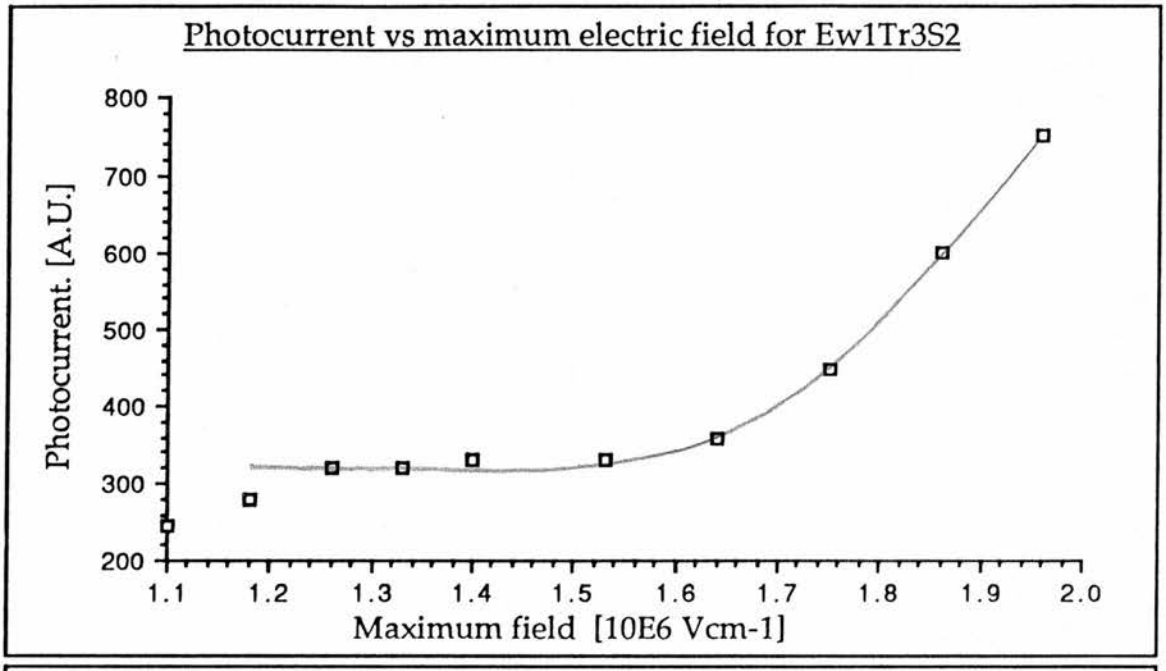

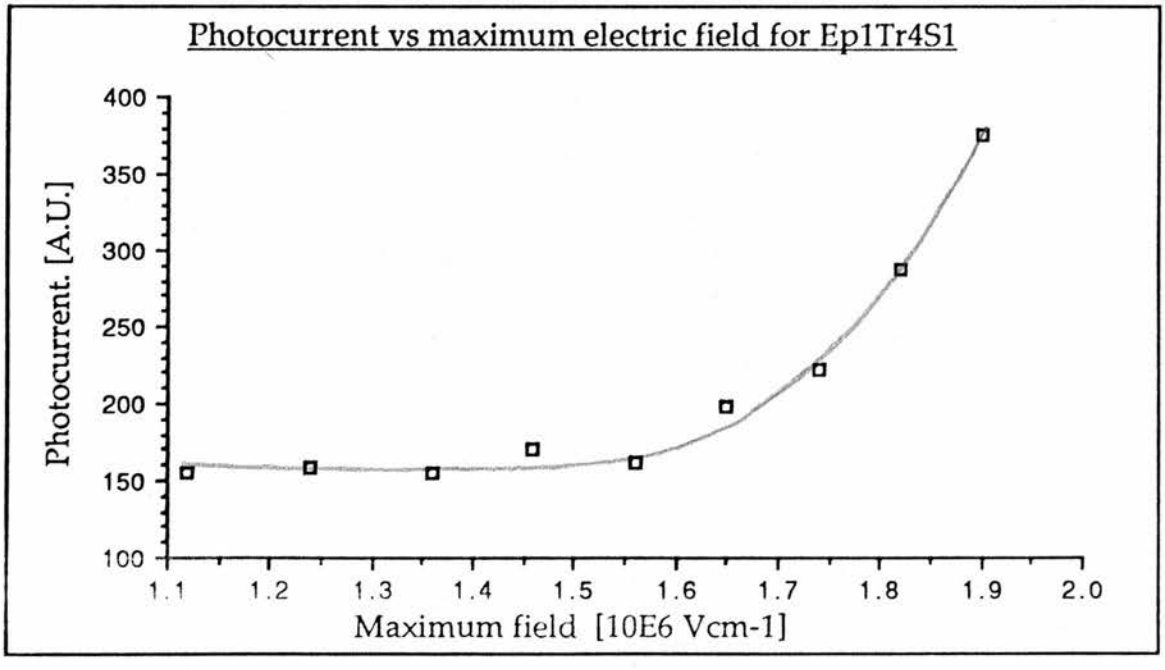

Below is an equivalent multiplication plot to those on the previous page except that the photocurrent was induced by hard ultraviolet light only. There are thus no ionised deep centres in this diode and $N_{d(dark)} = N_{d(effective)}$. The shape of the curve is the same as the others and the breakdown field is the same as that for the same diode measured using a mixed excitation light. The error bars are simply an indication of the noise observed on the photocurrent signal when the light intensity is reduced by using a monochromator.

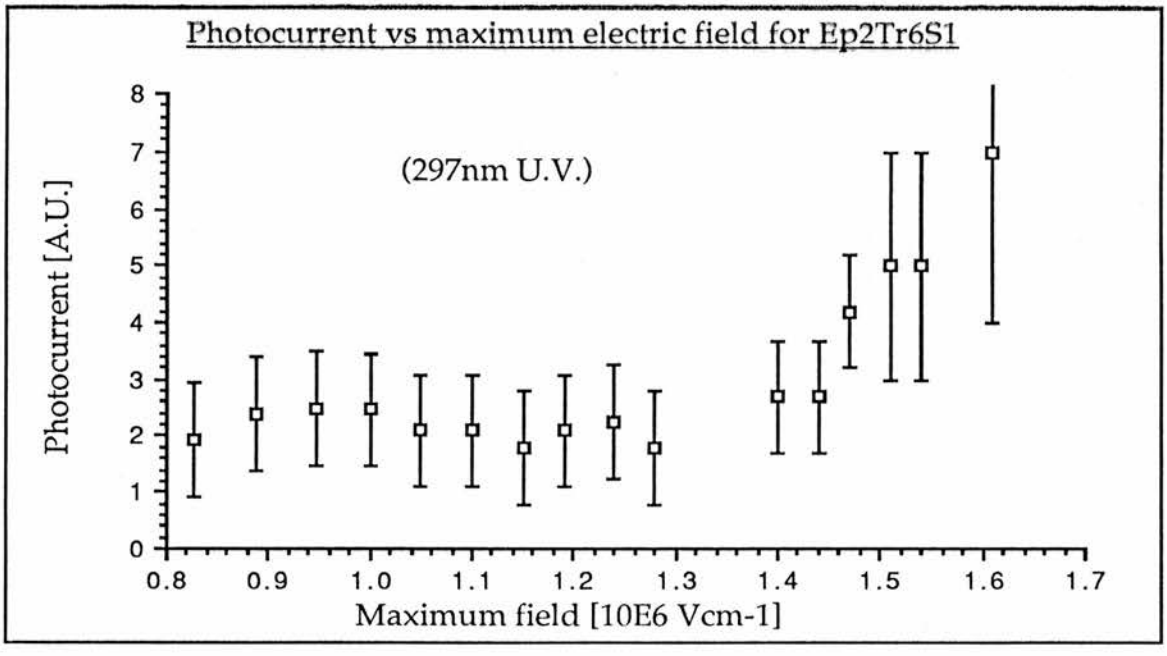

From the multiplication factor M it is possible via an iterative process to find $\alpha(E)$ as described by Moll[15] and outlined below.

(1) M is deduced from the ratio of the photocurrent at a given field to that before multiplication. (In this case the pre- band-to-band plateau is the sensible choice of a unity multiplication level). In the case of data

with considerable scatter M is taken from a smooth curve drawn through the photocurrent points.

(2) [1-1/M] is tabulated from M and appropriate values of the maximum junction field and depletion region width (calculated from N_d) and voltage are entered alongside each point.

(3) α is calculated from,

$$\alpha = [1\text{-}1/M] / W_{(effective)}$$

Initially the width is taken as the junction width.

(4) A first value for "b" is obtained from a plot of $Log_e\alpha$ against 1/E

(5) This value of "b" is used to calculate the ratio of $W_{(junction)}$ to $W_{(effective)}$. A graph of the theoretical variation of $W/W_{(eff)}$ against b/E is provided by Moll [15]

(6) The new values of width are used in (3)&(4) to get the next value of "b" which in turn is used to generate a new set of values for $W/W_{(eff)}$.

If logα is plotted against 1/E the gradient of the line gives the ionisation parameter "b". Such a plot is shown below for both vapour and melt grown material.

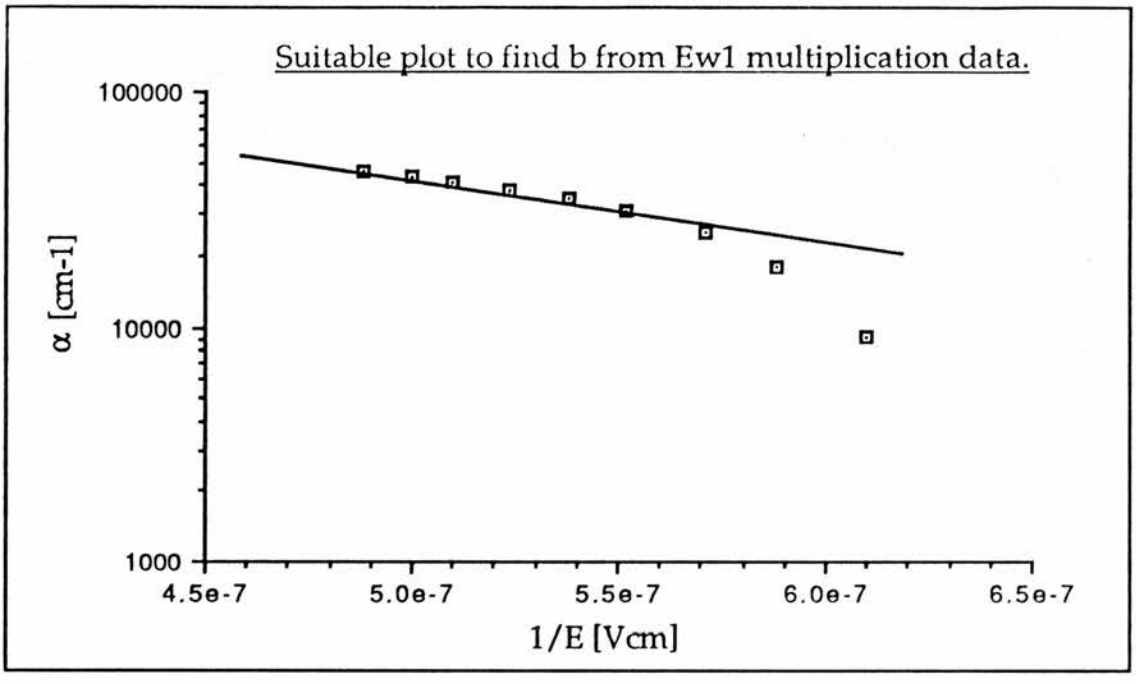

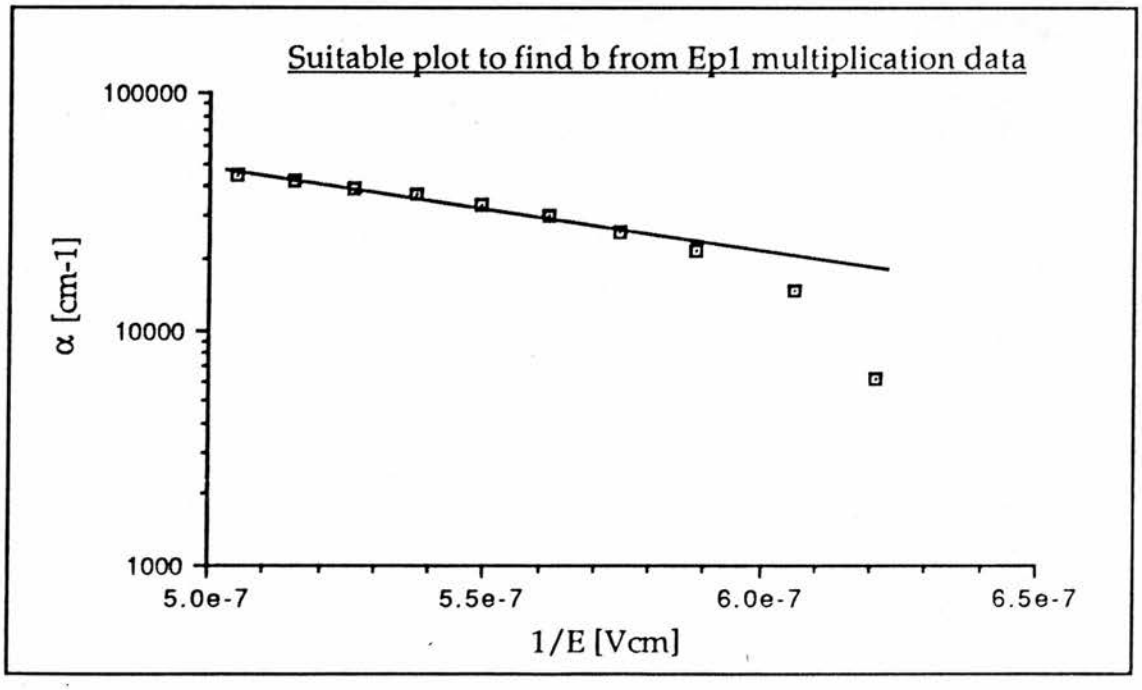

(6) Discussion.

The capacitance^{-2}-voltage plots were straight lines indicating a uniform distribution of donors over the surface region of the ZnS. Donor densities in the range 10^{16} to 10^{17} cm^{-3} (in darkness) were achieved with the conductivity treatment. If one assumes an electron mobility of 150cm^{2}V^{-1}s^{-1} at room temperature[24] the material has resistivity of 0.8 to 8 Ωcm^{-1} when all these donors are ionised. This is comparable to values achieved by other workers using slight variations on this conductivity treatment. For example Katayama[19] achieved 10-100Ωcm and Lukyanchikova[20] claims 1-10Ωcm as typical. The conductivity process is not well understood at present. Some workers eg.[20] quote aluminium as the shallow donor in ZnS(n). However, the situation is considerably more complex than simple substitutional doping because the aluminium forms complexes with native lattice defects and other impurities (Kukimoto[25]). In a crystal with 10^{16}cm^{-3} shallow donors chemical analysis might typically be expected to reveal ~10^{19}cm^{-3} aluminium atoms indicating the extent of the complex formation.

The value of $N_{d(effective)}$ was considerably higher when the material was illuminated than the dark value. The straight line (capacitance)$^{-2}$-voltage plots also indicate that the junctions are reasonably well behaved and that the usual theories regarding field distributions in Schottky diodes may be applied with confidence.

The increase in the number of ionised donors with illumination is in one sense at least a useful effect, in that it reduces the voltage that need be

applied in order to achieve a given field. However great care must be taken to perform the capacitance-voltage run under identical illumination conditions to the photocurrent measurements in order that the field may be known accurately. Failure to take this precaution can easily lead to an error in field of >200%.

The photocurrent vs voltage curve for the light emitting diode is essentially flat over a wide range of voltages. The signal was recorded at higher intensities as well to ensure this curve was not the result of saturation. Thus we can see that there are no major system anomalies and that we may be confident of our results.

The most striking feature of the photocurrent-field curves is the steep initial rise. The fields at which this occurs are rather small for the process to be band-to-band ionisation. Furthermore the effect appears to saturate at higher fields which would be very surprising behaviour for a band-to-band avalanche process. Various experiments including measurements of the linearity of the effect with light intensity and fits to theoretical curves have lead us to believe this is due to an impurity ionisation process. Such a process was described by Livingstone & Allen[26] for ZnSe diodes and is used by Petroff et.al.[27] in smaller gap materials to make a solid state photomultiplier. The impurity ionisation process is discussed fully in the next chapter. For the purposes of this chapter it is only the high field portion of the curve which is of interest.

The separate plots of photocurrent against field on linear scales look very much like those expected for a breakdown process. The field at which this occurs varies a little from sample to sample but is generally within the

range 1.4 to $1.7x10^6 Vcm^{-1}$. The small variation is probably due to different concentrations of impurities altering scattering behaviour. Measurements on thin film electroluminescent devices[28][29] indicate that the threshold of operation is around $1.3x10^6 Vcm^{-1}$. The small difference between this breakdown in electroluminescent devices and that in diodes is probably due to non-uniform field distribution within the devices. This means that measurements on thin films can only set a lower limit on the breakdown field. In a later chapter photocurrent vs field results are presented for evaporated thin films of ZnS and it is shown that the breakdown process begins at 0.9 to $1.1x10^6 Vcm^{-1}$.This is compatible with observations of thin film light emission thresholds[28][29] since significant current flow and thus light emission might only occur a little beyond the ionisation threshold when M is large.

When determining the ionisation parameter "b", it is desirable to make measurements over as many values of M as possible to maximise accuracy and investigate the nature of the rise. In most materials this presents little problem as current flow is minimal at fields below that required for band-to-band ionisation. However in our samples of ZnS there was an additional ionisation process occurring at lower fields than the band to band. Fortunately this impurity ionisation process saturates before band to band begins in most samples enabling us to measure M. However the small dark current leak from the Schottky contact (which is not ideal) is multiplied as well leading to a very large leakage current ($\sim 1.0 Acm^{-2}$) at the highest fields. When the band-to-band ionisation occurs the situation becomes even worse with the further multiplication

of the dark current. It is very difficult to obtain good reproducible data for M under these conditions because as discussed previously the contacts are of limited durability. Any non-reproducible value of M is of course unusable. This has restricted us to measuring only the lower values of M up to around 3 or 4. Shining visible light on the diodes appears to make the current leakage worse. This is believed to be due to impurity photoconduction in the oxide layer. With hard ultra-violet light multiplications up to around 6 were observable but the scatter was too bad to gain much useful information from these curves.

The number of iterations required to maximise the accuracy of the value of "b" depends to a large extent on the original data quality. Repeated iterations with poor data will not lead to a more accurate determination. In the case of our data three or four iterations were used.

The plots of Log α against 1/E are good straight lines for the majority of the data points suggesting that the behaviour is similar to that of the smaller gap semiconductors. However the first couple of low field points seem to show a much steeper rise. This could simply be due to the large errors involved in finding [1-1/M] when M is close to unity. There is of course some ambiguity in defining the unity level within the experimental scatter. This is of little importance at large values of M but could distort the first couple of measurements considerably. It is however interesting to note that Howard[30] had to assume α(E) had this form, ie. a steep initial rise followed by $\alpha_o \exp(-b/E)$ behaviour in order to model memory effects in ZnS thin film displays.

There is a small scatter in the value of 'b" obtained from various samples, (probably simply due to experimental error) but in general we can say that the value of the ionisation parameter for ZnS is,

$$1.3\ (+/-)\ 0.3 \times 10^7\ Vcm^{-1}.$$

To our knowledge this is the first time such a measurement has been made for ZnS. (The principal difficulties in the past have been the production of good contacts on a piece of ZnS with a well-defined field structure and overcoming contact destruction due to excessive dark current flow at high fields.)

Livingstone and Allen[7] pointed out that there is a trend amongst the tetrahedral semiconductors for b to increase with increasing energy gap. The figure overleaf shows how our data for ZnS fit the trend and also how the very large value of b for SiO_2[31] does not appear so strange considering the large energy gap of this material. This straight line fit must of course break down for the lower energy gap materials such as InAs since the log b scale has no zero. Andreev et.al.[32] have measured the ionisation parameter "b" for solid solutions of $InAs_{1-X}Sb_X$ over the field regions where their data fit the relation,

$$\alpha = \alpha_0 \exp(-b/E).$$

This point on the plot illustrates this inevitable low gap deviation.

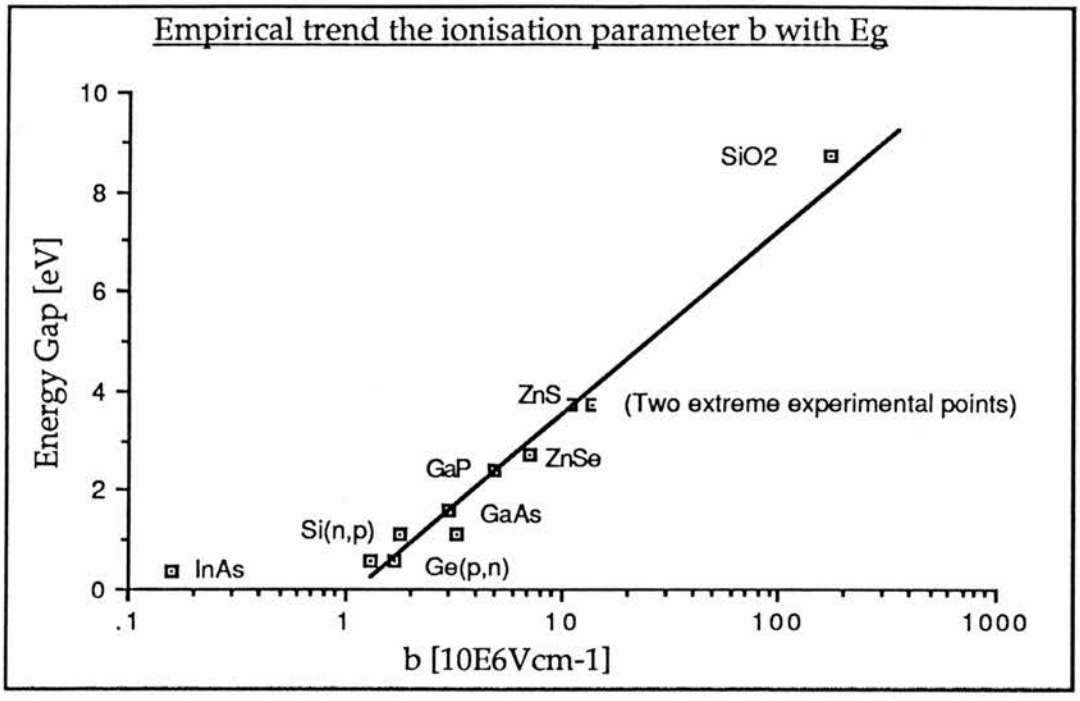

During this work we have only considered ionisation processes initiated by electrons. It is impossible to study processes initiated by holes at high fields in n-type Schottky diode because the forward bias would produce an unmanageable dark current.

(7) Concluding remarks.

We have shown that band-to-band impact ionisation in ZnS is in general, a similar process to that which occurs in other tetrahedral semiconductors, and as such need not be treated as a special case. It however, is possible that the onset of the multiplication is slightly more rapid than conventional theory would suggest, and this may be related to memory effects in thin film devices. We have calculated the band-to-band ionisation parameter for ZnS as,

$$1.3\ (\pm 0.3)\ x10^{7} Vcm^{-1}.$$

This is to our knowledge the first time this quantity has been measured. Finally, we may conclude that at the operating fields of most thin film electroluminescent devices band-to-band impact ionisation will occur. This means that a large number of holes will be generated within these devices.

Chapter 3

Hot electron effects in ZnS.

(1)Introduction.

The behaviour of hot electrons with energies >1eV in ZnS and ZnSe is of considerable interest from both a theoretical and technological view point. For example Inoguchi[3] type high field electroluminescent displays are gaining popularity due to their flat structure and large area. The emission from such devices is believed to involve the impact excitation of the manganese luminescent centre in ZnS by hot electrons, (Mach & Müller[5]). Much however remains unclear about the operation of these devices, particularly the electric fields at which various effects occur and the relation of the light emission to band-to-band impact ionisation and other high field processes.

ZnS is a particularly good material for the study of hot electron processes because of its large band-gap (3.7eV at room temperature) and the availability of comparatively large single crystals. There are however problems, the making of electrical contacts being at a more primitive state of technology than in GaAs for example, and the n-type doping process is not completely understood.

The behaviour of hot electrons in ZnS and ZnSe has previously been studied to some extent. For example, Rigby and Allen[10] have investigated light emission from hot electron transitions within the conduction band of ZnS, and from this derived information about the hot electron energy distribution. Turvey and Allen[33] have done similar work on ZnSe. Gordon[34], from measurements of the quantum efficiency of ZnS:Mn and ZnSe:Mn diodes, has also obtained some information

about the behaviour of hot electrons in these materials. Livingstone[26][35] has observed a two stage impurity ionisation process in ZnSe:Mn and ZnSe:Cu diodes. A hot electron impact ionises an impurity deep in the energy gap to produce a new conduction electron. Another hot electron may then impact ionise a valence electron into the resulting empty centre. Under favourable circumstances this can lead to an avalanche process.

We have measured the photocurrent as a function of electric field in ZnS Schottky diodes and found evidence of a similar two stage impurity ionisation process. We have been able to compare the field dependence of this ionisation process to the variation of the quantum efficiency of the manganese electroluminescence, by performing both types of experiment on the same sample. Ionisation measurements made on a diode from the same batch as those used by Rigby and Allen[10] have enabled us, by comparison to their emission data, to substantiate their ideas about the behaviour of hot electrons in ZnS at very high fields. Because, as far as possible, the various experiments were carried out on the same diodes the relationship of the different processes to electric field may be compared with confidence.

Photocapacitance measurements were made on the ZnS diodes, and these revealed a large concentration of deep neutral centres at ~2.2eV below the conduction band. We believe that these centres are responsible for the impurity ionisation mechanism.

Bryant et.al.[11] and Jiaqi et.al.[38] have studied the relative intensity of

the electroluminescence emission of manganese and rare earth centres as a function of applied voltage, in ion-implanted ZnS diodes and thin films. From this work Bryant and his co-workers have suggested that the hot electron distribution in ZnS is Maxwell-Boltzmann[47][51][48] and more recently, Druyvesteyn[37][49]. In either case they believe the hot electrons become significantly more energetic as the field increases. However, Rigby & Allen[10] have produced evidence which shows that this is not so at fields in the region 0.7 to $1.4 \times 10^{6} V cm^{-1}$. Because the ion-implantation process produces a high density of defect centres, we believe that an impurity ionisation mechanism will be present in ion-implanted diodes. We are able to offer an alternative interpretation to the results of Bryant and Jiaqi, based on this impurity ionisation, which is consistent with all the experimental evidence that is available.

(2) Theory of the two stage impurity ionisation mechanism.

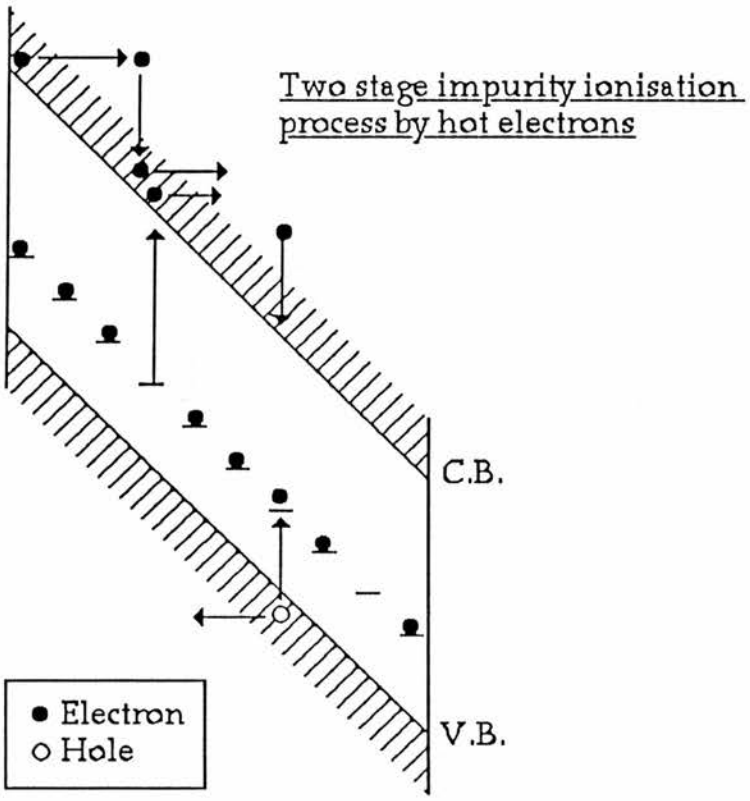

In the previous chapter "Band-to-band ionisation" we considered the theoretical model of the ionisation of a host lattice atom by a hot electron. In this section a theoretical model of impurity ionisation (originally proposed by Livingstone & Allen[26]) is outlined. The initial assumptions made are a little different to those for band-to-band ionisation.

Namely,

(1). Ionisation is caused only by electrons.

(2). The field in the junction is constant.

Four processes are considered, these are illustrated by the diagram overleaf. 1 & 2 are ionisation by hot electrons, 3 & 4 are recombinations.

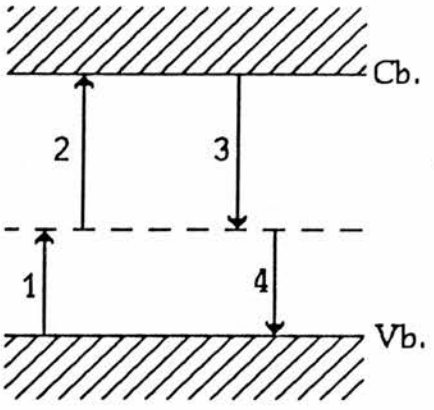

The following symbols are adopted,

N_t	Concentration of deep centres.
n_t	Concentration of electrons on the deep centres.
n,p	Concentration of free carriers. (electrons and holes respectively).
σ	Effective cross-section
v	Carrier velocity.

The general form of a rate equation is,

$$\text{Rate} = v\sigma n N_t. \tag{1}$$

In steady state the population of the centres is constant, so that the total number of electrons entering the centres must equal the total number leaving.

The corresponding rate equation is,

$$n\sigma_1 v_n(N_t-n_t) + n\sigma_3 v_n(N_t-n_t) = n\sigma_2 v_n n_t + p\sigma_4 v_p n_t . \tag{2}$$

Process —— 1 —— —— 3 —— —— 2 —— —— 4 ——

If (2) is expanded and rearranged, one has,

$$n/N_t = (\sigma_1 + \sigma_3) / (\sigma_1 + \sigma_2 + \sigma_3 + \sigma_4 [pv_p/nv_n]) . \quad (3)$$

This is an expression for the number of ionised centres, but it is inconvenient because it involves v_p and p. However, from current continuity, we have,

$$I = I_n + I_p = nev_n + pev_p . \quad (4)$$

(4) can be rearranged to give,

$$[p v_p / n v_n] = [I / I_n] - 1 . \quad (5)$$

We can substitute (5) into (3) to give,

$$\frac{n_t}{N_t} = \frac{\sigma_1+\sigma_3}{\sigma_1+\sigma_2+\sigma_3-\sigma_4+\sigma_4 I/I_n} . \quad (6)$$

We now have, in the form of (6), a convenient expression for the proportion of the deep centres which are occupied.

We now consider the net generation rate of conduction electrons. If the rate of electrons entering the centres is the same as that for electrons leaving, as one would expect in steady state, the rate of generation of conduction electrons g is simply,

$$g = \text{Rate 2} - \text{Rate 3} \quad (7)$$

$$\Rightarrow \quad g = n \sigma_2 v_n n_t - n \sigma_3 v_n (N_t - n_t) \quad (8)$$

We now consider the continuity equation,

$$dn/dt = g - (1/e) \nabla . J_n . \quad (9)$$

In steady state dn/dt = 0. That is, although multiplication may be occurring, the current at a particular field is not time dependent. In addition to this, at the high fields we are considering ($\geq 10^4$ Vcm-1) the mobility relation $v = \mu |E|$, no longer holds. Since the field is constant, the velocity of the electrons is also assumed to be constant across the high field region. This leads to a simplification of the continuity equation.

$$dn/dx = g/v_n. \tag{10}$$

We can substitute for g from (8) into (10), and after rearranging we have,

$$g / (v_n n N_t) = \sigma_2 (n_t / N_t) - \sigma_3 + \sigma_3 (n_t / N_t) . \tag{11}$$

We can substitute an expression for n_t/N_t (the proportion of empty centres), from (6) into (11), and after rearrangement we have,

$$g/v_n = n N_t \left[\frac{\sigma_1\sigma_2+\sigma_3\sigma_4 - \sigma_3\sigma_4 I/I_n}{\sigma_1+\sigma_2+\sigma_3-\sigma_4+ \sigma_4 I/I_n} \right] . \tag{12}$$

By comparison to (10) we can equate (12) to dn/dx, so that,

$$dn/dx = n N_t \left[\frac{\sigma_1\sigma_2+\sigma_3\sigma_4 - \sigma_3\sigma_4 I/I_n}{\sigma_1+\sigma_2+\sigma_3-\sigma_4+ \sigma_4 I/I_n} \right] . \tag{13}$$

Since $I_n = nev_n$, we have in effect a differential equation for n(x). It is convenient at this stage to let,

$$A = N_t (\sigma_1 \sigma_2 + \sigma_3 \sigma_4), \; B = (N_t \sigma_3 \sigma_4 I) / e v_n ,$$

$$C = (\sigma_1 + \sigma_2 + \sigma_3 + \sigma_4) \text{ and } D = (\sigma_4 I / e v_n) .$$

(13) may then be integrated as,

$$\int dx = \int \frac{(Cn + D)\, dn}{(An^2 - Bn)} \quad . \tag{14}$$

If we let $\alpha = -D/B$ and $\beta = C - \alpha A$, then (14) may be integrated by partial fractions to give,

$$[x] = [\, \alpha \log_e n + \beta/\alpha \log_e | An - B | \,] . \tag{15}$$

The appropriate limits for (15) are, x = 0 to x = W (the width of the high field region) and for n, I_0 / ev_n at x = 0 to MI_0 / ev_n at x = W. This gives us,

$$\alpha \operatorname{Log}_e M + (\beta/\alpha) \operatorname{Log}_e \left| \frac{AMI_0/ev_n - B}{AI_0/ev_n - B} \right| = W \ . \tag{16}$$

Now $I = MI_0$, so that once the original notation has been substituted for A, and B the modulus (| |) part of (16) can be written as,

$$| \, | = M [\, 1 + (1 - M)(\sigma_3 \sigma_4 / \sigma_1 \sigma_2)] \ .$$

(16) can thus be written in the form,

$$\alpha \operatorname{Log}_e M + \left[\frac{C}{A} - \alpha \right] \left[\operatorname{Log}_e M - \operatorname{Log}_e \left| \frac{1 + \sigma_3 \sigma_4 (1 - M)}{\sigma_1 \sigma_2} \right| \right] = W. \tag{17}$$

$$\frac{C}{A} \operatorname{Log}_e M - \left[\frac{C}{A} - \alpha \right] \operatorname{Log}_e \left| \frac{1 + \sigma_3 \sigma_4 (1 - M)}{\sigma_1 \sigma_2} \right| = W. \tag{18}$$

The original notation can now be substituted for α,C and A in (18),

$$\Rightarrow N_t W = \frac{(\sigma_1+\sigma_2+\sigma_3-\sigma_4)}{(\sigma_1\sigma_2+\sigma_3\sigma_4)} \text{Log}_e M \pm \left[\frac{\sigma_1+\sigma_2+\sigma_3-\sigma_4}{\sigma_1\sigma_2+\sigma_3\sigma_4} - \frac{1}{\sigma_3}\right] \text{Log}_e \left|1+\frac{\sigma_3\sigma_4(1-M)}{\sigma_1\sigma_2}\right| \quad (19)$$

This is too complex to compare with experimental results. However, if the carrier velocities are high in the high field region, recombination will not be a strong effect. We can follow the analysis through for a system with only two transitions as is shown below.

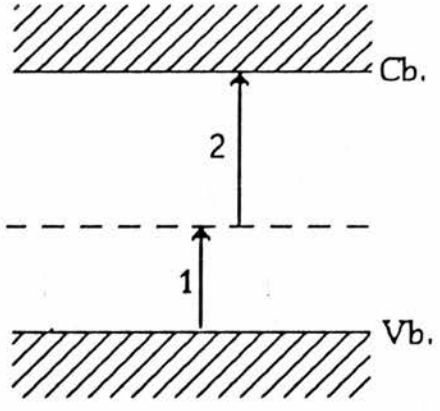

As in the previous case, in steady state the rate of carriers entering the centres must equal that leaving so that,

$$\sigma_1 \, n \, v_n \, (N_t - n_t) = \sigma_2 \, n \, v_n \, n_t \, . \quad (1a)$$

The number of occupied centres (n_t / N_t) is,

$$n_t / N_t = (\sigma_1 / [\sigma_1 + \sigma_2]) \, . \quad (2a)$$

The net generation rate of electrons is simply the number leaving the

centres,

$$g = n \sigma_2 v_n n_t = dn/dt \ . \qquad (3a)$$

The continuity equation remains unchanged,

$$dn/dx = g/v_n. \qquad (4a)$$

Substitution of (3a) into (4a) gives,

$$dn/dx = n \sigma_2 n_t \ . \qquad (5a)$$

We have an expression for n_t from (2a), substitution of this into (5a) gives,

$$dn/dx = (n N_t \sigma_1 \sigma_2 / [\sigma_1 + \sigma_2]) \ . \qquad (6a)$$

This can easily be integrated to give,

$$[\mathrm{Log_e}\, n] = [\ x N_t \sigma_1 \sigma_2 \ / \{ \sigma_1 + \sigma_2 \} \ ] \ . \qquad (7a)$$

The appropriate limits for this integral are x = 0 to x = W and the limits for n are n(0) and n(W). Since M = n(W)/n(0) This gives us an expression for M,

$$M = \exp [N_t \sigma_1 \sigma_2 / (\sigma_1 + \sigma_2)] \ . \qquad (8a)$$

If one of the cross-sections σ1, σ2 is much larger than the other, we can write a simple expression for M,

$$M = \exp (N_t W \sigma) \ . \qquad (9a)$$

(3)Experimental methods.

(3.1)Measurement of photocurrent and the making of contacts.

In outline

Mechanically chopped light from a Hanovia UV-100 ultraviolet lamp was used to generate a photocurrent in a reverse biased diode. The magnitude of this photocurrent as a function of applied bias voltage was measured on a P.S.D. A more detailed description of the experimental arrangement for photocurrent measurement can be found in the chapter "Band-to-band impact ionisation in ZnS". For low fields, electrolytic as well as metal contacts were employed. The light source used with the electrolytic contacts was a soft ultraviolet lamp (~360nm peak).

[During the course of this work several light sources were tried in addition to the ones mentioned above. Namely; 300nm ultraviolet alone, 300nm ultraviolet with DC blue light and ultraviolet/visible mixture. Although there are changes in the effective donor density (already discussed in the chapter "Band-to-band impact ionisation") these experiments produced the same photocurrent vs field characteristics as those using the Hanovia lamp and the 360nm lamp.]

(3.1a)The electrolytic contact on ZnS.

Hydrochloric acid in 10% aqueous solution was chosen as the electrolyte. The structure of a typical hydrochloric acid electrolytic contact is shown in the diagrams overleaf. The large area acid back contact serves the same purpose as the aluminium overcoating on the metal based Schottky diodes. That is it provides a large capacitance so that for the

1MHz signal used in the capacitance-voltage experiments the back contact is essentially a short circuit. The indium dots have finite contact resistance (100Ω to 10kΩ) which although very much less than the DC depletion region resistance presents an impedance comparable to that of the front contact capacitance at 1 MHz.)

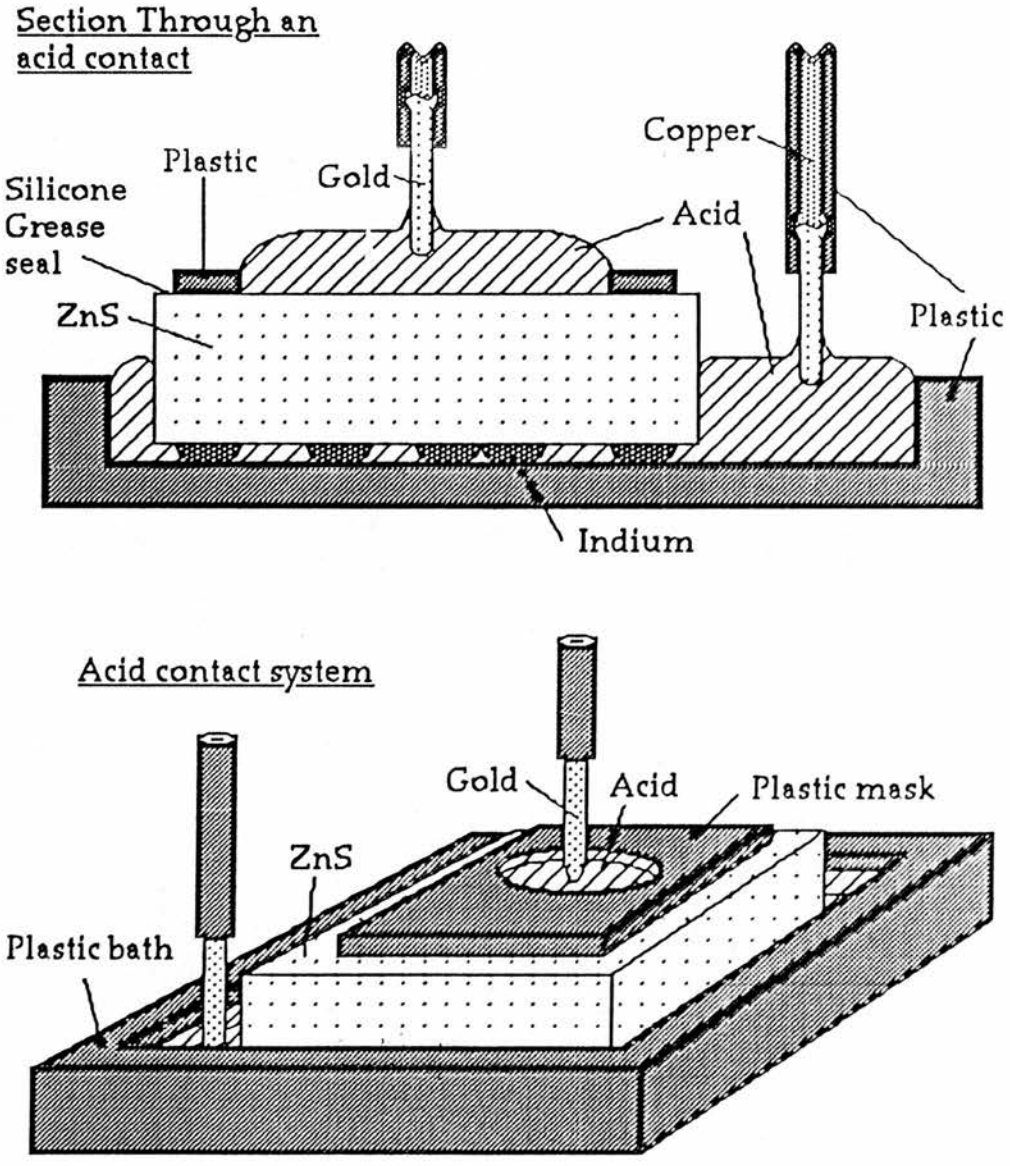

Electrolytic contacts have in general very much better electrical

characteristics than metal ones because the acid is constantly re-etching the surface and removing oxide. The disadvantage of such contacts is poor durability at higher voltages, due to electrolysis. Even current densities as low as $5mAcm^{-1}$ produce intolerable surface damage and gas bubbles. Gas bubbles are an acute problem because they cling to the crystal and reduce the effective surface area of the contact. This reduction in area invalidates the photocurrent data. It is electrolysis that limits the maximum bias voltage and consequently the maximum junction fields which can be achieved when using acid contacts.

One further potential problem exists with electrolytic contacts on wide gap materials such as ZnS. In order to produce electron hole pairs by excitation across the band gap one requires light with wavelength shorter than 335nm. Water (and consequently the acid solution) is opaque to such wavelengths. For this reason use of electrolytic contacts for photocurrent measurements on ZnS is only possible if there is an impurity photoconduction mechanism, so that light of lower photon energy than E_g can generate carriers. Fortunately such a mechanism was present in our samples.

(3.1b) Aluminium contacts on ZnS.

The experimental arrangement was the same as that for the acid contacts except that a semi-transparent aluminium Schottky contact was used, and the light source was a Hanovia UV-100 lamp instead of the softer 360nm lamp. With care it is possible to produce a mechanically sound aluminium contact with >50% transmission in the visible.

To investigate the possibility of any surface conduction effects contributing to the observed photocurrent characteristic, a guard ring was used in some cases. The guard ring increases the total contact area considerably and thus increases the leakage current. The consequent Joule heating makes guard rings impractical at very high fields. The observed characteristics remained unchanged when a guard ring was used. In view of this and the practical problems involved, the use of guard rings was abandoned.

(3.2) Photocapacitance studies of the deep levels within the band gap of ZnS.

(3.2a)Single beam method.

Semi-transparent Schottky contacts were made by evaporating aluminium onto an etched surface just as for the photocurrent measurements. The contacts made for this experiment were however considerably larger with diameters up to around 3mm. This was done in order to increase the sample capacitance and thus the sensitivity of the experiment. The capacitance was measured on a Wayne Kerr B601 capacitance bridge whilst a constant reverse bias of 10V was applied. The bridge was operated at 1MHz as this is optimum for sensitivity and is in the frequency regime where the capacitance is nondispersive. The DC bias and AC bridge signal were separated by a simple single pole filter based around a small inductor. The light source was a 150W tungsten-halogen lamp which was focused into a Bausch & Lomb high efficiency monochromator fitted with a 33-86-25-02 visible light grating. The

capacitance changes were so large that the bridge could be easily rebalanced each time the monochromator wavelength was changed. The sample capacitance was measured as a function of wavelength. The capacitance changes were slow and thus a considerable settling time had to be allowed between readings (1-10minutes). This is the princip al disadvantage of this method. It is also more than an experimental inconvenience because a capacitance change might be overlooked if it were very slow.

The resulting spectra were calibrated in terms of photon number by replacing the sample with the detector head of a U.D.T. flat spectral response silicon light meter.

(3.2b)Dual beam method.

The samples were prepared and mounted in the same way as for the single beam photocapacitance experiment and a reverse bias of 10V applied. However in this case two light sources were used. One was of fixed wavelength, and one was of variable wavelength. The fixed wavelength source was a tungsten/halogen lamp fitted with a Wratten 47B blue filter. This coupled with the naturally rapid fall off in spectral emission of such lamps in the violet gave a reasonably confined spectral range coupled with high intensity. The variable wavelength monochromatic light was produced by a second tungsten lamp focused through a Bausch & Lomb high efficiency monochromator fitted with a 33-86-25-02 visible light grating. Where necessary filters were also inserted to block second order light. This variable wavelength light beam could be interrupted by a mechanical shutter.

The Wayne-Kerr B-601 bridge was operated at 1MHz and a balance was set with the sample in situ and completely darkened. The off balance signal was monitored on a Farnell TM-2 AC millivoltmeter the output of which was linked to a chart recorder. The blue/violet pump light was switched on and the capacitance increased considerably. The offset null facility on the chart recorder was then used to centre the pen again. The sign of the capacitance changes could be determined from the direction of pen deflection. (The initial blue light can easily be observed to produce a positive change, so for example a decrease in the off-balance signal due to the monochromatic light represents a decrease in equilibrium capacitance). The experimental steps are shown diagrammatically below.

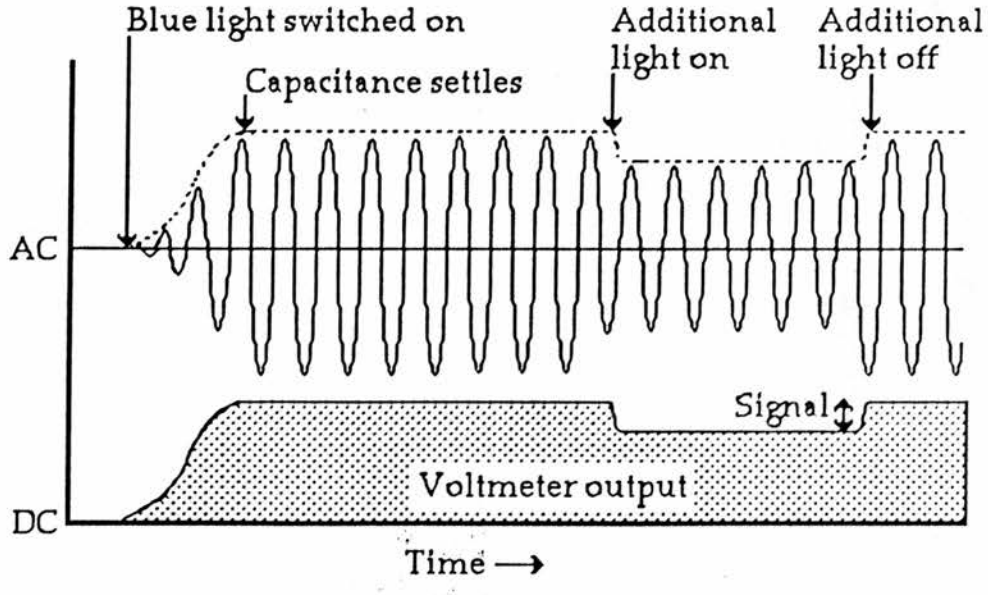

One advantage of this method is that the high photon flux (with energy $>E_g/2$) from the blue lamp produces rapid settling of the

capacitance when the much weaker monochromatic light is switched on or off.

The resulting spectra were calibrated in terms of normalised photon number by replacing the sample with a thermopile detector.

The monochromator bandwidth was measured using a low pressure mercury lamp and an interference filter to isolate the 546nm spectral line. A photomultiplier with an S-20 response was used as a detector.

(3.3)Optical absorption experiment.

The optical absorption of our ZnS samples was measured in the visible and near ultra-violet range. Samples were prepared with clean polished surfaces devoid of contacts and other optical obstructions. The experiments were carried out DC to avoid time dependencies. For the visible range a tungsten/halogen light source was used and for the near ultraviolet a high pressure mercury lamp. The detector was a U.D.T. silicon light meter. A spectrum of the light source alone was recorded and then the sample was inserted into the light path and the spectrum repeated. Subtraction of the two provides a measure of the absorption of the material. A prism monochromator was used for the longer wavelengths to avoid confusion with second order components, a grating was necessary in the ultra-violet. A diagram of the apparatus is shown overleaf.

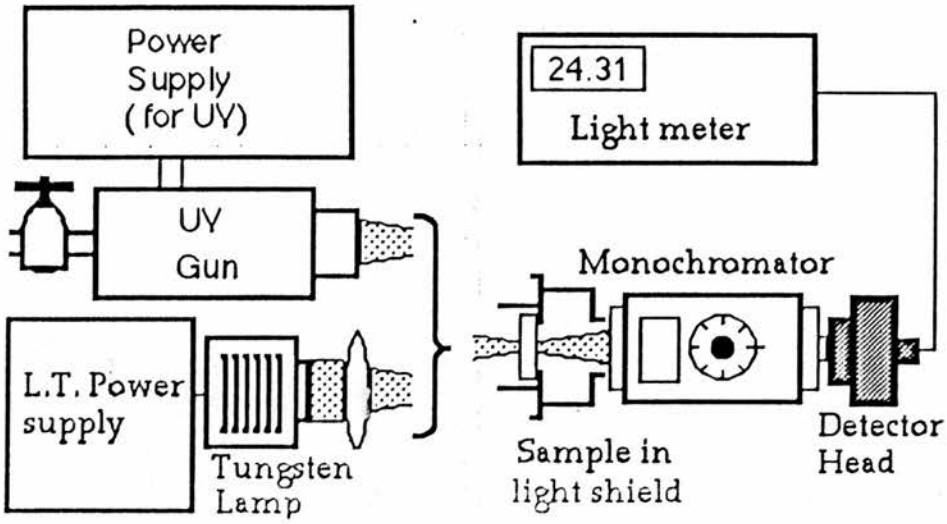

(3.4)Perturbation of ionisation.

We hoped that the photocapacitance and absorption experiments could be related to the ionisation measurements, by studying the perturbing effect of an additional monochromatic light, on the photocurrent in a diode biased into the impurity ionisation field region. In particular, the spectrum of such a perturbation can be compared to that of the photocapacitance spectrum, providing an indication as to whether or not the same centre is involved in both processes.

A Hanovia UV-100 ultraviolet gun was focused onto the diode contact to generate a large and stable photocurrent. An additional monochromatic light, produced by a tungsten/halogen lamp and a Bausch & Lomb high efficiency grating monochromator, was also focused onto the contact. The monochromatic beam was mechanically chopped so that the perturbation signal could be monitored on a PSD. The diagram overleaf shows the experimental arrangement.

Perturbation of photocurrent apparatus

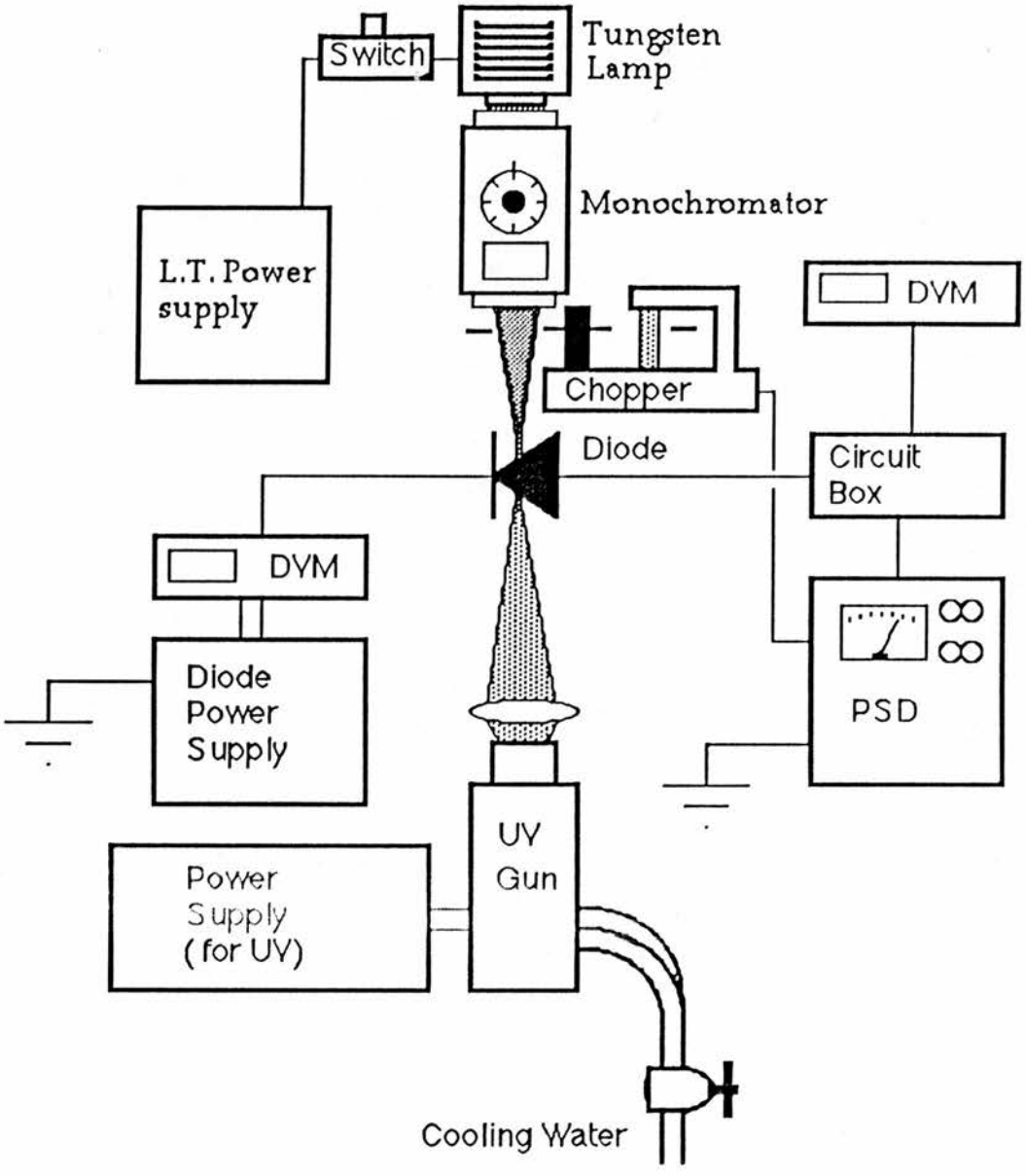

(3.5)Measurement of the quantum efficiency of a ZnS:Mn diode.

The emission spectrum of a diode fabricated out of the Ep2 (ZnS:Mn 0.5%) material was measured to ensure that the yellow manganese emission dominated the light output. This was found to be so and

consequently no optical filtering was necessary to isolate this emission during the quantum efficiency measurements.

The quantum efficiency measurements were made under pulsed field conditions because the diodes proved more stable than if driven DC. An Advance pulse generator was used to generate square voltage pulses which were applied to the diode. The current was measured with an oscilloscope and sampling resistor. The light emission was detected by a photomultiplier with an S-20 response, the signal from which was fed into a boxcar averager. The gate width was set to cover approximately the central 80% of the emission pulse. The boxcar thus gave an average value of the light emission based on many individual pulses.

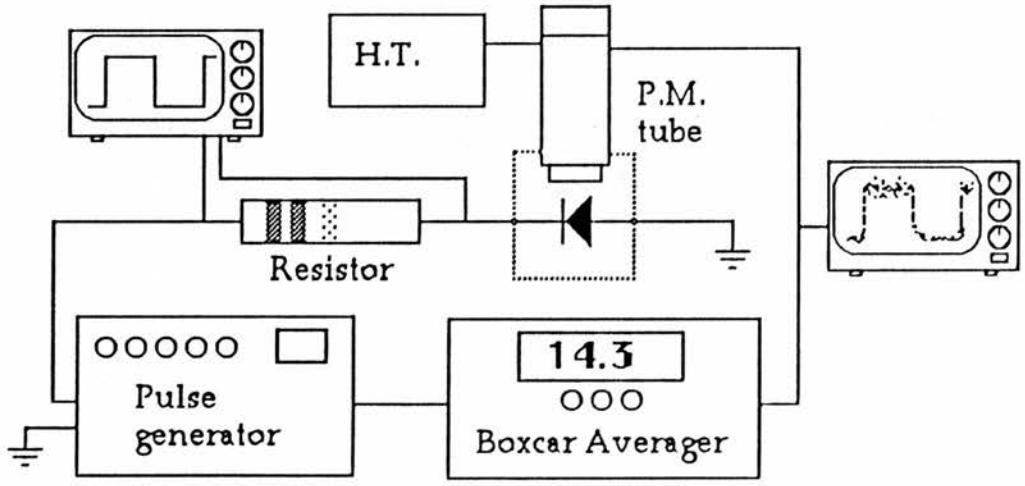

(4)Results.

(4.1) Contact performance and photocurrent measurement.

(4.1a) I-V characteristics of ZnS/Al and ZnS/HCl diodes.

A current voltage characteristic for a diode with one acid Schottky contact, and a multiple indium (immersed in acid) rear contact, similar to those described in "experimental methods" (3.1a), is shown in figure 1 (below).

Fig.1. A typical I-V curve with Acid/Acid&Indium contacts (See text)

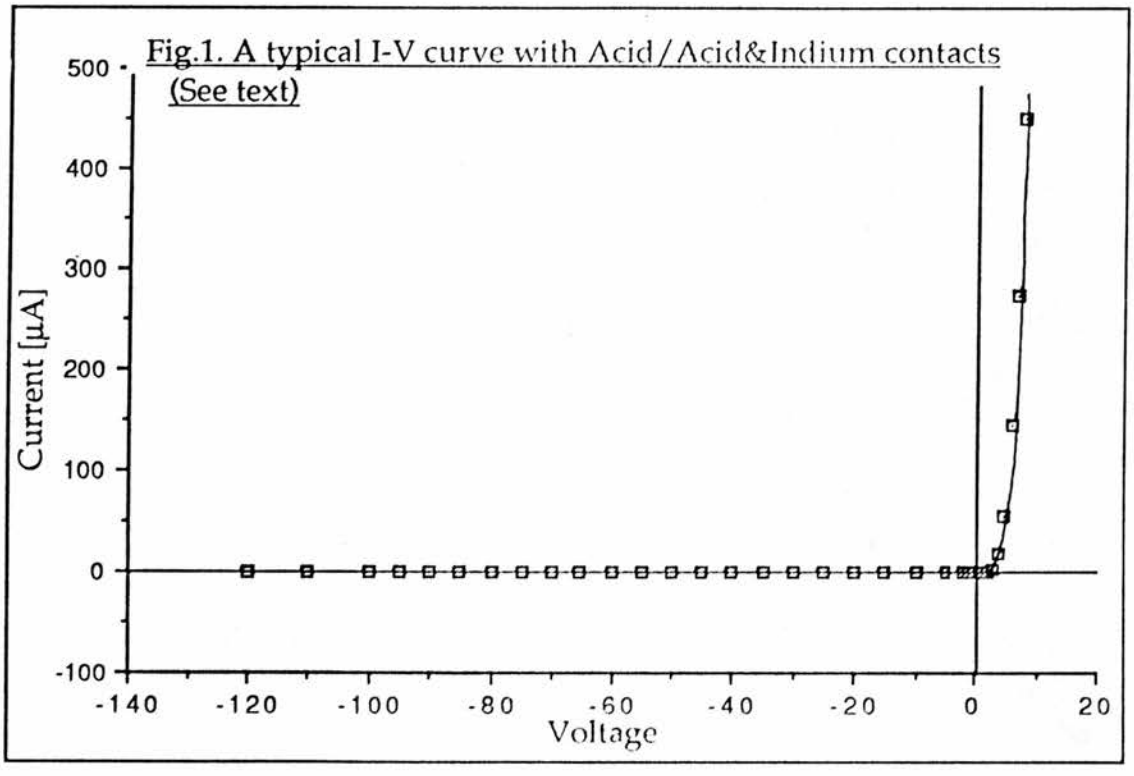

In this case we refer to positive voltages as those where the Schottky contact is positive with respect to the rear contact.

The current-voltage characteristic of a diode with one aluminium Schottky contact and an aluminium/indium rear contact is shown in figure 2 (below). The positive voltage is defined in the same way as for figure 1.

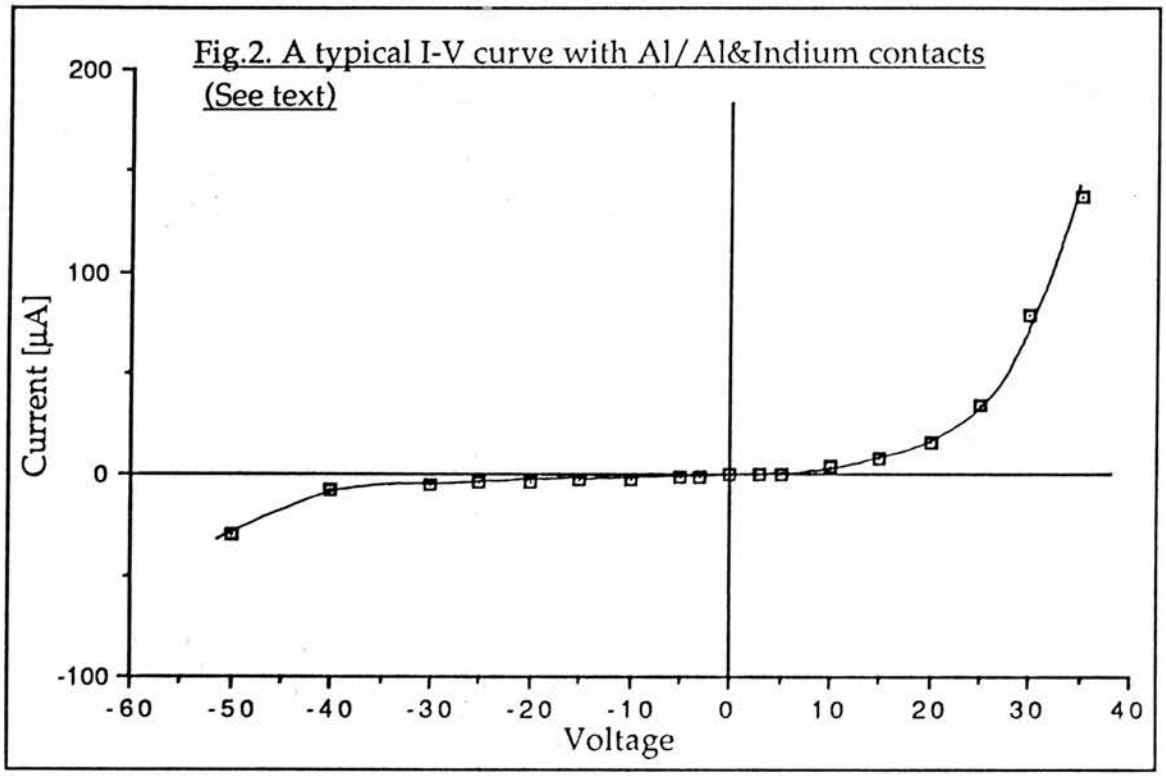

The graph above is by no means the best diode characteristic that was obtained with an aluminium contact on ZnS, but it is intended to show what might typically be achieved. In this way it can be compared directly with the typical electrolytic contact profile on the previous page.

C-V plots for both types of contact have already been described in the chapter "Band-to-band impact ionisation in ZnS".

(4.1b) Photocurrent measurements on Al/ZnS diodes.

The curve immediately below shows typical photocurrent-field characteristics obtained from diodes with aluminium contacts, based on Ep1 and Ew1 ZnS. The curve overleaf shows the variation of photocurrent with field for a diode made from Ep2 ZnS.

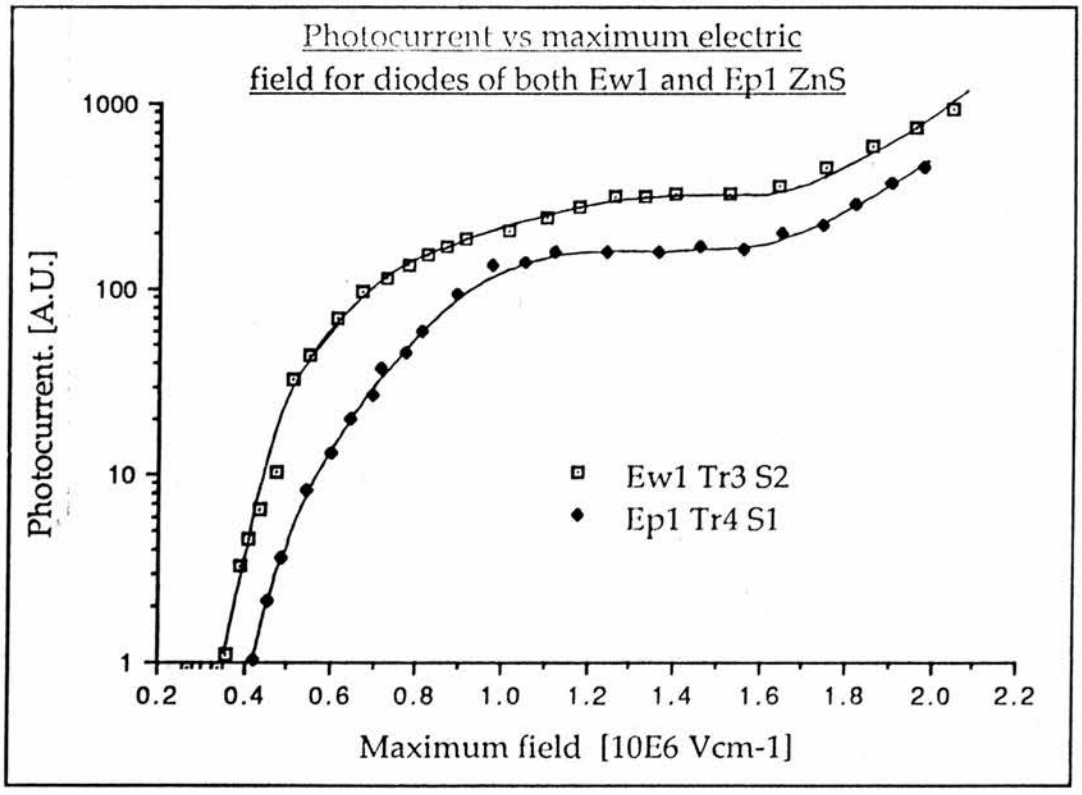

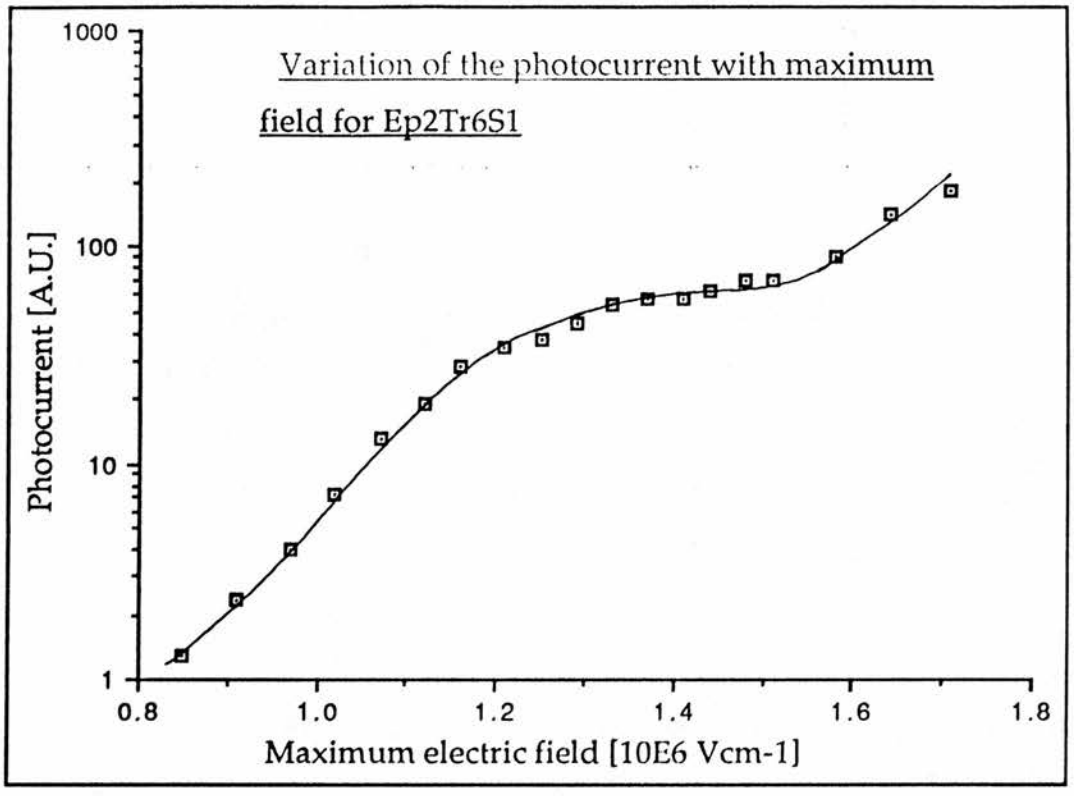
Variation of the photocurrent with maximum field for Ep2Tr6S1
Photocurrent [A.U.]
1000
100
10
1
0.8
1.0
1.2
1.4
1.6
1.8
Maximum electric field [10E6 Vcm-1]

(4.1c) Photocurrent measurements on HCl/ZnS diodes.

The curves below show typical examples of the variation of photocurrent with junction field for "electrolytic type" Schottky diodes.

Because the light ($h\upsilon < E_g$) is not strongly absorbed a correction for the variation of the collection volume (that of the depletion region) must be made. The data is normalised to unit collection volume by dividing the photocurrent by the depletion region width. The width can be easily calculated from the relation,

$$W = \{2\varepsilon_r/eN_d\}(V_{bi} + V_{app})^{1/2}$$

once Nd is known from a capacitance-Voltage experiment.

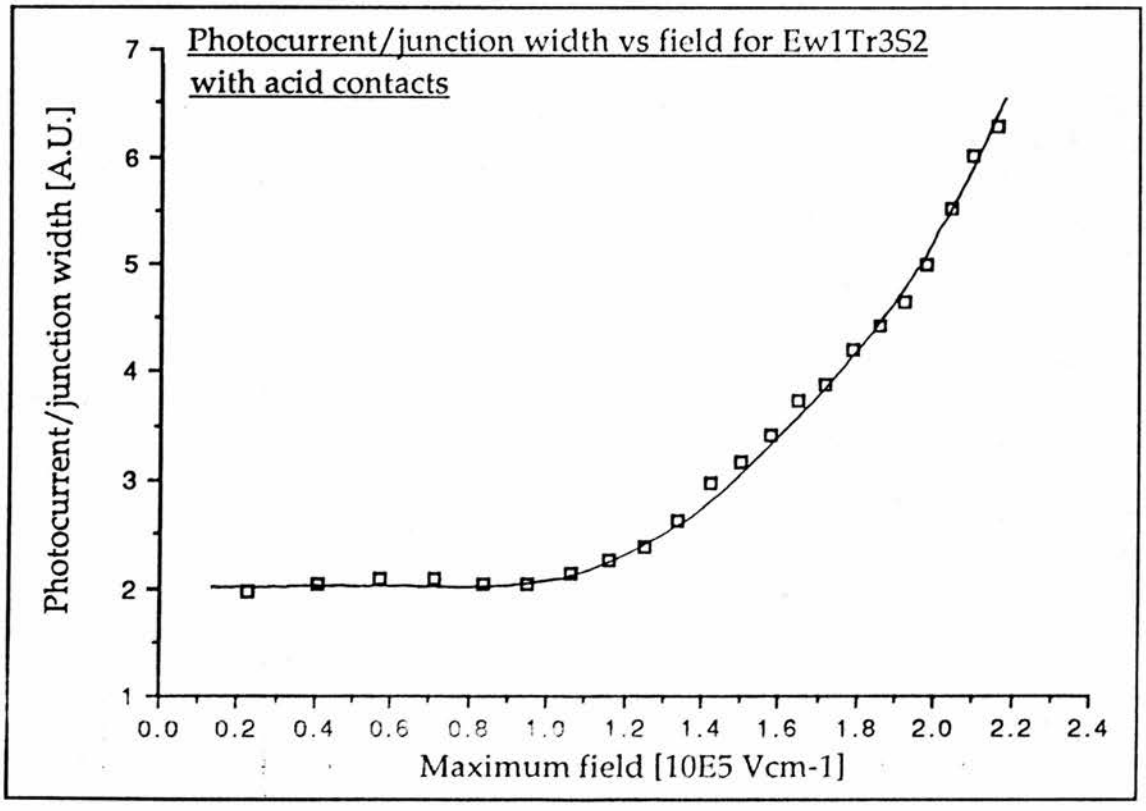

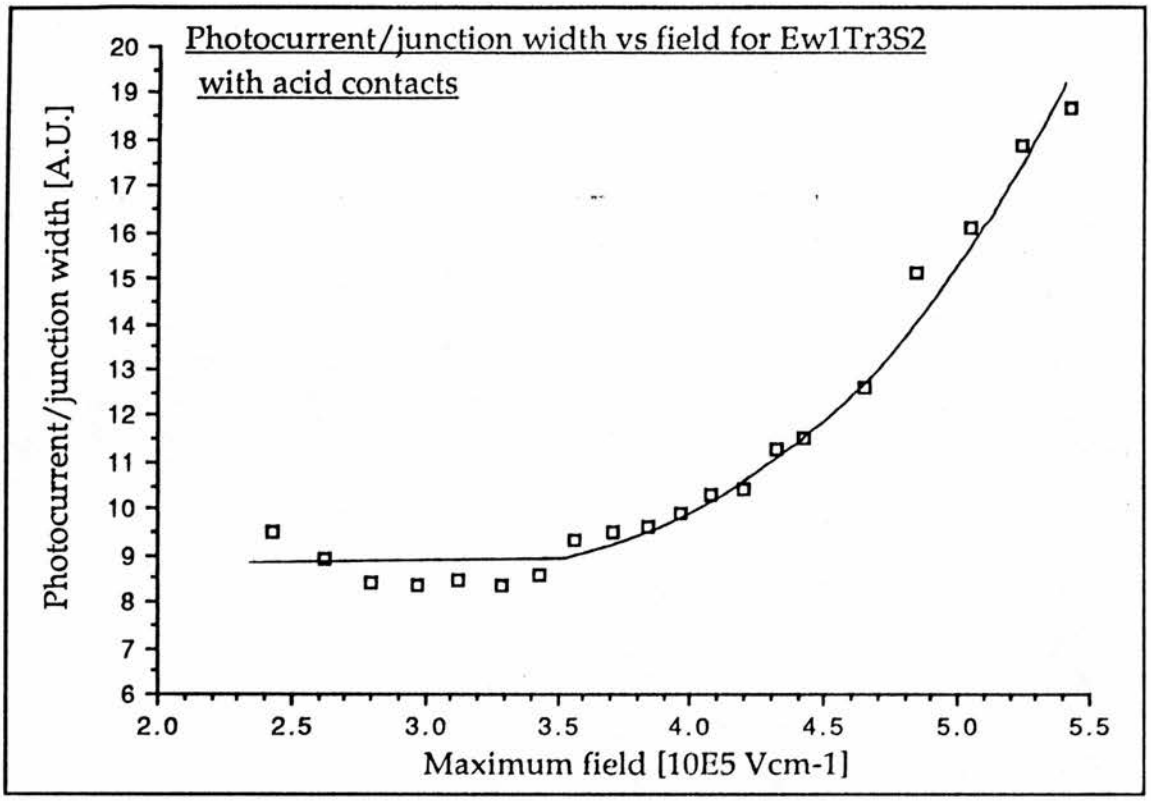
Photocurrent/junction width vs field for Ew1Tr3S2
with acid contacts
Photocurrent/junction width [A.U.]
20
19
18
17
16
15
14
13
12
11
10
9
8
7
6
2.0
2.5
3.0
3.5
4.0
4.5
5.0
5.5
Maximum field [10E5 Vcm-1]

(4.2)Photocapacitance studies of the deep levels.

(4.2a) Single beam method.

The plot below shows a typical capacitance vs photon energy characteristic for ZnS. Any differences between the Ep1 and Ew1 materials were smaller than differences between individual samples.

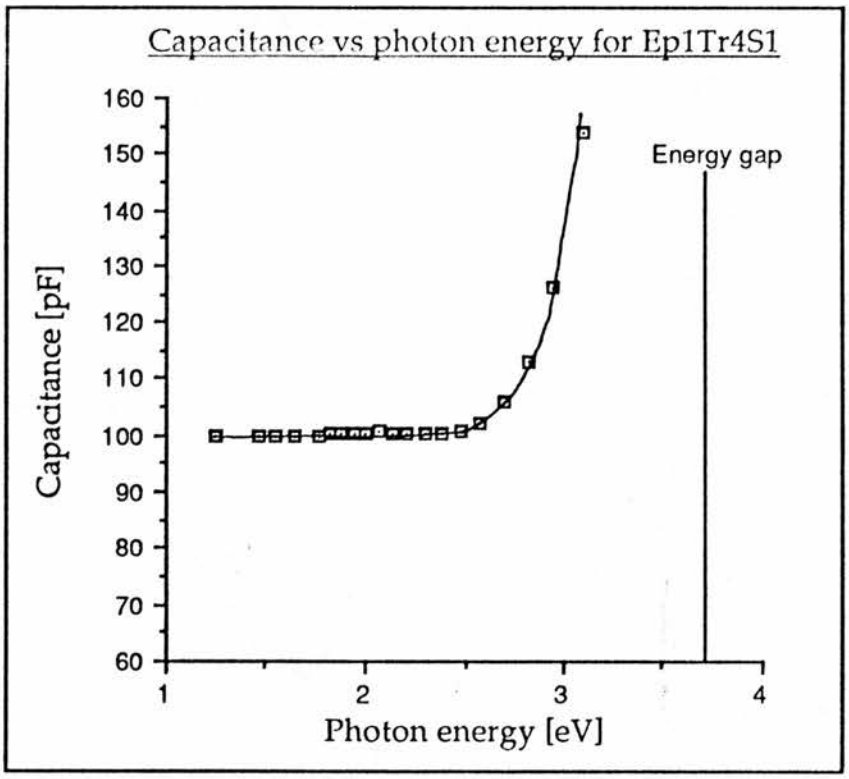

The threshold for the capacitance increase is more easily seen when the log of difference capacitance is plotted. Difference capacitance in this case is defined as $C_{h\upsilon} - C_{1.5eV}$ ($C_{1.5eV}$ being very slightly greater than C_{dark}).

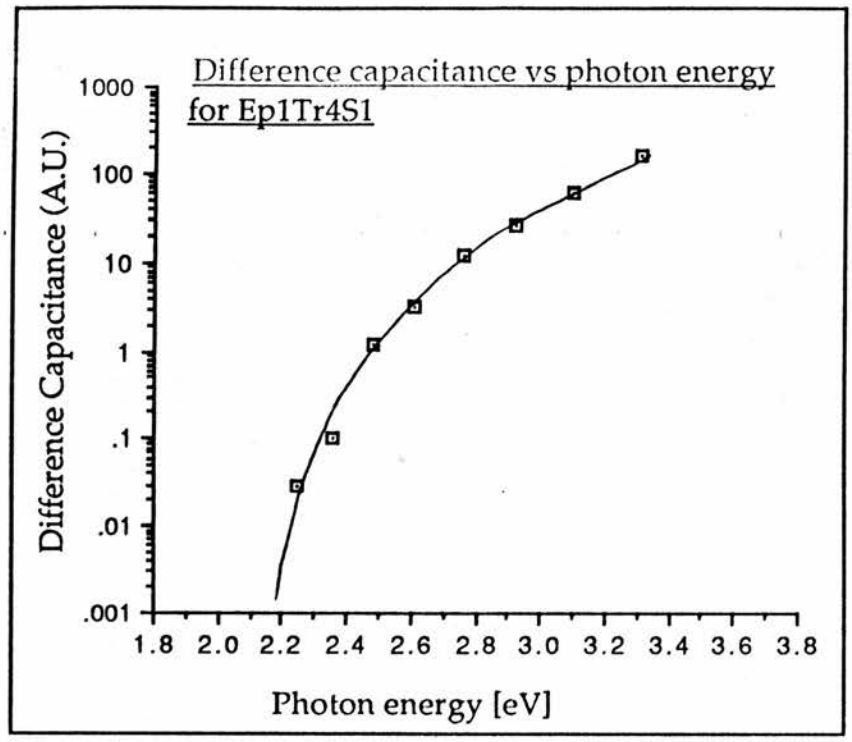
Difference capacitance vs photon energy
for Ep1Tr4S1
Difference Capacitance (A.U.)
1000
100
10
1
.1
.01
.001
1.8 2.0 2.2 2.4 2.6 2.8 3.0 3.2 3.4 3.6 3.8
Photon energy [eV]

(4.2b)Dual beam method.

The curve immediately below shows the variation of the equilibrium capacitance with the photon energy of the probe beam, for Ew1Tr2S2. The lower curve shows a similar plot for the melt grown diode Ep2Tr4S3.

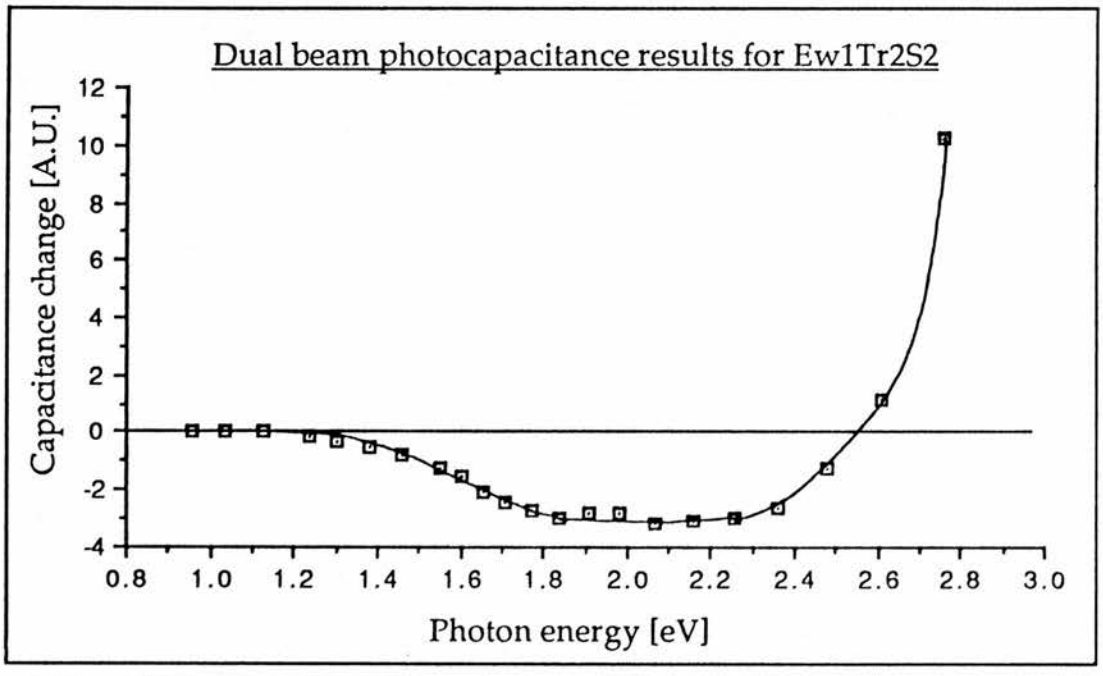

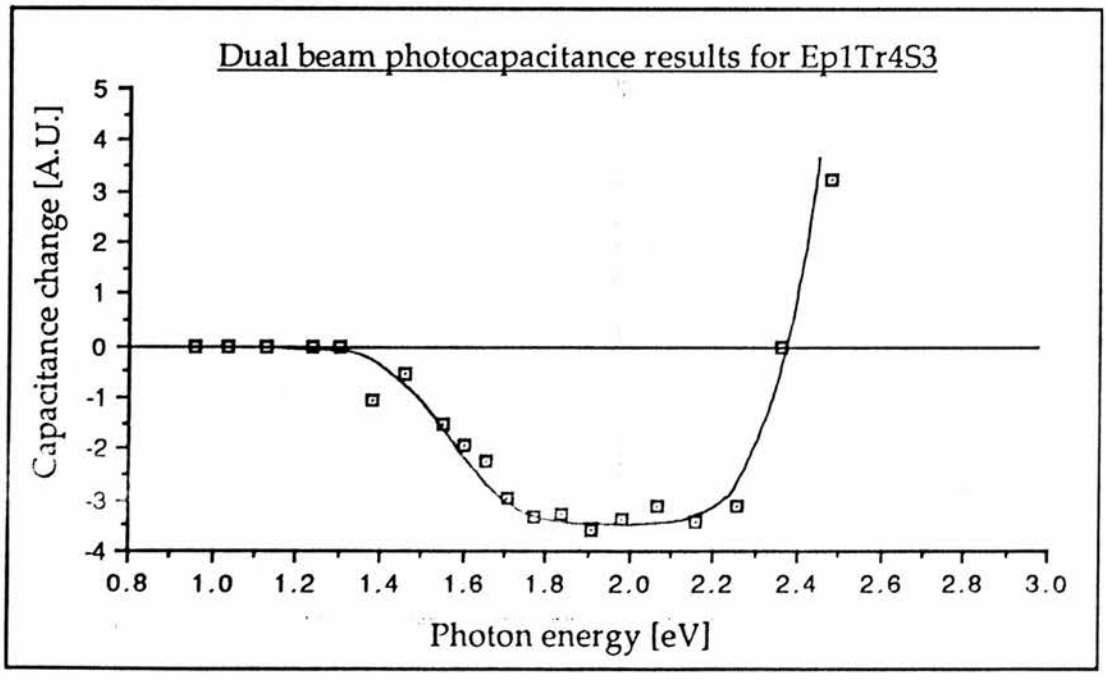

The two curves are typical in shape of all the diodes tested, however,

the exact values of the thresholds varied by around 0.1eV from sample to sample and between different contacts on the same sample. The latter variation indicates a considerable degree of inhomogeneity over the sample surface. It is for this reason that whenever possible different measurements which would later be compared (such as quantum efficiency and multiplication) were performed on the same contact. Any overall differences between the Ew and Ep materials were smaller than the the difference between the individual samples.

Below, the two plots are shown on a larger scale so that the overall shape can be seen. The rise in capacitance at shorter wavelengths is very much bigger than the fall that is induced by the light of hυ~2eV. The units on the ordinate of this graph are consistent with those in the previous two plots.

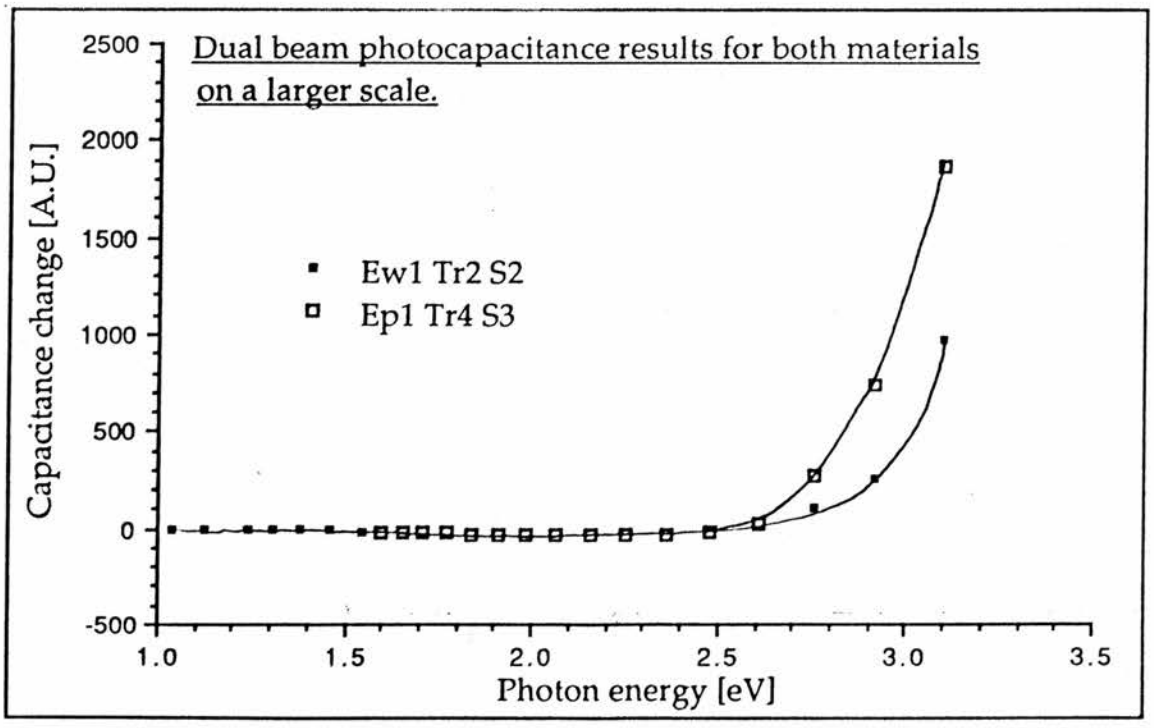

Monochromator bandwidth.

The graph below shows the band-width of the monochromator used to produce the probe beam in the dual beam photocapacitance experiments.

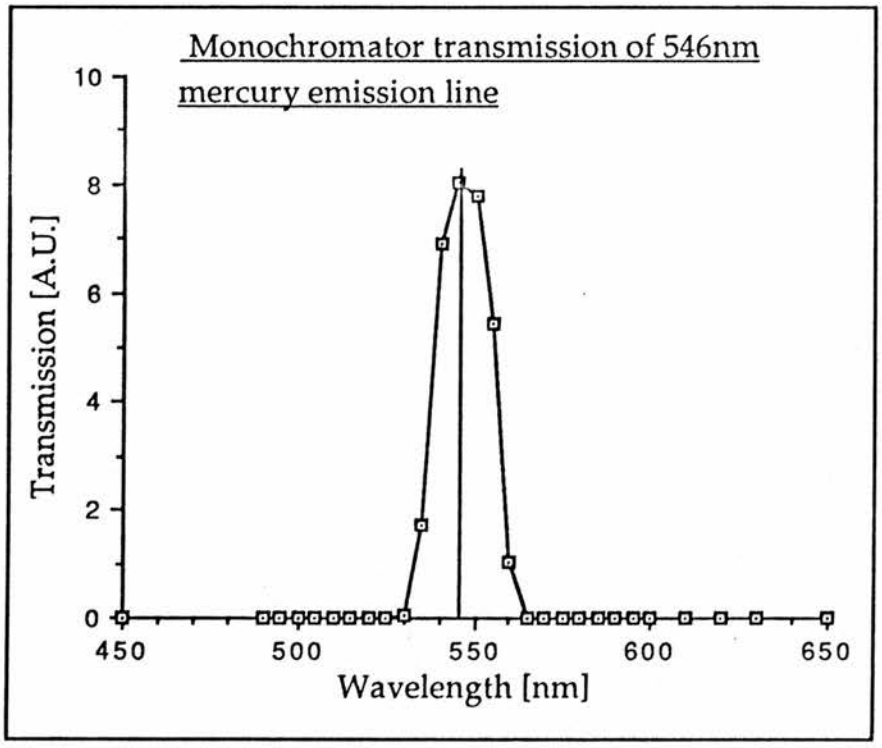

(4.3)Optical absorption experiments.

The transmission curve for Ep1Tr4S3 is shown below. An allowance for reflection from the surface of ~5% has been made so that the transmission is 100% at maximum. The crystal used was 1.8mm thick.

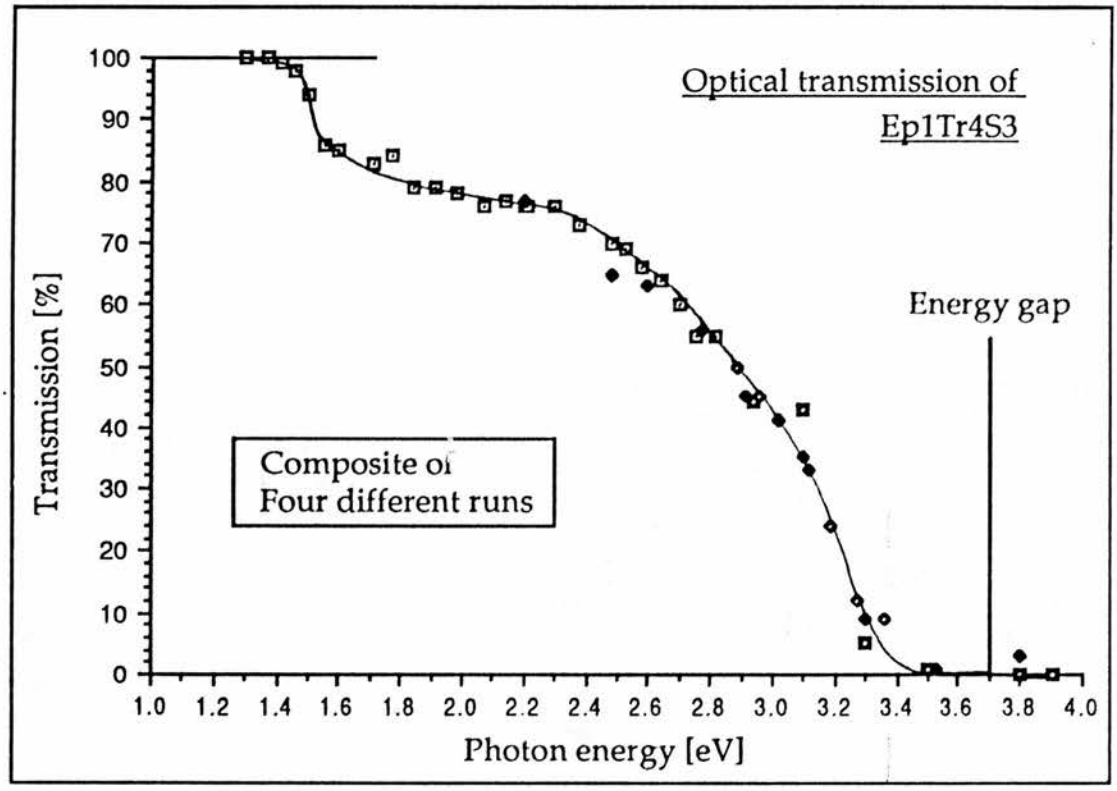

(4.4)Perturbation of photocurrent.

The graph below shows results of the perturbation of ionisation experiment for 3 samples. The only clearly resolvable feature is the threshold for a steep rise at around 2.3eV.

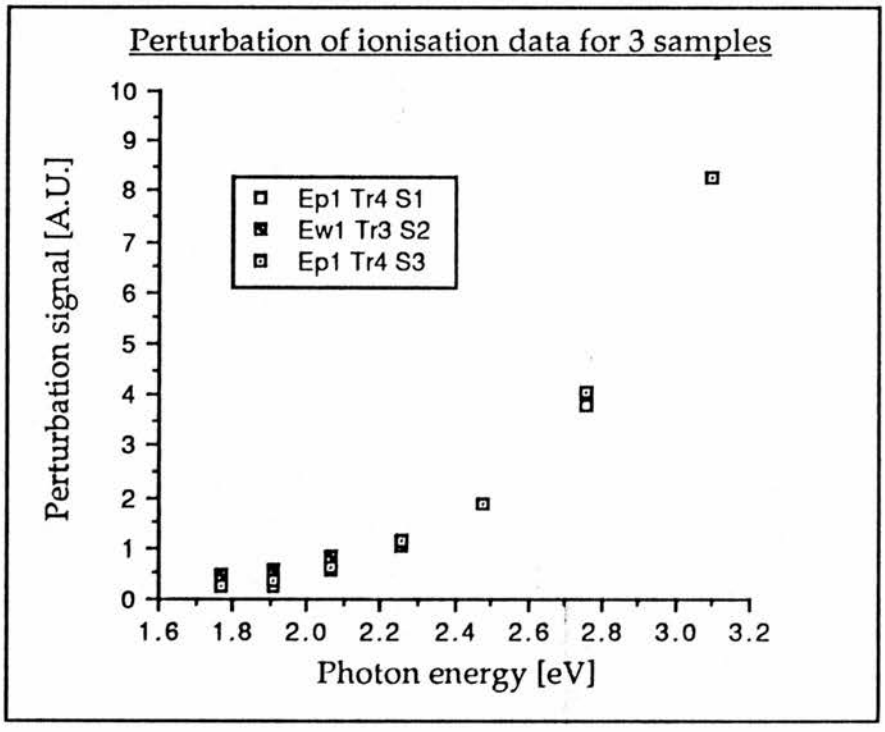

(4.5) Measurement of quantum efficiency.

The reverse bias (negative to Schottky) emission spectrum (calibrated from the manufacturers specification for the photomultiplier) for the diode Ep2Tr6S1 is shown below. The manganese emission completely dominates. The light from the diode was comparatively bright and characteristically yellow.

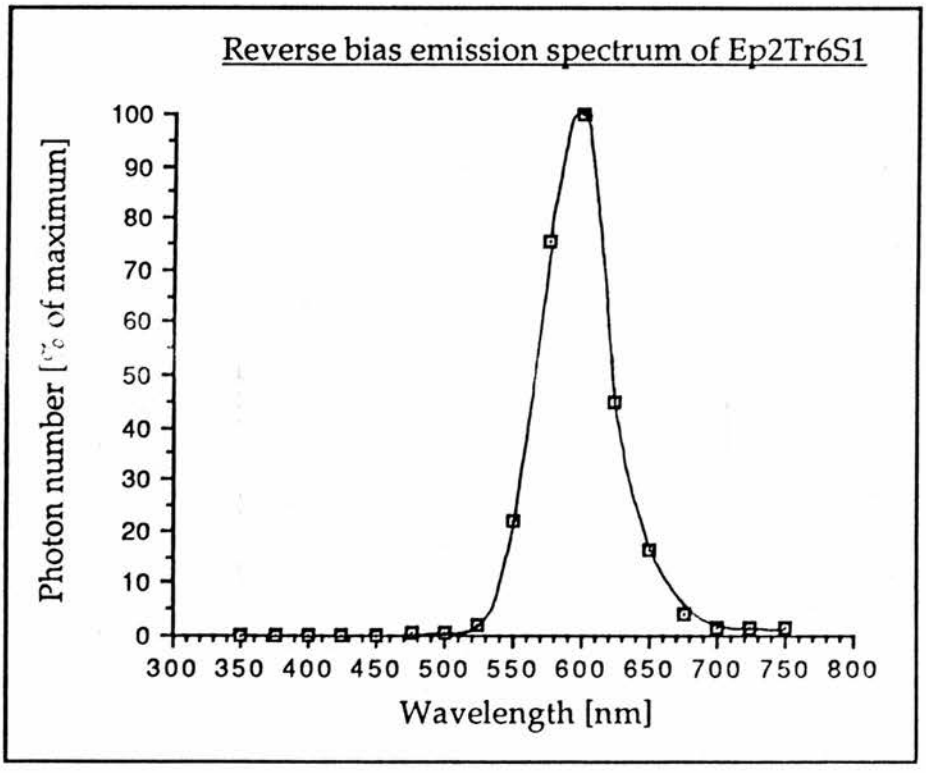

The curve below shows the variation of the quantum efficiency of the manganese emission with electric field for the diode Ep2Tr6S1. (The twin sample Ep2Tr6S2 exhibited a very uneven doping profile in its C-V characteristic and so we were unable to deduce a value of the electric field with confidence.)

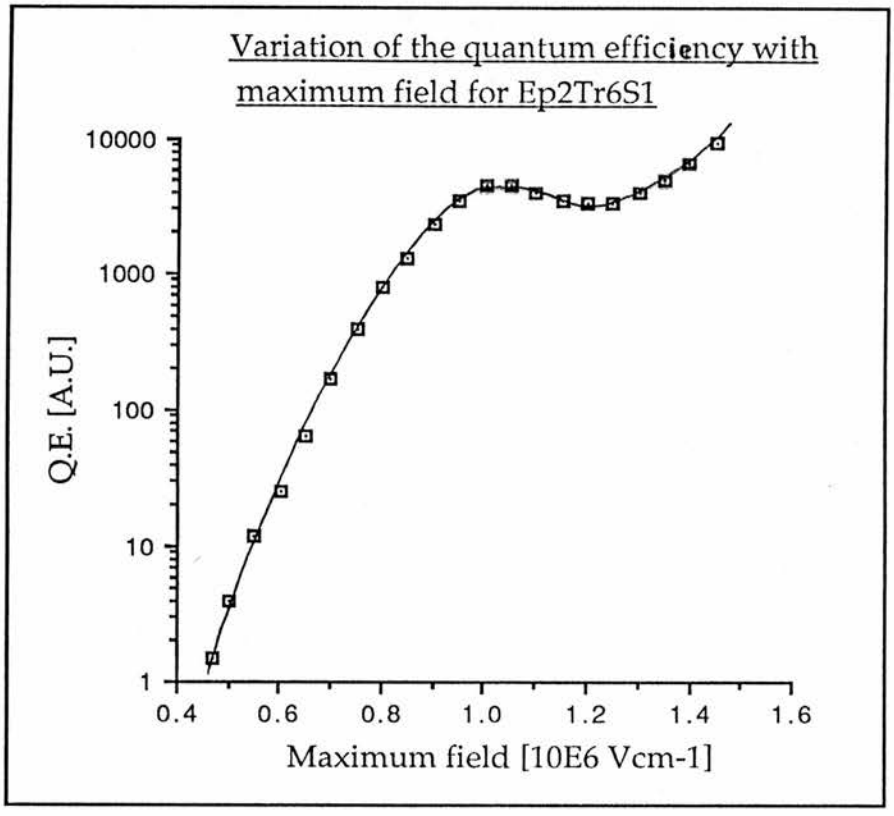

(5)Discussion.

The photocurrent in a Schottky diode is directly proportional to the number of carriers emerging from the depletion region. The steep rise in photocurrent observed in our samples at low fields, must therefore represent a significant change in the number of free carriers. We do not believe that this change in the carrier number is the result of a band-to-band ionisation process for two reasons. Firstly, the threshold field (~$2x10^5$ Vcm^{-1}) is very much lower than one would expect for such a process in ZnS, and secondly, the effect saturates at fields above ~$10^6 Vcm^{-1}$. Livingstone & Allen[26] have described a two stage impurity impact ionisation process in ZnSe, which produces an increase in the observed photocurrent of a Schottky diode at pre-band-to-band breakdown fields. They have also developed a theoretical model of the multiplication process (presented in the "Background theory"), which predicts the variation of the multiplication M as,

$$M(E) = \exp [N_t W_{eff} \sigma] .$$

If σ has the form $\sigma = \sigma_0 \exp(-b^*/E)$ It is possible to investigate a fit of this model to the experimental photocurrent data by plotting LnLnM against 1/E. Such a fit has been done for some of our data and the result is shown overleaf. From the gradient of the straight line one can deduce an impurity ionisation parameter b^*

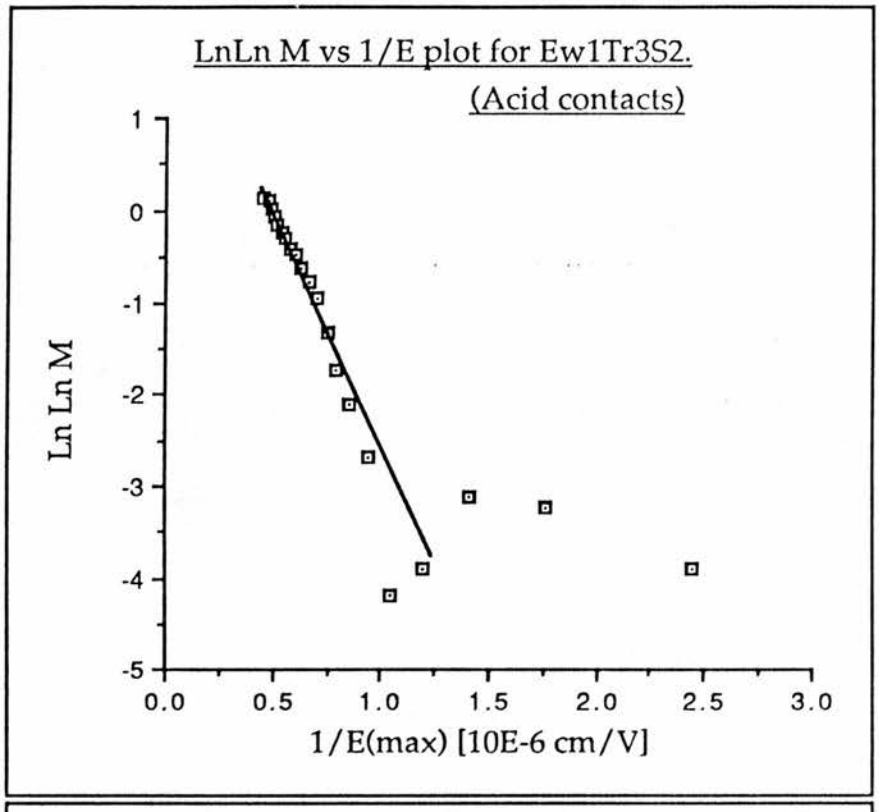

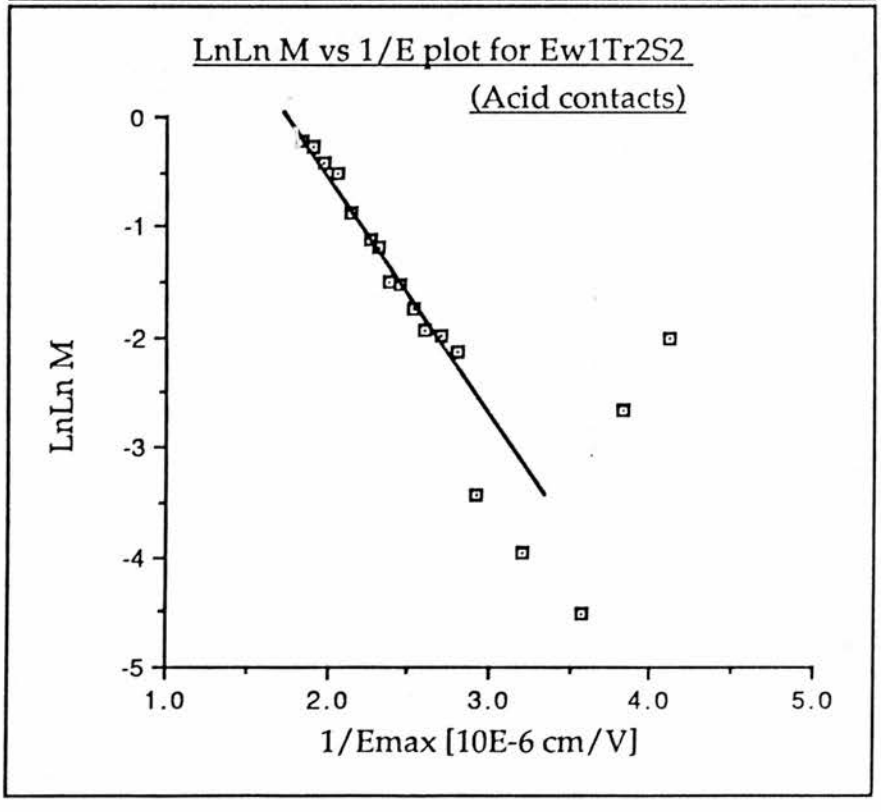

The scatter at low fields is due to error in determining the exact value of M as this approaches unity. The straight line represents a

fit to,

$$\mathbf{LnLnM = (-b^*/E).}$$

The data from the acid contacts appear to fit the theoretical multiplication model very well, yielding a value of b* in the range $2.5x10^6 Vcm^{-1}$ to $5.5x10^6 Vcm^{-1}$. This is comparable to the value of b* for ZnSe (4 to $6x10^6 Vcm^{-1}$), obtained by Livingstone[35]. Unfortunately, problems associated with the oxide layer, inevitably present in the Al/ZnS diodes, make it difficult to determine a convincing unity level prior to the start of impurity ionisation in most diodes. This prevents the calculation of M. However, for Ew1Tr3S2 (refabricated with aluminium contacts) an approximate unity level could be defined and the value of b* from the LnLnM vs 1/E plot, was $4.2x10^6 Vcm^{-1}$, which lies close to the value obtained from the acid contacts. Unfortunately none of the low field data from the Ep1 or Ep2 melt grown diodes was good enough to enable us to calculate a value of b* for these materials.

The impurity multiplication is much larger in ZnS than ZnSe. This is not entirely unexpected because the value of the multiplication M is critically dependent on the impurity concentration N_t, and the density of defect centres tends to be larger in ZnS than ZnSe. (The formation energy of lattice defects is typically of the order 2-3 eV largely irrespective of the material in question, thus defect concentration tends to increase with increasing energy gap.)

The single beam photocapacitance studies were dominated by a deep level approximately 2.2eV below the conduction band. The sign of the

capacitance change was positive which implies that the residual charge on the centre after ionisation is positive. The magnitude of the capacitance change when the sample was illuminated by a tungsten lamp was very large (~300% of dark value). This leads us to believe that density of the deep centres is very high. This is as one would expect if an impurity multiplication process is observed, because in order to achieve a value of M significantly greater than unity, theory predicts that a very large number of centres is necessary (~$10^{19}cm^{-3}$).

The dual beam photocapacitance measurements were in good agreement with the single beam experiment. Light of energy <~1.2eV does not perturb the equilibrium capacitance, where as light of ~1.4 to ~2.1eV produces a decrease in equilibrium capacitance and light with energy >~2.3eV produces a capacitance increase. These observations are consistent with transitions into and out of a centre with energy ~2.2eV below the conduction band. If this is the case, one would expect the combined thresholds of the two transitions to add up to ≥Eg. Values from each of the samples used are tabulated below.

Ew1Tr2S2	1.4±0.1eV	2.25±0.1eV	3.65±0.2eV
Ew1Tr3S2	1.3±0.1eV	2.2±0.2eV	3.5±0.3eV
Ep1Tr4S3	1.4±0.1eV	2.25±0.1eV	3.65±0.2eV
Ep1Tr4S1	1.3±0.1eV	2.4±0.1eV	3.7±0.2eV

Some of the combined values are slightly lower than one would

expect. However, the results are presented in convolution with the monochromator bandwidth, and this leads to an apparent lowering of the thresholds when a very steeply rising function (such as a photoionisation cross-section) is involved. Fornell et al[36] have performed photocapacitance experiments on vapour grown ZnS:Mn diodes and have detected several levels within the band gap. In particular they report a level 0.8eV above the valence band, although unfortunately, the spectral range of their experiment was insufficient to detect the presence of the deep centre 2.2ev below the conduction band, if indeed such a centre exists in their material. We have confidence that a 0.8eV centre, similar to that reported by Fornell, exists in our samples in addition to the 2.2eV level, in the light of detailed photocapacitance studies (using the Ep1 and Ew1 samples) performed by Zheng[12]. The pump beam for the dual beam photocapacitance experiment reported here was energetic enough to empty some of the 0.8eV centres. It is possible therefore, that transitions into this 0.8eV centre produce an extension of the low energy threshold that was observed in our experiments. This would lead to an apparently lower combined energy value for the 2.2eV centre than would be expected.

If a centre lies below Eg/2, as in this case, determining its concentration is difficult. Various dual beam photocapacitance methods are available to measure photoionisation cross-sections (see for example Grimmeiss & Kullendorff[39]), however to extract a value for N_t requires additional information usually provided by measurements on p-type samples. Brotherton[40] describes a thermal excitation method for measuring the

number of deep centres. Unfortunately however, this method cannot be applied to our diodes because of the large number of additional centres present, the low room temperature thermal ionisation of a 2.2eV centre and the non ideal nature of the contacts.

One would expect a crystal with a very large number of impurity centres to have large optical absorption at some wavelengths. The absorption spectrum for Ep1Tr4S3 has two principle features, an increase at ~1.4eV followed by a further increase at ~2.3eV. We believe that these two absorptions correspond to transitions into and out of the same centre because of their similarity to the photocapacitance results for this sample and their 3.7eV cumulative energy. The order of the apparatus in such absorption experiments is important and worthy of consideration. In this case, the "white" light passes through the sample before the monochromator. There are energetic components in this light which empty some of the deep centres enabling the absorption at 1.4eV to occur. If the order of the experiment was to be reversed (monochromator then sample) all the centres should be full and the 1.4eV absorption should not be seen.

In the absence of any intentional doping we speculate that the centre in question may be a defect rather than an elemental impurity. The fact that we see this centre in photocapacitance studies of both melt-grown and iodine transport grown material lends weight to this idea.

The results of the perturbation of ionisation experiment are difficult to interpret rigorously. There is, however, a change in the gradient of the

effect at ~2.3eV which coupled with the very large population of the 2.2eV centres indicates that these are likely to also be involved in the two stage ionisation process.

It is interesting to consider the implications of the presence and nature of this impurity ionisation mechanism to the hot electron distribution. For polar materials with only optical phonon scattering Stratton[41] has developed a formula for the threshold fields for electron runaway. In ZnS, LO phonon emission is the major scattering process at low fields, however, acoustic and impurity scattering mechanisms are not negligible (Rode[42]). Care must thus be exercised in application of Strattons' formula to this system. Rigby[10][43] has, using Strattons' formula, estimated the threshold field for runaway in ZnS to be $1.1 \times 10^4 V cm^{-1}$. Due to the presence of a built-in potential in our Schottky diodes almost all of the photocurrent and quantum efficiency measurements are taken at fields above this value.

Once an electron experiences runaway and begins to leave the bottom of the Γ_1 valley its velocity increases. (With higher velocity optical phonon scattering and impurity scattering have less effect and so the electron gains more energy.) The runaway is halted when the electron enters the X_1 and X_3 valleys. Because these valleys are shallow ($dE/dk \approx 0$), the electron velocity becomes very low (although its energy remains high). Low velocity favours optical phonon and impurity scattering processes and consequently these will act to keep the electrons in these valleys. The

band structure of ZnS is shown in the sketch overleaf (After Wang and Klien[9]).

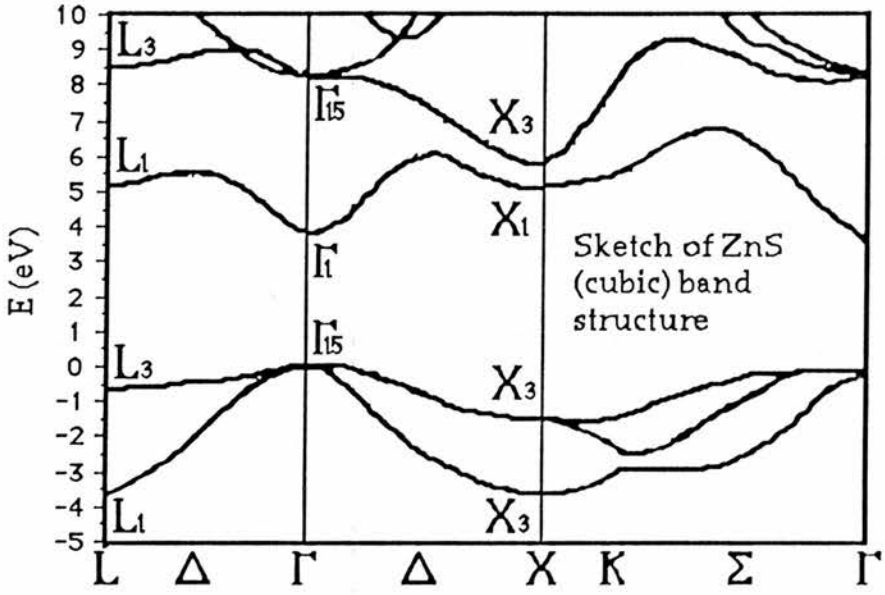

We thus believe that at all the fields we have made measurements at, the L_1, X_1 and X_3 valleys of the conduction band are at least partially populated.

Rigby and Allen[10] have shown that at fields in the range 0.7 to 1.4×10^6Vcm-1 the electron distribution is not strongly affected by the field. This was seen as evidence that almost all the electrons have left the Γ_1 minima and sit in the L_1 , X_1 and X_3 valleys of the conduction band. At higher fields still, ~$1.7 \times 10^6 Vcm^{-1}$, Thompson and Allen[6] have observed band to band impact ionisation in ZnS. This corresponds with the start of a second electron runaway, out of the X_1 and X_3 valleys. On the diagram overleaf the approximate energy thresholds for impurity ionisation of a 2.2eV deep centre and band to band impact ionisation across the energy gap are shown. (The energy for the latter process is greater than the band

gap because of conservation of crystal momentum. In a material with parabolic bands the energy for this process is typically taken as $(3/2)E_g$.

However in ZnS electrons at the Γ_{15} point have sufficient energy and the right momentum to impact ionise an electron from the top of the valence band into the conduction band. This point is thus taken as the threshold on the diagram below).

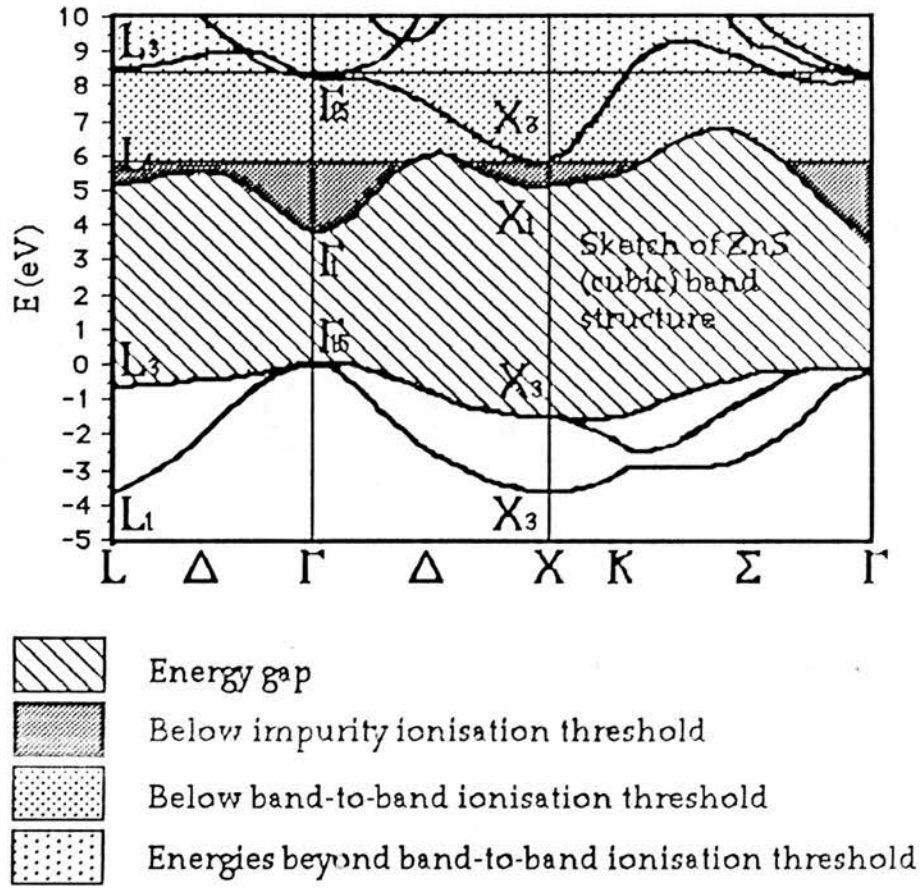

It is interesting to note that an electron in the X_3 minima has almost exactly the right energy to impact ionise a 2.2eV deep centre. The value of this inter-valley energy difference varies slightly between different

calculations of the band structure, and so it is unwise to put too much emphasis on this resonance at this stage. However, irrespective of the exact energy of the X_3 valley, such an electron has high energy and low velocity, a situation which would strongly favour an impurity impact event. There is a considerable momentum mismatch involved, if an electron in the X_1 or X_3 valleys, impact ionises a deep centre. The impurity centre itself could, however, easily absorb the necessary momentum difference. Ionisation of the deep impurities might thus be expected to be a strong effect if N_t is high enough. (A similar situation exists with the impact excitation of the manganese luminescent centre in ZnS, (Allen[44]). Resonance with the band structure makes this centre very much more efficient than most others.)

The valence band does not contain valleys similar to those of the conduction band and so although hot holes are probably present in ZnS at high fields, their behaviour will be very different to that of the electrons. The presence of these holes is however of significance and this point will be discussed later.

If the impact ionisation of impurities, excitation of the manganese luminescent centre and the hot electron transition luminescence all involve electrons in the X_1 and X_3 valleys, one would expect the variation of all these processes with electric field (and consequently electron distribution) to be similar. N.E.Rigby in this laboratory has measured the

hot electron transition luminescence quantum efficiency as a function of field for the diode Ew1Tr3S1. This is from the same batch as Ew1Tr3S2 on which we have made ionisation measurements. The two curves were plotted together and the result is presented below. (See also [14])

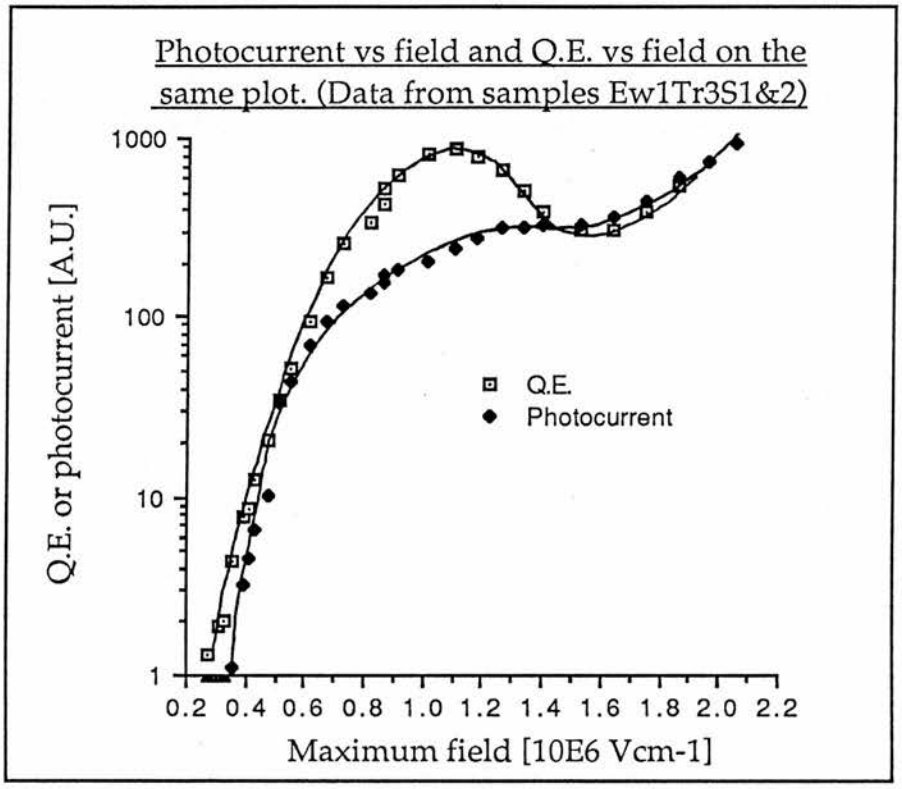

It can be seen from the figure that, in the field region where the impurity impact ionisation rate increases the quantum efficiency of the hot electron emission also increases. The quantum efficiency then goes through a broad maximum in the field region where the impurity ionisation tends to saturate. There is another increase in the quantum efficiency at higher fields ≈1.5x106Vcm-1 where band to band impact ionisation occurs.

The variation of the manganese quantum efficiency with field is shown overleaf together with a multiplication curve for the same diode.

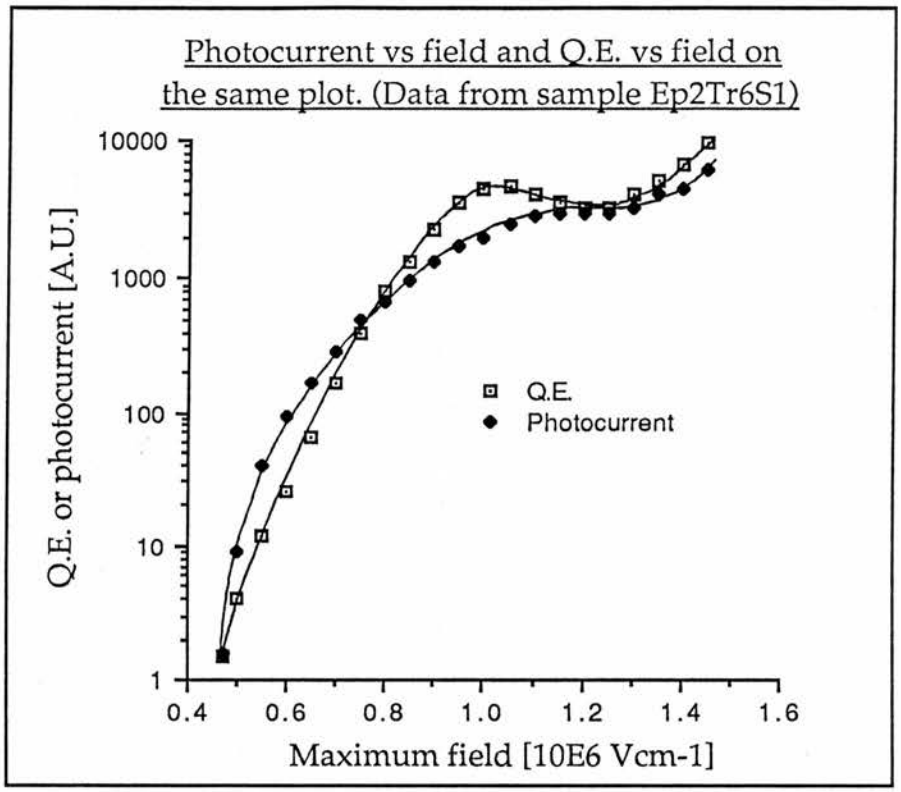

Again we observe a close correlation between the two curves, giving credence to the ideas of Rigby & Allen about the distribution of hot electrons in ZnS at high fields. The shape of the manganese quantum efficiency curve is quite similar to that observed by Gordon[34] for ZnS:Mn. Gordon suggested that the reduction in the quantum efficiency may be a band structure effect. At very high fields some of the electrons move out of the X_1,X_3 and L_1 valleys and consequently have higher group velocity. This combined with the loss of the resonant energy condition reduces the quantum efficiency of the manganese emission. The reduction

of the hot electron transition luminescence quantum efficiency, at comparable fields has also been attributed to depopulation of the X_1 and X_3 valleys, (Rigby & Allen[10]).

Because we have multiplication curves for the same diodes as our quantum efficiency measurements we are able to substantiate these ideas to some extent.

Depopulation of the X_1 and X_3 valleys would reduce the efficiency of the impurity ionisation process because of increased carrier velocity. The fact that we observe the onset of the reduction in quantum efficiency at the same field as the saturation of the impurity ionisation mechanism is in keeping with the idea of depopulation of these valleys. If , as we suspect, an electron must reach the Γ_{15} point in order to impact ionise a valence electron into the conduction band, there will be a field region where a significant number of electrons have left the X_3 valley, yet band to band ionisation will remain near unity. This is consistent with the observation of saturated impurity ionisation and reducing quantum efficiency. The final interesting feature of the curves is the increase in quantum efficiency that occurs when band-to-band ionisation begins. In the absence of more detailed knowledge about the precise form of the electron distribution at these very high fields the interpretation of this feature becomes very speculative. However if an electron at the Γ_{15} point impact ionises a valence electron the result will be two considerably less energetic electrons

in or around the central minima of the conduction band. Such electrons may then rise into the X_1 and X_3 valleys and serve to repopulate them, thus increasing the quantum efficiency.

In 1971 Krupka[45] suggested that luminescent centres such as Tb^{3+} ions could be used as a probe for the hot electron distribution in ZnS. Zhong & Bryant[46] have constructed ZnS thin film electroluminescent devices containing Cu,Cl and Nd and see multiple sharp emission lines from these devices. Bryant and his co-workers have used the variation of the relative emission intensity of such lines with applied voltage to infer that the hot electrons follow a Maxwell-Boltzmann distribution[47][51][48] and consequently that the distribution is strongly dependent on the electric field. The quality of such results is not sufficiently high to determine the precise form of the hot electron distribution (in later papers the same data was claimed to fit a Druyvesteyn distribution[37][49]). There is however, a general trend towards higher energies as the field increases. Bryant is not able to estimate the electric field in his devices, however, the voltages he applies are quite small (~10V). We believe that it is probable that the devices have low internal fields ,perhaps ~10^5 Vcm^{-1}, and that the changing electron distribution is simply due to electron transfer to the upper valleys of the conduction band. These thin film results are thus perfectly compatible with the ideas of Rigby & Allen.

There has been considerable interest recently in electroluminescence from ion-implanted ZnS Schottky diodes, for example see[11][38]. Once again, by comparison of the relative emission intensities of two or more

luminescent centres (eg. Mn & Er) with applied voltage, information can be obtained about the distribution of the hot carriers. The results of such experiments usually show a continuous change in the relative intensity of the emission from the two centres with increasing reverse bias. These results have also been interpreted as evidence for electron impact excitation of the luminescent centres, with a hot electron energy distribution that is strongly dependent on the field[49]. (In the case of diodes very high electric fields can be achieved quite easily without breakdown). This would at first sight appear to contradict the findings of Rigby & Allen[10].

There is however a serious problem associated with interpretation of the data as electron impact. The implanted centres all lie within ~10nm below the contact[50], whilst the depletion region in a ZnS diode might typically extend for 1μm below the surface (possibly further in an ion-implanted sample since the implantation damage will reduce the conductivity). At the observed threshold for electroluminescence an electron injected at the Schottky contact would not have fallen through sufficient potential drop (and consequently would not have sufficient energy) to excite the centres. Back scattering arguments cannot be applied since an electron returning towards the contact must work against the applied field and consequently lose energy.

In the light of our ionisation measurements we are able to offer an alternative explanation of the ion implanted luminescence results. In reverse bias a small number of electrons are injected into the depletion

region (perhaps by conduction through an oxide layer) and accelerate in the applied field. Deep in the depletion region they gain enough energy to impact ionise deep impurities and electron hole pairs result.

The density of defect centres will be very high in an ion-implanted sample due to the implantation damage which extends much further than the implanted luminescent centres. Consequently, we predict that the impurity multiplication will be very large. (An indication of the extent of the damage caused to diodes by ion implantation is the large forward biases (~60V Jiaqi[38]) which may be applied to these structures without breakdown.)

The holes that are produced by the impurity multiplication accelerate in the applied field, move towards the Schottky contact, and on arrival impact excite the luminescent centres. Since there are no valleys in the valence band there is no reason why the hot hole distribution should not vary continuously with the electric field. The holes fall through a large potential in crossing the depletion region and consequently can easily acquire the necessary energy to excite the centre. This idea is further supported by the observation by Jiaqi[38] that the emission intensity ratio (and thus the hot carrier distribution) does not vary much with applied voltage when the samples are driven in forward bias (+ to Schottky). Under these conditions it may well be electrons, injected from the bulk ZnS, which are crossing the region and exciting the luminescent centres. If the distribution of the hot electrons is not strongly dependent on field, over a finite range, as Rigby & Allen believe, then one would not expect to

observe a change in the relative intensity of the emission from different centres. The various processes are illustrated by the diagrams below.

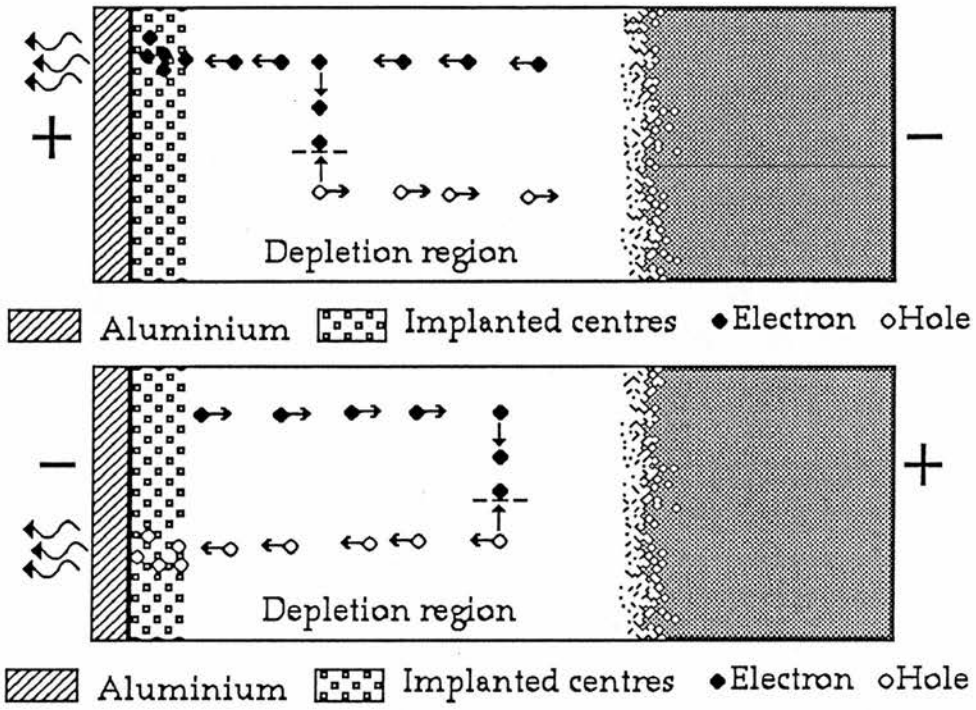

Reports on such electroluminescent emission rarely include data about the electric fields at which the measurements were taken. (It is difficult to determine the exact field distribution in an ion implanted diode due to the damage layer and consequent non-uniformity of field.) It would however be interesting to attempt to make such measurements so that the above hypothesis could be more rigorously investigated.

(6) Concluding remarks.

We have shown that a two stage impurity impact ionisation mechanism operates in ZnS. We have also shown that there are a significant number of deep neutral centres at ~2eV below the conduction band. These are responsible for the very high level of photoconduction in our ZnS crystals. There is some evidence which implies that the ~2eV centre may also be responsible for the impurity impact multiplication mechanism.

We have measured the variation of the electroluminescence quantum efficiency of the manganese centre in ZnS with electric field. We have compared this with photocurrent measurements made on the same sample. We have also compared the hot electron luminescence results of Rigby & Allen[10] with photocurrent measurements we have made on a twin diode. As a result of this we have produced further evidence to suggest that in ZnS under high fields the hot electrons transfer to the upper valleys of the conduction band.

We have pointed out that in ZnS under moderate fields, free holes are generated via the two stage impurity impact ionisation mechanism. With this in mind we have reinterpreted the ion implanted diode luminescence results of Bryant[11]. This has removed the contradiction between such experiments and the hot electron luminescence results of Rigby & Allen.

Finally we are able to say that the band structure of the host crystal has a very important role to play in governing the behaviour of ZnS high field luminescence devices.

Chapter 4

On the possibility of producing efficient blue LED's from ZnS and ZnSe.

(1) Introduction.

In 1936 Destriau[2] discovered that particles of ZnS phosphor suspended in oil, emitted light when subjected to large alternating electric fields. Progress from this discovery, towards marketable devices, has been sporadic, often halted by limitations in device fabrication technology. However, AC electroluminescent panels based on ZnS phosphor particles suspended in a solid binder are commercially available today, although problems persist. In particular, the working life of such devices, usually of the order of 1000 hours, is quite short .

During the 1960`s, Kahng[52] reported light emission from thin films of ZnS:RE, when these were excited by AC voltages. From this work, the so called "Lumocen" devices have emerged, although none of these devices have been produced commercially.

Perhaps one of the most significant recent advances has been the development by Inoguchi[3] of "Sharp" devices based on thin films of ZnS:Mn. Such devices have the necessary reliability and efficiency to be commercially viable.

All of the above mentioned devices offer considerable promise for large area flat displays. The principle disadvantages of these devices are that they all require large or complex drive voltages, and although great improvements have been made in efficiency, this remains lower than might be desired. Often there are fundamental limitations to the efficiency of such high field luminescent devices. For example, because of concentration quenching, increasing the manganese concentration in

ZnS:Mn devices beyond ~1% does not, as might be expected, increase the emission from these devices.

Although a great deal of progress has been made in the development of ZnS high field electroluminescent devices, there are at present no commercially available low voltage ZnS based display devices. Such devices, usually in the form of forward biased p-n junctions, have been made from other materials, such as $GaAs_xP_{1-x}$, for a number of years now. However, the comparatively small direct band gaps available in these materials limit efficient visible emission to red, yellow, green and shades thereof. Because of the large band gap of ZnS it would in principle be possible using this material to manufacture electroluminescent devices in any colour (including blue), by doping with the appropriate luminescent centre. Unfortunately, it is not at present possible to make low resistivity p-type ZnS, consequently construction of ZnS p-n junction devices, similar to the $GaAs_xP_{1-x}$ ones, is impossible.

In this chapter we propose a new type of ZnS device, based on hot carrier multiplication, which offers the possibility of high efficiency and multi colour emission coupled with comparatively low voltage DC operation. The structure of our proposed device is shown on the next page. When operated in forward bias, electrons from the bulk ZnS(n) are injected into the insulating layer, and accelerate in the high field thus gaining energy. These electrons could impact ionise deep impurities, giving rise to multiplication. If this ionisation were two stage (where both transitions into and out of the centres are produced), free holes would

result. These holes could accelerate in the opposite direction and be injected into the bulk ZnS(n). Here they could be trapped by suitable luminescent centres and recombine radiatively with conduction electrons.

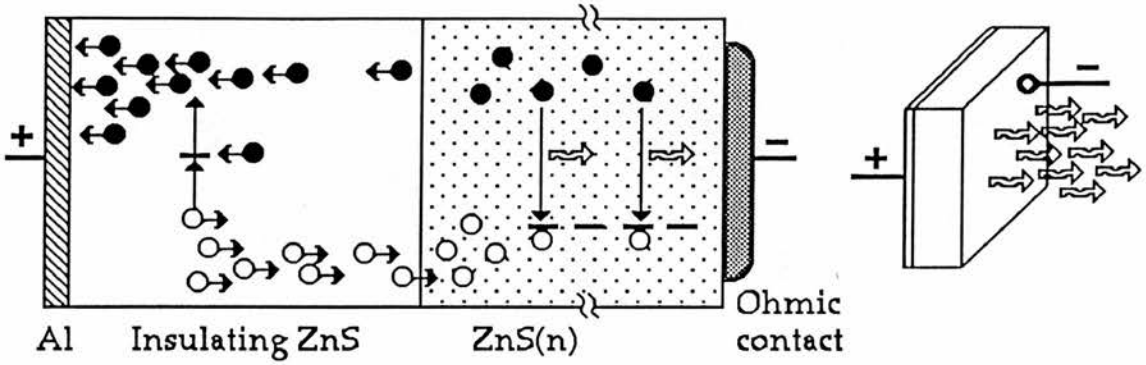

(On the diagram above solid circles represent electrons, whilst unshaded ones represent holes.)

The overall efficiency of a minority carrier injection based MIS device is given by the expression,

$$\eta_{TOTAL} = \eta_h \eta_r \eta_{ie},$$

where η_h is the hole injection efficiency (ie. the proportion of the total current carried by holes), η_r is the radiative recombination efficiency and η_{ie} is the ratio of the internal to external efficiency. η_{ie} is a measure of the proportion of generated photons which "escape" from the device and in practice this is typically of the order 0.3. If the multiplication M in the insulator is large, the number of holes will become almost equal to the

number of electrons and η_h will become large. Thus the maximum attainable device efficiency with a perfect trapping and luminescent centre might be expected to be around 15%. This is a very optimistic figure, however devices of this design with efficiencies better than 5% are not inconceivable.

Several variations on our proposed device are possible: Two stage impurity ionisation has been observed in ZnSe (Livingstone[26][35]), implying that ZnSe may also be a suitable host material. In the case of a ZnSe device, blue emission might be achieved by radiative free exciton recombination or a donor acceptor pair emission. The efficiency of this process, particularly at room temperature, would ultimately limit device performance. If it is for some reason not possible to produce two stage ionisation in the insulating layer, band-to-band ionisation could be used to generate free holes. The disadvantages of this approach would be the higher drive voltages required, and the probable reduction of device stability when operated at such high fields. To some extent the latter problem could be alleviated by pulsed voltage operation, although this complicates the drive circuitry requirements.

One of the key questions, in assessing the feasibility of a low voltage device, is the presence or absence of a two stage impurity ionisation process in insulating ZnS and ZnSe. Photocurrent measurements on thin films of ZnS, ZnS MIS devices and ZnSe MIS devices lead us to believe that such a mechanism is somtimes present. Light emission from the MIS

devices we have constructed was disappointingly weak. However, experiments performed on these devices lead us to believe that this is due to nonradiative recombination, and that with improved fabrication techniques efficient devices might be made.

Forward bias electroluminescence from ZnS and ZnSe MIS devices is of course not a new phenomenon. There are many reports in the published literature of emission from such structures. For example such emission is reported by; Bala et al[53] (ZnO on ZnSe(n)) , Fan et al[59] (ZnS on ZnSe(n)) and Katayama et al[19](ZnS on ZnS(n)). Katayama reports nitrogen temperature efficiencies of $1.5x10^{-3}$ for some of his ZnS devices which, although not remarkable by the standards of GaP devices, is higher than that reported by Kahng[52] for the first lumocen devices. None of the published reports of this light emission attribute the production of holes to impact ionisation. In the last part of this chapter we look at a few of these reports of MIS electroluminescence, in an atempt to determine whether the observed light emission can be attributed to impurity ionisation, or whether some other mechanism is responsible. We have also used information from these reports in order to make further improvements to the proposed design of the ZnS LED's.

(2)Experimental methods.

(2.1) Sample preparation.

MIS devices were produced by two methods, radiation damage of conducting ZnS and evaporation of a surface layer of ZnS on a conducting ZnS substrate. Before working on evaporated film MIS devices, we produced some thin films on aluminium coated glass substrates so that we could investigate the properties of these films in isolation.

(2.1a) Production of ZnS thin films.

Glass slides coated with a layer of aluminium (to act as one contact) were used as substrates for the evaporated films. ZnS is a particularly difficult material to evaporate. It has no stable liquid state below 30 atmospheres and thus must be evaporated by sublimation from a powder. The sublimation curve is sketched below together with the approximate point used in the production of our devices.

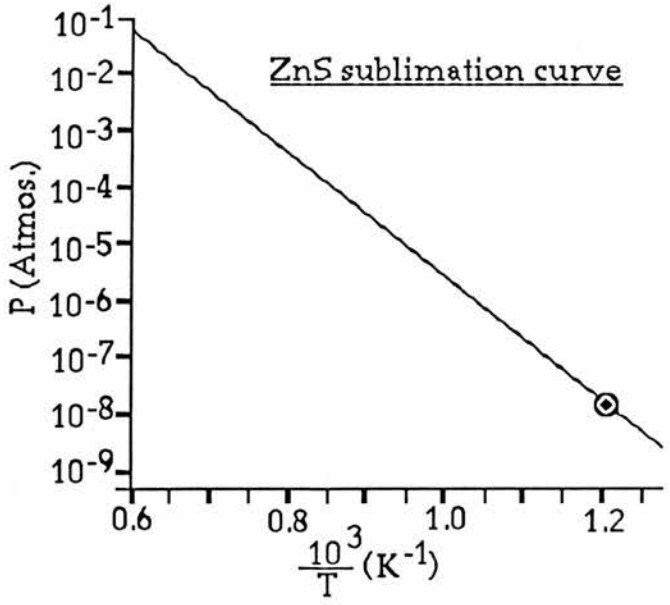

Evaporation of ZnS is made additionally difficult by the tendency of the powder to absorb water from the atmosphere. During sublimation of the ZnS this water evaporates violently and tends to blow the powder off the molybdenum boat. This problem was largely eliminated by storing the powder in a desicator prior to evaporation. As an additional precaution, once in the evaporator the ZnS powder was heated to 600K and de-gassed under vacuum for one hour before the temperature was increased to begin sublimation.

When all the powder had evaporated (this process typically took 30 minutes for a 2000Å film) the device was removed from the evaporator and multiple top contacts were made by evaporating aluminium through a mask in a separate machine. The sketch below shows the structure of a completed device.

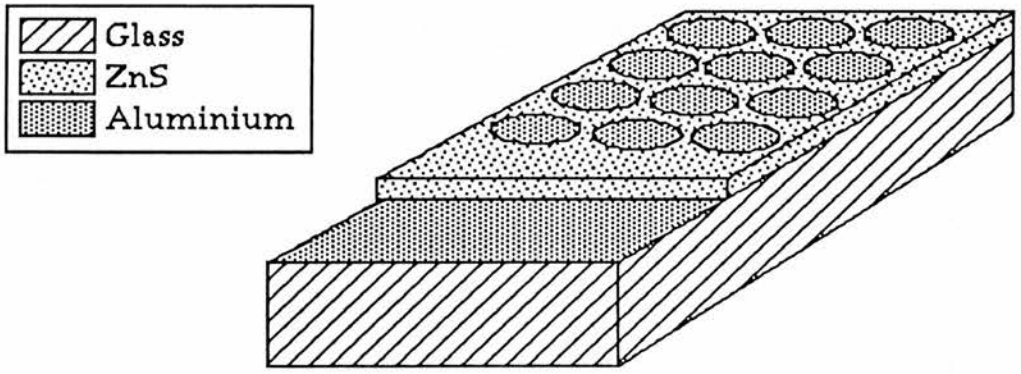

The film thickness (in general this was <1μm) has been exaggerated for clarity. The top contacts were as small as was practically possible (around 0.3mm diameter.) This was because these films had a tendency to contain many pin holes. If a top contact is evaporated over one of these pin holes

it will short circuit with the lower aluminium and thus be useless. For this reason multiple small top contacts give the best chance of producing a workable sample. The films were labelled D1,D2,D3 etc. in chronological order of production.

The thickness of the films was determined by contact capacitance. The capacitance was measured over a wide range of frequencies to ensure that it was not dispersive. Once the capacitance of a contact, with known diameter, is measured, a value for the film thickness can easily be determined from the parallel plate capacitor expression. This method does not provide absolutely accurate values for the film thickness, because the dielectric constant of the evaporated ZnS is slightly dependent on the conditions under which it is deposited. However, since the exact field distribution is not known for a polycrystalline film in any case, the small resultant error in assuming that $\varepsilon_{(Film)} = \varepsilon_{(Single\ crystal\ ZnS)}$ is not significant. For the D4 devices an additional thickness determination was made using a Newtons rings interference method. This was in agreement with the capacitance results to within 10%. Since the interference method is considerably more difficult and time consuming than the capacitance method, it was not generally used.

(2.1b) Production of M.I.S. devices.

(2.1b [i]) Evaporation of ZnS films on ZnS(n) single crystals.

In order to provide single crystal ZnS(n) substrates, contacts were removed from some of the diodes used for our earlier work.

[Nomenclature: The original sample name is retained, and the batch number of the film deposited on the surface is added to this to make a device name. For example Ew1Tr2S2 with a ZnS film grown along with the D6 thin films becomes the MIS device Ew1Tr2S2/D6.] The crystal surfaces were prepared by grinding with 1200 grade silicon carbide followed by cerium oxide powder to achieve a fine finish. The samples were then etched in 50% caustic soda solution followed by 10% HCl. Indium ohmic contacts were fused onto one side of the sample. The final polishing of the opposite (uncontacted) face was done with 1% HCl on chemically resistant filter paper. Once the ZnS(n) sample had been highly polished, it was transferred immediately to the evaporator and mounted on a heated stage. In this way the temperature of the substrate crystal could be controlled during the deposition of the films. Evaporation of the surface film was carried out in the same way as described in (2.1b). A pair of glass/aluminium substrates were loaded into the evaporator alongside the sample. The layer deposited on these substrates was presumed to be of the same thickness as that on the crystal, so that capacitance measurements on the films gave an indication of the thickness of the layer on the ZnS(n) crystal (on which it is more difficult to determine the thickness by this method). Once the surface film had been deposited circular aluminium contacts were evaporated on to it and an overcoating of aluminium was applied to the back (indium side) of the sample. The sketch on the next page shows a finished device.

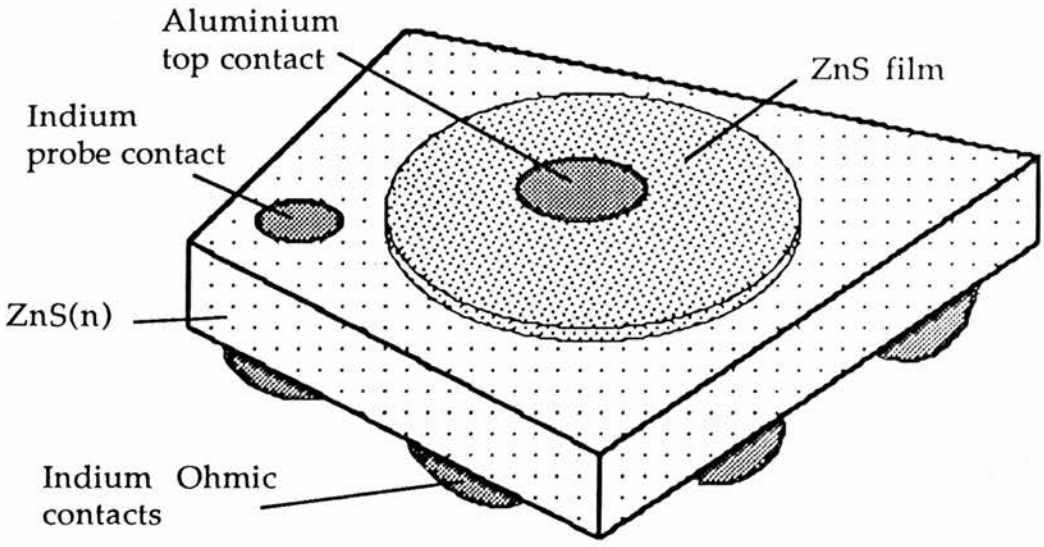

(2.1b [ii]) Production of insulating layers by α particle bombardment.

ZnSe was chosen as the substrate for these devices for two reasons. Firstly it is possible to fabr cate ZnSe diodes with very much better electrical characteristics than ZnS diodes. This means that the characterisation of the insulating layers by electrical means is more accurate. Secondly the exciton asociated emission in nominally undoped ZnSe is blue which is considerably more easily detected than the ultra violet emission from ZnS. In addition to this our absorption experiments on ZnS (see "Hot electron effects in ZnS"Page 88) indicated that any violet emission may be largely self absorbed in this material.

The starting material for the ZnSe MIS devices was single crystal high resistivity ZnSe grown from constituent elements by vapour transport, by other workers in this laboratory. The crystal was cut into dice and made conducting by immersion in molten zinc at 950K for 150hours. Apart from the absence of aluminium, the practical details of the process were similar

to the zinc/aluminium treatment for ZnS, which was described in the chapter "Band-to-band impact ionisation in ZnS" (4.1). ZnSe diodes were made by polishing the ZnSe(n) single crystals with cerium oxide and etching in 10% bromine/methanol followed by 50% caustic soda solution. Aluminium Schottky contacts and indium ohmic contacts were made on opposite faces of the sample. The resulting diodes were placed, Schottky side uppermost, under the curium 244 α particle source to produce the insulating layers.

[It became necessary at this stage to introduce a nomenclature for the ZnSe samples. The general form used previously for the ZnS samples was followed. There was only one starting material ZnSe1, each successive conductivity treatment led to a batch of samples Tr1, Tr2 etc. and each sample within a batch was randomly allocated a number S1, S2 etc. Each sample was irradiated with α particles only once so that a substrate sample number became a device number without introducing any ambiguity.]

The zero bias capacitance after α particle bombardment was very much smaller than that before. This being the case, the thickness of the insulating layer is, to a first approximation, the same as that of an equivalent ZnSe parallel plate capacitor. The reduction of contact capacitance and the implied film thickness, although useful in showing that an insulating layer has formed, cannot be used to determine an accurate value for the field in such devices because of their complex structure.

Initially α particles with energies of ~5MeV were used. A significant insulating layer was produced in 7 days. For the last batch of devices an aluminium film absorber was used to lower the energy of the α particles to ~1MeV. With the less energetic α particles the layer took only 2 days to form.

(2.2) Experimental techniques.

(2.2a) Photocurrent experiments.

Measurements were made of the variation of the photocurrent with applied reverse bias voltage for all the samples. The basic technique is to illuminate the front aluminium sample contact with chopped light of photon energy >Eg, and measure the AC photocurrent as a function of applied bias voltage. The general techniques are discussed in more detail in the chapter "Band-to-band impact ionisation in ZnS"(4.3). For the ZnSe material (band gap 2.7eV room temperature) a tungsten lamp with a Wratten 47B (blue) filter was used as the light source. For the ZnS devices, a Hanovia UV-100 ultra-violet gun was used. The variation of the photocurrent characteristic with temperature was investigated for a ZnSe MIS device. Temperature control was achieved by mounting the sample on a coldfinger in a Thor continuous flow cryostat during the photocurrent experiment. Nitrogen gas from a liquid nitrogen reservoir was used as the cryogen, the flow rate being adjusted in order to vary the temperature.

(2.2b) Quantum efficiency measurements.

The variation, with both voltage and temperature, of the forward bias quantum efficiency of the MIS structures was measured. A photomultiplier tube with an S-20 response was used to detect the emission when a DC forward bias was applied to the samples. No optical filtering was used during these measurements on either the ZnSe or ZnS MIS devices.

To record the variation of quantum efficiency with voltage, the applied voltage, sample current and photomultiplier output voltage were monitored simultaneously on three digital multimeters. (The voltmeter connected across the sample was, however, switched to open circuit during the sample current measurements.) These measurements were performed at low temperature in the continuous flow cryostat.

To record the variation of quantum efficiency with temperature, the MIS devices were mounted in the cryostat. Nitrogen gas from a liquid nitrogen reservoir was used as a cryogen, once again the flow rate was adjusted to vary the temperature. A constant voltage was applied to the sample and the sample current and photomultiplier signal were monitored at various temperatures.

(2.2c) Recording the emission spectrum of a ZnSe MIS device.

The emission spectra of the ZnSe MIS devices were recorded. The samples were cooled to 110K in the continuous flow cryostat, in order to increase the light emission to an acceptable level. The devices were driven by single polarity pulses with a 1:4 duty cycle, so that comparatively high currents, and consequently large light output, could be sustained for the

duration of the experiments. The light from the sample was passed through a Bausch & Lomb high efficiency monochromator, which was sealed to the cryostat with plasticene to exclude stray light. The detector was a photomultiplier tube with an S-20 response. A PSD, synchronised with the pulse generator, was used to measure the photomultiplier tube output signal. Spectra were recorded for increasing wavelength followed by decreasing wavelength to ensure that the output was not time variant. The spectra were calibrated in terms of photon number from the manufacturers specifications for the photomultiplier and the monochromator dispersion.

(3) Results.

(3.1)Thin films.

The curve below shows that the contact capacitance of a D4 ZnS film is essentially independent of frequency, over the range 20kHz to 1MHz. Such invariance cannot be taken for granted, as some early D1 and D2 films which were of lower quality exhibited considerable dispersion. A thickness determination based on capacitance is of course only valid if the capacitance is independent of frequency.

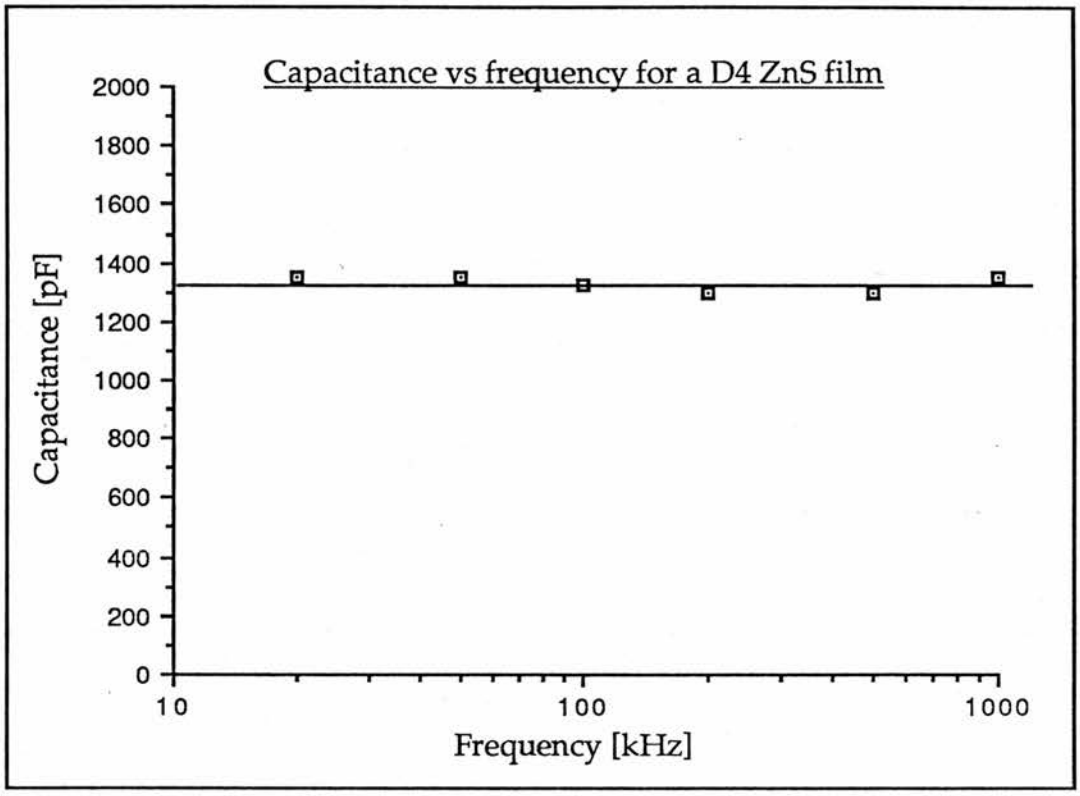

The three curves, below and over leaf, show the variation of the photoconductivity with electric field for three thin films of ZnS. Photoconductivity (photocurrent / voltage) is plotted rather than photocurrent, because the Hanovia lamp has considerable emissions in the visible, which cause bulk photoconduction effects. The multiplication processes are more easily seen if this ohmic component is removed by dividing the photocurrent by the applied voltage. Behaviour of such devices at high fields is erratic, and so the curves cannot be described as typical of device behaviour in general. However, they are typical of the behaviour of stable contacts on the ZnS films.

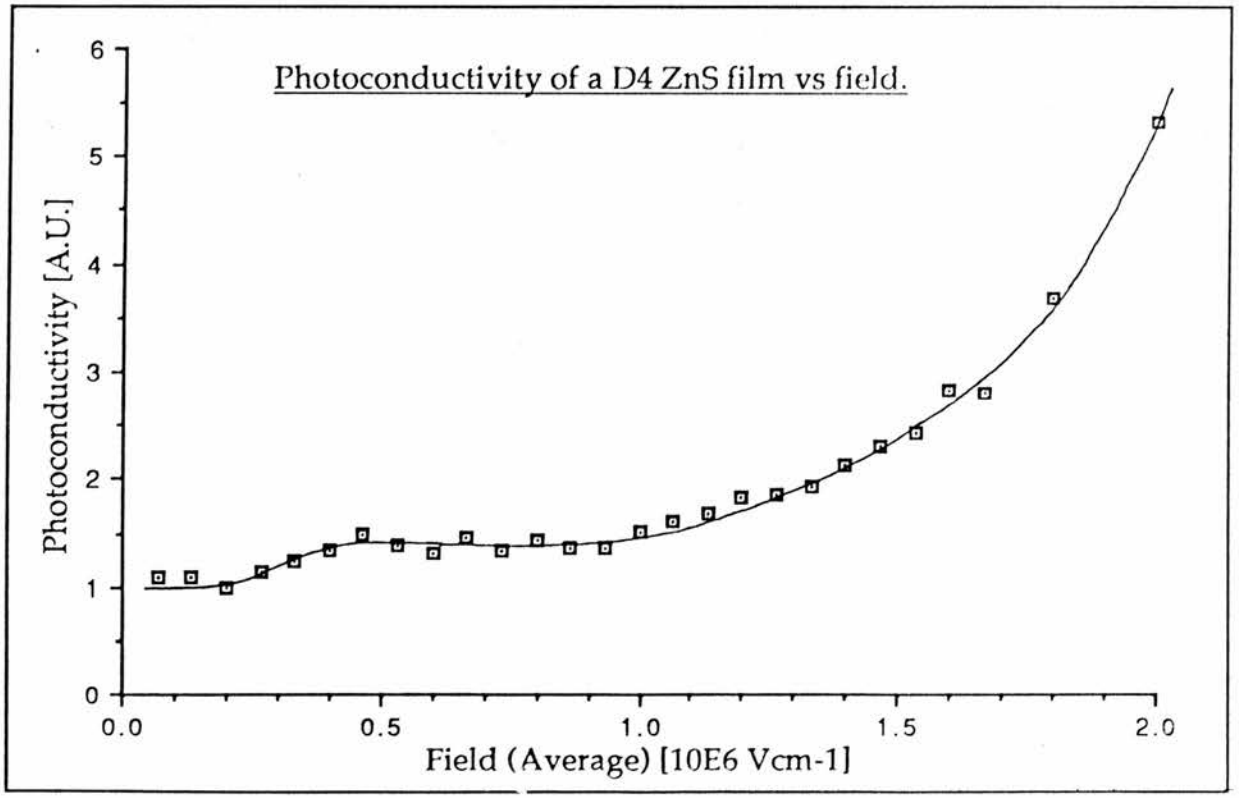

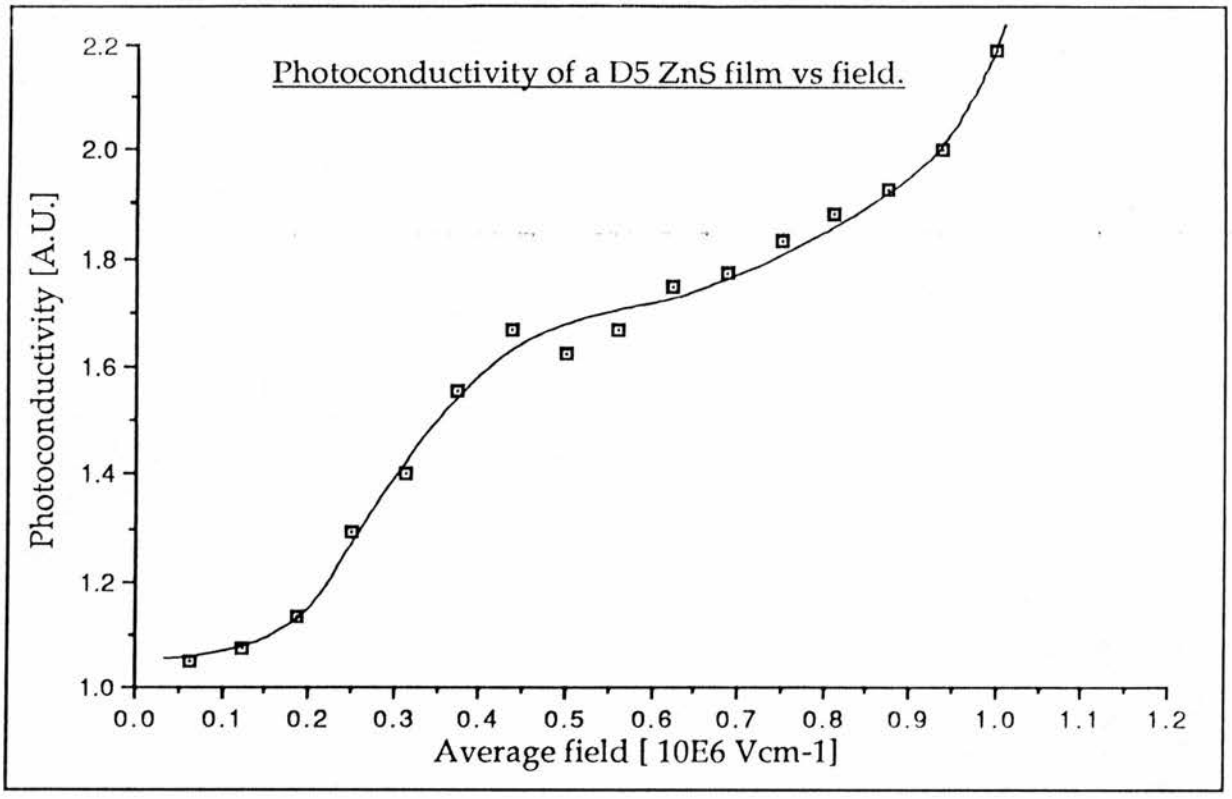
Photoconductivity of a D5 ZnS film vs field.
Photoconductivity [A.U.]
2.2
2.0
1.8
1.6
1.4
1.2
1.0
0.0 0.1 0.2 0.3 0.4 0.5 0.6 0.7 0.8 0.9 1.0 1.1 1.2
Average field [10E6 Vcm-1]

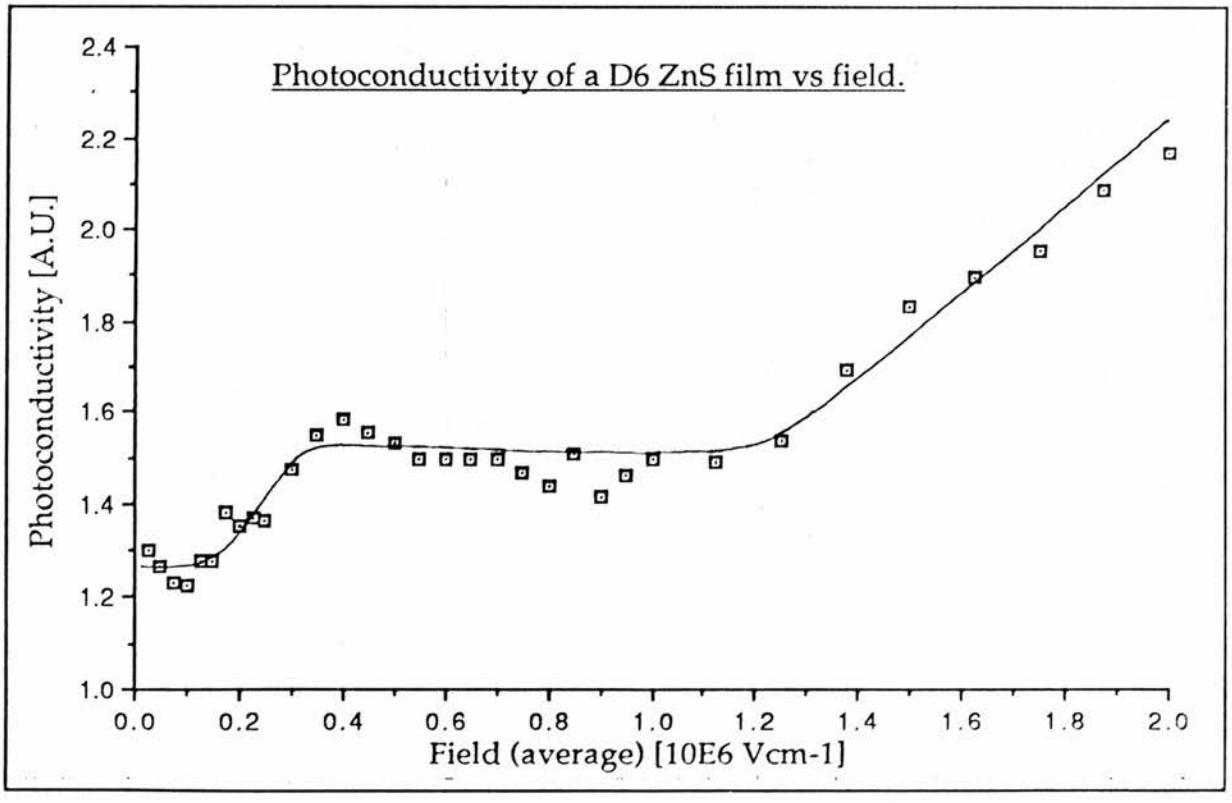
Photoconductivity of a D6 ZnS film vs field.
Photoconductivity [A.U.]
2.4
2.2
2.0
1.8
1.6
1.4
1.2
1.0
0.0 0.2 0.4 0.6 0.8 1.0 1.2 1.4 1.6 1.8 2.0
Field (average) [10E6 Vcm-1]

(3.2) M.I.S. devices.

Throughout this work forward bias is defined as the aluminium contact directly on the insulating layer, being at higher potential than the indium back contacts.

(3.2a) Thin films of ZnS grown on Single crystal ZnS.

The curve below shows the variation of the photocurrent with voltage for the MIS device Ew1Tr2S2/D6. Since almost all of the applied voltage is dropped across the surface film we believe that, as with the isolated film , it is more appropriate to plot photoconductivity than photocurrent for these devices.

Photoconductivity vs bias voltage for the MIS device Ew1Tr2S2/D6 under reverse bias.

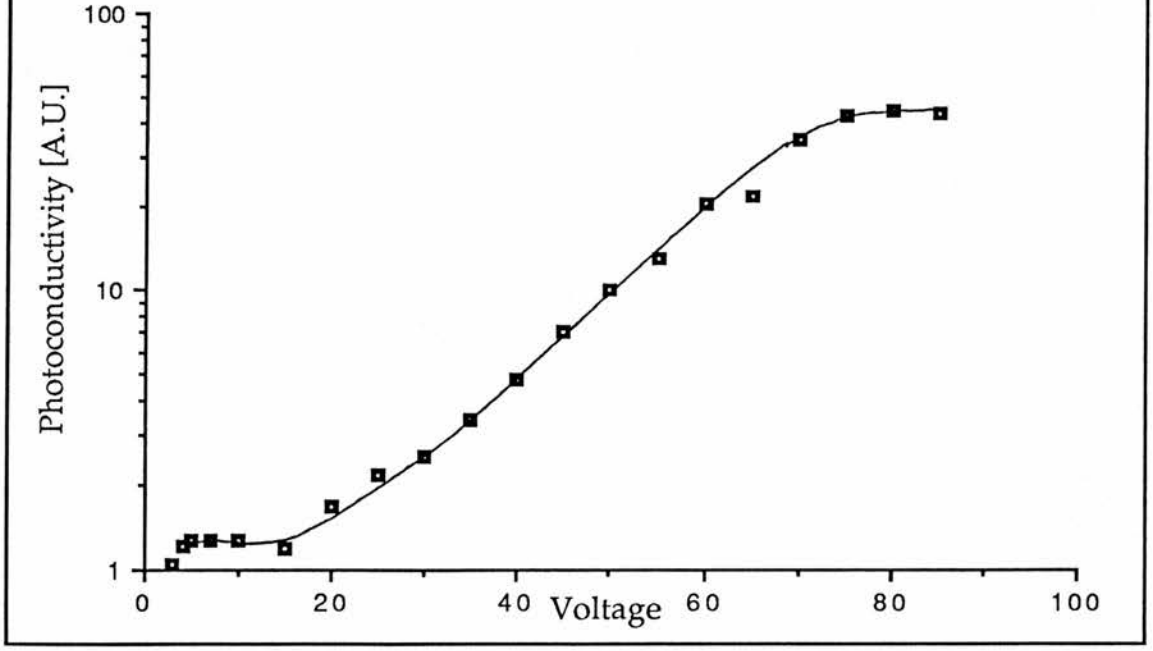

The plot below, shows for the Ew1Tr2S2/D6 MIS device, the proportion of the applied voltage that is dropped across the film itself in forward bias. This was measured with a probe contact similar to the one in the diagram at the bottom of the page.

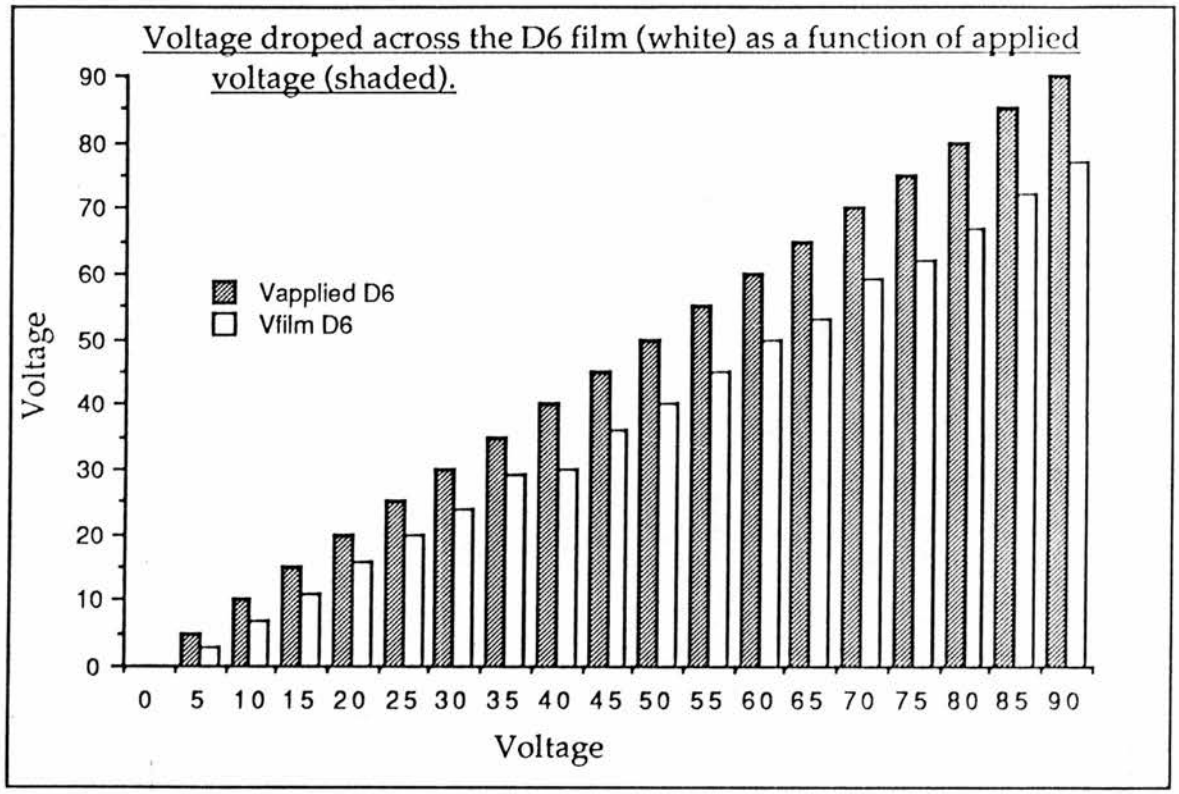

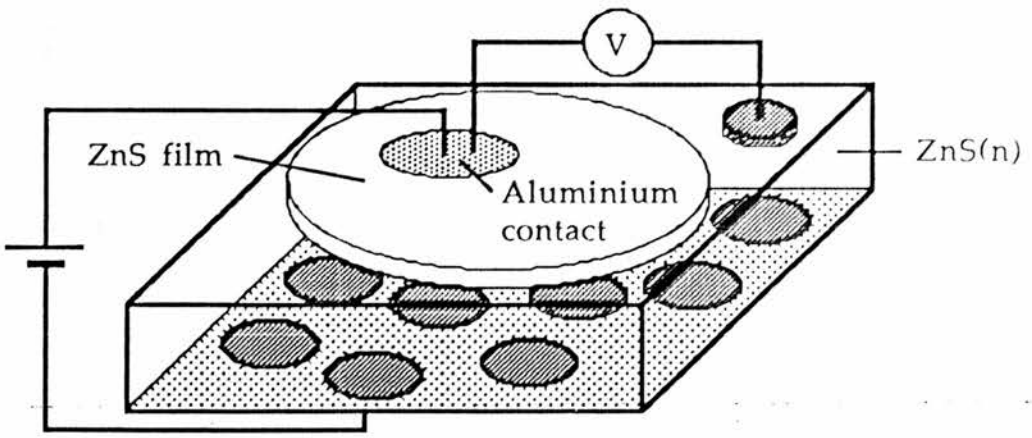

The variation of the quantum efficiency with temperature was investigated for the Ep1Tr4S3/D7 MIS device. (Unfortunately, the device Ew1Tr2S2 was destroyed during experiments prior to the quantum efficiency temperature run. Data for the similar device Ep1Tr4S3 is thus presented in substitute.) The curve below shows this variation for two forward bias voltages, 30V and 100V. The vertical spacing between the two sets of data on this plot is arbitrary. That is the units on the ordinate for each set are not consistent with each other.

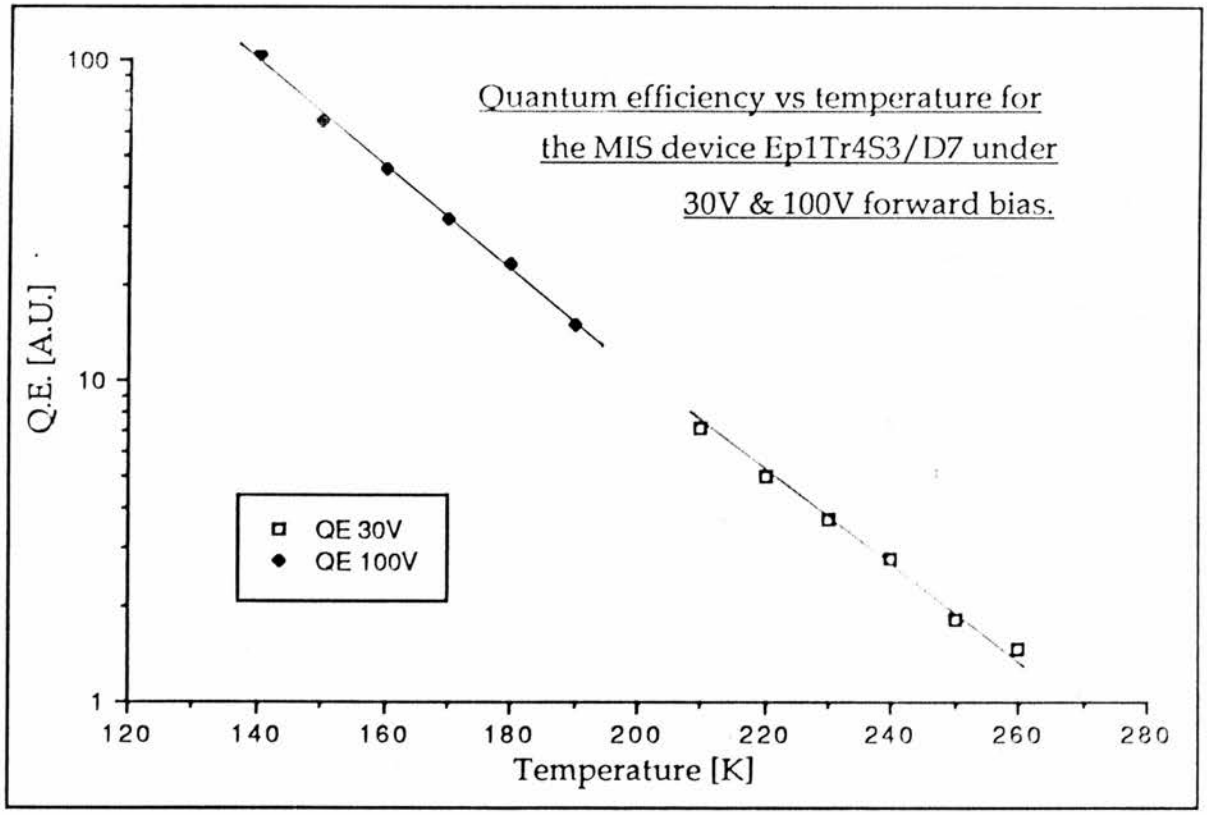

The variation of the quantum efficiency with applied forward bias voltage, for the Ew1Tr2S2/D6 MIS device, is shown in the graph below. The curve is composed of data from two separate runs, R1 & R2. The experiment was performed at 115K.

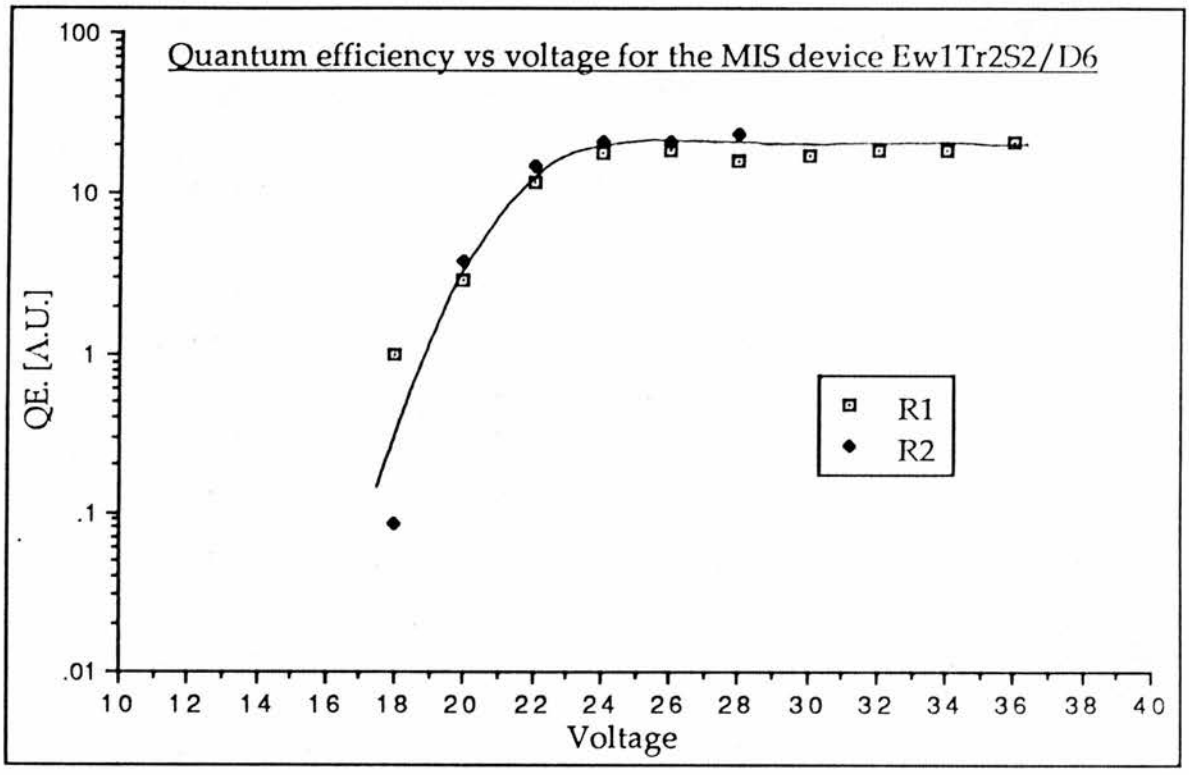

The curve below shows the variation of the capacitance of the MIS device Ew1Tr2S2/D6 with applied reverse bias. The rear of the sample is coated with aluminium to provide a large back capacitance, so that the capacitance measured is essentially that of the contact on the insulating film. The results were obtained at 1MHz and room temperature. The error bars indicate the resolution of the bridge, in terms of the divisions on the dials.

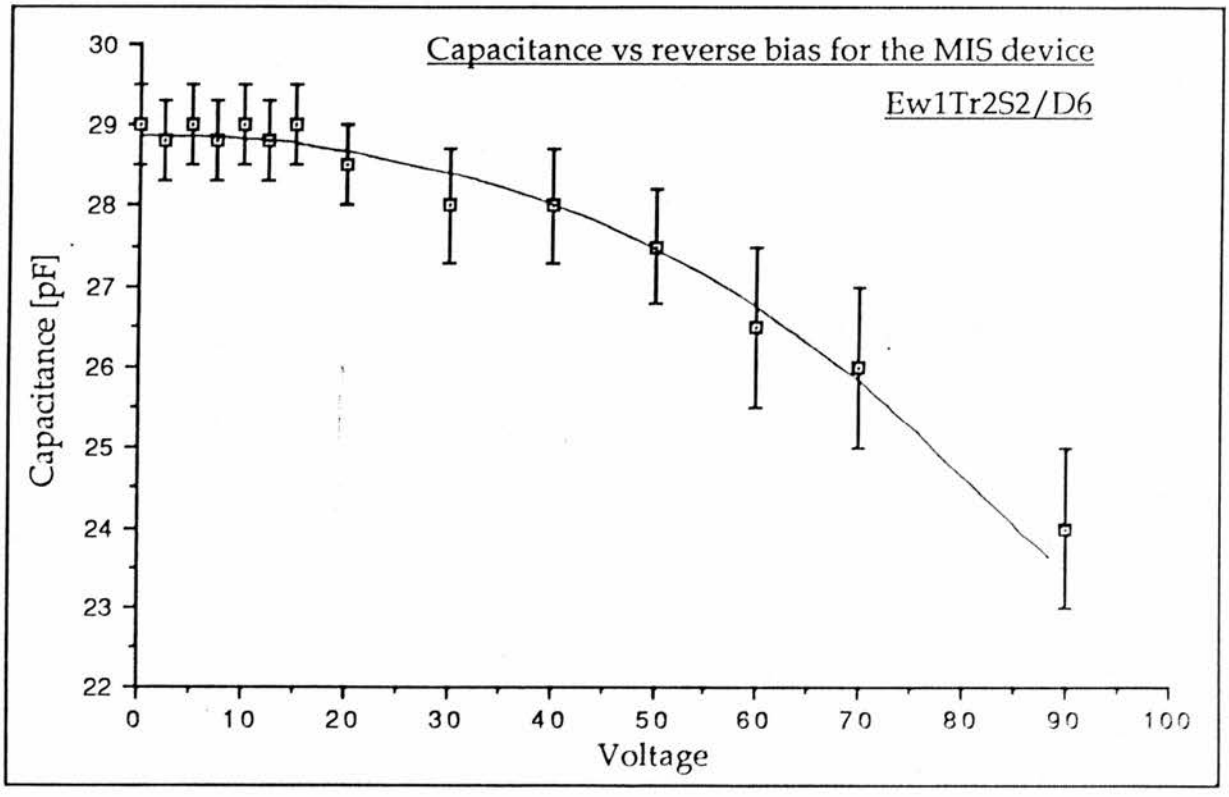

(3.2b) ZnSe MIS devices, produced by α particle bombardment.

The current-voltage (below) and capacitance^{-2}-voltage (overleaf) curves of the ZnSe/Al diodes before bombardment show very much better diode characteristics than the ZnS diodes discussed in previous chapters. The indium back contacts have DC resistances of the order of 1Ω, so that it is not necessary to overcoat the back surface with aluminium in order to make capacitance measurements.

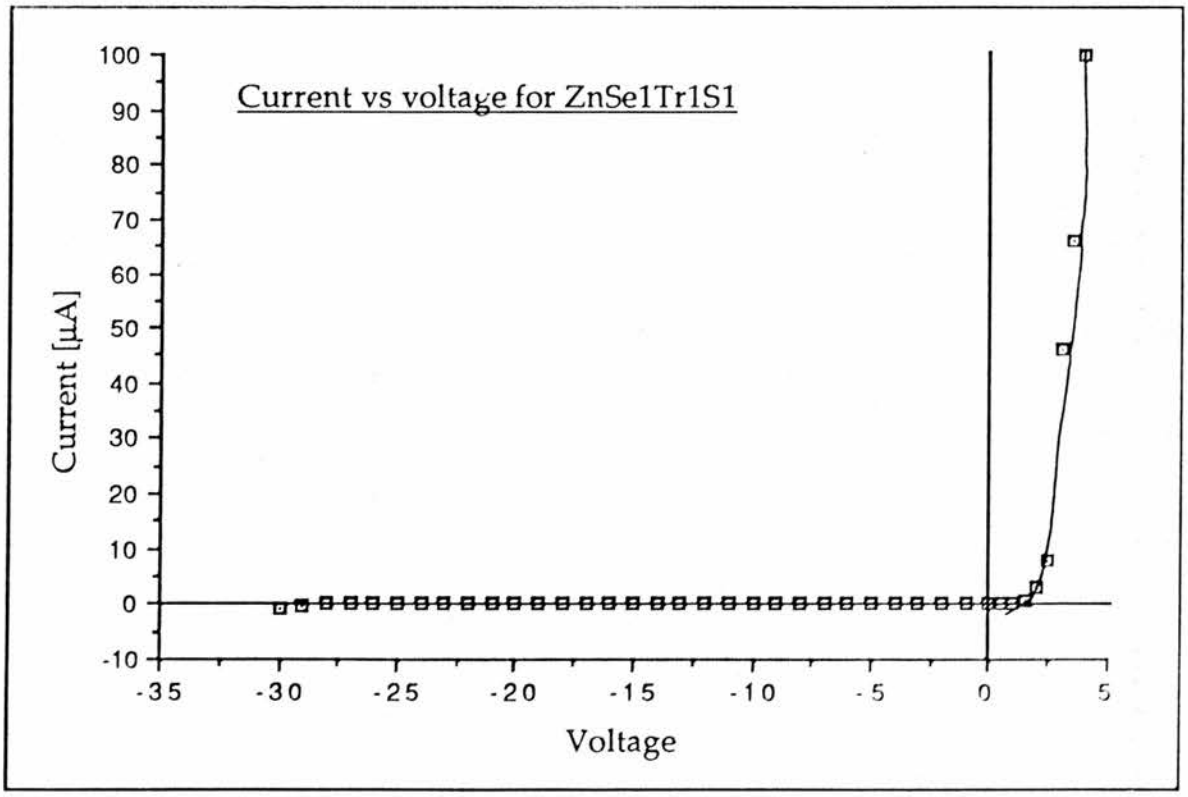

The graph below shows a typical capacitance^{-2} -voltage plot for a ZnSe/Al diode. Unlike the ZnS/Al diodes, the capacitance and junction width of ZnSe diodes was not significantly light dependent.

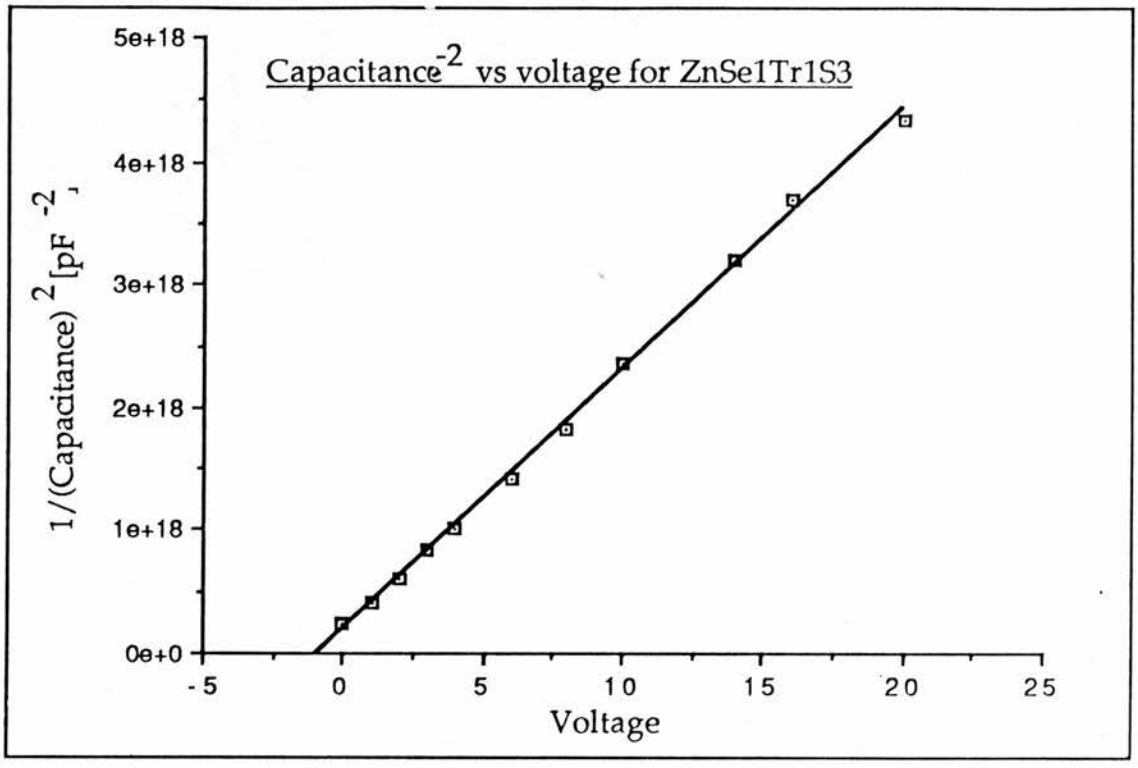

The curve below shows the variation of photocurrent with reverse bias for ZnSe1Tr1S1. The photoconductivity is also shown. In the case of these devices there is some uncertainty as to which is the most appropriate variable to plot because the insulating layer does not completely dominate the electrical characteristics of the device. To a large extent the most appropriate plot must depend on the precise structure of the individual device. This is not too much of a problem because the two exhibit similar behaviour over most of the range.

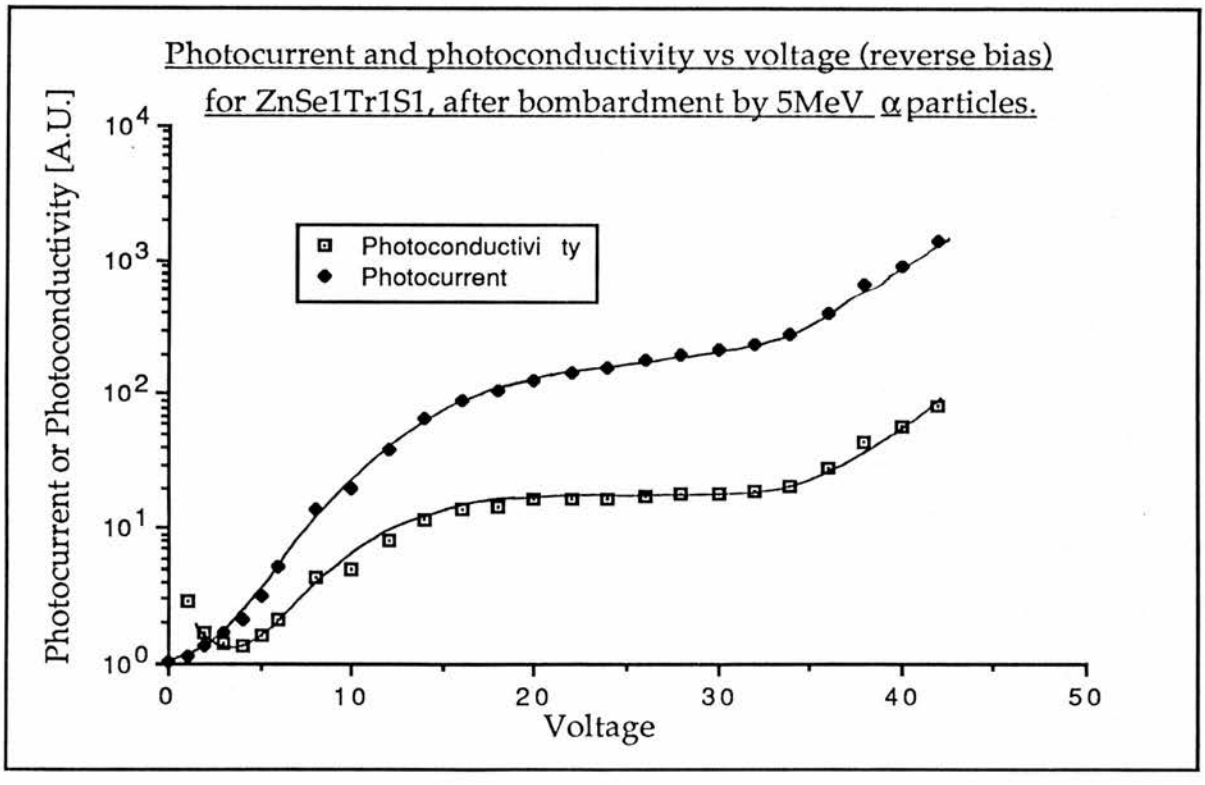

The curve below shows the variation of the quantum efficiency with forward bias, of an MIS device (ZnSe1Tr1S1) operated at 95K,

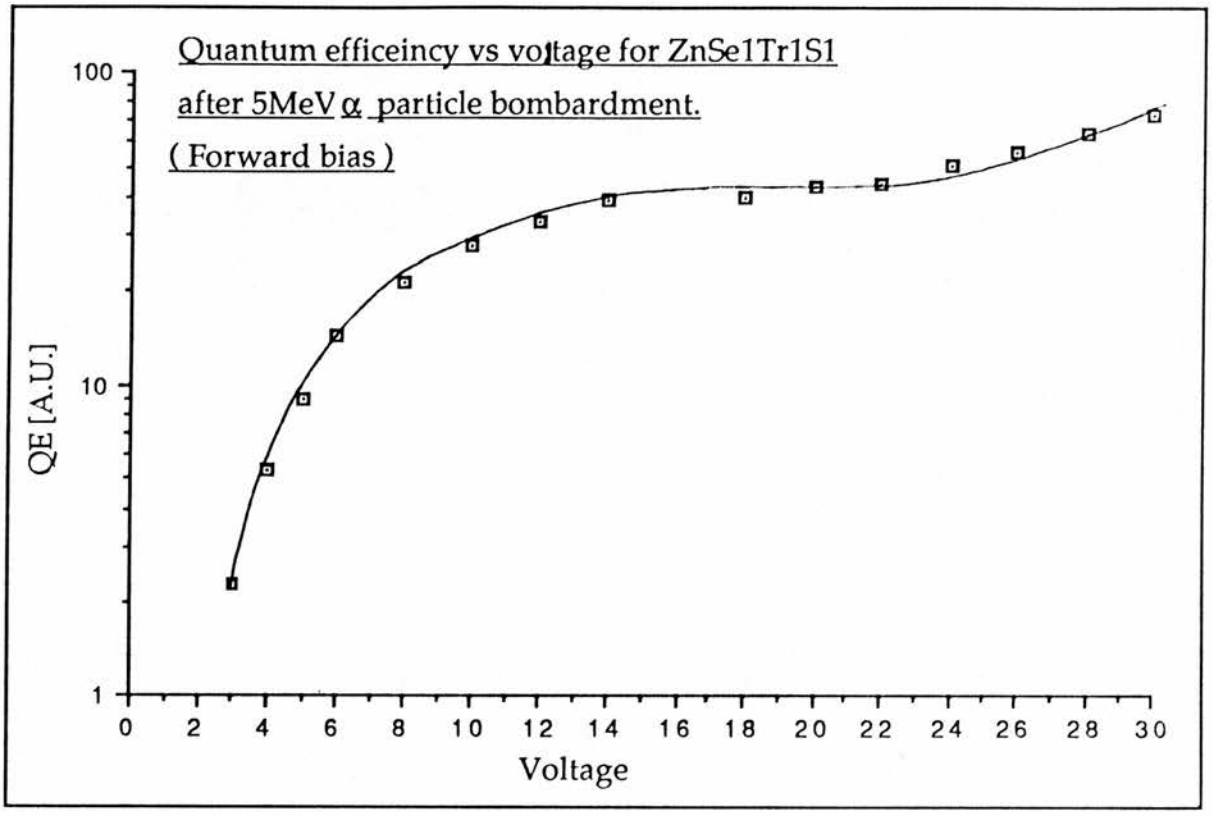

The curve below shows the variation of the quantum efficiency with temperature of the MIS device ZnSe1Tr1S1. The the measurements were taken with constant applied voltage.

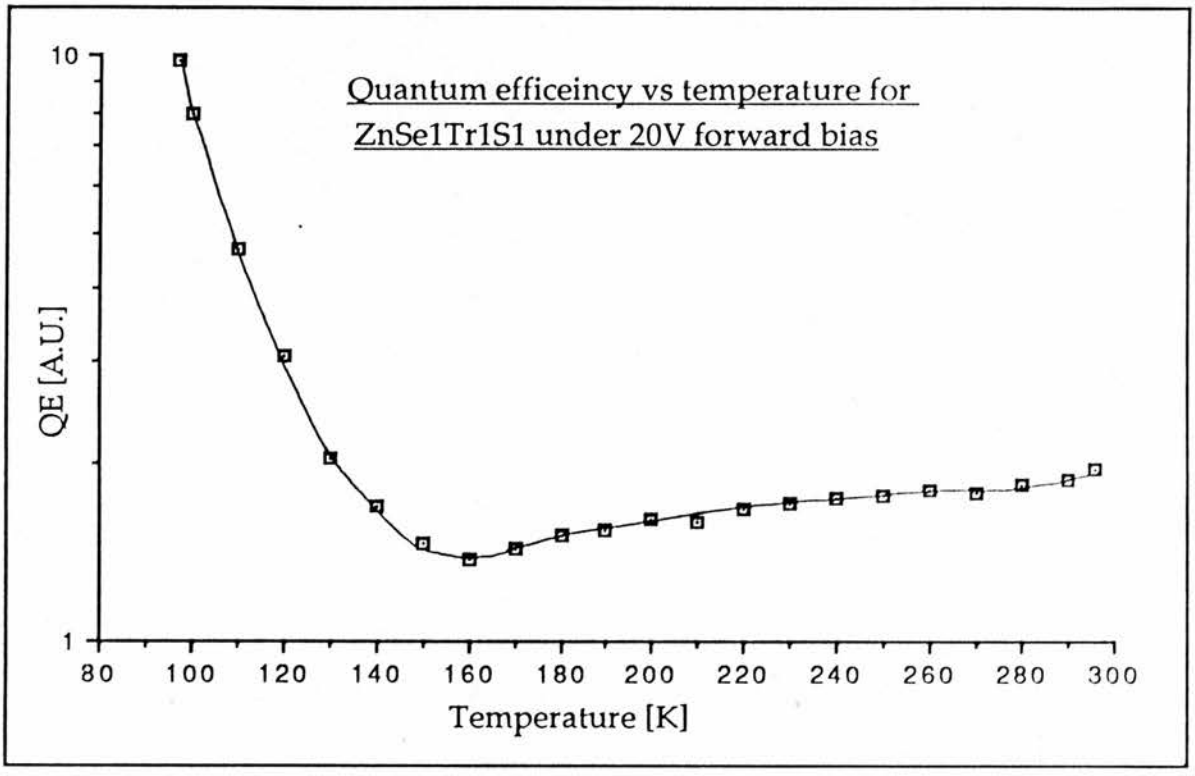

The curve below shows the forward biased emission spectrum of the ZnSe1Tr1S1 MIS device at 100K. The comparatively weak emission meant that the monochromator slits had to be wide and consequently the resolution is not high. There is however, clear evidence of blue emission extending to $h\upsilon = E_g$.

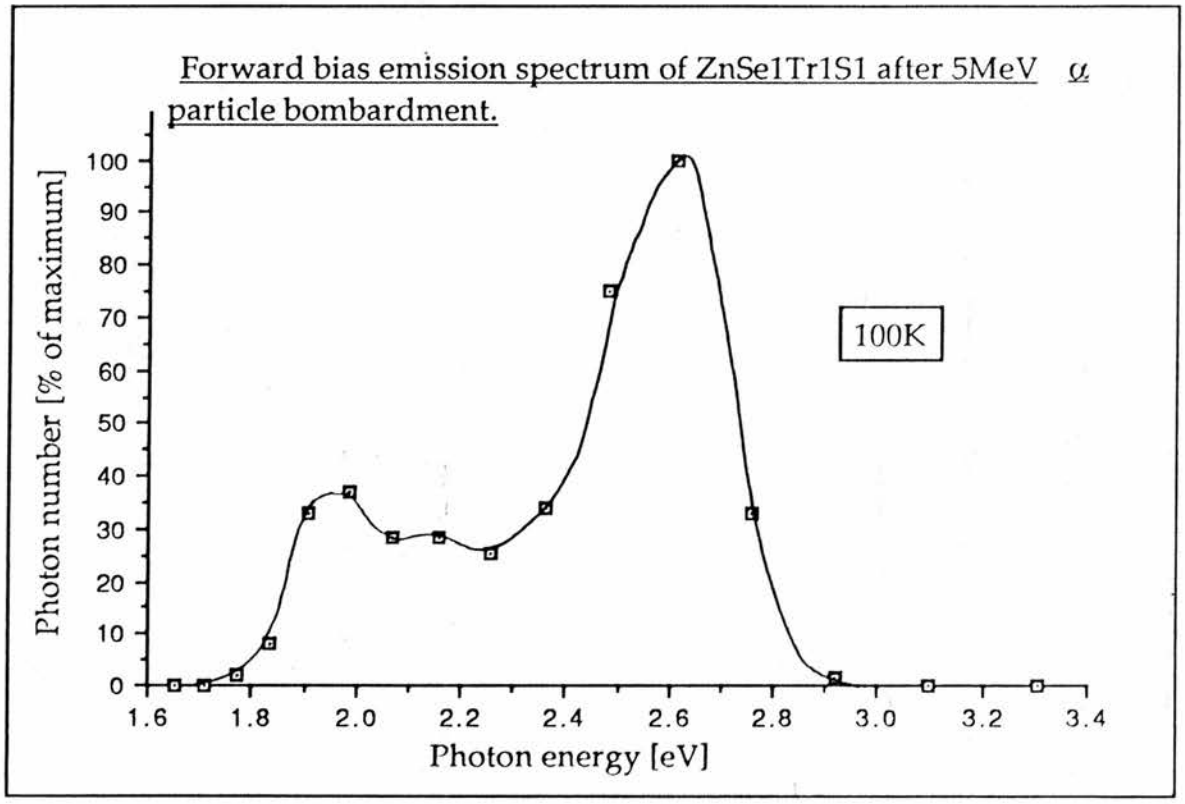

The curve below shows the variation of the photocurrent-voltage characteristic with temperature for the MIS device ZnSe1Tr1S2. (As for ZnSe1Tr1S1 this device was exposed to 5MeV α particle radiation.) The data was taken under reverse bias.

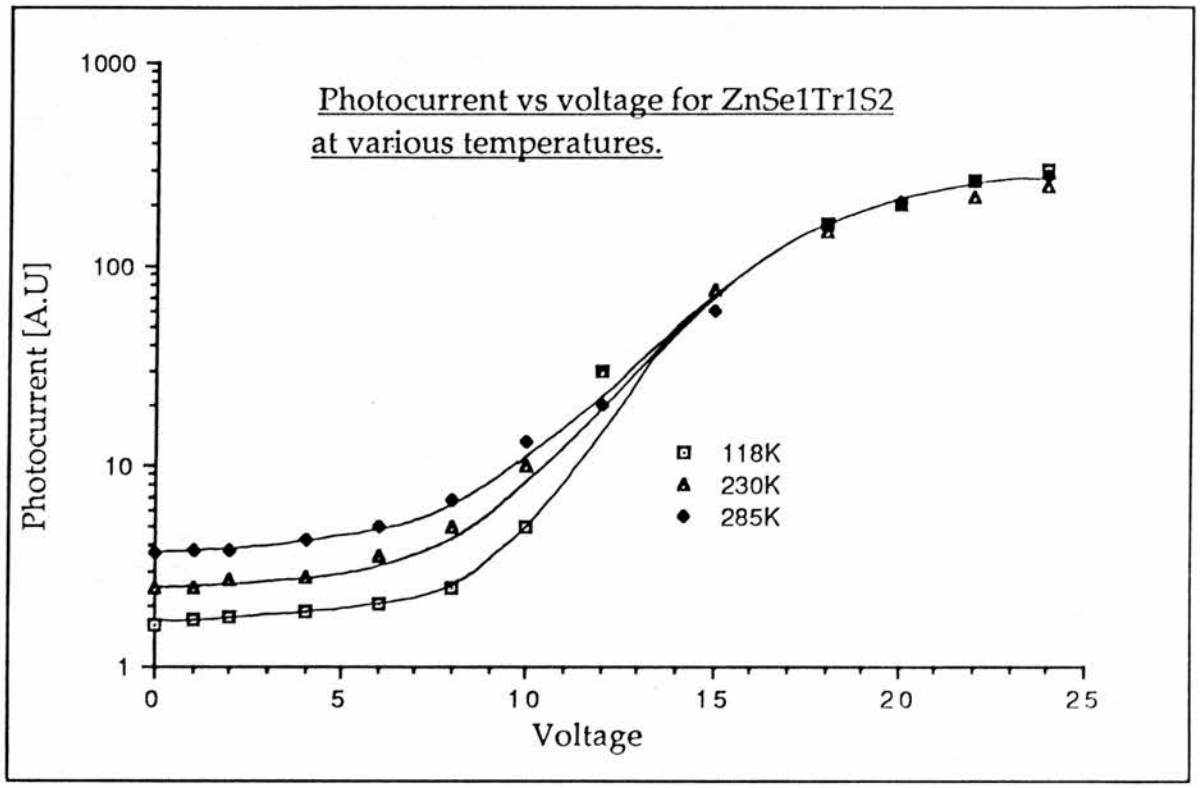

Lighting conditions were identical for each of the separate photocurrent-voltage runs, so that they may be directly compared.

We now move on to the device ZnSe1Tr1S3 produced by 1MeV α particle irradiation. The plot below shows the forward biased emission spectrum for such a device before (curve A) and after (curve B) annealing at 140C for 4 hours. Once again the monochromator band width had to be large so no fine structure is resolved. The spectra were recorded at 100K.

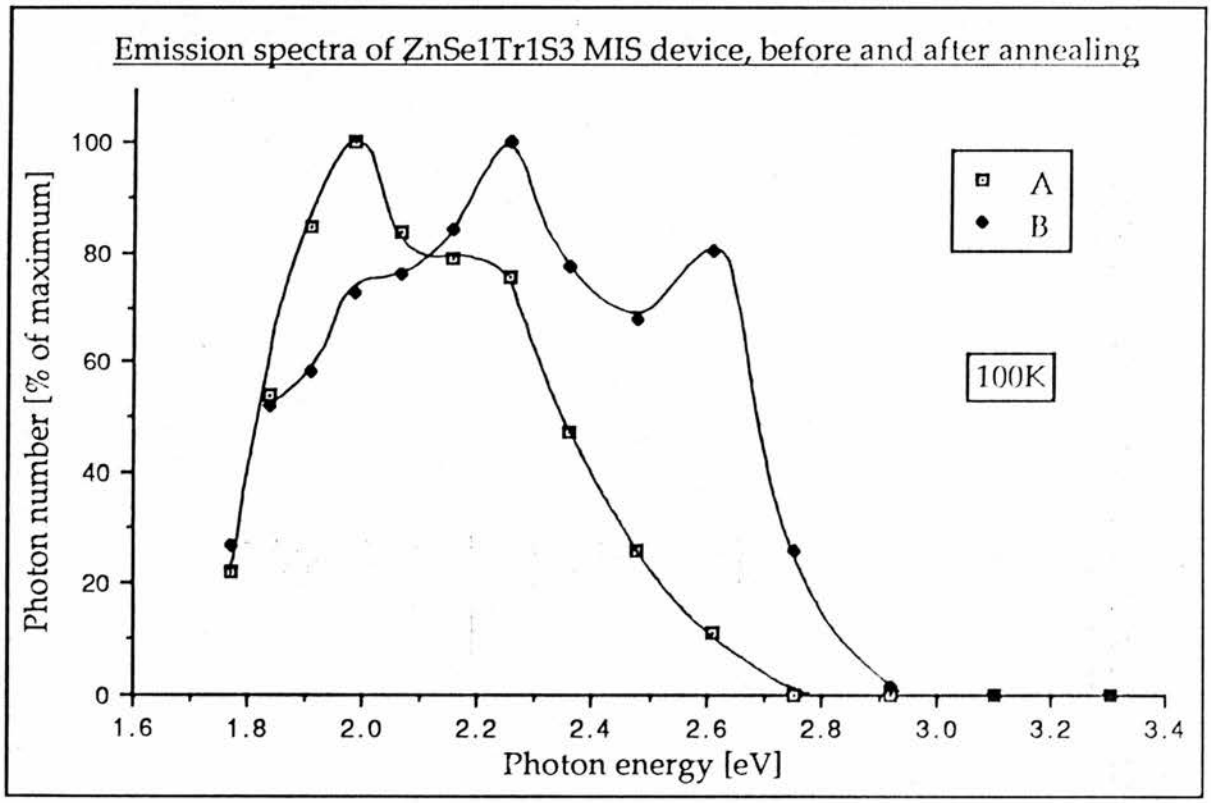

The graph below shows the photocurrent-voltage characteristic of the MIS device ZnSe1Tr1S3 before (curve A) and after (curve B) annealing at 140C for 4 hours. (This is the same device as mentioned on the previous page) The data is for room temperature (295K).

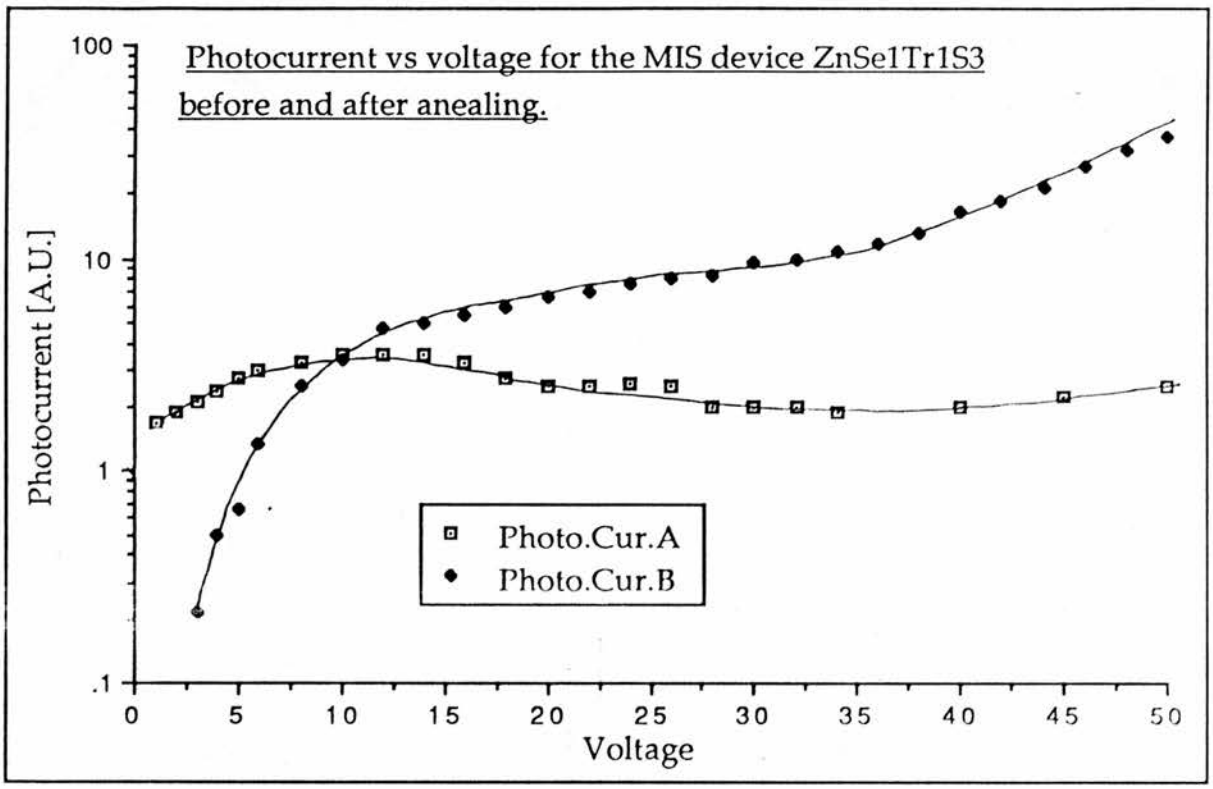

(4) Discussion.

(4.1) Ionisation processes in ZnS thin films.

The photoconductivity-field curves for the D4, D5 and D6 ZnS films all exhibit similar behaviour. The conductivity is approximately constant until $2x10^5 Vcm^{-1}$ (average field) beyond which it begins to rise. At $4x10^5 Vcm^{-1}$ the rise saturates and the conductivity is once again constant until $\sim 10^6 Vcm^{-1}$, where a second rise begins, this time limited only by the failure of the device.

[The D5 film exhibits a slight rise in photoconductivity between $4x10^5 Vcm^{-1}$ and $10^6 Vcm^{-1}$, however photoconductivity can only be taken as an approximate measure of the carrier number, when many other factors, such as bulk conductivity, are involved. The behaviour of this film is thus taken to be qualitatively similar to that of the D4 and D6 devices.]

Evaporated thin films are highly polycrystalline and consequently the electric field distribution within them is not homogeneous. The average field (voltage/thickness) at which an effect is observed in such a film must always be viewed as the minimum threshold field for the effect. In other words although the average value of the field may be say $10^6 Vcm^{-1}$, there may be some regions within the film where the value of E is larger than this. In view of this we believe that the second rise in photoconductivity at $\sim 10^6 Vcm^{-1}$ is due to band-to-band impact ionisation despite the fact that the onset of this effect in ZnS diodes occurs at slightly higher fields ($1.4x10^6 Vcm^{-1}$ to $1.7x\ 10^6 Vcm^{-1}$ (Thompson and Allen[6]).

By comparison to the behaviour of the ZnS diodes, we have attributed the initial rise in the photoconductivity of the films, between $2x10^5 Vcm^{-1}$ and $4x10^5 Vcm^{-1}$, to impurity impact ionisation.The size of the carrier multiplication M due to this impurity impact ionisation (M = 1.2 to 1.5) is very much smaller than was observed in ZnS diodes. There are two possible reasons for this. Firstly the number of impurity centres N_t might be smaller in evaporated films than in the diodes, and if as in the diodes, $M = \exp[N_t \sigma W]$, this would result in a smaller observed multiplication. The second reason that M might be smaller in evaporated films is related to the polycrystalline nature of these films. If a film contains many grain boundaries and major discontinuities, an electron may not be able to fall through the necessary potential drop for an ionising impact, without crossing at least one of these structures. If a significant number of electrons is scattered in crossing, and the scattering energy loss is large, the value of M will be much smaller than for more homogeneous material with the same impurity concentration. We believe that the presence of large scale structural defects is also the reason for the slow rise of the band-to-band multiplication beyond $10^6 Vcm^{-1}$, as compared to that observed in the diodes.

Although impurity impact ionisation is present in the thin films, it is a small effect, and consequently evaporated films do not appear to be particularly good candidates for the insulator in MIS LED's. Better fabrication techniques such as MBE or MOCVD would undoubtedly result

in better quality films, and possibly much higher values of M.

(4.2) MIS devices.

Before discussing the evaporated film and α bombarded MIS devices separately, we consider the operation of a multiplication based LED in more general terms. If the light emission is due to the recombination of injected holes in the n-type material, then,

$$\textbf{Brightness} = \eta_r \times \textbf{hole current} \qquad (1)$$

where η_r is the radiative recombination efficiency. We now consider current continuity in the insulating layer of the MIS device.

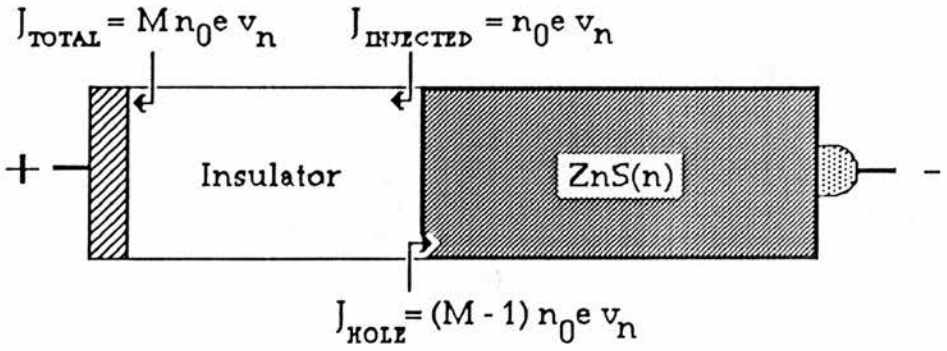

If a constant number of electrons, n_0, are injected at the negative edge of the insulator in unit time, the current at the positive contact will be,

$$J_{TOTAL} = M\, n_0\, e\, v_n \qquad (2)$$

where the symbols have their usual meanings. For current continuity the hole current at the negative contact must be,

$$J_{HOLE} = (M - 1)\, n_0\, e\, v_n. \qquad (3)$$

The quantum efficiency is defined as,

$$\text{QE.} \propto \text{Brightness/Total current} \tag{4}$$

and from (1) brightness = η_r x the hole current, so that,

$$\text{QE.} = \eta_r (M - 1)\, n_0\, e\, v_n / M\, n_0\, e\, v_n. \tag{5}$$

$$\Rightarrow \quad \text{QE} \propto (M - 1)/M. \tag{6}$$

M is a function of field, and consequently of applied voltage. If the multiplication due to impurity impact is of the order of 5, the variation of quantum efficiency with voltage should look something like the sketch below.

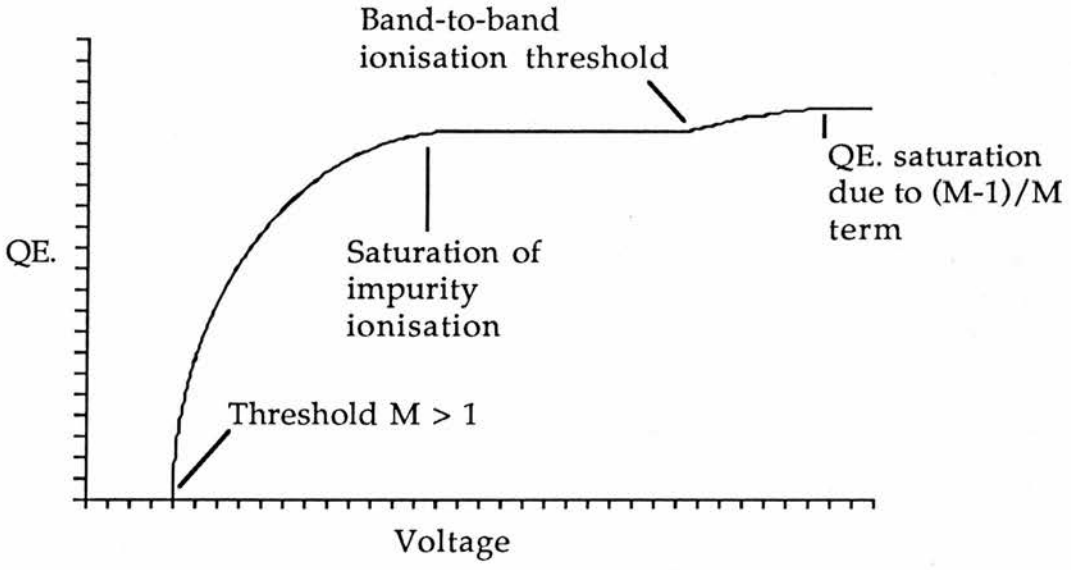

This provides us with a basis for qualitative comparison between the MIS devices we have produced and the theoretical behaviour of the multiplication based MIS LED's we propose.

(4.2a) Evaporated film MIS devices.

Because indium contacts on ZnS exhibit considerable resistance, it was necessary to check that most of the voltage applied to the device

was dropped across the film and not the rear contacts. This was done by means of a probe contact. The results show that despite the large contact resistance almost all of the voltage drop is across the ZnS film.

The emission from these devices was too weak to see at room temperature. At 130K there was a very feeble blue-white emission. Unfortunately this was too weak for a spectrum to be taken. The photoconductivity-voltage curve for the MIS device is different to that for the isolated D6 film, in that, although the threshold voltages for the impurity ionisation are similar, the size of the effect is much larger in the MIS device. The capacitance-voltage plot for this device shows that beyond the insulator there is some residual depletion region, which widens when a reverse bias >20V is applied. Consequently we believe that much of the large rise observed in the photoconductivity-voltage of this device plot beyond ~18V is due to impurity ionisation taking place in this depletion region rather than in the thin film. In forward bias the depletion region will be compressed, so that it should not affect the multiplication process as much. Hole injection in forward bias may thus not be as great as the multiplication measurements imply.

The quantum efficiency-voltage plot shows a threshold for emission around 17V. This is very similar to the threshold for the impurity impact ionisation in this device (18V). The quantum efficiency voltage characteristic has a very steep rise above threshold followed by a rapid saturation. In order to achieve a curve like this with impact ionisation M would have to be very large indeed (of the order of 100). Since we do not

believe this to be the case, we are not able to fully understand the origin of this rapid saturation of the quantum efficiency above 25V in terms of a multiplication process.

The quantum efficiency increases continually with increasing temperature over the range 130K to 260K. If the hole injection mechanism is impact ionisation, one would not expect a variation in η_h with temperature. Consequently this increase in the quantum efficiency with decreasing temperature is believed to be due to an increase in the radiative recombination efficiency.

(4.2b) MIS devices produced by α particle bombardment of ZnSe.

Prior to irradiation, the ZnSe/Al Schottky diodes exhibited very good rectification and the C^{-2}-voltage plots gave intercepts of around 1V, indicating the absence of any significant oxide layer. None of these diodes emitted any visible light in forward bias. Insulating layers were produced by irradiation by 5MeV α particles from a 505μCi curium 244 α source. After 7 days under the α particle source the contact capacitance had dropped to a fraction of its starting value (typically 10pF from 220pF). One of the four sample contacts was covered with a thick metal shield during irradiation to act as a control. The capacitance of this contact did not change during irradiation indicating that the capacitance drop observed in the other contacts is due to radiation, rather than some other process, such as surface oxidation. The reduction of device capacitance is taken as evidence for the formation of a high resistivity layer beneath the Schottky

contacts.

For some samples an aluminium foil absorber was used to attenuate the energy of the incident α particles to around 1MeV. ZnSe samples subjected to this radiation formed highly insulating layers in only two days. When operated in forward bias the "5MeV" devices emitted blue light whilst the "1MeV" diodes produced yellow light.

The insulating layer thickness can be estimated by the zero bias capacitance of the device. In the case of the "1MeV" devices this was ~ $5x10^{-4}$cm, which is very close to the expected range of the α particles in ZnSe ($4x10^{-4}$cm). [The range of the α particles in ZnSe was estimated from that in similar materials such as silicon and aluminium. (Watt[55])] For the "5MeV" diodes the insulating layer thickness was less than half of that on the "1MeV" devices despite the fact that the more energetic particles have almost five times the range. Other workers have found that if ZnSe is bombarded by electrons of comparable energy, zinc vacancies are produced (Watkins[56]), At room temperature these vacancies are immobile[56]. The resulting interstitial zinc is however, highly mobile at room temperature and could migrate to the surface[56]. However, interstitial zinc in ZnSe resides in the form of the double donor Zn^{++}[56], and thus it is hard to envisage that an accumulation of this could produce an insulating layer. At present we do not understand the precise mechanism of the formation of this layer. However, since its thickness is sometimes significantly less than the range of the α particles,

defect migration might be expected to play an important role. The nature of the defect involved is not known, but it is unlikely to be isolated interstitial zinc or an isolated zinc vacancy.

The experimental results for the "5MeV" devices are more easily interpreted than those for the "1MeV" diodes, for this reason we focus our initial attention on these devices and in particular ZnSe1Tr1S1.

Because of the instability and comparatively weak emission from the diodes, the monochromator used to record the emission spectra had to have a large bandwidth, consequently the spectra do not resolve any fine features. The low temperature emission spectrum is dominated by a blue peak centring on ~2.6eV. This is believed to be due to radiative recombination of excitons. In addition to this there is a peak at ~1.95eV and some evidence of a third peak at approximately 2.2eV. The origin of the two lower energy peaks must be associated with luminescent impurity centres, light being emitted either as a result of electron impact excitation in the insulator or radiative hole recombination at a centre. The most important information we can derive from the emission spectrum is that the majority of the light from these diodes is produced as a result of hole injection into the bulk material.

The reverse bias photocurrent curve shows an increase above a low voltage threshold followed by a second increase at higher voltages. By comparison to the ZnS diodes, the results of Livingstone[35] for ZnSe and our thin film work, we attribute these two rises to impurity impact and band-to-band ionisation respectively. The observed threshold for the

initial rise is ~5V. This coupled with an estimated layer thickness of $1.5x10^{-4}$ cm yields an average electric field of ~$4x10^{-4}$ Vcm^{-1}. Although a little lower than expected this is of the right order for an impurity impact ionisation process, particularly since the field distribution is probably highly inhomogenous in these MIS devices. The multiplication from the impurity impact process is considerably bigger than was observed in the thin films, this is probably due to the absence of grain boundaries and the large number of defect centres produced by the irradiation.

The quantum efficiency voltage curve has a very similar shape to the sketch of the expected behaviour of such a plot for a multiplication based hole injection mechanism (see 5.1b). The capacitance voltage plot shows that, as for the ZnS MIS devices, there is still some residual depletion region in reverse bias. One would thus expect the threshold voltage for a high field process in reverse bias to be larger than that in forward bias. For this reason it is not valid to compare the photocurrent-voltage and quantum efficiency-voltage results on the same voltage scale.There are however, striking similarities between the two. The threshold for light emission in forward bias is ~3V. This is a sufficient potential drop for some of the electrons to gain enough energy to impact ionise a centre of ~2eV below the conduction band. (2eV is a value we have taken from our ZnS results, in ZnSe similar centres may be shallower than this). This is also very close to the threshold for impurity multiplication (~4V) as one would expect. Furthermore at high voltages, probably due to the onset of band-to-band impact ionisation, the quantum efficiency once again

increases. However due to the "saturation" of the (M-1)/M term this rise in the quantum efficiency is very much smaller than the corresponding rise in the photocurrent.

One final aspect of the behaviour of these devices worthy of consideration is the variation of the emission with temperature. The photocurrent voltage curve for ZnSe1Tr1S2 (also exposed to 5MeV α particles) shows that above 12 volts the photocurrent is not temperature dependent. At lower voltages there is a small decrease in photocurrent as the temperature is lowered. One would not expect an ionisation process involving hot electrons to be dependent on the host lattice temperature. The low voltage decrease in the photocurrent with decreasing temperature is interpreted as trapping and recombination of the optically created electron hole pairs, possibly at the crystal surface. As the voltage is increased the carriers move more quickly and this mechanism becomes ineffective. In general there are no significant differences between the photocurrent-voltage curves taken at different temperatures. Qualitative comparison of room temperature multiplication measurements with low temperature quantum efficiency measurements thus seems justified.

If the multiplication, and consequently the injection efficiency, is independent of temperature, the increase in quantum efficiency below 160K must be a result of an increased radiative recombination efficiency at these temperatures. The cause of the slight decrease in quantum efficiency from room temperature to 160K is unclear. It is however, possible that this is due to quenching of one of the other (yellow or red) components in the

emission.

We now consider the "1MeV" devices. After the insulating layer is produced, the emission spectrum shows no clear evidence of exciton emission. The corresponding photocurrent-voltage curve is strange but shows no convincing multiplication effects at all. We believe that multiplication does take place in the insulating layer of these devices, but that the free holes produced are trapped by additional defect centres within the insulator. The trapped holes may then recombine sometimes radiatevley with electrons resulting in the yellow-red emissions observed. No net multiplication should be observed for such a system, and very few holes should be injected into the bulk material to produce exciton emission. This is consistent with observation. In an attempt to reduce the concentration of the trapping centres the MIS device was annealed at 400K for 4 hours under 10% hydrogen/nitrogen. This process caused significant oxidation of the contacts, so the sample was etched in caustic soda and the contacts were replaced. Capacitance measurements confirmed the insulating layer had not been removed by this process. After annealing the photocurrent shows a slight rise with increasing reverse bias indicating that some net multiplication is occurring in the insulator. A small exciton emission peak also appears in the spectrum. It is interesting to note that the low energy peaks which dominate emission from the "1MeV" devices (1.97eV & 2.25eV) have very similar energies to the low energy emissions in the "5MeV" devices (1.95 & 2.2eV). It is thus possible that the residual yellow emission in the "5MeV" devices is also due to trapping losses at

similar centres.

(4.3) Some reports of forward bias emission in ZnS & ZnSe from the literature.

Within the scope of this discussion it is impossible to consider every report of light emission from ZnSe and ZnS MIS diodes, we have thus chosen representative work, from which we can derive useful information.

(4.3a) ZnSe/ZnO MIS devices.

Exciton electroluminescence has been observed from forward biased ZnSe MIS diodes made with a chemically produced oxide layer (Ryall & Allen[57]). Livingstone & Allen[60] observe a threshold for luminescence in such devices at 1.3V forward bias. Immediately this alone would appear to preclude an ionisation based hole injection mechanism. In addition to this the quantum efficiency-voltage characteristic of these diodes is totally dissimilar to that expected for a multiplication based device. Livingstone & Allen[60] propose an electroluminescence mechanism involving hole injection from around or above the metal Fermi level into the semiconductor valence band. This is more consistent with their experimental data than the ionisation model. Lawther & Woods[58] have observed yellow emission from similar chemically produced oxide layer ZnSe devices. They report a threshold for the emission of 1.08V. Since this is considerably less than $E_g/2$ for ZnO a two stage impact ionisation electroluminescence mechanism would also seem out of the question in these devices. We conclude that the light emission from these ZnSe/ZnO

MIS diodes is unlikely to involve impurity impact ionisation.

(4.3b) ZnSe/ZnS MIS diodes.

Fan & Woods[54] have observed blue exciton electroluminescence in forward bias for a MIS structure with a 2000Å ZnS layer grown by electron beam deposition on a ZnSe substrate. It is possible that Fan & Woods have superior growth conditions to ours, and that their films contain fewer major discontinuities. Consequently, scattering of the hot electrons within such a layer might not hinder multiplication. If this is the case and there are sufficient deep centres within the film, impurity impact ionisation might be expected to attain significant levels. Later work by Fan et al[59] discusses the spatial distribution of the blue electroluminescence. This appears to be localised in many small spots. It is possible that most of the holes (however they are produced) are lost in non-radiative recombination processes at the materials boundary. Bright spots may occur near areas where the two materials have a good interface so that holes may cross into the bulk without significant loss.

In the absence of more detailed information, in particular a quantum efficiency voltage plot, it is difficult to investigate the possibility that these devices operate by impact ionisation, any further.

(4.3c) ZnS based MIS devices.

Lukyanchikova et al[20] report blue light emission from ZnS MIS devices with a variety of insulators. This luminescence is seen when polythene and gelatine up to 30,000Å thick form the insulator as well as with layers of ZnS and SiO. It is hard to imagine that polythene might

exhibit similar behaviour to SiO or ZnS when used in an MIS diode. However, the authors mention that light emission from their ZnS MS diodes is weaker than their ZnS/ZnS(n) MIS diodes. Most authors believe (and most of the proposed theoretical models require) an insulating layer of some kind between the metal and the semiconductor in order to observe light emission at all in forward bias. We therefore suspect that there is a layer of oxide on the surface of their ZnS so that what is referred to as an MS diode in in reality a MIS diode with an oxide insulator. This would explain the emission in forward bias. We further suspect that the polythene layers contain pin holes (although the authors specifically claim that this is not the case) so that it is the behaviour of a ZnS/ZnO diode, not a ZnS/polythene diode, that is observed. The threshold for the emission from these structures is 1.7V. The situation thus appears analogous to that in ZnSe/ZnO MIS structures reported by Livingstone et al. Lawther & Woods[58] report blue emission from forward biased ZnS/ZnS(n) MIS diodes produced by electron beam deposition. The quantum efficiency of these devices is constant from the threshold ~2V to currents several orders of magnitude larger than that at threshold. A mechanism other than ionisation would thus appear to be responsible for the hole injection in their devices. The authors proposed an Auger process, where an energetic electron leaving the conduction band of the semiconductor enters the metal and excites a second electron leaving a free hole in the metal. This hole is then believed to enter the semiconductor valence band. There are however, serious problems

associated with this argument. The life time of a free hole in a metal is very short, in order for there to be significant injection, the free holes would have to move out of the metal into the insulator very quickly. Since there is no electric field in the metal it is hard to imagine why a significant number of holes should move towards the junction.

Katayama et al[19] report blue emission from ZnS/ZnS(n) MIS diodes with quantum efficiencies of 1.5×10^{-3} at 77K. Insulating layers were made by annealing under vacuum, so that the lattice match from the insulating ZnS to the bulk ZnS(n) should be very good. Our measurements on ZnS have led us to believe that the concentration of deep impurities N_t is sufficiently high for significant impurity impact ionisation to take place. The threshold for this emission is 5V, which is enough for ionisation to begin. However, the quantum efficiency of these devices is constant with current over the range 10^{-4}A to 5×10^{-2}A, which at first sight does not appear to be consistent with an ionisation based injection mechanism. However, if one refers to the current-voltage plot for these devices, one can see that although the quantum efficiency has been measured over a considerable range of current, the corresponding voltage range is very small. The constant quantum efficiency is in fact only maintained over the range ~14V* to ~22V, despite the 5V threshold quoted for emission. If the variation of M with voltage in these devices is similar to the sketch overleaf,

* The author has not provided an I-V plot for the particular diode from which the quantum efficiency current data is taken. Instead, two typical I-V charicteristics are provided for the devices. One implies a voltage range of 8 to 22V, the other 20 to 22V. 14 to 22V is quoted as an average of the two.

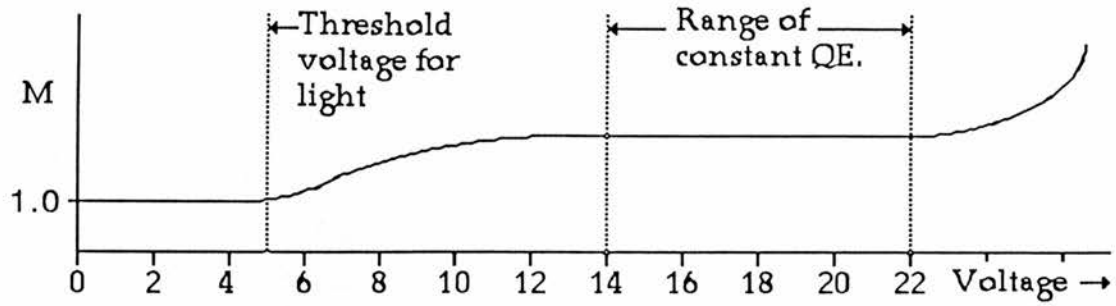

the results are consistent with our impact ionisation model.

If the overall efficiency, η_{TOTAL}, is 1.5×10^{-3}, and if η_{ie} is taken as ~0.15, the product $\eta_h \eta_r$ must be ~1%. The diodes are not deliberately doped with luminescent centres, so the radiative recombination efficiency might not be expected to be very high. (Blue emission in ZnS MIS diodes fabricated in this way has been attributed to donor-accoptor pairs comprising aluminium donors and Al/Zn vacancy acceptors (Katayama[19]).) This would imply a large hole injection efficiency, which is also consistent with an ionisation process.

(5) Conclusions.

In order to achieve efficient luminescence from a multiplication based MIS device three conditions must be satisfied.

(1) There must be a large net multiplication in the insulating layer.
(2) There must be very little non-radiative recombination loss at the insulator-semiconductor interface.
(3) The radiative recombination efficiency in the semiconductor must be large.

The evaporated film based Ew1Tr2S2/D6 devices failed because the poor quality polycrystalline nature of the film means that M is small so (1) is not satisfied. Furthermore, the emission from this device was spatially inhomogeneous, this effect is common in deposited film devices. For example Fan et al[59], report similar inhomogeneity of electroluminescence in electron beam deposited ZnS/ZnSe(n) MIS devices.We believe that there are usually large non-radiative hole losses at the interface in such deposited film devices. This problem might be overcome by using a high quality growth technique such as MBE or MOCVD and retaining the same material in the film as the substrate so that a lattice match can be achieved. Finally our ZnS(n) substrates do not exhibit visible photoluminescence when excitation light of $h\upsilon > E_g$ is used. One might thus expect that there are very few of the optically produced electron hole pairs recombining radiatively at luminescent centres. In

view of the failure of these devices to satisfy any of the above three conditions their disappointing luminescence might be expected.

The α particle bombarded ZnSe devices exhibit multiplication in the insulating layer, however, there is evidence that recombination loss is also present so that a large net value of M is not guaranteed. Since the insulator should have a reasonably continuous lattice with the semiconductor, condition (2) can be assumed to be satisfied. This idea is supported by the observation of spatially homogeneous electroluminescence in these and similar devices. We believe that the efficiency of our ZnSe devices is principally limited by the low efficiency of the radiative recombination in the bulk material. (Once again there is no significant photoluminescence when excitation light of $h\upsilon > E_g$ is used). This situation might be improved changing the impurity centres that are present in the crystal, so that non-radiative recombination is minimised.

We propose that the best candidate for an efficient device might be ZnS on ZnS(n) produced either by radiation damage or annealing (Katayama[19]). This would have large multiplication and low interface losses. The substrate crystal must be doped with an optimum concentration of efficient hole trapping luminescent centres. In this way very large efficiencies might be achieved.

Finally it is worth considering the following question. Why, when moderately bright, blue ZnS MIS LED's have been reported in the literature for over a decade now, are none in commercial production? The answer to this is two fold. Firstly, with present fabrication techniques,

there is very little consistency in production. In other words only a few diodes in a large batch may be anywhere near as efficient as the ones reported in the literature. A better understanding of the processes associated with light emission should help to improve this situation considerably. The second problem lies with the durability of the devices. From our experience, with present contact technology it is difficult to maintain a stable DC current flow through the contacts for a prolonged period without device deterioration. Continual improvements in the technology of making contacts to II-VI compounds might soon overcome this difficulty, particularly if there is the incentive of efficient ZnS LED's with multi-colour emission.

Chapter 5

The origin and time dependency of the photoluminescence emissions of ZnS:Te

(1) Introduction.

Under suitable circumstances the introduction of a substitutional isovalent impurity into a semiconductor can produce a localised trapping level[61]. Examples of this include nitrogen in GaP and tellurium in CdS. In 1968 Cuthbert & Thomas[62] produced experimental evidence for the presence of such a trapping level in CdS doped with tellurium. They also discovered that as the concentration of tellurium was increased, a second, lower energy level produces a new luminescence peak. They have attributed this to an exciton binding level formed by tellurium doublets on nearest neighbour cation sites. In 1969 Iseler & Strauss[13] reported the observation of such luminescence in ZnS:Te. At high tellurium concentrations they too observed a second lower energy peak, which by analogy to the work of Cuthbert & Thomas they believed to be also due to tellurium doublets. At very high tellurium concentrations (>3%) Heimbrodt & Goede[63] observed a still lower energy peak which they believe to be due to complexes of three tellurium atoms.

Some of the luminescent emissions from ZnS:Te are reported to have large quantum efficiencies even at room temperature, and consequently there would appear to be considerable potential in such materials for device manufacture. Our initial interest in the ZnS:Te system was as a possible substrate for the MIS LED's described in chapter 4. Tellurium substituted for sulphur in ZnS produces a hole trapping level, but the empty centre has little affinity for electrons. If used as the substrate for a

minority carrier injection MIS LED this material would, under suitable conditions, trap a significant proportion of the injected holes. Once a hole is bound to a tellurium site there is a strong Coulomb attraction for electrons. Since the substrate in these devices is n-type there are plenty of free electrons available to bind to such trapped holes and form excitons. Radiative recombination of these excitons might very probably result in efficient light emission. Tellurium singlets have a characteristic violet emission (395nm) which could be used to produce violet LED's. However, the emission is quenched above 200K so room temperature operation would be highly inefficient. When the tellurium concentration is increased, the singlet emission disappears and is replaced by a lower energy blue peak which several authors believe to be due to tellurium doublets[13][63][64]. This blue emission remains essentially unquenched up to around 300K. If such an emission really is due to tellurium doublets, these might also act as hole traps in the MIS devices, giving rise to efficient blue electroluminescence, even at room temperature.

Previous work on ZnS:Te has concentrated on powder samples and ion-implanted single crystals. We have grown ZnS:Te crystals in this laboratory, although unfortunately the material was of insufficient quality for device production. It was however possible to isolate small (~2mm side) single crystals of ZnS:Te from this material on which we were able to perform some optical experiments. The crystals were found to exhibit weak green/blue photoluminescence at room temperature, under

excitations with $h\upsilon > E_g$. This is evidence that free electrons and holes can recombine radiatively at centres within the material which means that it might be a suitable substrate for hole injection based MIS devices. As a control, experiments were also performed on nominally undoped vapour transport grown Ew1 ZnS, and this has highlighted a problem. Under both 365nm and 297nm excitation the photoluminescence emission from the Ew1 ZnS was found to be very similar to that from the ZnS:Te material. This coupled with other observations has led us to believe that the blue emission band in our ZnS:Te is probably due to the well known self activated centre rather than tellurium complexes. Subsequent examination of the literature has revealed some degree of ambiguity associated with the attribution of the blue emission in ZnS:Te to tellurium pairs. In fact, in the case of some reports there is more evidence to support the idea of the emission being due to a donor acceptor pair than a tellurium complex.

During the course of this work, it was noticed that under 365nm excitation the photoluminescence of both materials took a considerable time (~20 seconds) to build up. Since this might have significant consequences for electroluminescence an investigation of the ZnS:Te system and its time dependence was undertaken. The build up of the photoluminescence with time, at various wavelengths and intensities, was investigated, and on the basis of this and some other simple thermoluminescence observations we have proposed a qualitative

model for this process. This involves the ionisation of the luminescent centres and subsequent trapping of the free electrons by an electrically neutral centre or complex within the energy gap.

(2) Experimental methods.

(2.1) Sample mounting and cryogenics.

The ZnS samples were mounted on a specially constructed cold finger in a Thor continuous flow cryostat. The crystals were secured to the metal with black nail varnish. Although this seems a strange material to use, it was found to exhibit no visible fluorescence under 365nm or 297nm excitation, whereas conventional materials such as GE varnish do give a slight emission. In addition to this the varnish is rapid drying and does not out-gas when the cryostat is pumped down. Cementing of the samples to the cold finger is preferred to mechanical fixing because it produces a better thermal contact. A diagram of the sample mounting and coldfinger is shown below.

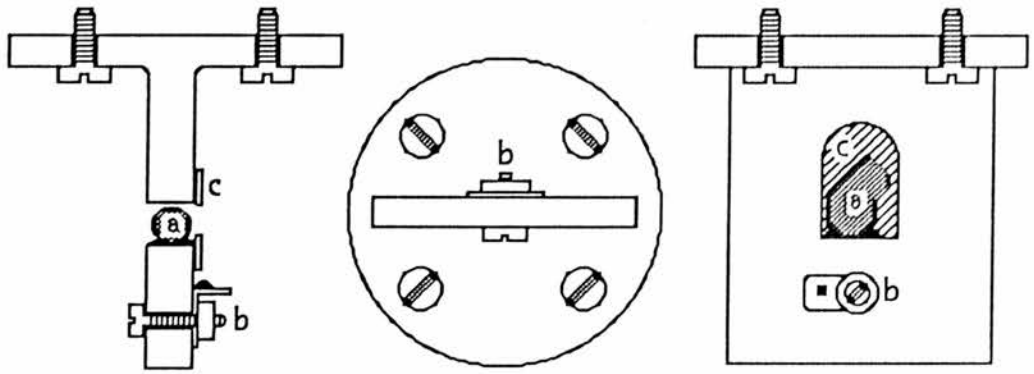

[a].. Sample [b].. Thermocouple [c].. Light baffle

Liquid nitrogen was used as the cryogen. Temperature control was achieved using a Control & Readout Ltd. 405 temperature controller coupled to the cryostat internal heater. Temperature was monitored with a copper/eureka thermocouple which had its cold junction secured to the

cold finger.

(2.2) Photoluminescence spectra.

The light source for the photoluminescence experiment was a Hanovia UV-100 water-cooled mercury arc lamp. This was fitted with an internal optical system producing a fine focus outside the lamp. The lamp emission consisted of a broad background on which were superimposed 365nm,313nm and 297nm spectral lines. The lamp was focused into a Bausch & Lomb high efficiency monochromator to isolate the appropriate spectral line. The resulting ultraviolet beam was directed at one side of the sample via one of the cryostat quartz windows. The emission light from the sample left the cryostat via the opposite window and was mechanically chopped by a Bentham 218 chopper unit. Light baffles were used to eliminate excitation light which had not passed through the sample since this contains some residual visual components which limit the sensitivity of the experiment. The chopped light emerging from the cryostat was focused into a Zeiss single prism monochromator. (This was chosen in preference to grating monochromators of higher efficiency and resolution, because of its absence of second orders.) A photomultiplier with an S-20 response was used as a detector. The signal from the photomultiplier was measured on a lock-in amplifier, which took a reference from the chopper. The emission intensity at each wavelength was recorded manually. The emission spectra were corrected for the photomultiplier response using the manufacturers data.

In order to investigate the variation of the emission spectrum with

intensity, a series of neutral density filters were inserted into the ultraviolet light path These took the form of wire grids and consequently had to be located away from focal planes. The optical density of these grids was measured for the visible wavelengths with a silicon light meter and a tungsten lamp.

The diagram below shows the general experimental arrangement.

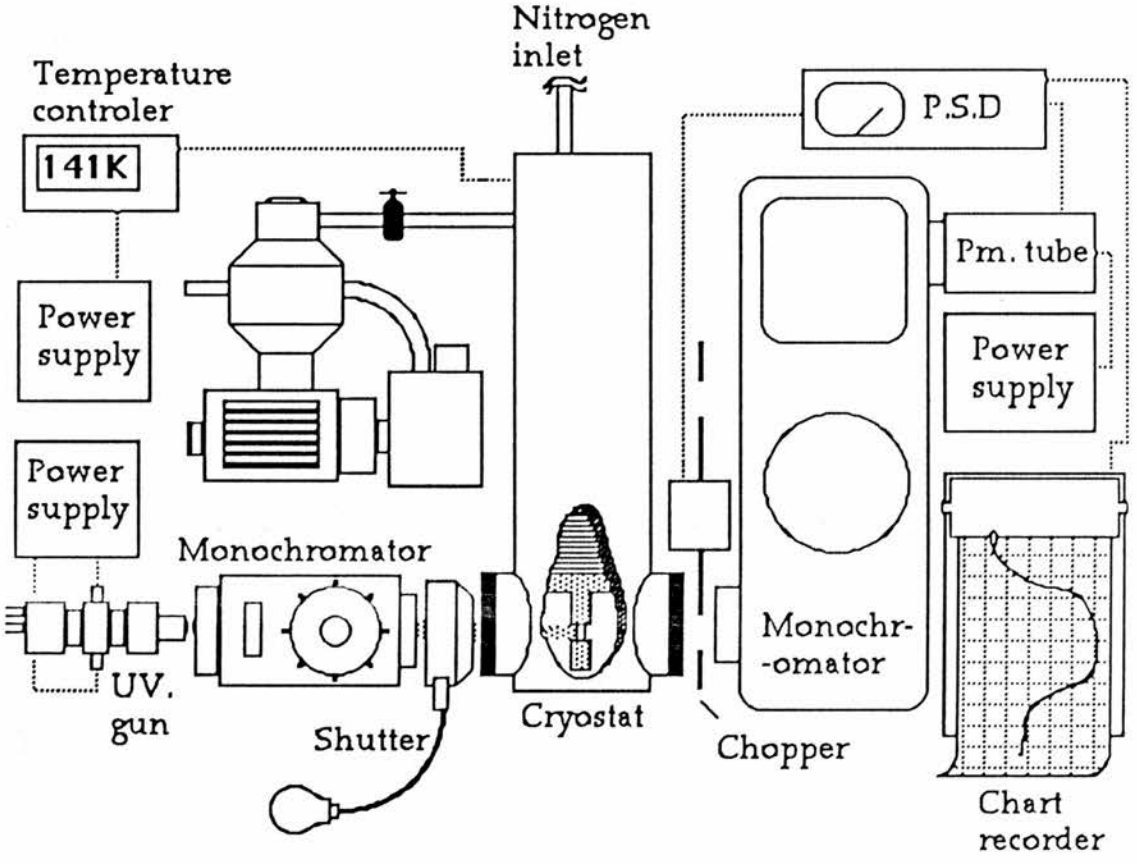

(2.3) Measurement of the time variance of the emission.

The Zeiss monochromator was retained during the time dependence measurements so that we were able to isolate the time variance of individual parts of the emission spectrum. The samples were mounted on

the cryostat coldfinger in the usual way. During this experiment the ultraviolet light beam was interrupted by a camera shutter resulting in a fast (<1ms) turn-on time. Initially the phase sensitive detection system was removed in order to minimise the system response time. However the output signal proved to be excessively noisy when the system was operated DC. Subsequently the chopper and lock-in amplifier were replaced. The response time of the system was minimised by increasing the chopping frequency to its maximum value of 500Hz, and setting the external time constant of the lock-in amplifier to its minimum value of 10ms. The system response time was tested by setting the two monochromators to the 546nm mercury line (which passes through the sample unhindered) and measuring the variation of the output signal with time. This is a good way of assessing the system response because the experimental arrangement remains unchanged. The system response was found to be much faster than any of the photoluminescence build up times that were recorded with the 365nm excitation. With both monochromators set to 365nm, it was also possible to investigate any time dependence of the sample absorption.

The variation of the photoluminescence rise time with excitation intensity was investigated by inserting wire grid neutral density filters into the ultra violet light path.

(2.4) Thermoluminescence.

Both the Ew1 and the ZnS:Te material exhibited bright thermoluminescence. A brief qualitative assessment was made of this.

Samples were immersed in a liquid nitrogen bath which was placed under a 365nm lamp. After 30s, the samples were removed from the nitrogen and placed on a large metal block which was at room temperature. As the samples warmed up they emitted a comparatively intense light. If one watched the process through Wratten filters one could see that the light emission from the ZnS:Te had significant components in the blue (corresponding to the 2.6eV peak) and the red (corresponding to the 1.9eV peak). The Ew1 material showed significant emission in the blue (corresponding to the 2.6eV peak), and the yellow/green (corresponding to the 2.3eV peak).

(3) Results.

Unless otherwise stated, all the spectra presented in this section are corrected for the photomultiplier response using the manufacturers data.

(3.1) The nature of the emissions.

The two graphs overleaf show the photoluminescence emission spectrum of the ZnS:Te (S1) material. The upper graph (Fig.1.) is for 297nm excitation and the lower graph (Fig.2.) is for 365nm excitation. The spectra were recorded at 5 temperatures ranging from room temperature to ~100K. The excitation intensity was identical for the five temperatures within each plot, as was the experimental geometry. Thus the five curves on each plot are directly comparable with each other. There is however no correlation between the intensity of the upper and lower plots.

Spectra were recorded for increasing wavelength. At the end of each run back checks were made to ensure that there was no significant drift in the emission.

Fig 1. Photoluminescence emission spectrum of ZnS:Te (S1) when excited by 297nm light. (5 temperatures).

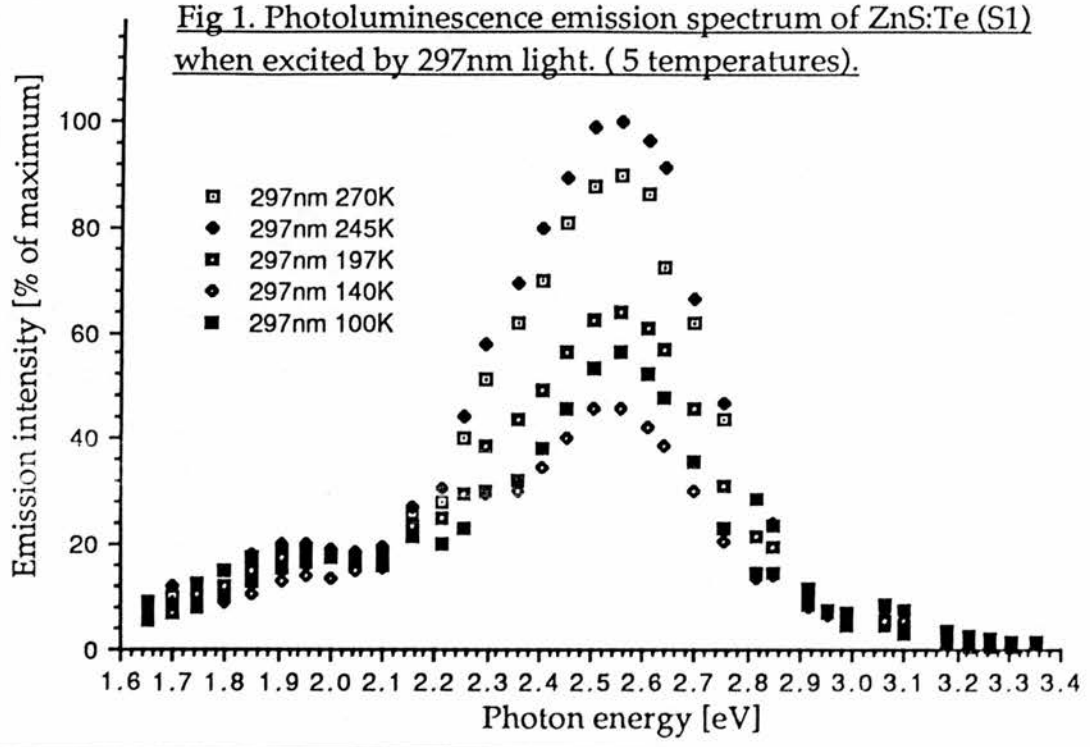

Fig.2. Photoluminescence emission spectrum of ZnS:Te (S1) when excited by 365nm light. (5 temperatures).

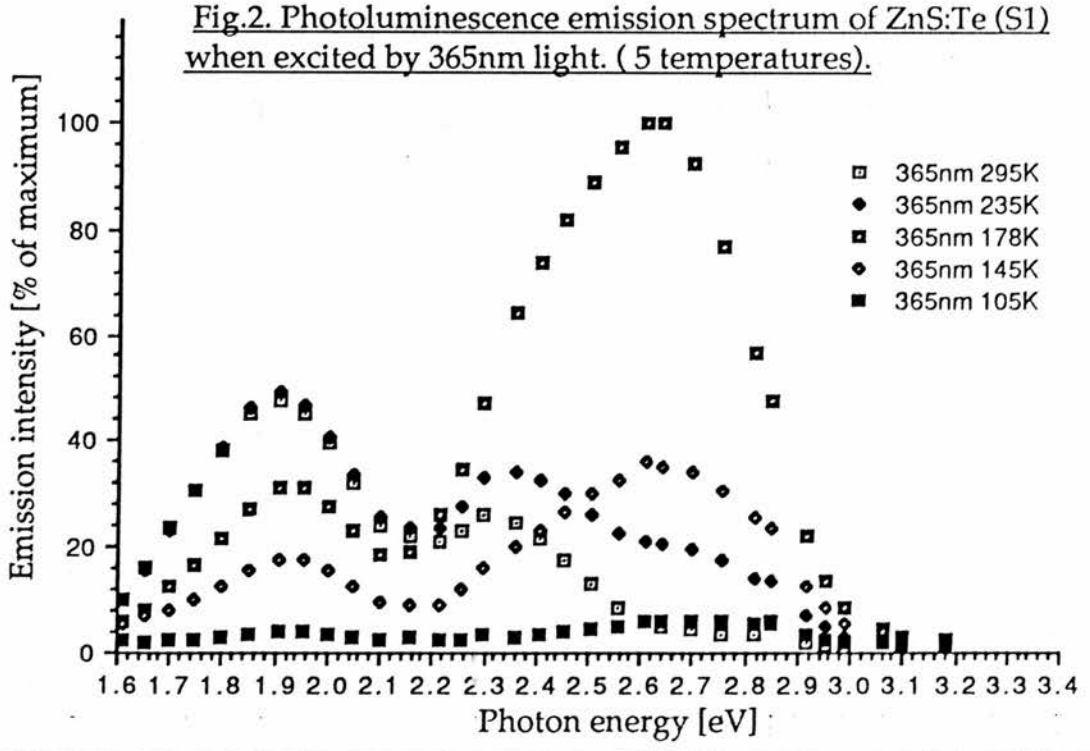

The two graphs overleaf (Fig.3 and Fig. 4) show the photoluminescence emission spectrum of Ew1 ZnS under 365nm and 297nm excitation respectively. The "365nm" spectrum was recorded at three different temperatures and once again the units on the ordinate are consistent for each curve. The shape of the sample was such that quite a large amount of the excitation light passed straight through into the monochromator. As a consequence of this there are some mercury lines superimposed on the spectrum. The energies of the three principal contaminant lines are marked on the graph.

Initially the sample Ew1 ZnS showed no visible photoluminescence with 297nm light. However after a 20 hour etch in 10%HCL it was possible to record the spectrum shown in Fig.4. Once again there are several mercury lines contaminating the spectrum.

Fig. 3. The photoluminescence emission spectrum of Ew1 ZnS when excited by 365nm light. (3 Temperatures).

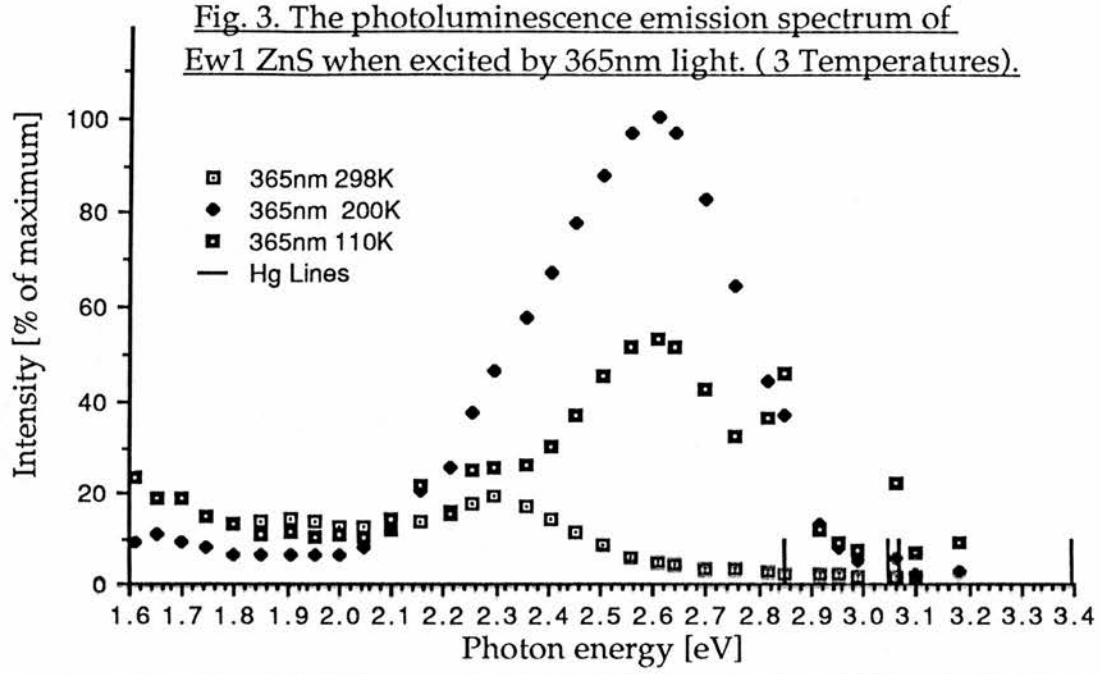

Fig. 4. Photoluminescence emission spectrum of Ew1 ZnS when excited by 297nm light. (298K)

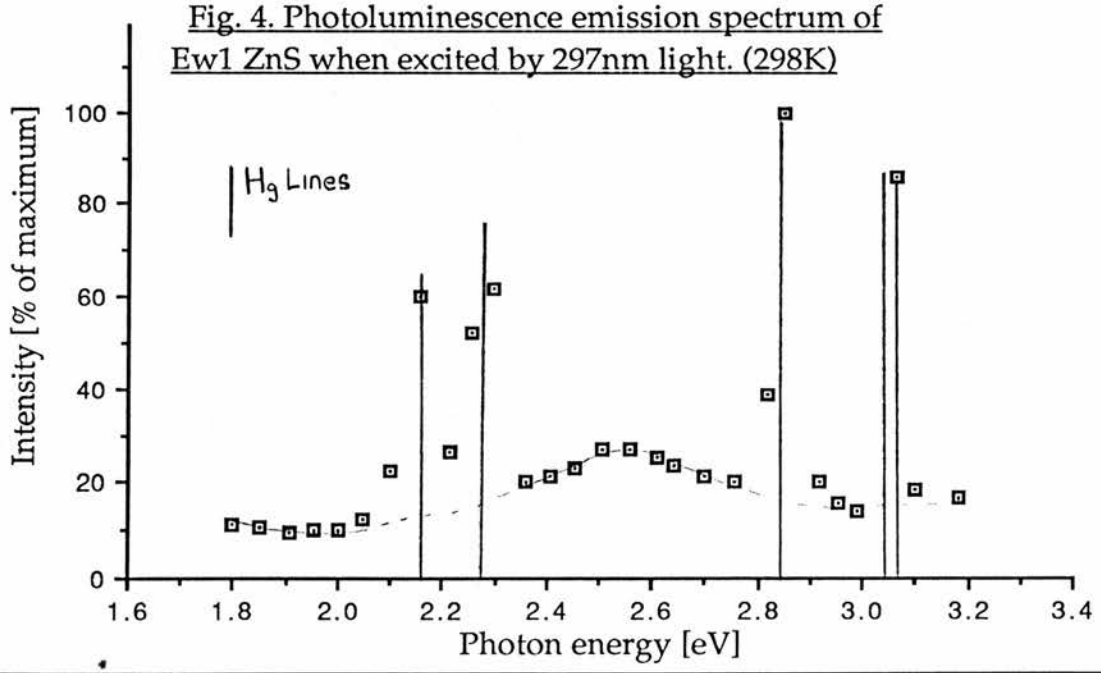

The two plots overleaf show a detail of the photoluminescence emission spectrum of ZnS:Te (S1) under 365nm excitation. The upper plot (Fig.5.) shows the results obtained when the maximum practically attainable excitation intensity was used. The lower graph (Fig.6.) shows the same spectral region when the lowest excitation intensity that still gave good results, was used. Although only two curves are presented, several runs were made at each intensity to ensure that the small difference between the two is real.

The spectrum is left uncalibrated since the peaks are only to be compared with each other.

The units on the lower ordinate are consistent with those on the upper, so that the emission intensity on the lower plot is only ~2% of that on the upper.

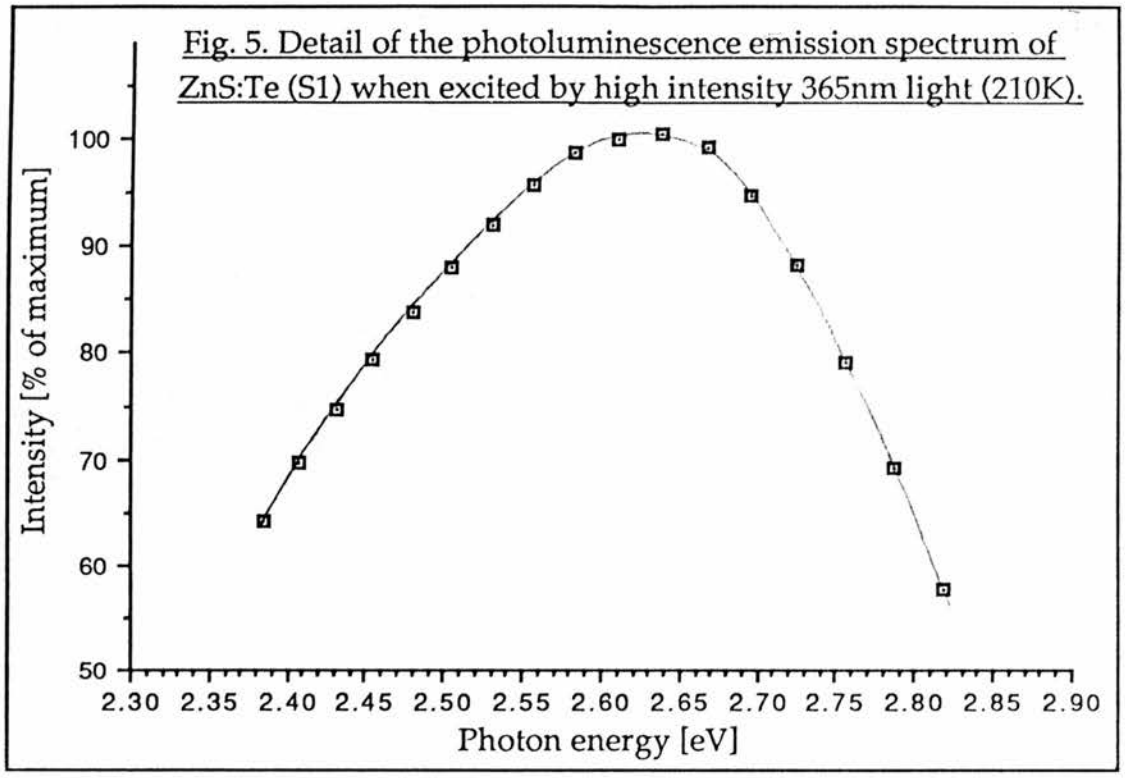

Fig. 5. Detail of the photoluminescence emission spectrum of ZnS:Te (S1) when excited by high intensity 365nm light (210K).

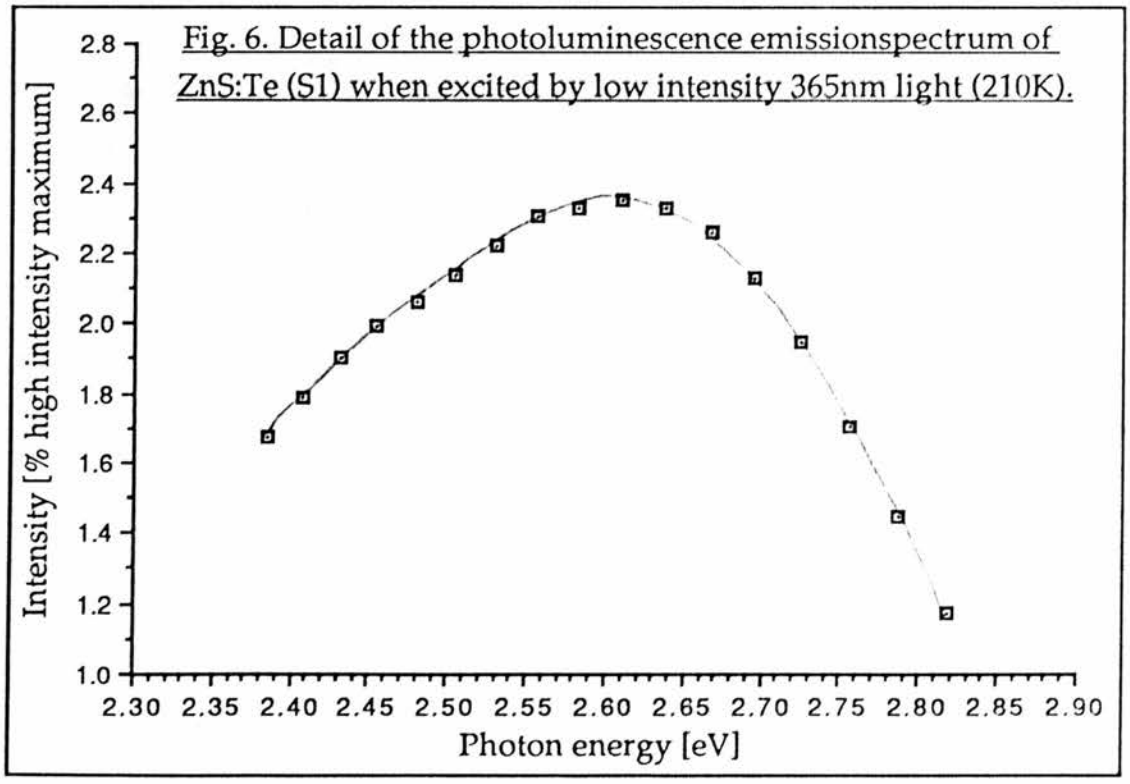

Fig. 6. Detail of the photoluminescence emissionspectrum of ZnS:Te (S1) when excited by low intensity 365nm light (210K).

In a similar manner to the previous page , the two plots overleaf show a detail of the photoluminescence emission spectrum of Ew1 ZnS under 365nm excitation. The upper plot (Fig. 7) shows the results obtained when the maximum practically attainable excitation intensity was used. The lower graph (Fig.8) shows the same spectral region when the lowest excitation intensity that still gave good results was used. Again although only two curves are presented, several runs were made to ensure that the small difference between the two is real. The spectrum is uncalibrated.

The units on the lower ordinate are consistent with those on the upper, so that the emission intensity on the lower plot is only ~6% of that on the upper.

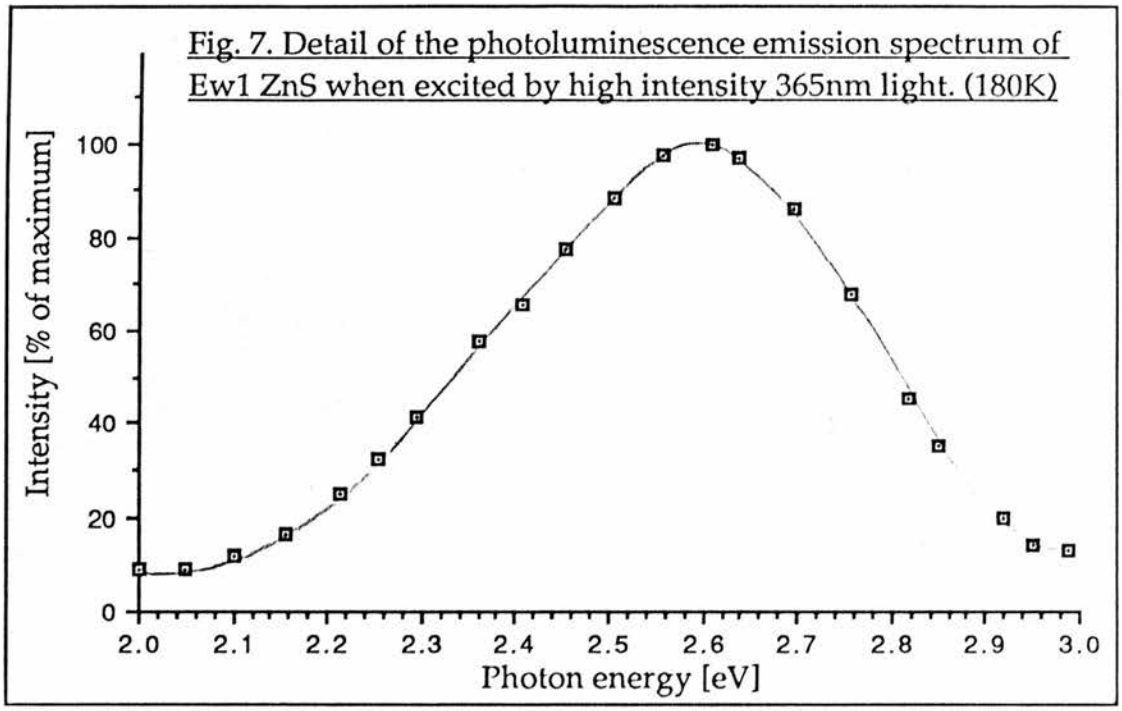

Fig. 7. Detail of the photoluminescence emission spectrum of Ew1 ZnS when excited by high intensity 365nm light. (180K)

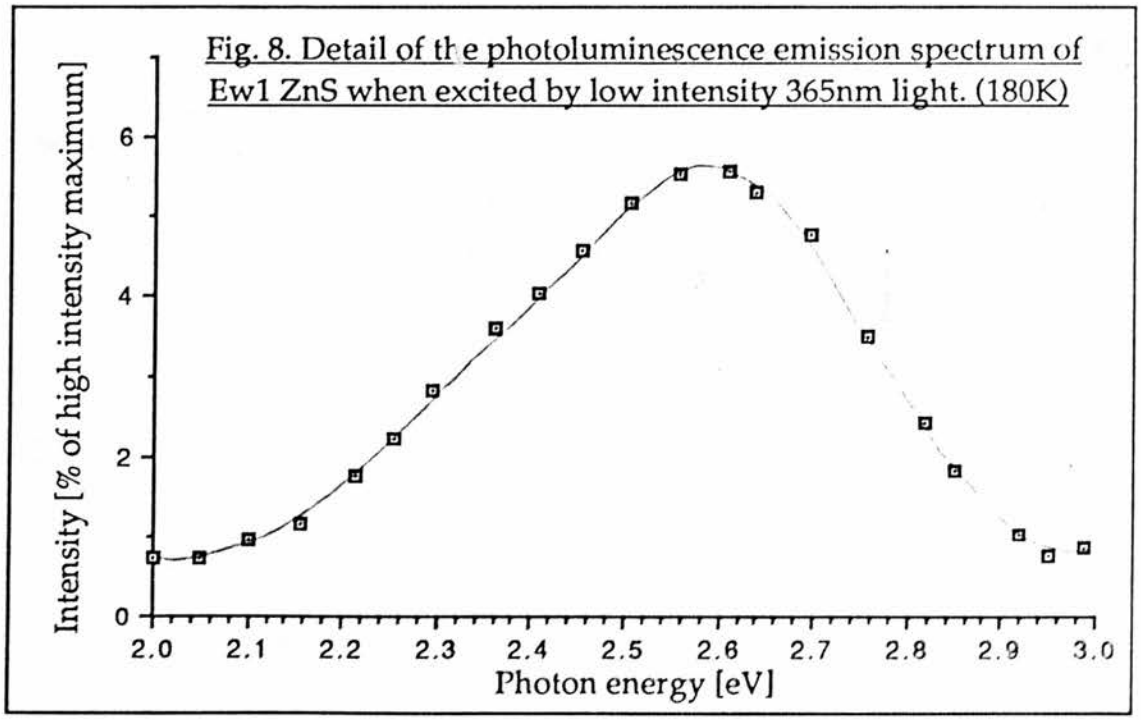

Fig. 8. Detail of the photoluminescence emission spectrum of Ew1 ZnS when excited by low intensity 365nm light. (180K)

The graph below (Fig.9) shows the "red" region of the photoluminescence emission spectrum of ZnS:Te (S1) under two different excitation wavelengths (313nm and 365nm). Both sets of data are for 234K but the intensity of the two excitations is not the same.

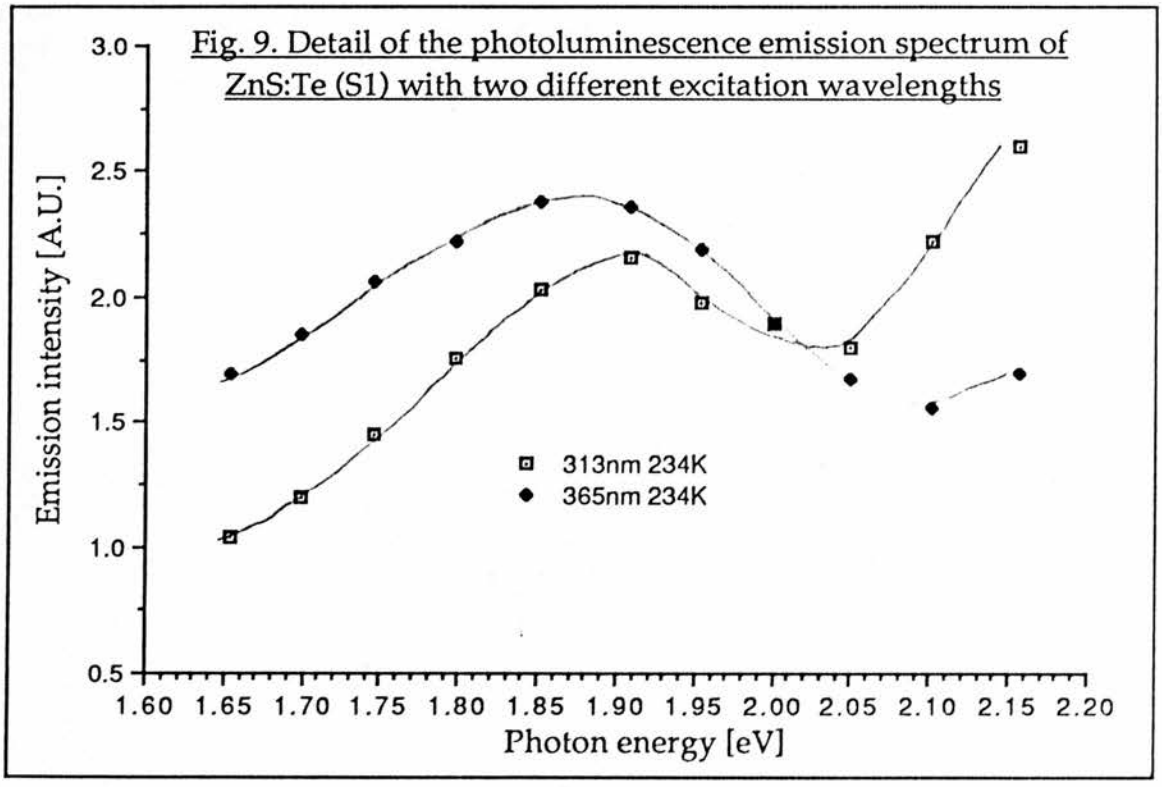

The two plots overleaf show the temperature variation of the photoluminescence emission of ZnS:Te (S1) under 365nm and 297nm excitation.

Fig.10 shows the variation of the emission at 484nm and 640nm with temperature, for 297nm excitation. The intensity of the two emissions are consistent with each other so that the two curves may be directly compared.

Fig.11 is a similar plot for 365nm excitation. Once again the intensity units for each plot are the same.

The wavelengths chosen for this experiment correspond with the peak emissions of the sample under the appropriate excitation.

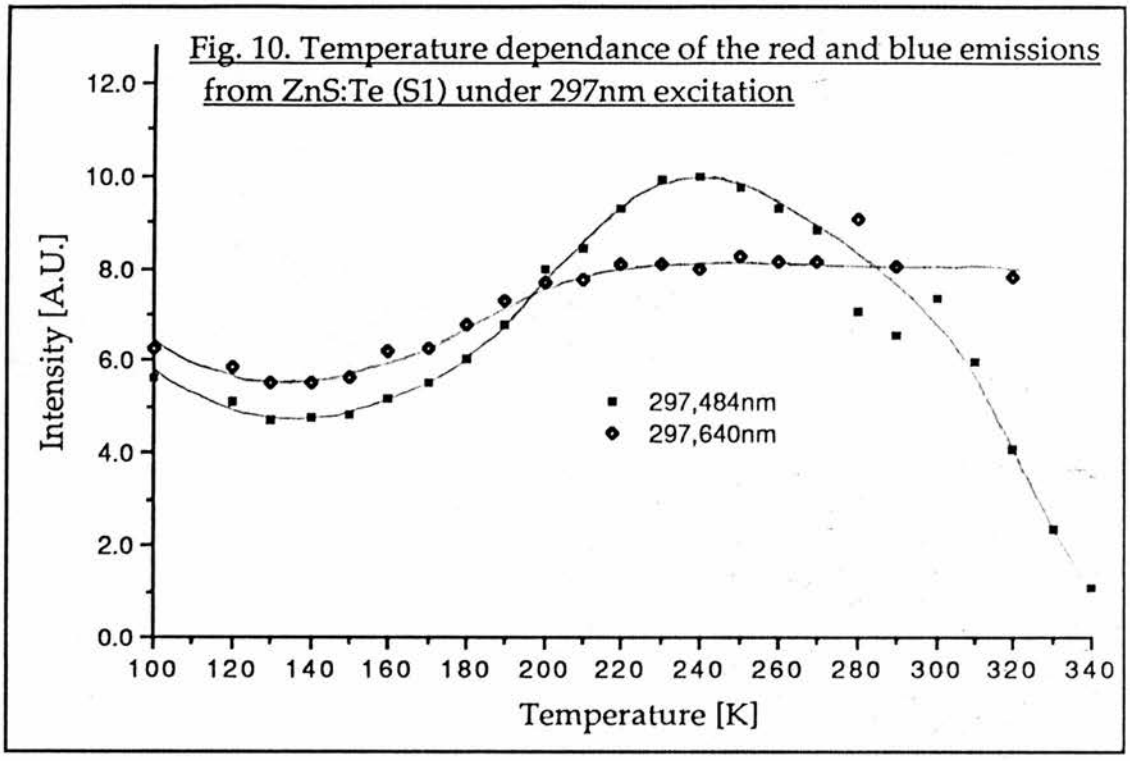

Fig. 10. Temperature dependance of the red and blue emissions from ZnS:Te (S1) under 297nm excitation

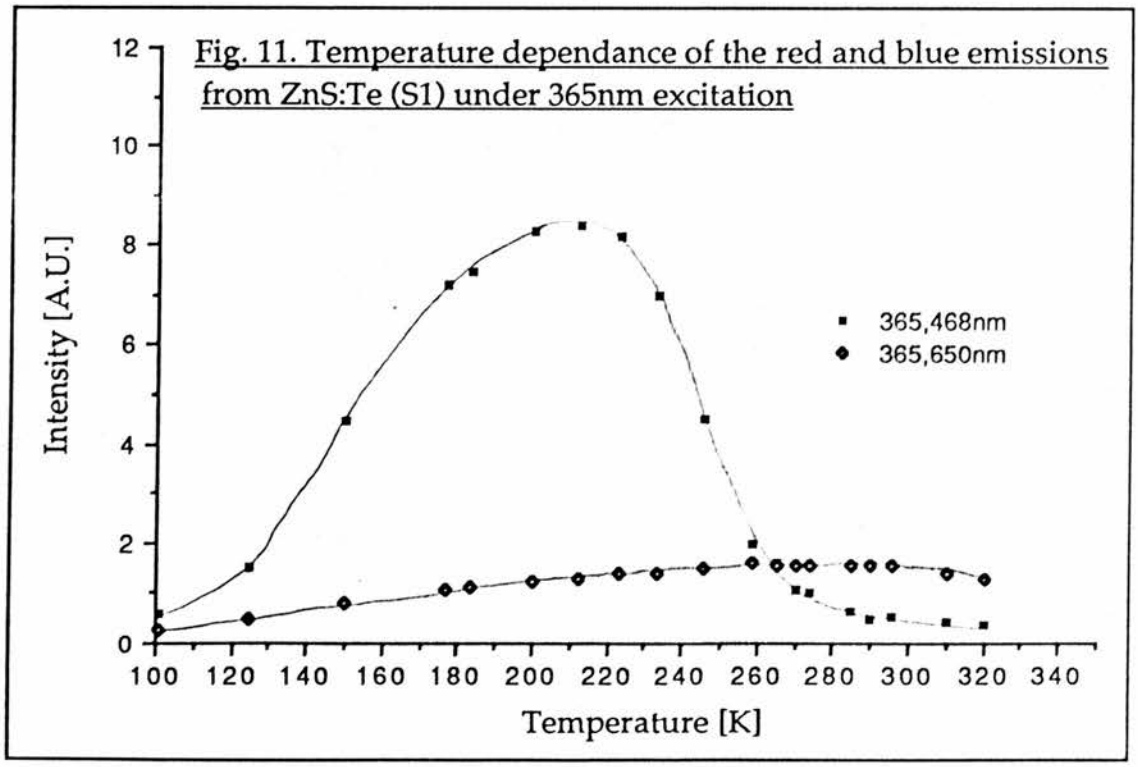

Fig. 11. Temperature dependance of the red and blue emissions from ZnS:Te (S1) under 365nm excitation

(3.2) The time dependence of the emissions.

The two curves overleaf (Fig.12 & Fig.13) and those on page 184 (Fig.14 & Fig.15), show the variation of the photoluminescence emission intensity of ZnS:Te with time for two different excitation wavelengths and two different emissions. A more quantitative description of the rise time can be made by fitting the data to the curve

$$I = I_0 (1 - \exp [- t / \tau]).$$

The four curves presented here are simply intended to illustrate what the photoluminescence build up and decay typically look like. The system response for an identical pulse length is shown on Figs.12 & 15 as a solid line, the squares on the same plots show the photoluminescence emission from ZnS:Te (S1). The recorded rise time for both the red and blue peaks was limited by system response when the 297nm excitation was used.

The 2.6eV and 2.3eV emissions from the Ew1 material also behaves in a similar manner.

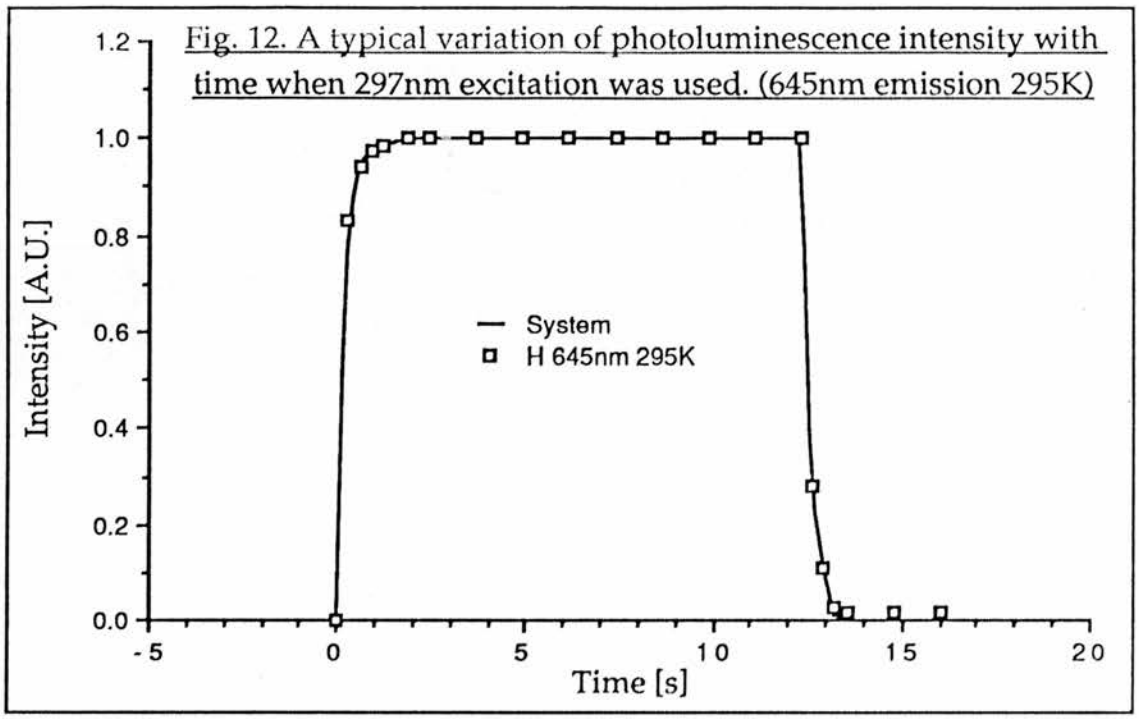

Fig. 12. A typical variation of photoluminescence intensity with time when 297nm excitation was used. (645nm emission 295K)

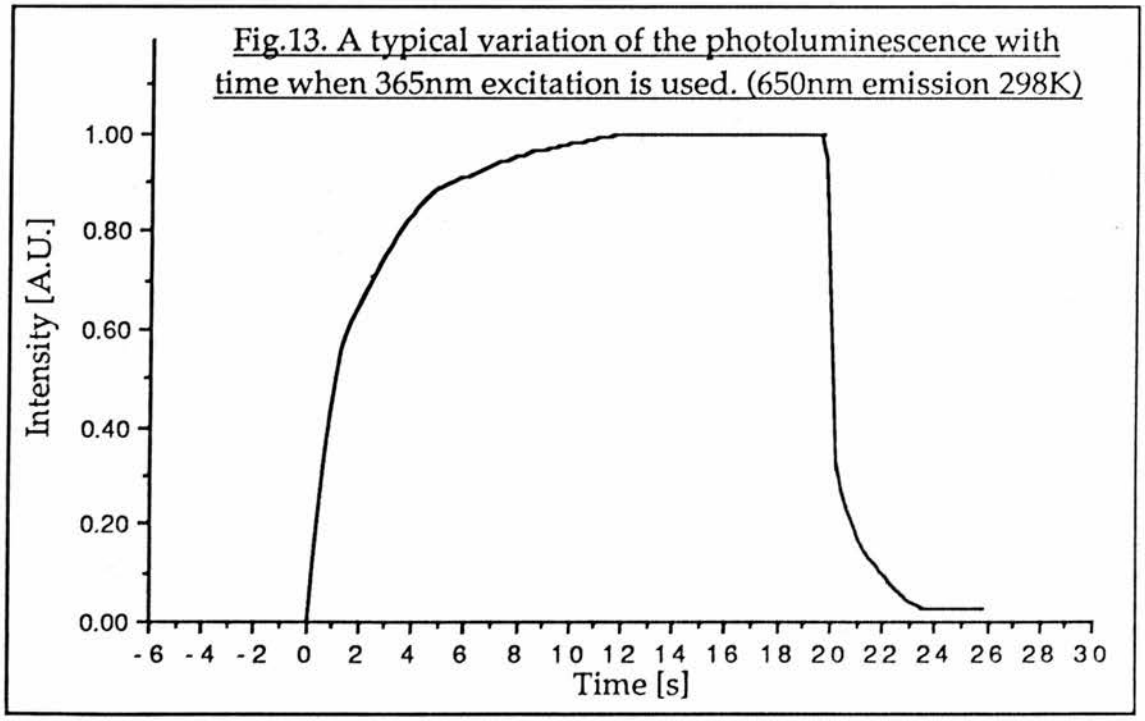

Fig.13. A typical variation of the photoluminescence with time when 365nm excitation is used. (650nm emission 298K)

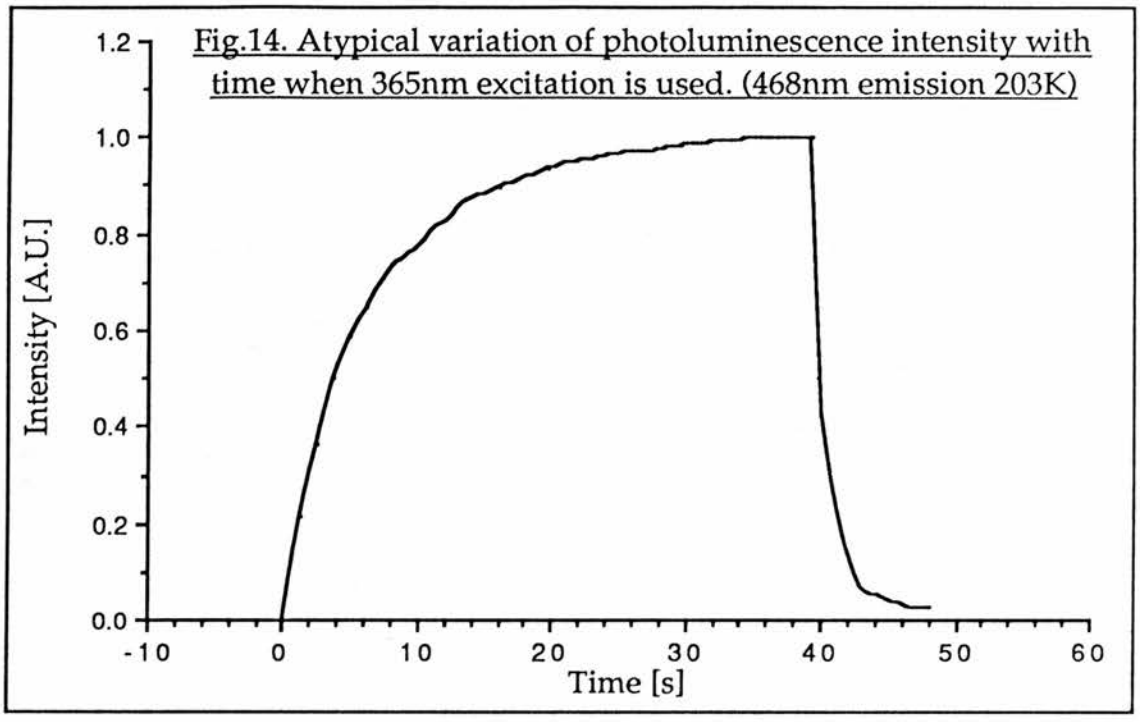

Fig.14. Atypical variation of photoluminescence intensity with time when 365nm excitation is used. (468nm emission 203K)

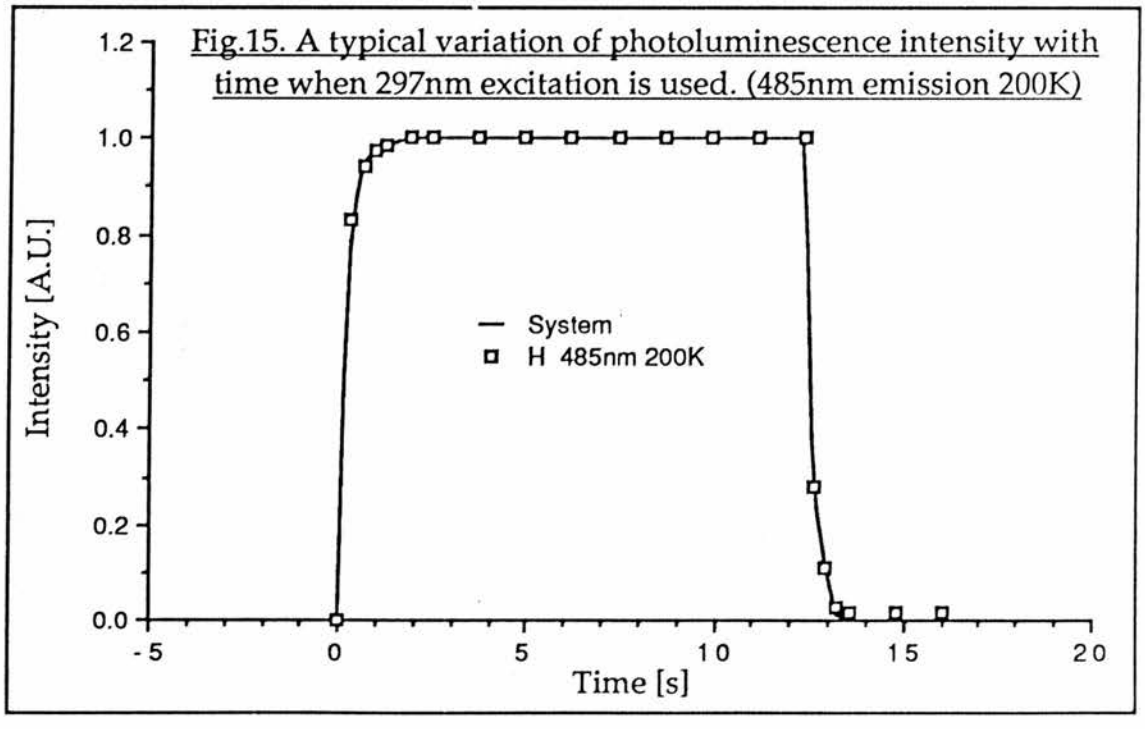

Fig.15. A typical variation of photoluminescence intensity with time when 297nm excitation is used. (485nm emission 200K)

When lower intensity excitation light was used the photoluminescence emission took considerably longer to build up. This is illustrated by fig 16 (below) which shows the 468nm fluorescence build-up and decay for two intensities of excitation differing by a factor of approximately two. A further illustration of this is given by Fig 17 (overleaf) which shows the rise in 468nm emission intensity for four different excitation intensities. Fig 18 (also overleaf) shows the data from fig 17, plotted as 1-[I(t)/I(max)].

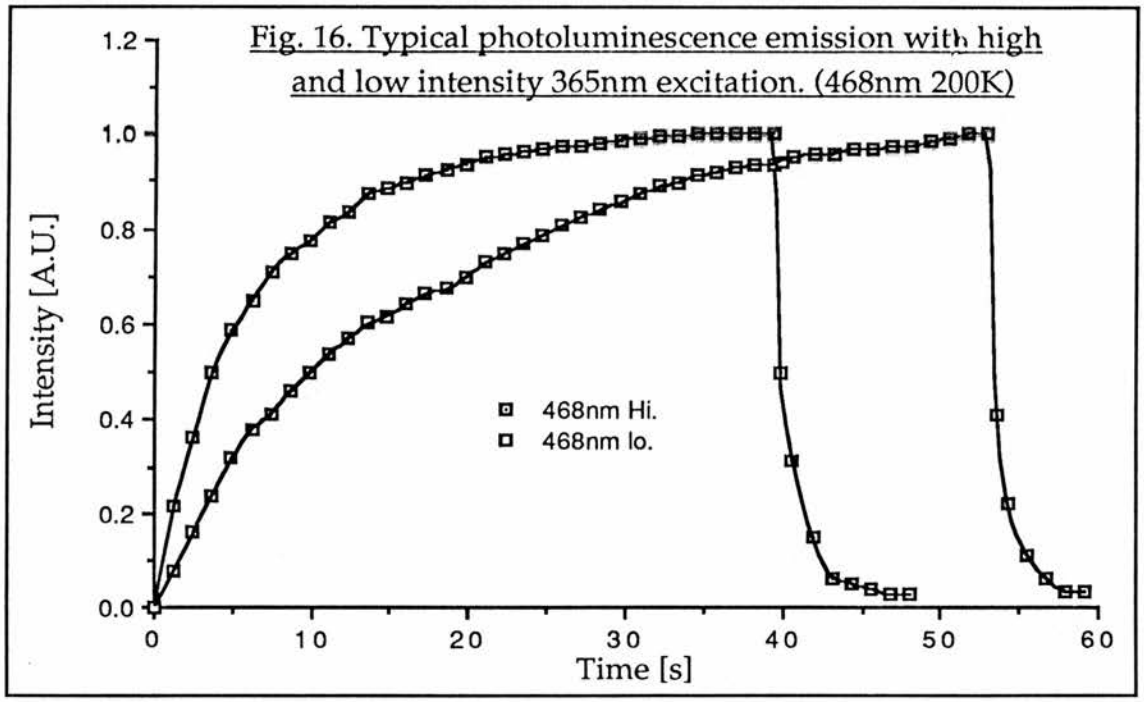

Fig. 16. Typical photoluminescence emission with high and low intensity 365nm excitation. (468nm 200K)

Fig.17. The build up of the 468nm photoluminescence emission at four 365nm excitation intensities (200K)

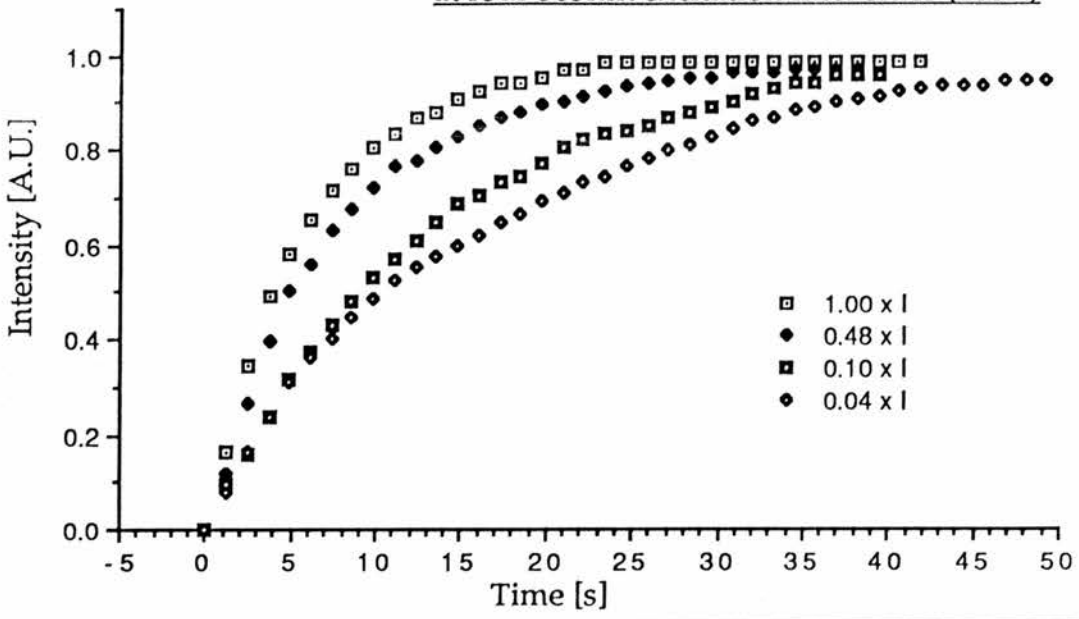

Fig. 18. Plots of [1-I(t)/I(max)] for the 468nm emission at 4 different 365nm excitation intensities (200K)

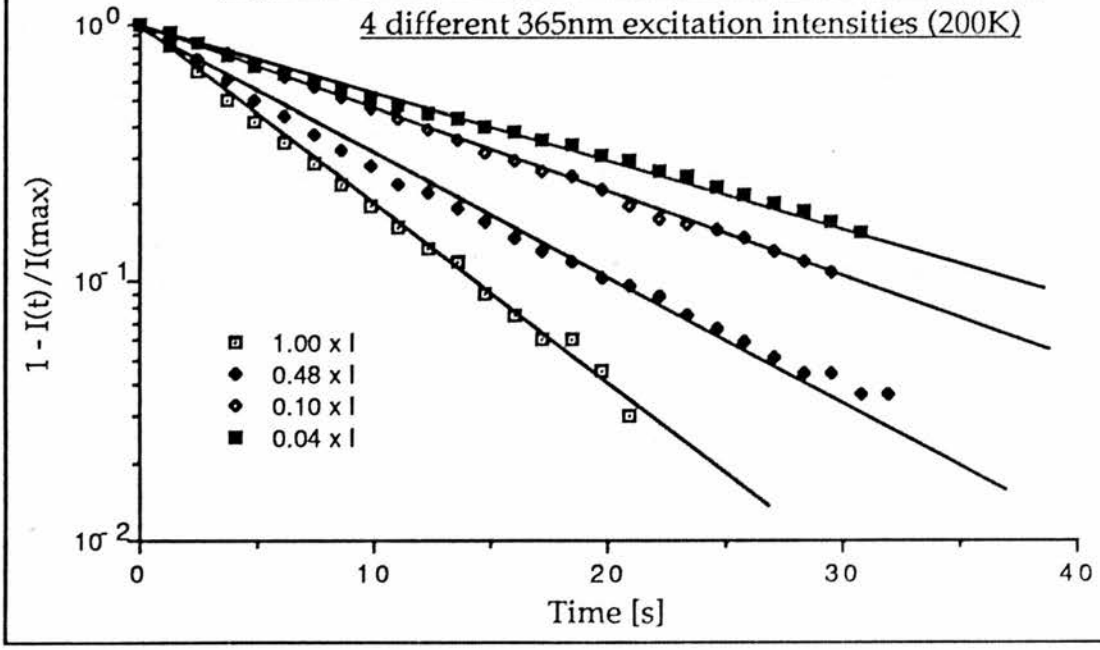

Fig. 19 (below) shows a 1-[I(t)/I(max)] plot for the 650nm emission at four different intensities. The values of the time constant obtained from these runs and those from the 468nm emission are plotted together as a function of intensity in Fig.20 (overleaf). For practical reasons the intensities of the two runs could not be exactly the same, however they are of similar order.

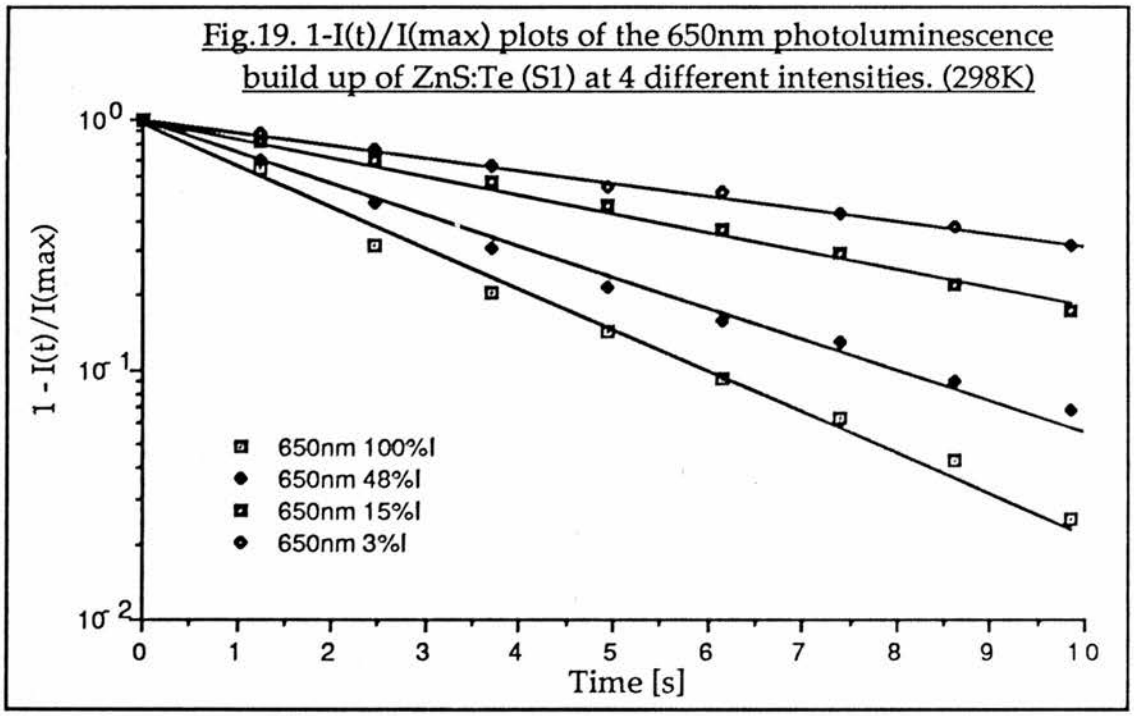

Fig.19. 1-I(t)/I(max) plots of the 650nm photoluminescence build up of ZnS:Te (S1) at 4 different intensities. (298K)

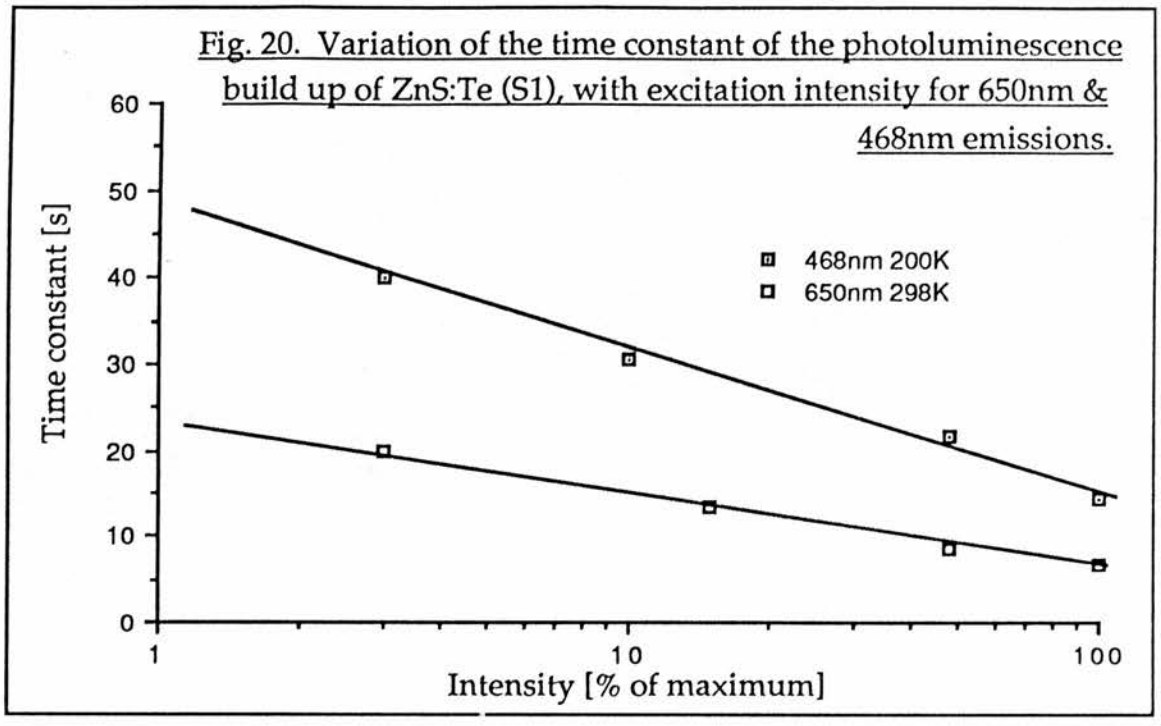

Fig. 20. Variation of the time constant of the photoluminescence build up of ZnS:Te (S1), with excitation intensity for 650nm & 468nm emissions.

The absorption of the 365nm excitation light by ZnS:Te (S1) (at 200K) was investigated. The results are shown in Fig.21 (below). Light baffles were used to ensure that the signal recorded was due only to light passing through the sample. The 468nm photoluminescence emission for a similar pulse is also shown.

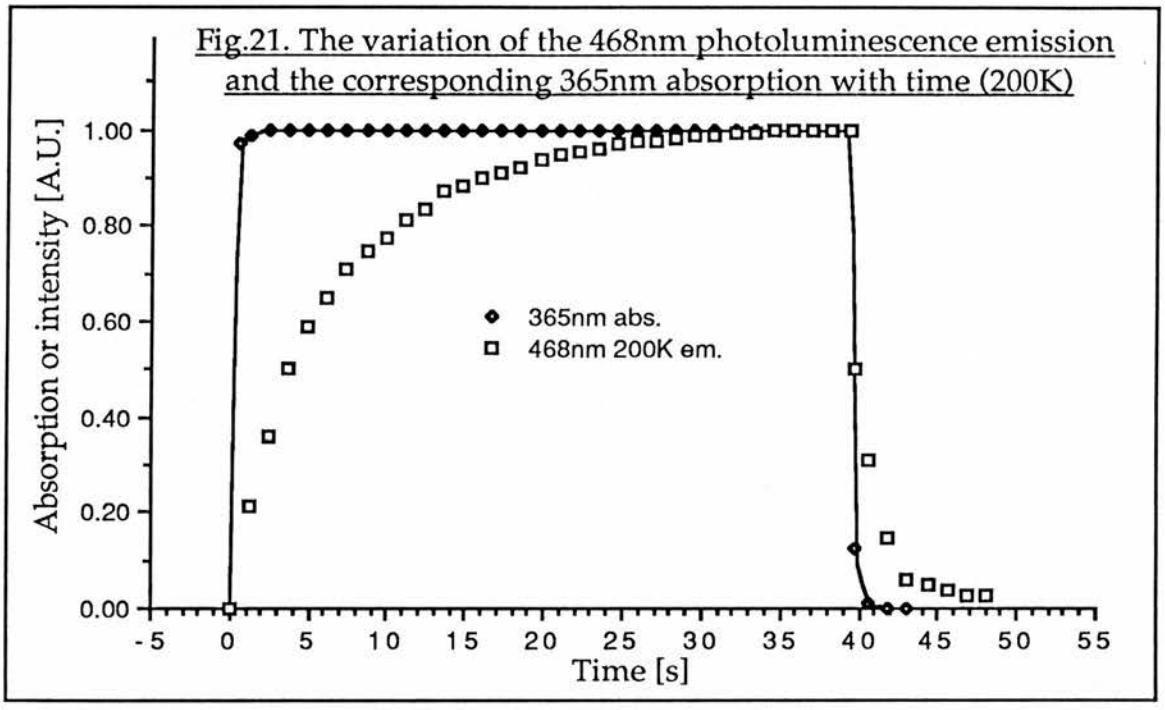

Fig.21. The variation of the 468nm photoluminescence emission and the corresponding 365nm absorption with time (200K)

During the course of experimentation, it became apparent that the recovery time of the inhibitor mechanism was very much longer at 200K then it was at 300K. Fig 22 shows 1-I(t)/I(max) plots for the 650nm emission from ZnS:Te (S1). The experimental procedure used to obtain these data is illustrated by the diagram on the same page.

Test runs were necessary in order to set the photomultiplier bias and the chart recorder sensitivity to appropriate levels at each temperature.

Run [A] produces the usual long rise time, however run [B] (performed 5 minutes after a test run at 200K) yields a very much shorter time constant. If the crystal is heated to room temperature and then recooled, all in darkness, the inhibitior mechanism is restored. Run [C} thus yields a time constant very similar to that at room temperature.

Unfortunately, quenching of the 468nm emission at 300K prevents an identical experiment being performed on this peak. However longer recovery times were also observed with this emission at low temperature.

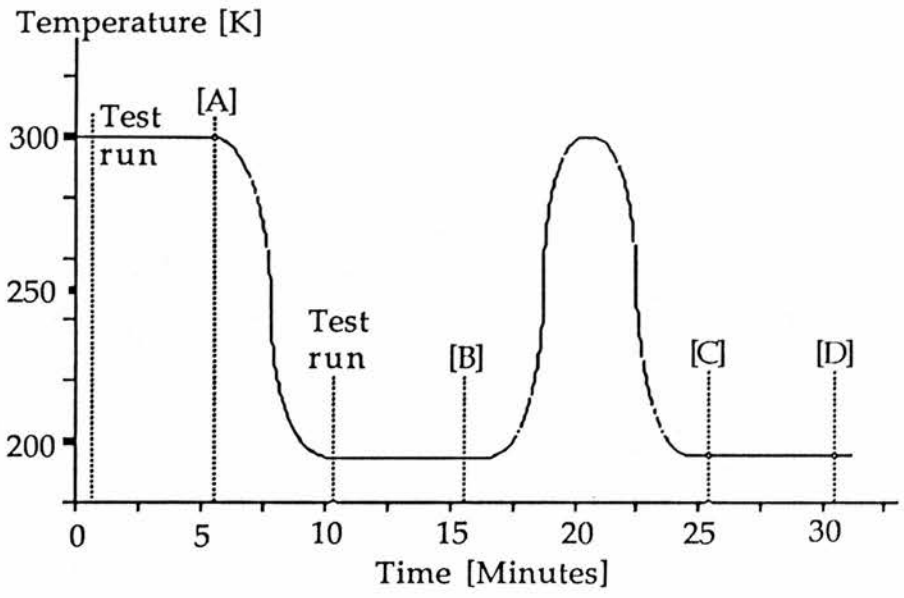

Fig.22. Curve fits to the photoluminescence build up of ZnS:Te (S1)
[A],[B],[C]&[D] as in acompaning diagram.

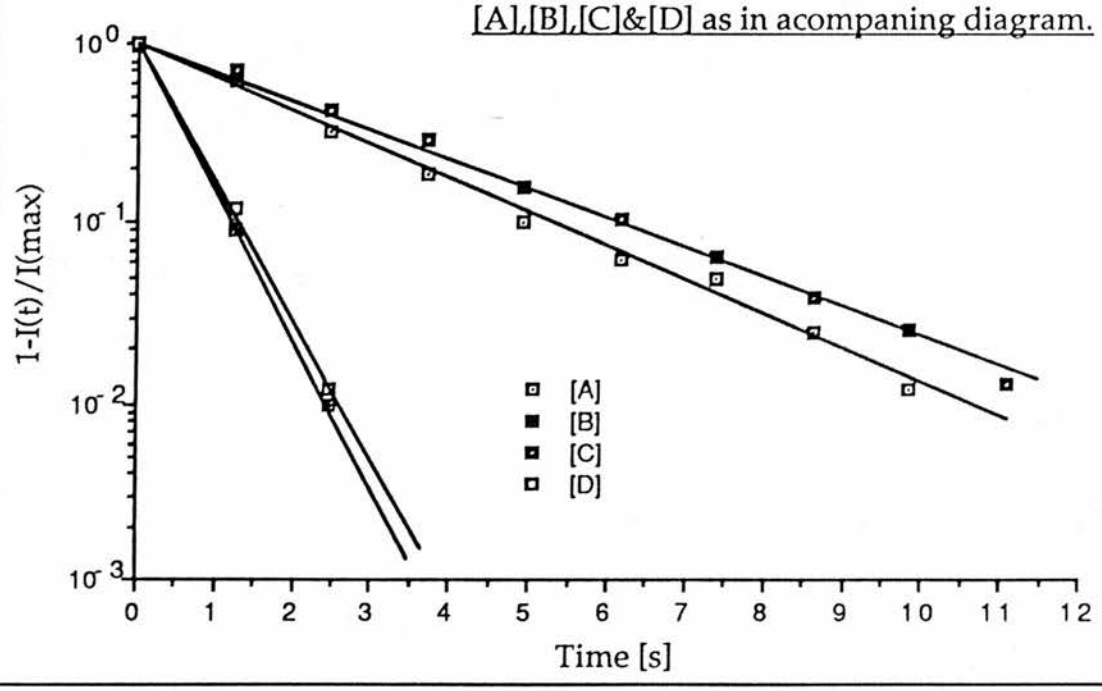

(4) Discussion.

(4.1) The origin of the emission.

Three distinct peaks are visible in the emission spectrum of the ZnS:Te material, one at ~2.65eV, one at ~2.3eV and one at 1.92eV. The 2.65eV and 1.92eV peaks show a very slight shift towards higher energies as the temperature decreases. However this is not remarkable as the band gap also increases slightly as the temperature is lowered.

At 200K the dominant emission peak from the ZnS:Te material is at 2.65eV. This lies very close to the 2.63eV which Fukushima et al[64] observe in their ZnS:Te, and believe to be due to exciton recombination on tellurium doublet centres. The characteristic excitation peak for this emission, is, according to Fukushima, at 3.5eV, very close to the 3.4eV excitation light which we have used for our photoluminescence spectra. The half width of our peak is also in good agreement with that quoted by Fukushima, for similar temperatures. One might at first sight be inclined to look upon this as evidence that our emission peak is due to tellurium doublet states. However, if one examines the emission spectrum of the nominally undoped Ew1 material there is an equally large peak at at a very similar energy (~2.6eV). Furthermore this peak is of similar width to that in the ZnS:Te material.

It is well known that in ZnS, zinc vacancies form complexes with donors to produce the self-activated luminescent centre. The precise energy of the emission from this centre varies slightly with various external factors, but is generally close to 2.6eV(Leverenz[65]). Since the Ew1

material is free of intentionally added activators, it is reasonable to presume that the observed 2.6eV luminescence peak is due to the self-activated emission. The question which must now arise is, 'how can one justify that 2.65eV emission from the ZnS:Te material is different in its origin to that from the Ew1 material? With this in mind we have looked at some of the available literature about the ZnS:Te and related systems.

In 1968 Cuthbert and Thomas[62] reported luminescence due to isolated tellurium traps in CdS. At higher tellurium concentrations they observed a second lower energy peak which they believed to be due to tellurium doublet states. Tellurium doublet emission in ZnS was first claimed by Iseler & Strauss[13] in 1969. They formed a series of solid solutions of $Zn_xCd_{(1-x)}S$:Te with varying composition. Starting with the two peaks in CdS, reported by Cuthbert & Thomas, they showed that the peaks moved smoothly to higher energy as the composition of the material changed towards ZnS. The sketch below illustrates the results that are typically obtained. [13]

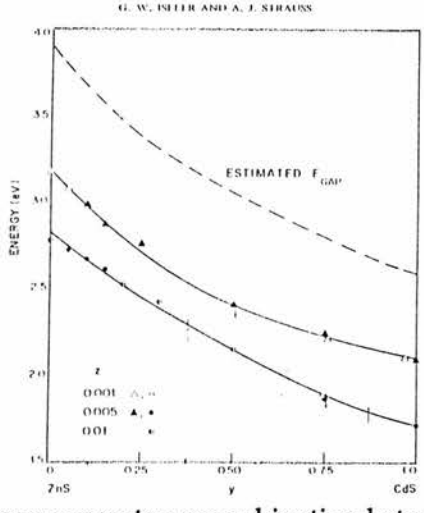

*The self-activated emission results from a donor-acceptor recombination between the defect related "A" centre acceptor and a remote donor.

However, this in itself is not proof that the emission in ZnS is due to tellurium doublets, particularly since Iseler & Strauss took no rigorous account of the emission efficiency of half width, as the composition varied. The self-activated centre also behaves in this way as the composition changes, as is illustrated in the graph below. (Data for the self-activated peak is taken from Leverenz[65]).

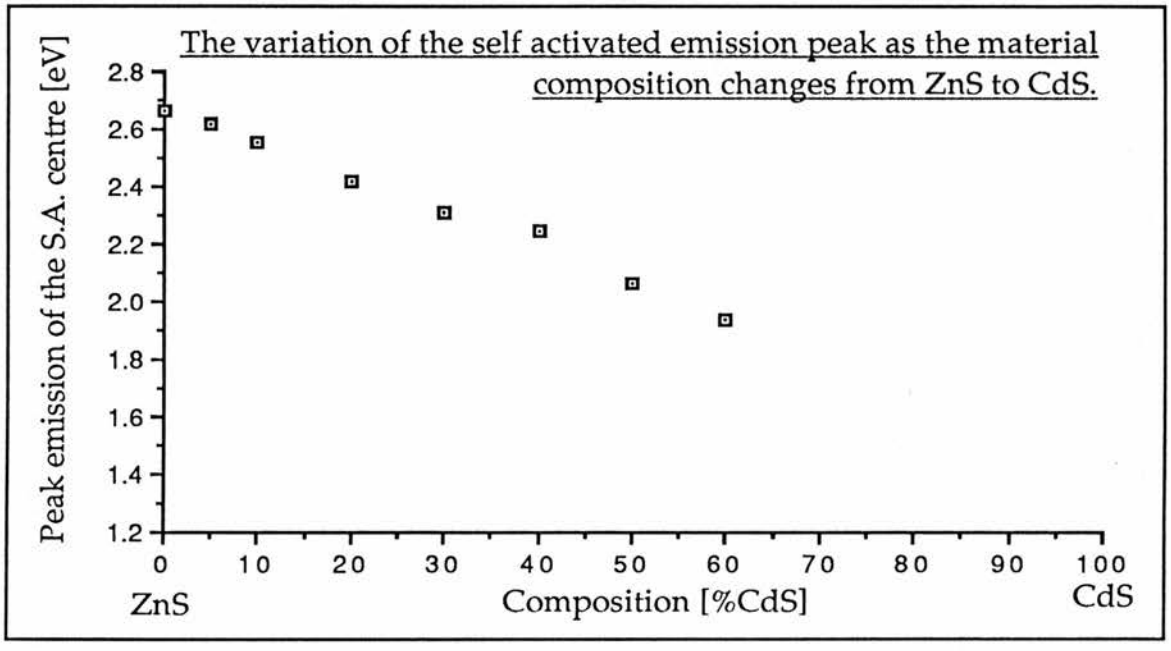

Additional evidence that the 2.6eV emission in ZnS:Te is due to tellurium pairs has been drawn from the change of the emission spectrum as the tellurium concentration is increased. Such spectra have been presented by Abdel-Kader et al[66] for ZnS:Te of different tellurium concentration. The general form of such results is illustrated by the sketch overleaf. (This sketch shows an idealised situation. In ZnS the transition

from high energy band (HEB) only to low energy band (LEB) only is quite rapid with few samples showing both peaks.)

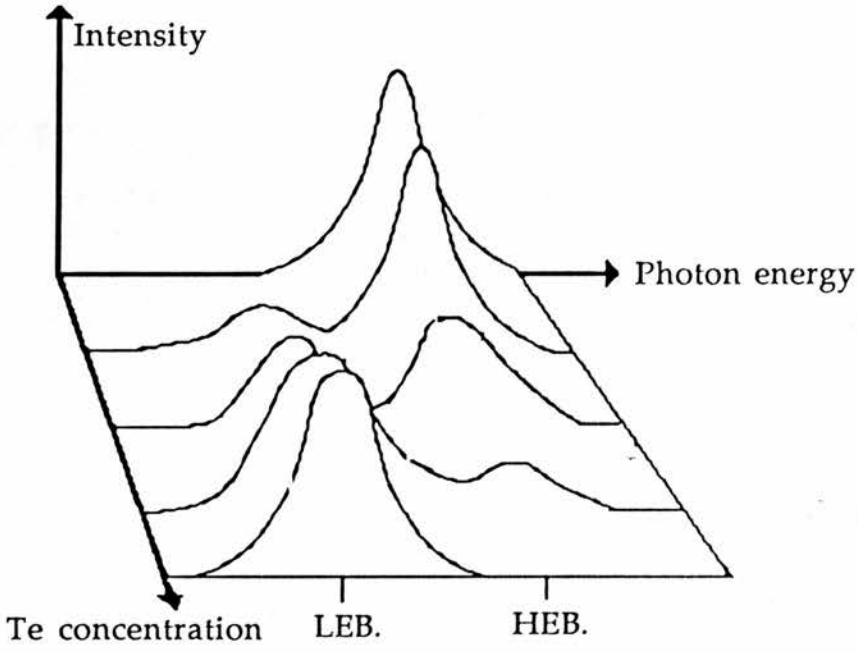

Such variations of spectra with composition are, however, still not evidence for the existence of a doublet, they only show that the singlet emission disappears and is replaced by another lower energy peak as the concentration of tellurium increases. An alternative explanation of this might be that the substitution of large numbers of the very much bigger tellurium atoms produces significant disturbance of the lattice which in turn leads to large numbers of zinc vacancies. These vacancies are the activator for the self-activated emission, and thus this might be enhanced resulting in the appearance of a new peak.

Further information about the nature of a luminescent centre can be obtained by examining its characteristic excitation spectra. It is claimed that

the tellurium doublet emission has a characteristic excitation at ~3.55eV[63][64]. However if one looks at a typical excitation spectrum of the self-activated emission (see for example Koda & Shionoya[67]) one also sees a peak at 3.5eV. The graph below is composed of experimental data from the following sources, self-activated emission Era[68] self-activated excitation, Koda[67] and tellurium doublet emission and excitation, Fukushima[64]. A complete 4K spectrum of the self-activated and the proposed tellurium doublets is thus formed.

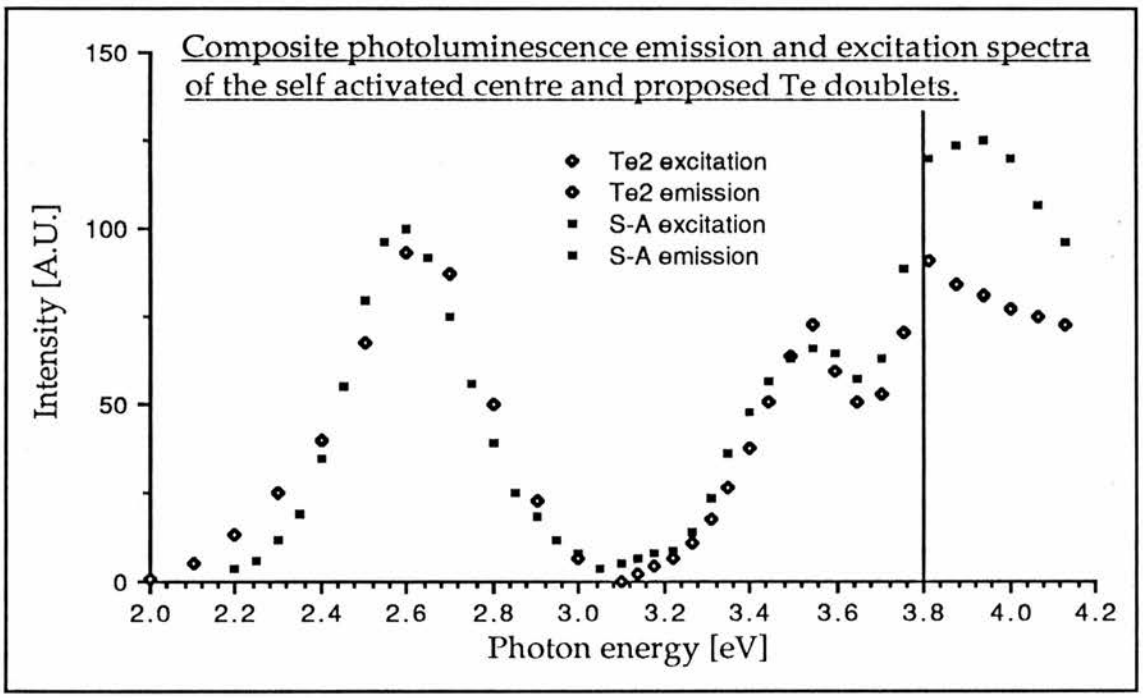

The difference between the two spectra is slight. Both show a characteristic excitation around 3.5eV and an emission around 2.6eV.

Further illustration of the similarity between the self-activated centre and the proposed tellurium doublets can be seen if one looks at the nitrogen temperature excitation spectra that is claimed to be due to

tellurium doublets and that for the self-activated centre. (In this case 77K data is taken from Heimbrodt[63] and Koda[67].)

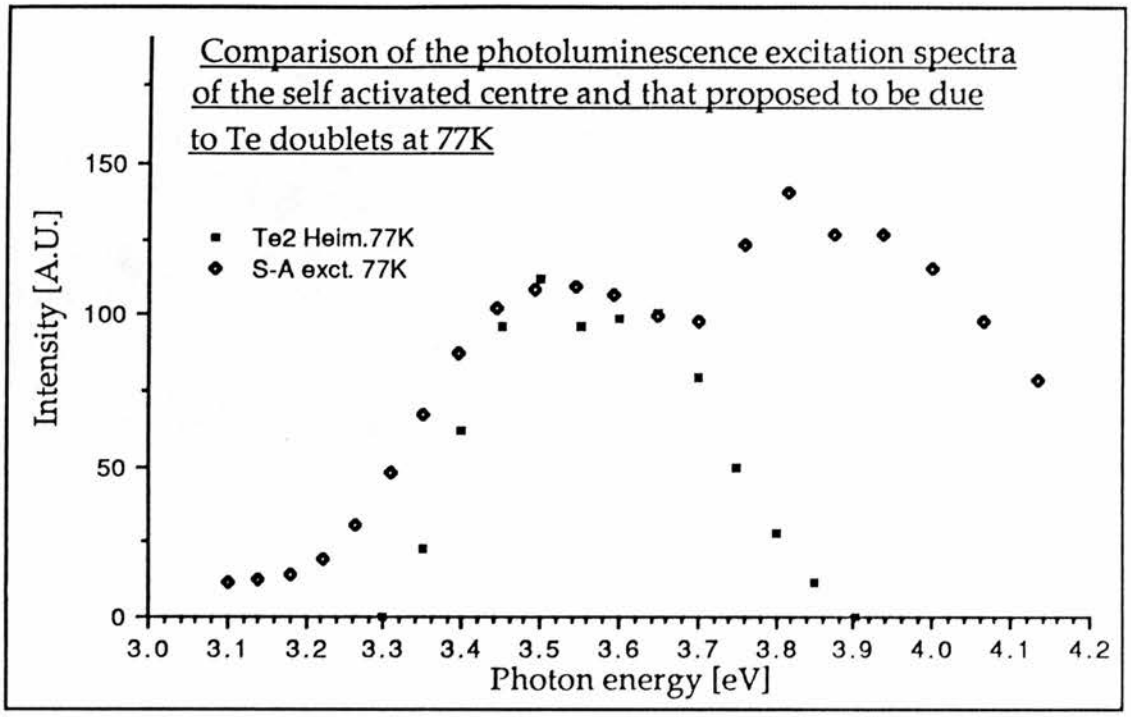

Both curves show a maxima at ~3.5eV. There are some differences between the spectra at high energies, however, an excitation spectrum above band gap (where the light is very strongly absorbed in electron hole pair production) is unreliable. Such results reveal more about the surface preparation of the crystal than the nature of the centres.

Abdel-Kader et al[66] do mention the possibility of a self-activated emission leading to confusion in a ZnS:Te system. However they imply that a self-activated emission can only occur in a material with intentionally added donors. Although it is true that aluminium or chlorine are often added to ZnS as co-activators in order to enhance the self-activated emission, their addition is not essential. This is because in all ZnS there are significant levels of residual impurities, some of which

may be donors.

[This does not mean that the material is conducting, it is widely believed that these donors are compensated in ZnS prior to the zinc conductivity treatment. The formation of the self-activated centre is itself an example of such compensation. The Ew1 material also has a strong self-activated emission yet it is highly insulating.]

Abdel-Kader et al[66] have used the fact that the variation of the emission intensity with temperature, for intentionally co-activated ZnS:Al, is different to that for the ZnS:Te peak of similar energy to argue that the emission peaks have different origins. Since the ZnS:Al and ZnS:Te material from which this data were taken were from different melts it may be presumed that they contain different concentrations and possibly even different species of additional impurities. Further to this it is not advisable to place much emphasis on temperature variation data, unless one knows precisely all the processes occurring within the sample. A good illustration of this can be drawn from our own data for the variation of the emission of the ZnS:Te material with temperature. When excited by 297nm light, below 240K the 1.9eV and the 2.55eV emissions show very similar temperature variation, yet we have no reason to suppose that the two centres responsible are related. Conversely, it is probable that the 1.9eV emission observed with both the 297nm and 365nm excitation is due to the same centre. However the temperature variation of these emissions is largely dissimilar for the two different excitations.

Our emission intensity temperature results were taken mainly for practical reasons. When luminescence transitions involve free carriers the temperature variation of the overall efficiency of a luminescent system is strongly dependent on the behaviour of all the centres within the crystal. Since we do not know the nature of all the centres that are present, any attempt to derive information from such results would be purely speculative.

Abdel-Kader et al[66] have performed time resolved cathodoluminescence spectroscopy on ZnS:Te samples of various compositions. For samples exhibiting only the HEB luminescence they found no shift in the emission peak as the luminescence decays after excitation this is as one might expect for an exciton/isoelectronic trap system. In the one sample which gives both HEB and LEB emission, this was also found. However in the samples with only a LEB, the emission peak shifts by -0.055eV during the first 10μs of the luminescence decay. Era et al[68],[69] working on self activated emission in ZnS:Cl, have also observed such a shift in the emission peak as the luminescence decays. In this case the size of the shift was very similar (-0.045eV in the first 10μs). Such energy shifts are characteristic of donor-acceptor pair emission, indeed this was one of the criteria used by Era et al[68] as evidence that the self-activated emission was itself due to donor-acceptor pairs. The presence of such a similar shift in ZnS:Te to that in ZnS:Cl lends weight to the idea that, at least in the higher tellurium concentration samples, the 2.6eV

emission is due to the self activated centre and not tellurium doublets.

Heimbrodt & Goede[63] have taken the idea of doublet states a stage further and propose that a 2.55eV peak which appears in material with ≥3mol% Te, is due to triplet states. Abdel-Kader et al[66] do not see this emission in 3%Te material, however, they do see a shift of the LEB to 2.55eV in material with 10% tellurium. (They do not attribute this to triplet emission). The shift of the LEB by ~0.1eV in 10% tellurium material is probably simply a consequence of the ~0.13eV change in energy gap as $Zn_{0.99}Te_{0.01}S$ becomes $Zn_{0.90}Te_{0.10}S$ and as such is unremarkable. It is more difficult to explain the observations of Heimbrodt and Goede[63] in this way because of the lower tellurium concentration at which their shift occurs.

To summarise, although it is possible that the blue emission observed in high tellurium concentration ZnS:Te might be due to tellurium doublet states there is little evidence in the literature to support this idea in favour of a self-activated emission mechanism.

Returning to the emissions observed from our samples, the idea that the Ew1 2.6eV emission is due to the self-activated centre is further supported by the slight shift towards higher energies observed when the excitation intensity is increased.

The 2.6eV peak observed in the ZnS:Te material also shifts slightly towards higher energy when the excitation intensity is increased. This observation is difficult to explain in terms of bound excitons on two nearest neighbour tellurium centres. Such shifts are, however,

characteristic of donor-acceptor pair emissions. This coupled with the very close energy correlation between our peak and that of the self-activated centre leads us to believe that it is this, and not tellurium doublet emission that we see in our samples.

The 2.3eV peak in the Ew1 material is due to an as yet unknown impurity centre. The ZnS:Te material also shows some evidence of an emission at 2.3eV which may well be due to the same impurity.

The emission spectrum of the ZnS:Te under 297nm excitation shows two peaks, one around 1.9eV and a second larger one at 2.55eV. It would seem reasonable to suppose that the peak at 1.9eV is related to the emission at similar energy under 365nm excitation. For practical reasons it was not possible to investigate the variation of this emission peak with intensity directly. However with light of $h\upsilon > E_g$, most of the photons are absorbed within a few nanometers of the surface resulting in electron-hole pair formation. These free carriers can recombine at suitable impurity centres, sometimes resulting in light emission. Since there are large numbers of pairs created in a small volume, the effective excitation density is very high. This being the case one might expect the emission peak due to a donor-acceptor pair mechanism to be shifted slightly relative to that obtained with sub band gap excitation of similar intensity. The red emission under 297nm or 313nm excitation occurs at slightly greater energy than under 365nm excitation, leading us to believe that this emission may possibly be donor-acceptor pair related. The shift cannot, in

this case, be viewed as strong evidence of pair emission since factors other than excitation density are also different for the two spectra. Copper is known to give a red donor acceptor emission in ZnS, but this is usually at around 1.7 to 1.8eV. The precise energy of this emission is known to vary slightly with crystal preparation conditions, so the energy discrepancy alone would not discount copper as an activator in our crystals. However, in order to observe a red copper emission in ZnS special preparation conditions are required and in general such an emission is quite difficult to achieve. Thus it seems improbable, though not impossible, that these conditions have been coincidentally met, and that the red emission we observe is due to copper contamination.

By far the largest emission from the ZnS:Te under 297nm excitation, was at 2.55eV. Under the 297nm excitation the photoluminescence is generated very close to the surface of the crystal. With the experimental arrangement that we used, this light has to pass through the crystal before it is detected. It is probable that significant self-absorption of this light occurs particularly of the higher energy components, leading to the impression of an energy shift. [Although no rigorous absorption experiments have been carried out on ZnS:Te (S1), other ZnS samples grown in this laboratory have had significant preferential absorption of blue light.] Initially the Ew1 ZnS showed no visible photoluminescence with 297nm excitation, however, after surface damage had been removed by 20 hours etching in 10% HCL a slight blue emission was seen. Although the spectrum is heavily contaminated by residual mercury lines, the peak

of this photoluminescence emission is clearly at lower energy than under the 365nm excitation. There is thus no significant difference between the blue photoluminescence of the Ew1 ZnS and that of the ZnS:Te. On the basis of the measurements we have made there is no reason to believe that the blue/green emission from the ZnS:Te under 297nm excitation, is due to a centre other than the self-activated.

(4.2) The time dependence of the emission.

Under 365nm excitation the intensity of the photoluminescence emission from both the nominally undoped Ew1 ZnS and the ZnS:Te exhibited a readily observable build up over a period of several seconds.

If such a build up was simply due to the centre having an exceptionally long luminescence lifetime, one would expect to observe a decay time similar to that of the rise. Since this is not the case, we may eliminate this possibility.

The rise time has been empirically fitted to the relation,

$$I_{(time)} = I_{(max(t=\infty))} [\, 1 - \exp\{ -t/\tau \}]$$

The time constant for the build up, τ increases significantly as the intensity of the excitation is lowered. This increase is proportional to the log of the intensity. The time constants for the two emissions are not exactly the same, but they maintain a constant ratio at all intensities measured. Intuitively an excitation intensity dependence leads one to believe that the intensity of the emission as a function of time, is related to the number of excitation photons that have been incident on the crystal

since the start of the excitation pulse. Such photon number dependence is consistent with the idea that some inhibitor level must be populated before luminescence is allowed. As more of the inhibitor centres are populated more luminescent transitions are permitted leading to the slow build up. Such an inhibitor level would have to have a long lifetime, and might be a metastable level within the luminescent centre itself or some other more spatially remote trapping level.

One form that this mechanism might take is competitive photon absorption by some non-luminescent centre, present in greater numbers than the luminescent centres. Such a centre might operate by absorbing excitation or emission photons, in a transition to a long lived state, thus giving the appearance of a luminescence build up. With this in mind the absorption of the crystals as a function of time was measured. At both 365nm and 546nm no time dependence in the absorption was found. thus we do not believe that the buildup is due to competition for photons. The only possibility this leaves us with is that electrons are released from the luminescent complexes by the excitation light and are trapped by some level before they can radiatively recombine. Such a level is unlikely to be an isolated donor or acceptor since these are in general only attractive when they are ionised, where-upon they have already contributed one free carrier. We do not believe that the trapping mechanism is intrinsically related to the nature of each of the luminescent complexes because in monochromatic measurements of the rise times one can see that the 2.6eV and 2.3eV emissions in the Ew1 ZnS both have slow build up times, as do

the 2.6eV and 1.9eV in the ZnS:Te. We have no reason to believe that the 2.3eV emission in Ew1 ZnS or the 1.9eV emission in ZnS:Te are related to the self-activated emission at 2.6eV. The observation of this build up at all these wavelengths would require the same metastable level to be present in all these centres, which seems improbable. An external electron trapping level provides a more likely explanation of the results. However on the basis of the previous argument alone one cannot eliminate the possibility that it is one of the luminescent centres that serves as the trapping level for the others. It is possible that the excited state of one centre is metastable and serves as an electron trap.

The presence of a large population of trapping levels is also implied by the large thermoluminescence observed. All the luminescent emissions are present in the thermoluminescence, which is in keeping with the idea of the excitation light ionising the centres rather than simply exciting them. If a carrier leaving a deep trap can produce luminescence from all the centres, the loss of a carrier to such a trap might inhibit all the centres.

Initial experiments to measure the time constant, τ, at 200K led to the impression that this was very much shorter than that at 300K. This effect transpired to be due to the way the experiment was carried out rather than an intrinsic property of the material. During the initial measurements a test pulse was used to set the photomultiplier voltage and chart recorder sensitivity. At 300K the allowed 5 minutes dark time for system recovery was sufficient, however at 200K most of the traps remained full after this time, leading to the impression of a shorter time constant at these

temperatures. Warming the sample to 300K, followed by recooling to 200K, empties all the traps and results in the observation of a time constant very similar to that at 300K. This experiment could not be exactly duplicated for the 468nm peak since this emission is quenched at room temperature. However at 200K very much longer recovery times were also needed for this centre too, as one would expect from our model of the luminescence processes. The diagrams overleaf summarise our ideas about some of the mechanisms which operate in our ZnS:Te .

The simple situation of electrons being released from a single trapping level is complicated to some extent by the presence of the second luminescent centre. If, as is probable, the trapping cross-section of one centre is significantly larger than that of the other, that centre will be better able to "compete" for the free electrons that become available as the traps become full. This may be the reason that the time constants for the two centres are different.

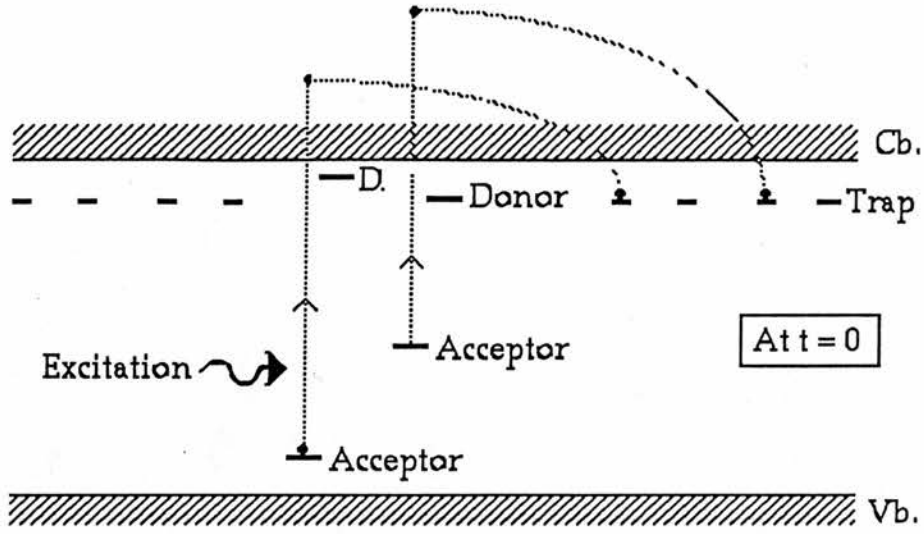
Cb.
D.
Donor
Trap
Acceptor
At t = 0
Excitation
Acceptor
Vb.

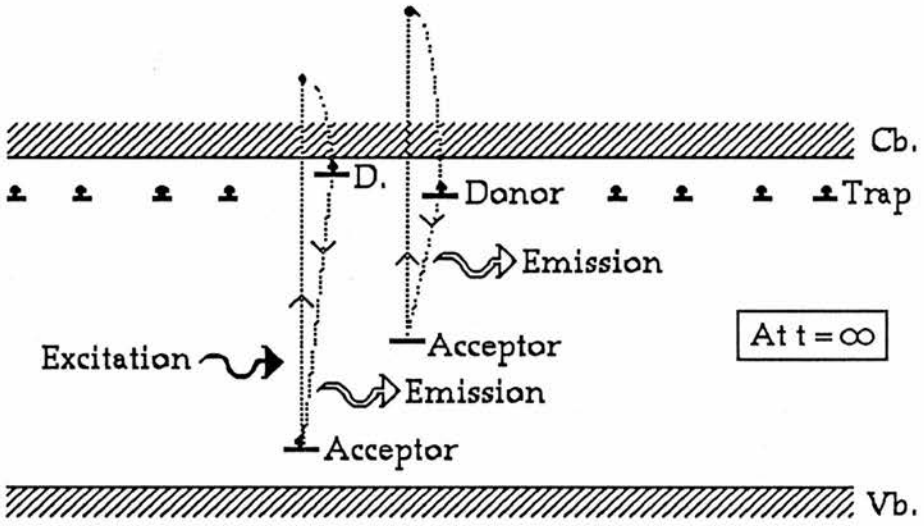
Cb.
D.
Donor
Trap
Emission
At t = ∞
Acceptor
Excitation
Emission
Acceptor
Vb.

(5) Concluding remarks.

When ZnS is lightly doped with tellurium we believe that the resultant high energy photoluminescence emission band is due to an exciton binding to the single tellurium centre, as is widely accepted. However, we believe that in heavily doped material, the lower energy emission band which is observed may well be due to the self-activated centre rather than a tellurium doublet centre as some workers suggest[13][63][64]. Our own photoluminescence measurements on ZnS:Te and nominally undoped material (presumed to exhibit self-activated emission) have failed to produce a convincing difference between the two materials. Furthermore, the peak energy of the ZnS:Te emission was found to be slightly dependent on the excitation intensity. Such behaviour is characteristic of donor-acceptor pair emission. Photoluminescence and time resolved cathodoluminescence results for heavily doped samples from the literature are more consistent with the self-activated centre than a tellurium doublet. In contrast results for the singlet emission are, in the main, quite different to those for donor-acceptor pair centres. The introduction of high concentrations of the large tellurium atoms must presumably exert considerable stress on the host lattice. We believe that defects associated with this stress enhance the self-activated emission in heavily doped material. The quantity of literature on the ZnS:Te system has to date been somewhat limited, however, to our knowledge there has been no rigorous justification of the doublet model.

Both the ZnS:Te and the undoped material that we have worked on

exhibited a slow build up of photoluminescence emission after the excitation began. We have found that the time constant of the build up was strongly dependent on the excitation intensity. We believe that the mechanism responsible for this build up is competitive trapping of electrons that are ionised from luminescent centres. When all the traps are full the inhibitor mechanism is removed and the emission increases. Our observations of the temperature dependence of the inhibitor recovery time are also consistent with this model.

Chapter 6

A frequency domain phosphor decay time thermometer

(1)Introduction.

If suitably excited, many phosphors produce a comparatively long (typically milliseconds) luminescence decay after the excitation ends. In the simplest cases this decay is exponential, although it is often followed by a long afterglow. Both the time constant and the intensity of the exponential portion of the decay are often strongly temperature dependent over a certain range. (Generally the decay becomes shorter and less intense as the temperature is increased). The time constant and efficiency are of course also dependent on the material used, as is the temperature range over which large variation occurs. The diagram below shows the temperature dependence of the decay time and intensity for two hypothetical phosphors A and B. Such behaviour is representative of the materials used in temperature sensing. The temperature variation of intensity or life time can be used as the basis of a temperature sensor.

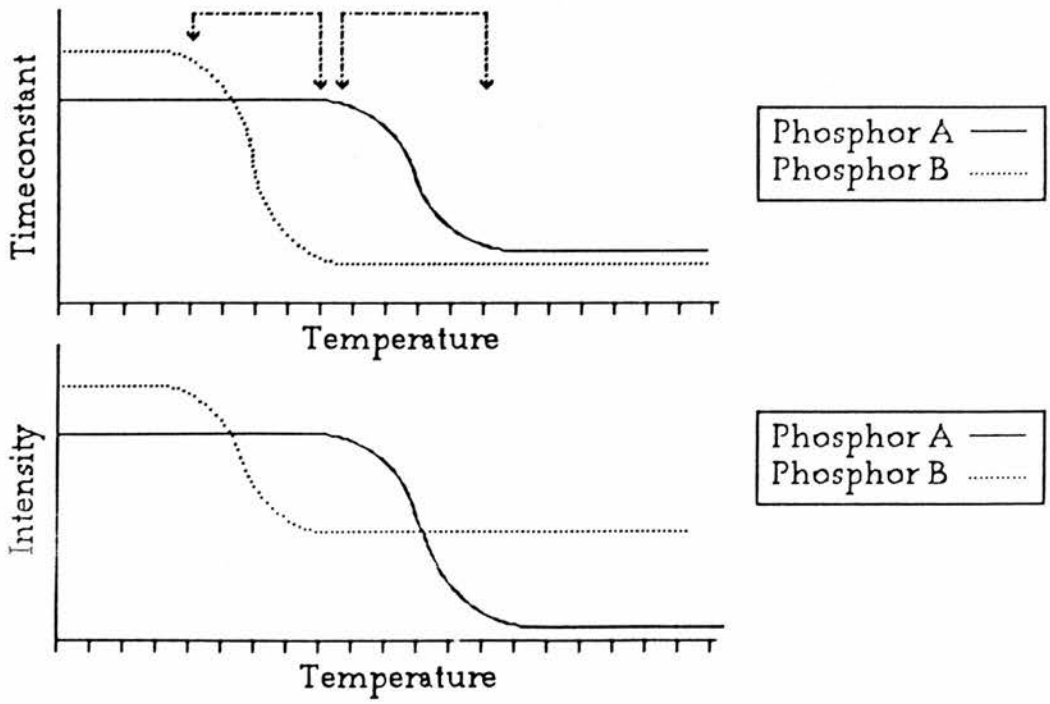

The useful ranges of both phosphor A and phosphor B in temperature sensing are indicated by the dashed arrows.

Although for many applications phosphor sensors do not offer an economically viable alternative to thermocouples and thermistors, they do have applications in some specialised areas of temperature measurement. Typically the phosphor is mounted on a surface, the temperature of which is to be measured. Because the links from the instrument to the phosphor are optical, perhaps in the form of glass fibres, they are of very low electrical conductivity. Consequently a phosphor sensor offers a considerable improvement in safety when used in high voltage apparatus. Furthermore thermocouples are unreliable in the presence of large amounts of electrical or magnetic interference, for example transformer cores, radio transmitters and engine interiors.*

The extent of current interest in the field of phosphor based temperature sensing is reflected by the ~600 papers and articles listed by Dowel et al[70] in their "Thermal phosphor research survey". However, most of this literature is devoted to materials (ie. phosphors) rather than the instrumentation necessary to produce a working sensor.

The aim of this work was to investigate the possibility of producing a phosphor emission decay based instrument for temperature measurement, that was considerably less complex than those at

* This is true, despite the fact that a thermocouple operates essentially DC whilst the interference is AC, because most metal or metal/solder junctions exhibit slight rectification. This phenomena can be seen particularly well in the pick up of AM radio signals on record players

present[71]. We began by considering phosphor temperature sensing from first principles. Two measurable parameters may be used, variation of the intensity with temperature and variation of the decay time with temperature. This leads to three possible approaches.

(i) Intensity measurement.

(ii) Time domain decay time measurement.

(iii) Frequency domain temperature measurement.

Of these (i) and (ii) have been used in commercial instruments[71], (iii) has not. We now consider each approach in turn.

(1.1) Methods of using phosphors as temperature sensors.

(1.1a) Intensity measurement as a guide to temperature.

A simple system using emission intensity as a guide to temperature would have to have constant optical efficiency and constant excitation intensity. This would be difficult to achieve in commercial applications. To get around this problem one could use a mixture of two phosphors in the detector head, one with a strongly temperature dependent emission over the required range and one with more constant characteristics. If the wavelengths of the two emissions were significantly different then signal separation by optical filtering would be comparatively easy. The instrument could compare the intensities of the two emissions and from this calculate the temperature of the phosphors. The diagram overleaf outlines the principle.

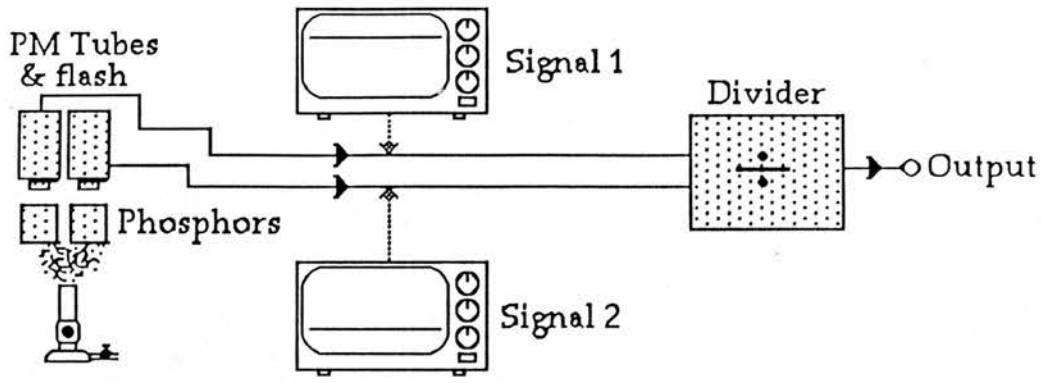

This method does however, have intrinsic problems. If the system were operated DC then any background light (such as afterglow, stray light or black body radiation) would invalidate the data. AC operation would overcome these problems but would increase the complexity of the instrument by introducing the need for some form of integrators. More importantly, this would impose the further restriction that the two phosphors would have to have comparable time decay characteristics over the entire working temperature range. Perhaps one of the most serious difficulties with this design is that many phosphors change their efficiency with aging particularly at high temperatures. This change would of course invalidate the calibration. All these factors make the system commercially unattractive.

(1.1b) Decay time measurements as a guide to temperature.

For this method only a single phosphor is required. An initial approach might be to measure the emission intensity with time after an optical excitation, and from this calculate the time constant. One might envisage this being done by a series of voltage comparators. If the trip voltages were all linked to the overall signal size then constant intensity

would become unnecessary. The diagram illustrates such a sensor.

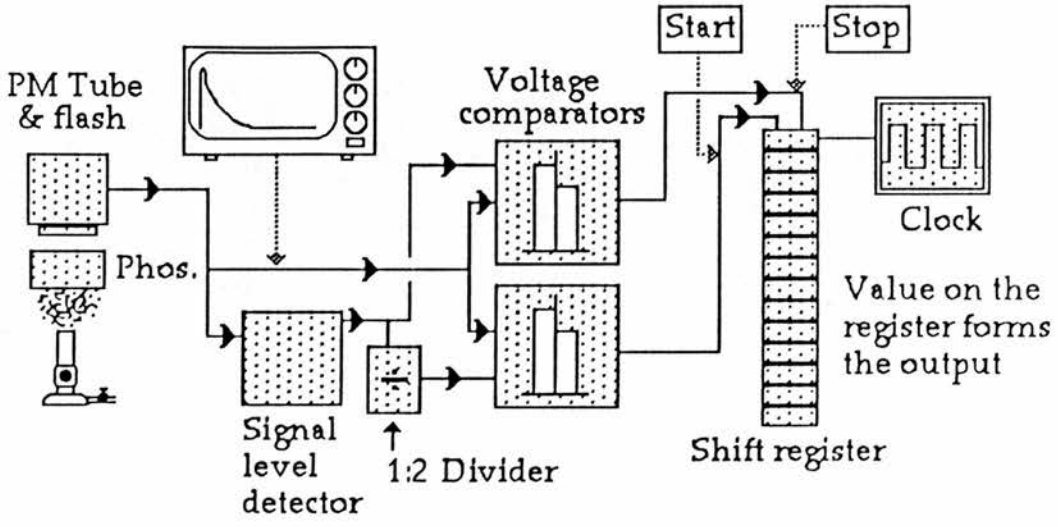

The decay is often noisy (particularly if the signal has fallen off at the "hot end" of the range) and so some form of averaging would be required. However this method still suffers from the problem of DC backgrounds affecting the results. To overcome this the signal may be digitised and computers might be used to calculate exponential curve fits. However, the hardware necessary for this would, and has, made such sensors very expensive.

A more subtle approach might be to consider the frequency domain. Any periodic function can be expanded as a Fourier series (effectively split into spectral components). For example, if this is done for a periodic exponential decay with time constant "t" and period "p", (with a 50:50 duty

cycle excitation) one has,

$$\frac{\text{Intensity}(3^{rd})}{\text{Intensity}(1^{st})} = \frac{1}{3}\left[\frac{\pi^2(t/p)^2+1}{(t/p)\pi^2+1}\right]^{1/2}$$

where 1st and 3rd refer to the first and third harmonic components of the signal respectively. (Parker [72]).

The decay time constant can thus be determined from the ratio of these harmonic components. Such a system has the advantages that it is not affected by a DC background and that the hardware required is comparatively simple. The first and third harmonics are an obvious choice since they are largest and thus offer the best signal to noise characteristics. An outline of such a sensor is shown in the diagram below.

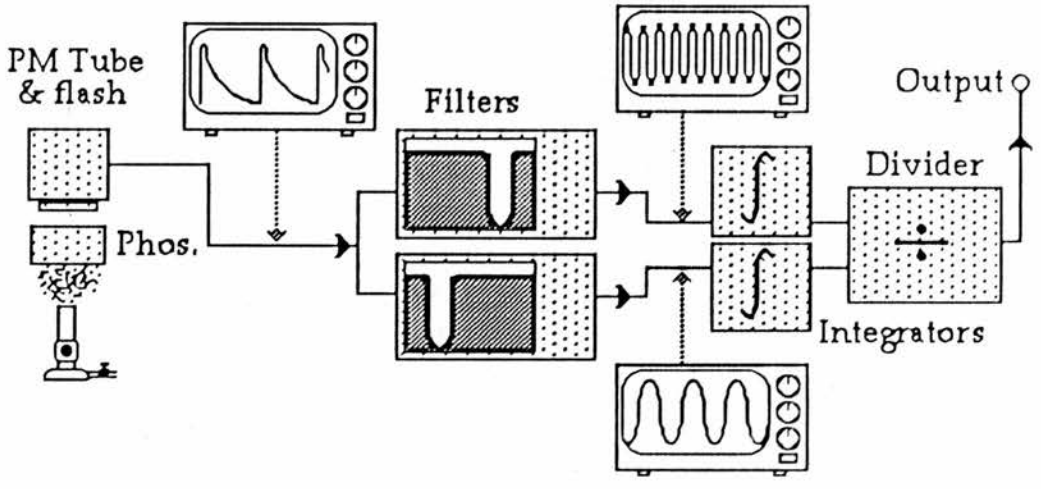

The frequency domain analysis of the decay time was adopted as the principle of our temperature sensor.

After completion the viability of the prototype sensor was illustrated using the commercial phosphor P-31 (ZnS;Cu,Ag).

(2) Experimental methods.

The following "experimental methods" section describes the design of instrumentation electronics necessary to produce a temperature sensor and the construction of an experiment to test the system performance.

(2.1) Design Details

The basic schematic is given in the diagram overleaf and accompanying it is a full circuit diagram of the prototype sensor.

The incoming signal from the photomultiplier was buffered by a 741 operational amplifier which also introduced a small gain. (A resistor in series with the input ensured a minimum input impedance under all possible operating conditions) Following the buffer is a constant level circuit. This was added after initial testing revealed that although the immunity to signal level variation was good, it could be improved by this simple piece of circuitry. (The slight residual dependence of the output on signal level is believed to be due to non-ideal component behaviour). The constant level circuit consisted of two 741 operational amplifiers and an electronic attenuator (MC3340P). (The attenuator passes a proportion of the incoming signal, the size of which is dependent on a DC voltage on a control pin.) The higher the control voltage the greater the attenuation. The buffered emission signal was fed into the attenuator and the attenuated output connected to the first 741.

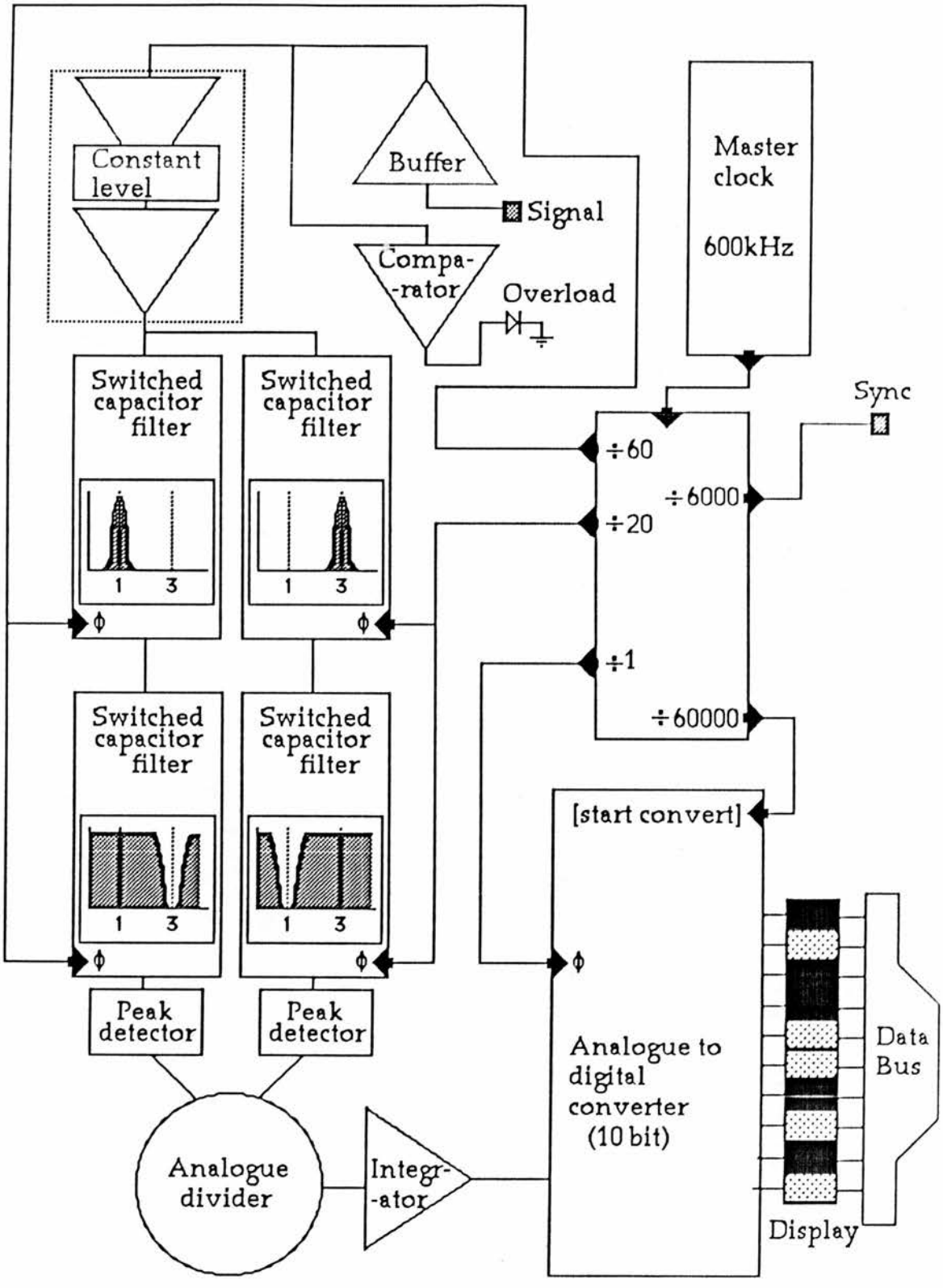
Constant level
Buffer
Signal
Compa-rator
Overload
Master clock
600kHz
Sync
Switched capacitor filter
Switched capacitor filter
Switched capacitor filter
Switched capacitor filter
1 3
1 3
1 3
1 3
÷60
÷6000
÷20
÷1
÷60000
[start convert]
Peak detector
Peak detector
Analogue divider
Integr-ator
Analogue to digital converter (10 bit)
Data Bus
Display

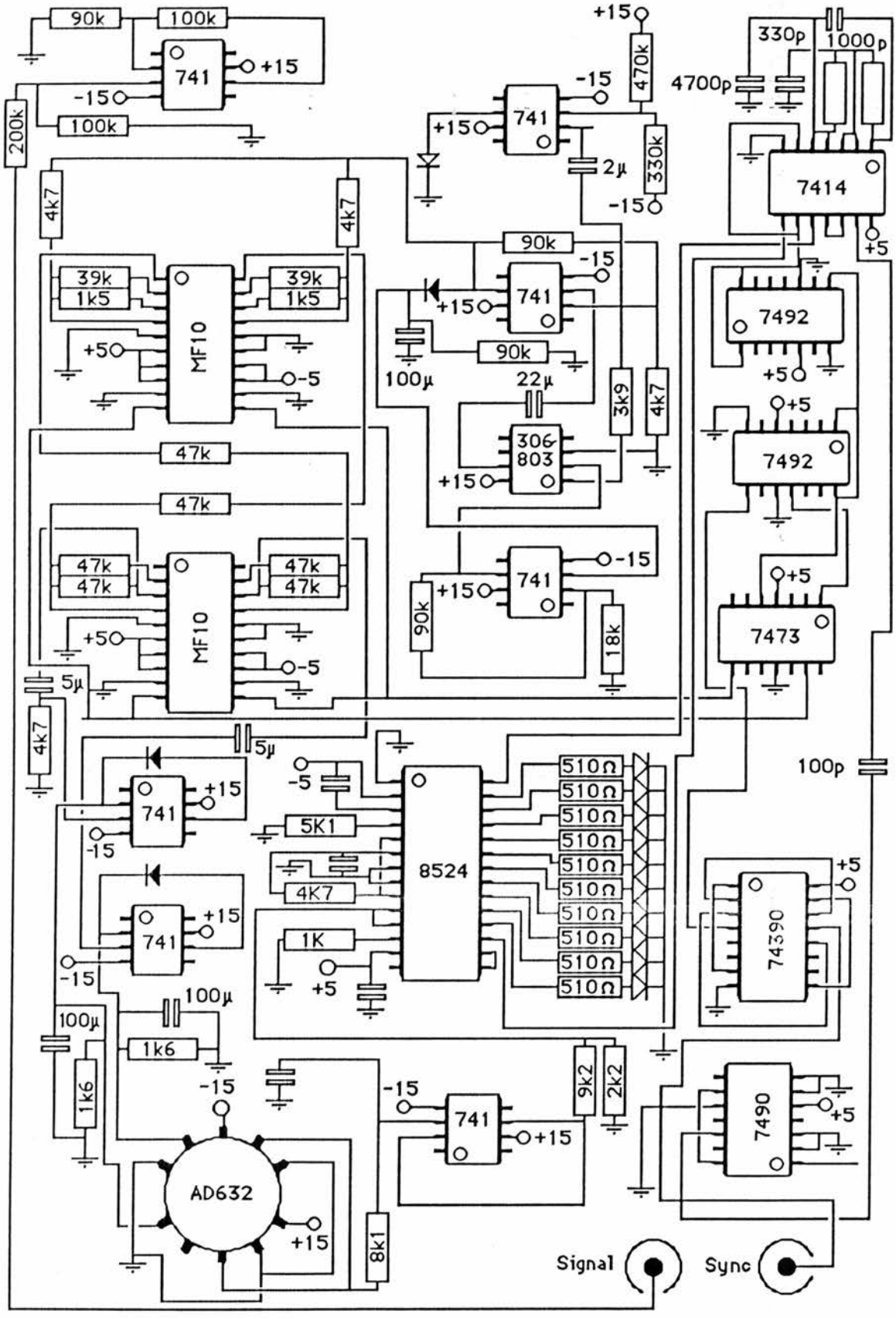
90k
100k
741
+15
-15
100k
200k
4k7
4k7
39k
1k5
39k
1k5
MF10
+5
-5
47k
47k
47k
47k
47k
MF10
+5
-5
5µ
4k7
5µ
741
+15
-15
741
+15
-15
100µ
100µ
1k6
1k6
-15
AD632
+15
8k1
+15
470k
-15
741
+15
2µ
330k
-15
90k
-15
741
+15
90k
100µ
22µ
306
803
+15
3k9
4k7
741
-15
+15
90k
18k
-5
5K1
4K7
1K
+5
8524
510Ω
510Ω
510Ω
510Ω
510Ω
510Ω
510Ω
510Ω
510Ω
-15
741
+15
9k2
2k2
330p
1000p
4700p
7414
+5
7492
+5
+5
7492
+5
+5
7473
100p
+5
74390
+5
7490
+5
Signal
Sync

The output of this 741, was branched two ways, one to form the output of the constant level circuit,the other to a diode capacitor peak detector. The output of this peak detector was buffered by a second 741 and forms the control voltage for the attenuator. In this way, overall feedback was achieved. The diagram below shows a schematic of the constant level circuit.

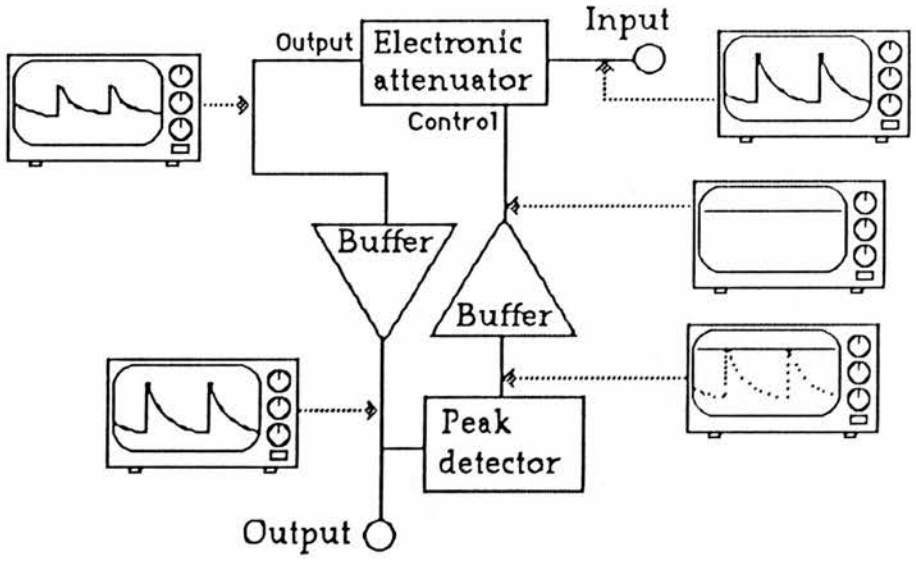

The only penalty for having this constant level circuit was a slight increase in the overall noise level. However since we were employing a signal averaging technique later in the circuit, this was not important.

The next stage was to isolate the two spectral components of interest ie the first and the third harmonics of the incoming signal. This can be done using conventional analogue active filters. However, high selectivity analogue filters are difficult to make. They are also difficult to tune and are prone to drift in operation. Such problems make them a

poor candidate for a commercial system which must be reliable and easy to use. (The intention at this stage was to design a system which was free from drift, self tuning and requiring no operator adjustments.)

Very high quality factors and freedom from drift were achieved by the use of switched capacitor filters in the form of the MF-10 integrated circuit. The precise principle of operation of such filters is complex[73] and will not be discussed here. Essentially the centre frequency of the band pass filter is dependent on an external reference frequency rather than component values. (In this case the centre frequency is one hundredth of that of the reference).

Since digital division is a precise process it was possible to produce reference signals for the two filters that differed by a factor of exactly three. This meant that if the first filter was tuned to the first harmonic the second was automatically locked on to the third. A further advantage of this method was that if the flash tube was also triggered by the master clock the system became self tuning. That is the filters were permanently locked onto the correct frequencies for the flash and emission. This being the case it was not necessary to make the passbands wide to allow for tuning errors and thus the selectivity could be high. This increased accuracy and reduced noise. The main limit to how sharp the passbands could be was an allowance for the flash trigger consistency.

In practice the clock consisted of a feedback oscillator based around a hex inverter integrated circuit. The master clock ran at approximately 600kHz, the lower frequencies such as filter references and flash trigger

being provided by digital division of this. The dividers were based on a series of jk flipflops and serial shiftregisters (The system adopted was based on components that were available, however, in a working model a reduction in hardware would be possible).

A refinement to the filtering was made by considering the nature of the signals. The largest contaminant to the third harmonic signal is the first harmonic and vice-versa. Thus, to improve the purity of the two harmonics each band pass filter was followed by a band reject filter centred on the opposite harmonic. Any remaining first harmonic was thus removed from the third harmonic signal and visa-versa.

After filtering, the two harmonic signals (now in the form of sine waves) were fed into peak detectors each based on a 741 operational amplifier and a diode capacitor network. Peak detection eliminated the need to consider relative signal phase. The capacitors in the peak detectors also provided a degree of noise averaging. The DC outputs of the peak detectors were used as inputs for an analogue divider (AD-632).

For a system where 32 levels of resolution (temperature increments) will suffice , the following alternative method may be adopted. Two 6 bit converters could be used, one for each of the two harmonic components. The output of these could be used as the address for an EPROM, The two data buses could be simply put end to end to form a 12 bit address. The EPROM could be programmed to have the result of division of the two numbers stored at the appropriate location. For example, suppose that the

first harmonic signal level was 011110 (dec30) and the third harmonic 001010 (dec 10). The number stored at the address location 011110001010 would be 000011 (dec3) the result of the division. In the future the size and price of read only memory is likely to fall and so this may represent a viable alternative to analogue division in all the temperature sensors.

The output of the AD-632 was used as an input for a 10 bit analogue to digital converter. The clock for the analogue to digital converter was taken directly from the master clock. The analogue to digital converter was used to drive a display ur it. The display was updated each time a start convert pulse arrived at the converter. For human monitoring the fastest useful update frequency was about 10Hz so this is the frequency that was used. The 10Hz signal came from a further division of the master clock. One problem did arise. During the start convert low cycle the converter was dormant and the display dark. This gave the impression of a flickering display. This problem was overcome in the following way. In order to initiate a conversion, the start convert signal need only be low for a few nanoseconds. Thus the display need only be dark for this time plus the conversion time (~50μs). The start convert signal was converted into pulses of short duration so that the off period became invisible. This was done by passing the 50:50 duty cycle 10Hz signal through a differentiator formed from spare channels of the hex inverter. The square edges produced sharp spikes when differentiated which formed the start conversion pulses.

The emission decay of the P-31 and many other phosphors was not perfectly exponential, thus an EPROM look up table would be the only sensible approach to calibration.

The output of the system was found to be independent of intensity over a large but finite range. Should this range be exceeded the operator must be warned that the system accuracy is reduced. This was done by feeding the incoming signal into a peak detector in order to convert it into a DC level. This level was then used as an input to a voltage comparator based on a 741 operational amplifier. The comparator output was sent to a polarity sensitive indicator, a light emitting diode in this case. If the signal level fell below a certain value the LED lit up. In a final version it would be desirable to have an overload light as well.

The power supply was constructed on a separate board and produced stable voltages to supply the main circuit. The circuit diagram is shown overleaf. An electronic phosphor simulator was also constructed so that the system could be demonstrated without the need to set up the rest of the experiment. The schematic for this is shown below.

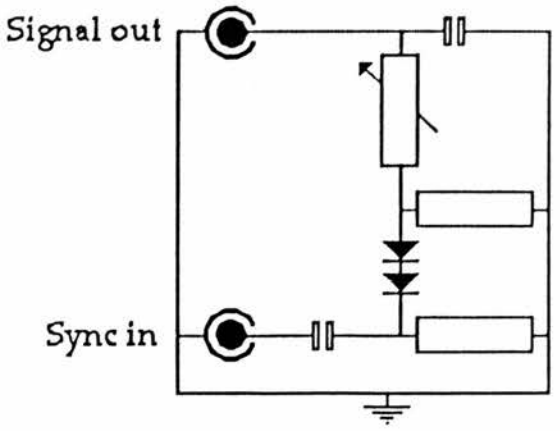

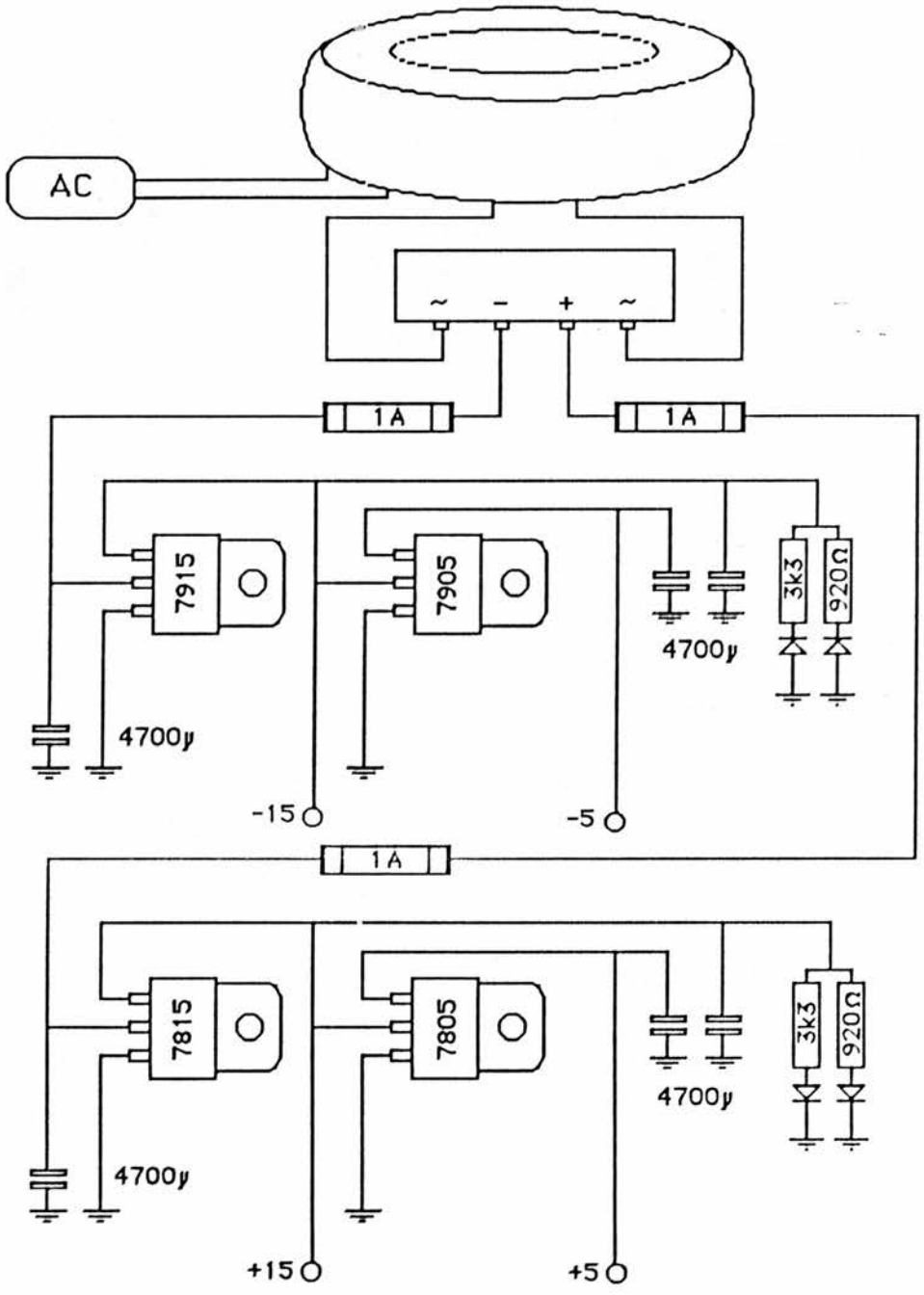
AC
~
-
+
~
1A
1A
7915
7905
4700µ
3k3
920Ω
4700µ
-15
-5
1A
7815
7805
4700µ
3k3
920Ω
4700µ
+15
+5

The sync pulse which would normally be connected to the flash was used to provide the simulator input. The sync signal was in the form of a square wave. Inside the simulator this was differentiated to form spikes. The positive going ones are suppressed leaving a string of negative spikes of around 4V in amplitude. These were then passed through a resistor-capacitor time constant circuit to simulate the decay output of the photomultiplier. The time constant and thus the decay speed could be varied by turning an external potentiometer.

(2.2) System testing.

Two principal tests were performed on the sensor. Firstly, the output of the system was measured as a function of incoming signal amplitude (with constant decay time). This enabled us to measure the immunity of the system to input signal level variation. Secondly, an experiment was set up with a real phosphor (P-31 ZnS:Cu,Ag) so that the overall performance of such a sensor could be investigated.

(2.2a) Immunity of the sensor to signal level variation.

In order to keep as many parameters as possible constant, the phosphor simulator was used in preference to a real phosphor. During this experiment the output of the simulator was amplified (to enable deliberate overload) and then passed into a variable attenuator. The output of this attenuator then provided the incoming signal for the sensor. The output (Temperature reading) was recorded as the input signal level amplitude was varied. This was done for two different decay time constants. The experiment is shown below.

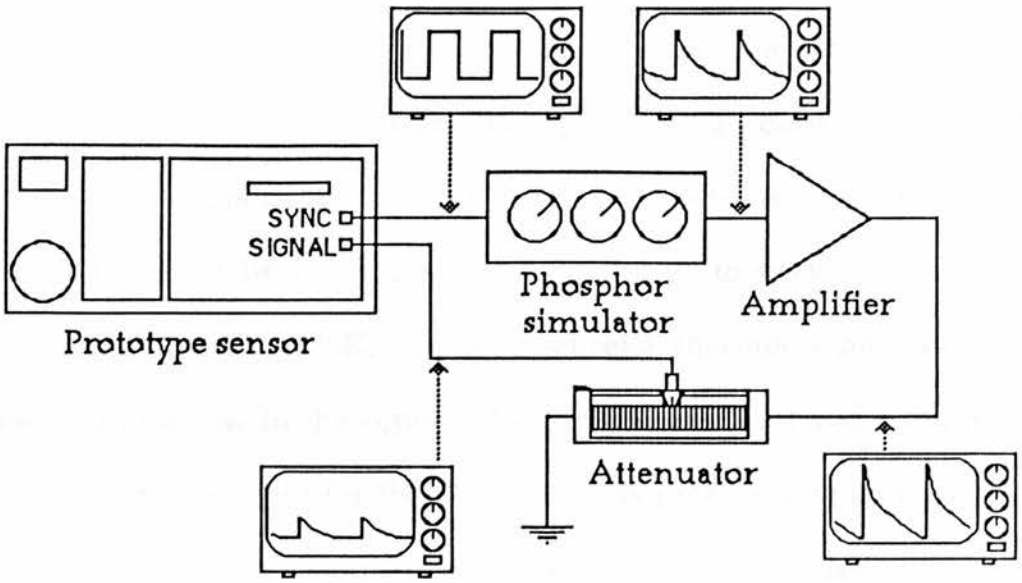

(2.2b) Operational testing with the P-31 phosphor.

The external apparatus was set up as in the diagram below.

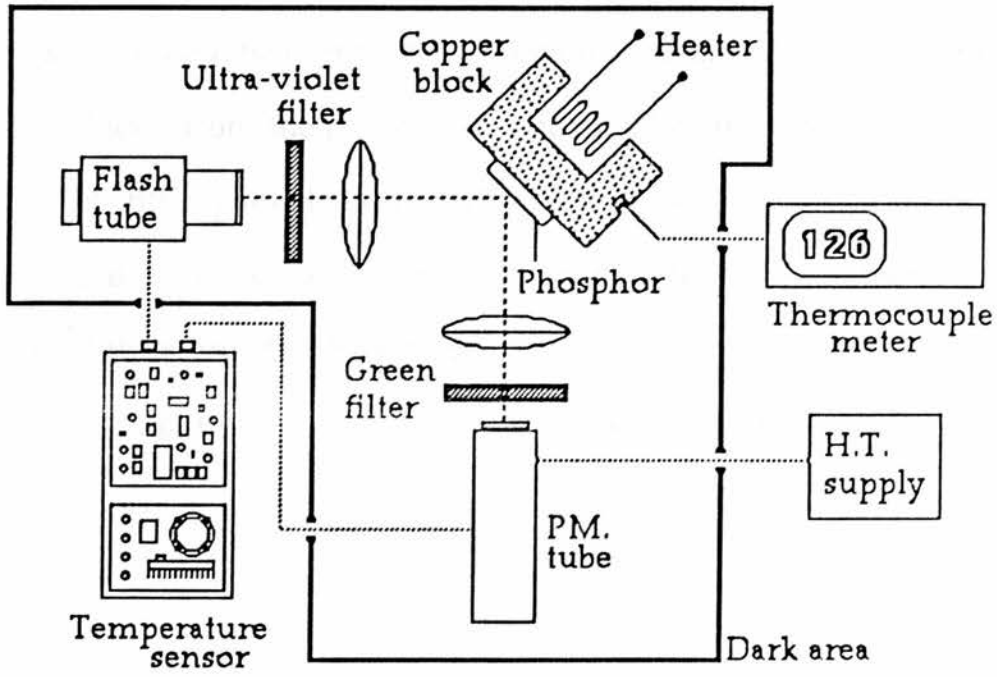

The P-31 phosphor (in powder form) was mixed with sodium silicate

powder and water to form a paste. This paste was applied to one face of a 0.5kg copper block to form a spot around 1cm in diameter. When dry the mixture hardens to form a mechanically strong coating which adheres well to the copper. The copper block was mounted on an electrically heated thermostatic hot plate. This enabled us to vary the temperature over the range 300-520K. A copper-eureka thermocouple junction was mounted in a hole in the copper block to provide a reference temperature.

The excitation light for the phosphor was provided by an Irwin EA0374 flash unit. This was set to external trigger mode and driven by the "sync" signal from the temperature sensor. The maximum flash rate was 120Hz limited by the lamp recharge time. The light from the lamp was passed through a Kodak Wratten 18A filter to isolate the ultra-violet. This 18A filter prevented visible light from the lamp simply reflecting off the phosphor surface and swamping the emission. The ultra-violet excitation light was excluded from the photomultiplier by a Wratten 58 (green pass) filter. The "58" filter passed the majority of the phosphor emission. The emission was detected by a IP28 photomultiplier tube, the output from which formed the signal for the sensor.

The digital output of the circuit was monitored as the temperature was varied.

(3) Results.

The graph below shows the variation of the digital system output (temperature on the final sensor) with peak signal amplitude. The two curves represent results obtained using two different time constants for the decay, ~5ms & ~15ms. Decay 1 and 2 respectively. 1% accuracy is maintained over the input voltage range 0.3 to 3.0 Volts.

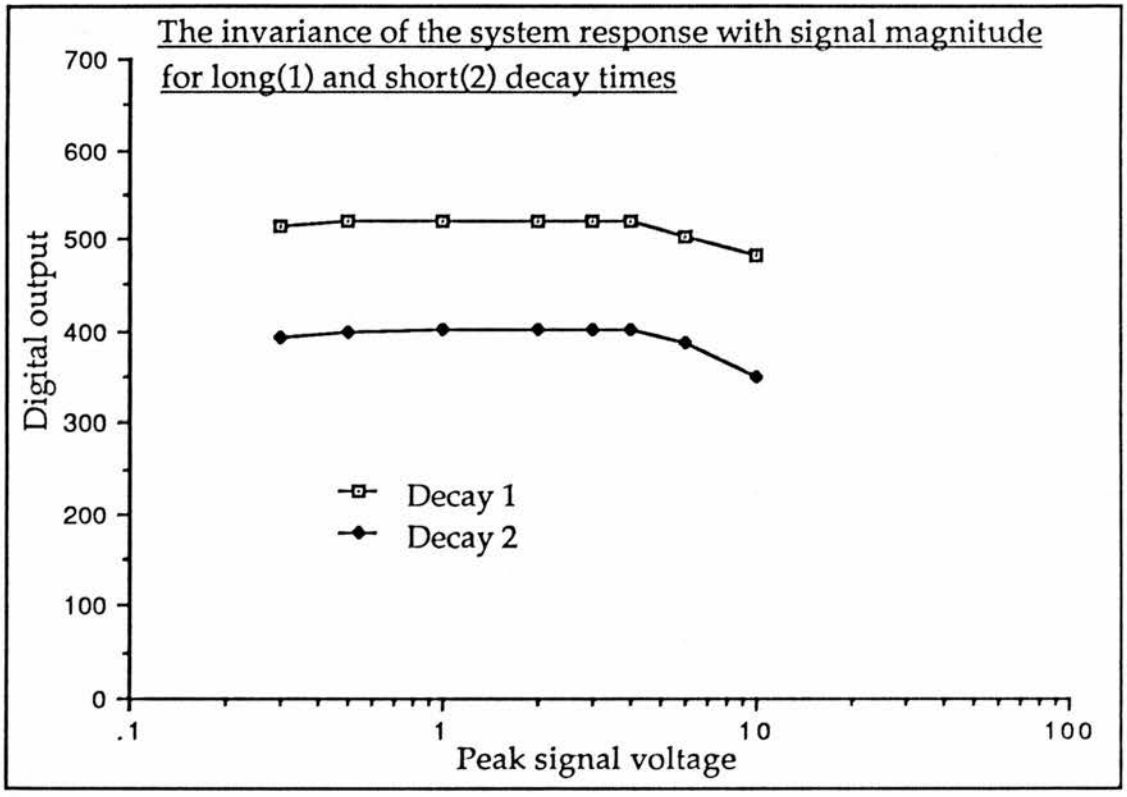

The graph below shows the variation of the digital system output with the temperature of the P-31 phosphor. Providing that the copper block temperature is given adequate time to stabilise there is no hysteresis effect on the characteristic. The jitter on the signal in operation was around ±1 in the least significant bit.

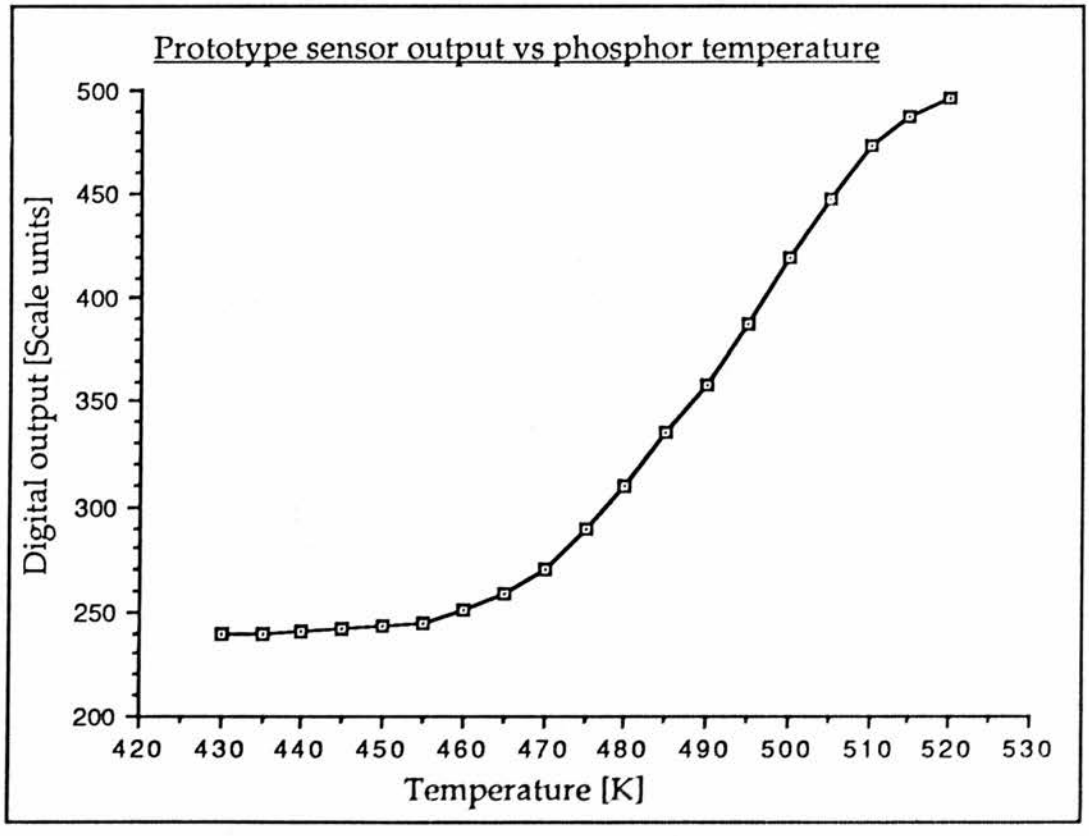

(4) Discussion and conclusion.

(4.1) System performance.

The phosphor temperature sensing system has been demonstrated to work well over the range 465 to 520K with 0.5K resolution. The system is independent of signal amplitude over a finite but useful range (0.3-3V with ±1 in least significant bit)

(4.2) Improvements to the prototype.

The prototype sensor was assembled on a single custom made printed circuit board. In operation electrical interference from the digital pulses that run some of the circuit elements often caused problems. In order to improve this the digital electronics could be mounted on a separate circuit board with an independent route to system ground.

A greater variety of suitable phosphors would enable the sensor to be used over a much wider temperature range and thus expand its usefulness.

Fibre optic light guides would improve optical efficiency and make the system easier to operate.

Chapter 7

Optically induced deep level electron hopping in GaAs:Cr and ZnSe

(1) Introduction.

The wave function of an electron bound to a localised level within the energy gap of a semiconductor has small but finite values beyond the immediate locality of the centre. If the wave function of such an occupied state overlaps an empty state there is a small probability that the electron will "hop" in to the empty state. Normally such hopping results in no overall current flow or polarisation since the movement is spatially random. However, in the presence of an electric field net movement can occur and the resulting charge transfer is usually called impurity conduction. This is of course a very simple view of the process, many detailed theoretical treatments are available (see for example Austin & Mott[74] and Scher & Lax[75][76]), although these need not concern us here. If the process is modelled by an electron hopping between adjacent centres, it can be shown that the AC conductivity of the sample becomes dispersive. If the hopping is continuous in real space, that is the electron executes a random walk by hopping from one centre to the next and then the next, then there will be a component of DC conductivity. Dispersion in the AC conductivity has become the hall-mark of hopping conduction processes in semiconductors.

Low temperature work on shallow level hopping has been carried out on many materials. Examples include, silicon (Pollak & Geballe[77]), GaAs (Kahlert[78]) and ZnSe (Rentzsch[79]). The general method adopted in such work is measurement of the AC conductivity of the sample as a function of frequency at low temperatures. If the material contained only donors,

these would all be full at very low temperature, and consequently no hopping would be seen. For this reason all of the above mentioned work has been carried out on partially compensated samples.

Dispersive capacitance has previously been reported in semi-insulating GaAs by Jonscher & Pickup[87]. In their samples the dispersion was observed in darkness at comparatively high temperatures. Jonscher & Pickup believe that four separate processes are occurring in the sample, and that there is a "phase transition" at 250K. In the work presented here, we have observed light induced dispersion in insulating GaAs:Cr, which we believe is due to hopping between deep acceptors within the energy gap. We have also performed similar experiments on ZnSe in which we believe we have seen hopping between deep centres of unknown origin. The samples we have used are highly doped, yet almost fully compensated and as such are highly insulating. With particular reference to the GaAs:Cr system, in darkness all the deep acceptors are full and thus no hopping can occur between them. However when the sample is suitably illuminated, some of these acceptors are emptied and a dispersion of the capacitance is seen. Such deep level studies are in a sense easier than shallow level work because apart from the simplified cryogenics the hopping process can effectively be switched on and off. This provides a background against which the dispersion can be compared. When working with shallow level systems one has to substitute undoped material as a control. Deep level studies also offer the possibility of gaining additional information about the nature of the process from the spectrum of the photo-effects.

In the GaAs:Cr system we have found strong evidence for the existence of a deep level hopping process. For the ZnSe material we have similar results, however, because of the nature of the sample we are unable to draw such definite conclusions from these.

Experiments were also performed on partially compensated GaP:Co and InP:Fe, however other processes were found to dominate the conductivity of these samples.

Jonscher[80] has proposed that a universal dielectric dispersion law exists for almost all materials. We have briefly discussed this and its relation to our work and that of Pollak and Geballe on silicon.

(2) Experimental methods.

(2.1) Sample preparation and mounting.

Five samples were used during this work. Two of melt grown GaAs:Cr supplied by S.E.R.L. One of melt grown InP:Fe supplied by Plessey. One of melt grown GaP from Eagle Picher into which cobalt was diffused and one of vapour grown ZnSe. All were in the form of lamina approximately 0.5cm^2 in area and between 0.1 and 2mm thick.

In order that the sample temperature might be varied, the samples were mounted in a Thor continuous flow cryostat. The capacitance was measured at various frequencies on a Wayne Kerr 601 or a General radio 1615-A capacitance bridge. The electrical requirements of the capacitance bridges used imposed restrictions on the method of sample mounting. One such restriction was that neither of the sample contacts must be common with the cryostat ground and consequently the coldfinger. It is however important to ensure good thermal contact between sample and coldfinger. The samples were fixed to a brass stud with epoxy resin. (This can be removed with toluene and ultrasound.) A thin mica sheet was sandwiched between the back contact and the metal stud to ensure electrical isolation. The brass stud was then secured to the coldfinger. Contacts were made onto the samples by evaporating aluminium, with the exception of the InP:Fe which was supplied with gold contacts. The diagram overleaf illustrates the sample mounting system. The copper tags ensure that the contact is mechanically strong. Electrically conductive silver paint was used to fix the copper tags to the aluminium contacts. The

silver paint is highly soluble in toluene and consequently ensures the safe release of the sample from the epoxy.

The front contact is large, and obscures around 50% of the sample face. A balance must be reached between increasing the capacitance and maximising the light collection area. One might at first sight think that light which is normally incident on the sample will not penetrate beneath the contact and thus no effect will be seen. However the refractive index of the sample is large and the sides smooth so that total internal reflection serves to scatter the light throughout the sample.

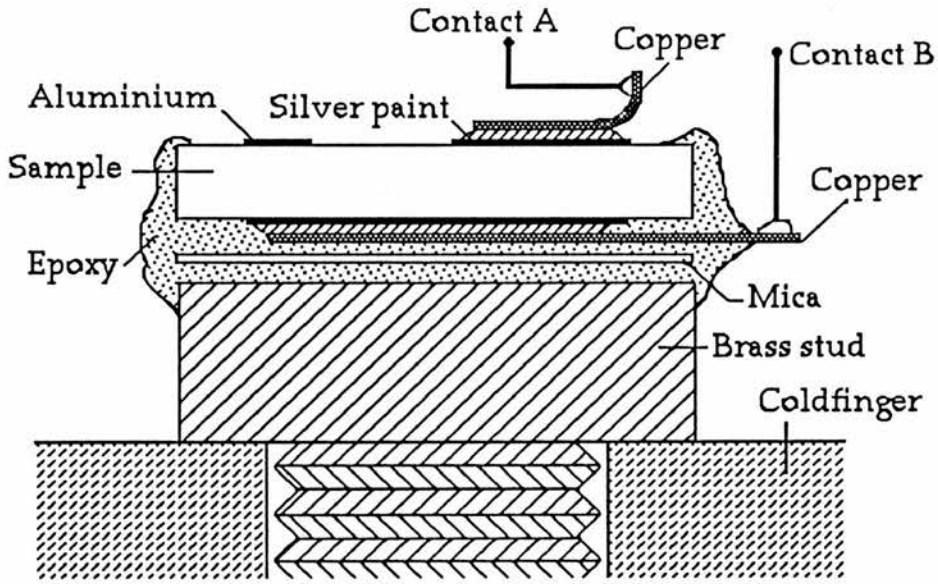

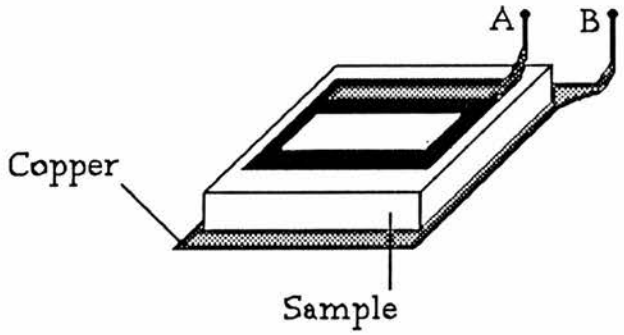

(2.2) Cryogenics.

The temperature of the sample was monitored with a thermocouple. This was based on copper/eureka junction, and the wires were continued outside the cryostat with the same metals. The temperature was monitored on a Control and Readout Ltd. 405 temperature controller which is already calibrated for these wires. The accuracy was checked by lowering the coldfinger directly into ice water and liquid nitrogen. The two temperatures recorded were 273K and 78K respectively which seemed acceptably accurate.The cryogen used was nitrogen in gaseous form. The arrangement can be seen in the diagram of general apparatus (overleaf).

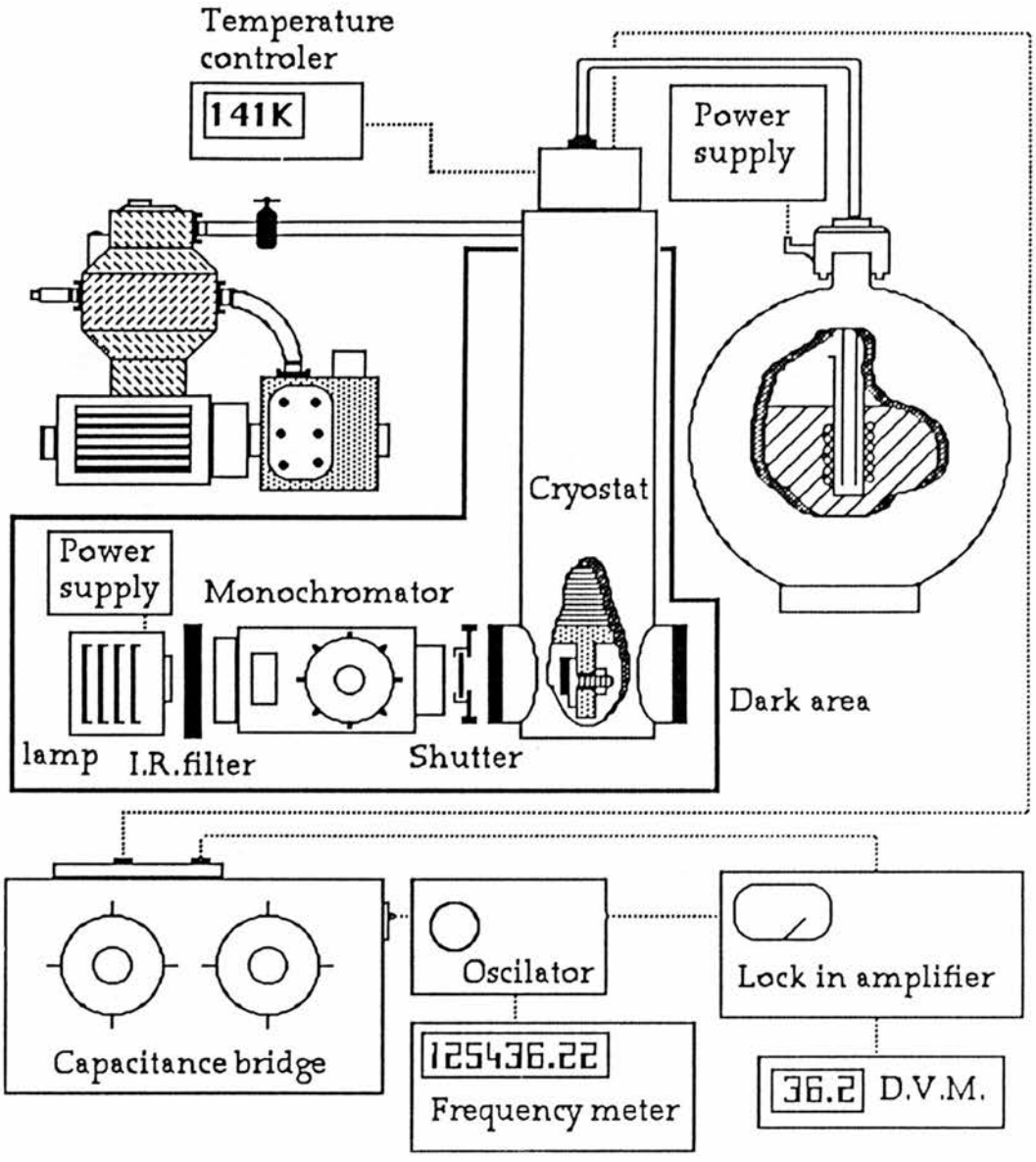

A metal dewar containing approximately 15 litres of liquid nitrogen had secured into its neck an adaptor for the transfer tube. Around the base of this adaptor (inside the dewar) is a heater element which is used to boil off the nitrogen and thus raise the pressure in the vessel. This forces gaseous nitrogen (at ~ 77K) through the transfer tube and thus into the cryostat. Once inside the cryostat the gas passes through a heat exchanger and then out of an exhaust port. Since

nitrogen is not expensive it was allowed to escape into the atmosphere at this point. When the transfer tube and cryostat were evacuated to below 0.01 mTorr it was possible to achieve a temperature of 105K at the sample using this method. (Radiative exchange and leakage conduction through the metal joints of the cryostat provided a thermal loss such that the lowest temperature that could be reached was greater than 77K). The temperature could be controlled by the flow rate of the gas which could in turn be controlled by the current passing through the heater in the nitrogen.

(2.3) Electrical measurements.

The two bridges used for the capacitance measurements were a Wayne Kerr 601 (15kHz to 15MHz) and a General Radio 1615-A (50Hz to 150kHz). Both of these measure equivalent parallel capacitance and resistance. The 1615-A bridge was more accurate (both systematically and randomly) in addition to being more convenient to use and was thus used in preference for measurements at frequencies within its range. The 1615-A bridge is designed to automatically null any capacitance between the connecting leads and the system earth. Advantage was taken of this facility by earthing the cryostat body and isolating the sample contacts from this. Thus an accurate null was provided at all frequencies. The 601 does not have this facility but instead is fitted with a manual null control to set the zero. The cryostat leads have a capacitance of something like 100pF, whilst the sample may have a capacitance of as little as 2pF. This poses a problem, in that the bridge has to be on a scale

such that 100pF will balance out, but the sample may exhibit changes in capacitance of as little as 1pF at maximum so that the overall change would be one percent of the total rather than fifty percent. This problem was overcome by breaking the connection to the sample inside the cryostat right next to the coldfinger in order to perform the null so that almost all of the stray capacitance due to the cryostat and mounting was compensated for. Unfortunately the null control on the bridge is not independent of frequency and thus a null must be made at each frequency during a run. Clearly it is not possible to open and re-evacuate the cryostat each time a measurement is made. A small reed switch was fixed on the cold finger so that the sample could be disconnected with a magnet outside the cryostat body and thus a null could be conveniently made at each frequency during a run.

In order to ensure that the capacitance effects observed in the samples were genuine and not artifacts of the experiment a series of fixed known value capacitors and resistors were placed in the cryostat as near as possible to the position of the sample. The capacitance was measured at a range of frequencies so that limits of confidence of the experiment would be known. The capacitance measured was within manufacturers stated tolerances and was almost completely non-dispersive over the range in which the experiments were to be conducted (100Hz to 800kHz). Typical results of such tests for both bridges are shown overleaf.

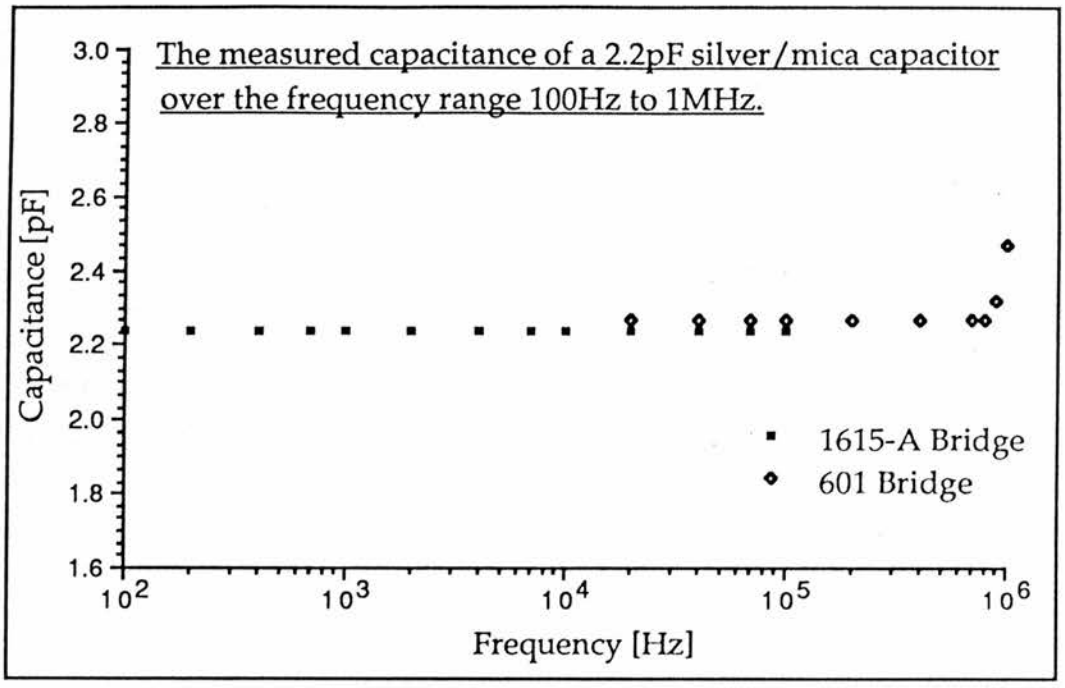

The 1615-A bridge is designed to perform tests on commercial capacitors (whose impedance is dominantly reactive) and for this reason the resistive phasor is expressed as a loss factor. The bridge is optimised for low loss systems so difficulty arises when the parallel equivalent resistance becomes the dominant conduction process (as in some of the samples used). This problem arises particularly when photon excitation is used to generate carriers. It was found that the bridge became systematically inaccurate when the loss factor exceeded one, furthermore the inaccuracy was slightly frequency dependent. This problem was solved by introducing a metal film fixed resistor in parallel with the sample to dominate the loss, and balancing this with a potentiometer in the opposite arm of the bridge. Thus the dispersion dial could be kept at 0 throughout a run irrespective of the sample resistance. The accuracy was thus restored.

This procedure did of course prevent the measurement of resistance when using this bridge. The in phase resistive component is in any case, dominated by carrier movement in the conduction band when the sample is illuminated.

Two signal generators were used as a source for the bridge, an Airmac 399 video oscillator and an Advance jib audio frequency generator. The frequency markings on the dials of the signal generators was not completely accurate, and so the frequency was monitored on a Dawe 719a frequency meter.

The illumination was provided by a tungsten lamp of high intensity. The power for this came from a stable DC 120W supply, the maximum load condition ripple being around 0.1%. The use of a DC light source avoids interaction between the modulated light and the AC electric field.

The light was passed through a Bausch & Lomb high efficiency monochromator before being focused onto the sample. Wide pass infrared filters were also used to cut out second order components. The bridge was nulled at each frequency (for the 1615-A bridge this is automatic), and the light and dark capacitance were recorded manually from the dials. In this way a plot of capacitance against frequency was built up. For the GaAs:Cr S1 sample a spectrum of the photo effect was recorded.This was done by manually recording the out of phase off balance signal from the bridge at each wavelength. In order to calibrate the spectrum the sample (and cryostat) was replaced by a

thermopile detector. This voltage is proportional to the total incident energy but can be easily converted into photon number. The calibration factors were calculated on the basis of a normalised incident photon number.

(3) Results.

(3.1) GaAs:Cr Samples 1&2.

The graph below (Fig.1), shows the variation of the capacitance of GaAs:Cr S2, with frequency both in darkness and under 1.75nm monochromatic illumination.

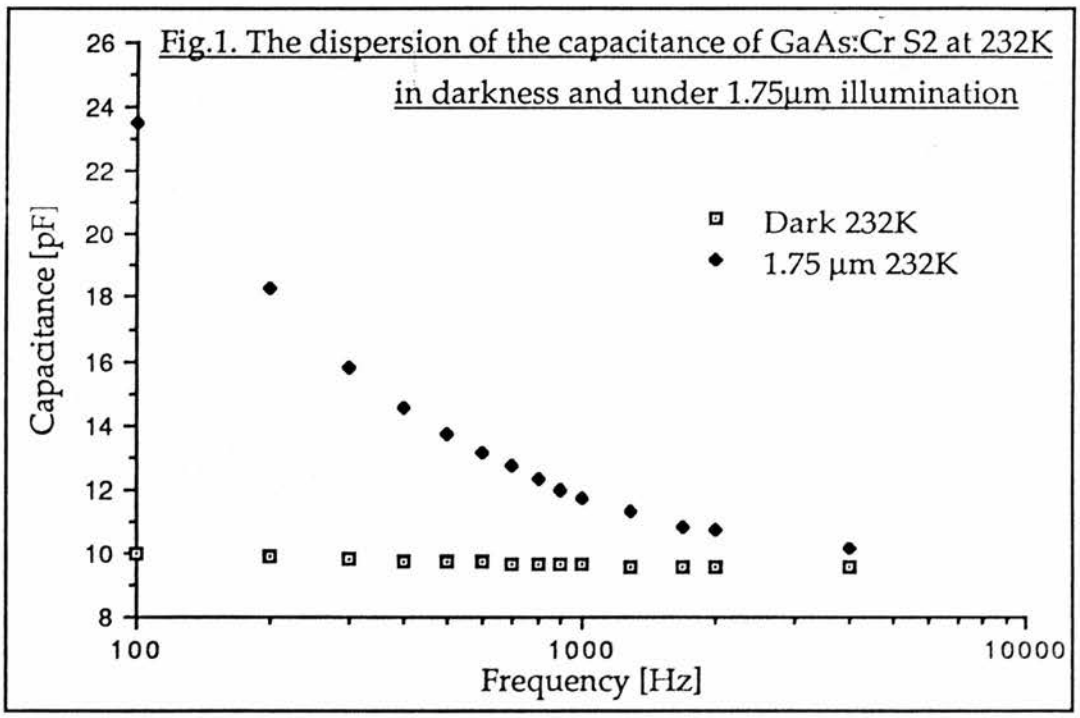

The two plots overleaf (Figs.2&3) show the variation of the difference capacitance with frequency and temperature for GaAs:Cr S1 and S2 respectively. Difference capacitance is defined as,

$$C_{(Diff.)} = C_{(light)} - C_{(Dark)}.$$

1.75μm monochromatic light was used to induce the capacitance change. The straight lines represent power law curve fits to the data, from which the dispersion parameter "s" can be defined according to,

$$C_{(Diff)} = A\omega^{s}$$

where A and s are constants and ω is the angular frequency.

Fig.2. The difference capacitance as a function of frequency at six temperatures for GaAs:Cr S1

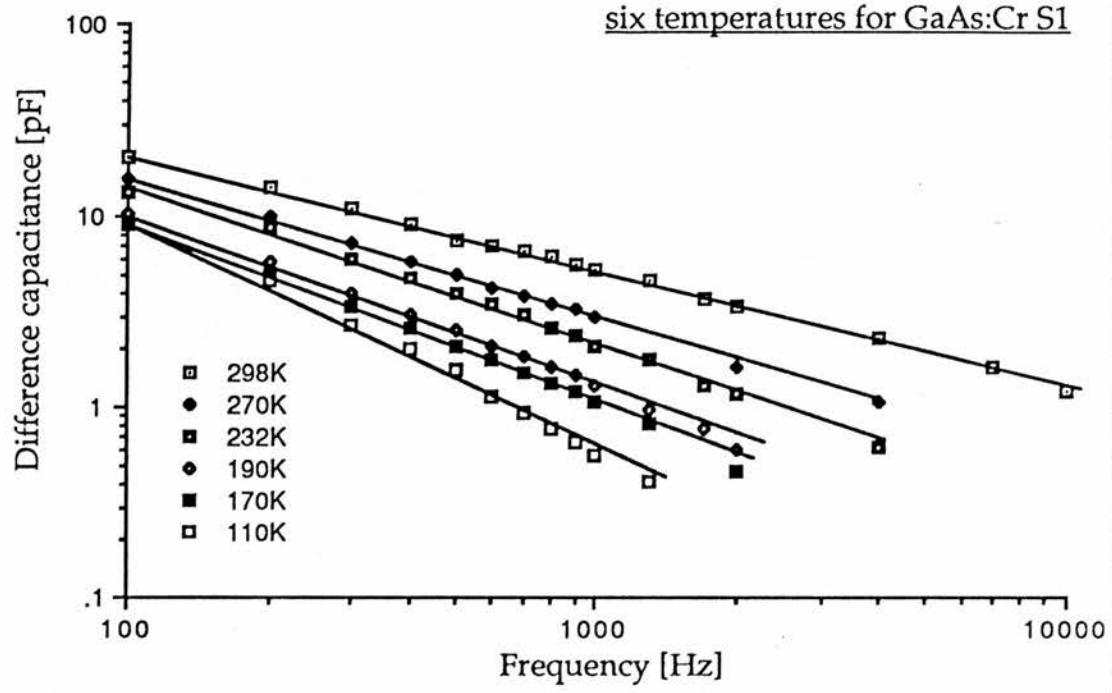

Fig.3. The difference capacitance as a function of frequency at six temperatures for GaAs:Cr S2

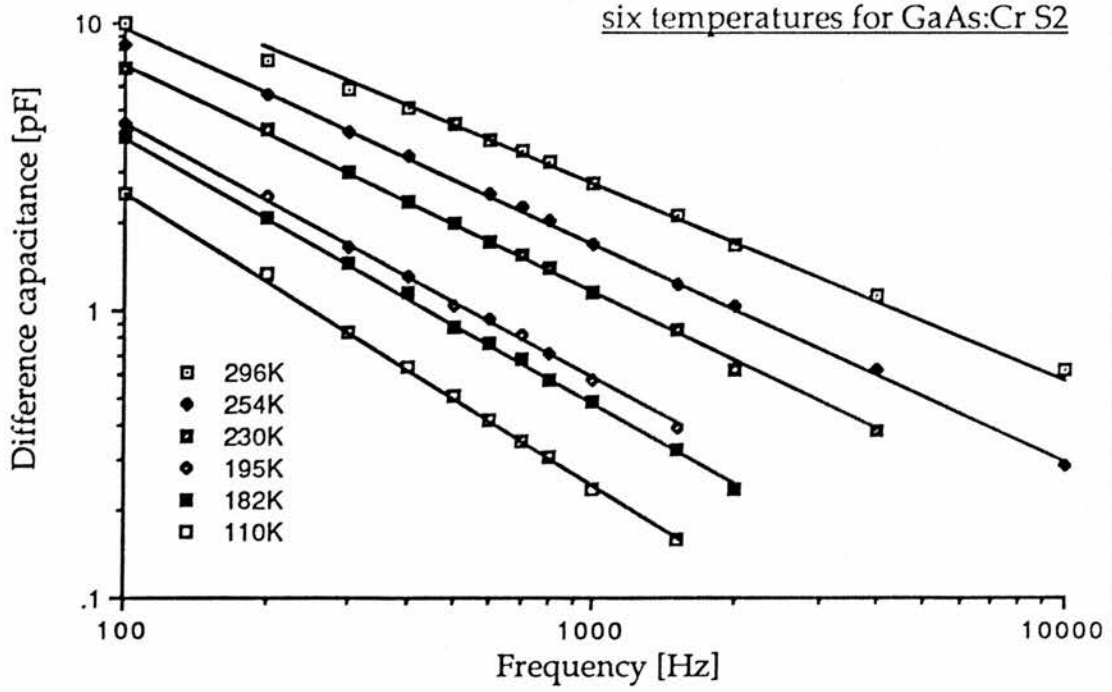

The two plots overleaf (Figs. 4&5) show the gradient of the straight line fits to the $C_{(Diff)}$/frequency data (from Figs. 2&3), plotted against temperature. The gradient of these lines represents "s" in the

$$C_{(Diff)} = A\,\omega^{s},$$

power law relation. The straight lines on Figs. 4&5 represent curve fits to this data.

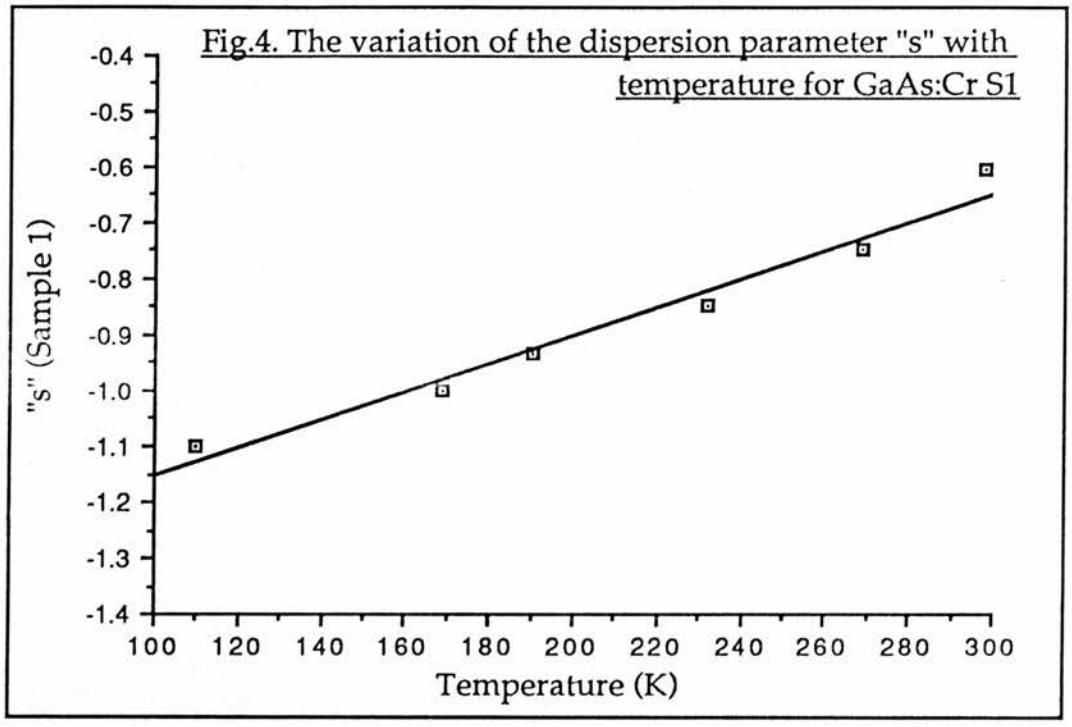

Fig.4. The variation of the dispersion parameter "s" with temperature for GaAs:Cr S1

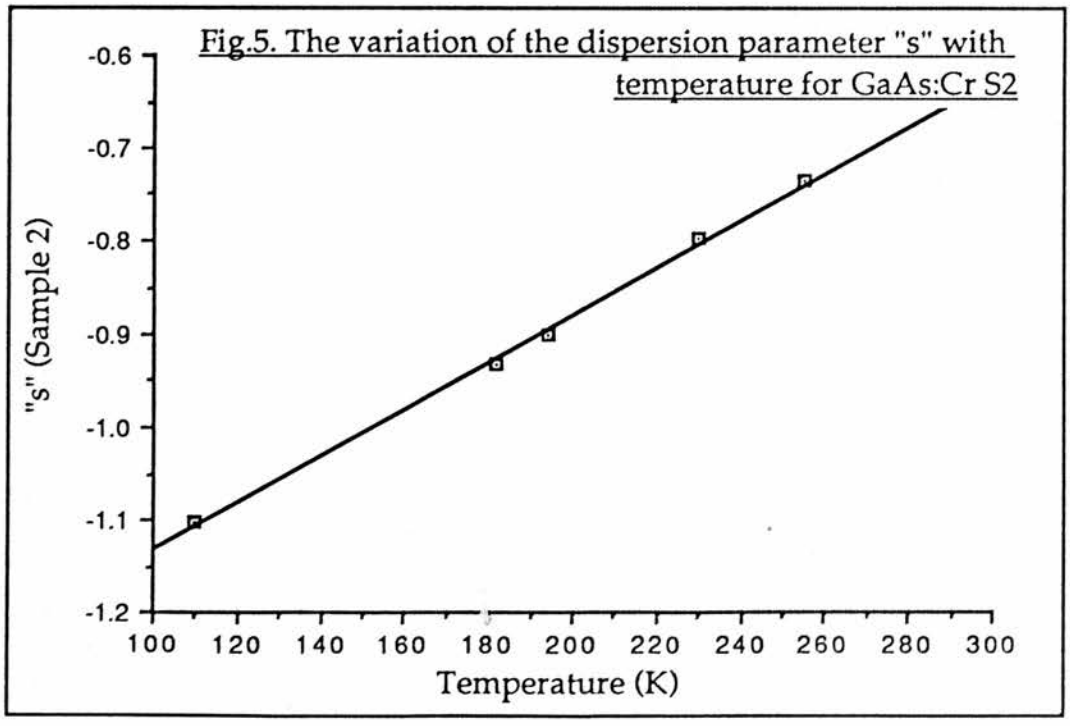

Fig.5. The variation of the dispersion parameter "s" with temperature for GaAs:Cr S2

The graph below (Fig.6) shows the magnitude of the difference capacitance of GaAs:Cr S1 as a function of photon energy. The frequency for this run was fixed at 1kHz and the data were recorded at 185K. The spectrum was calibrated in terms of photon number by replacing the sample with a thermopile detector.

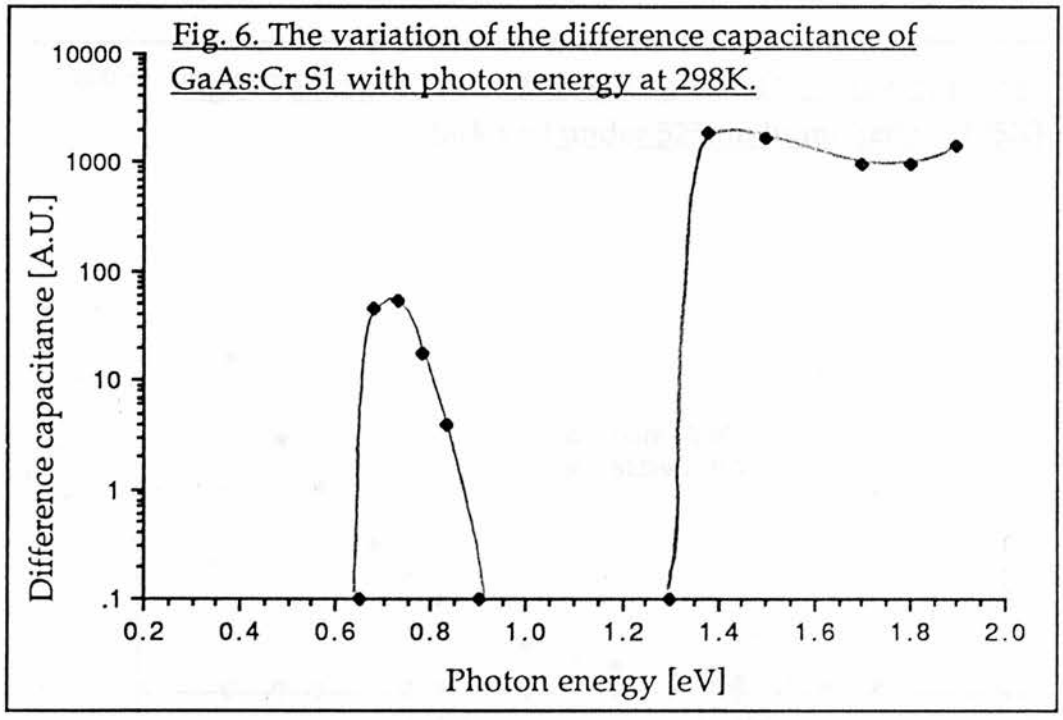

(3.2) ZnSe

Fig.7 (below) shows the capacitance of the sample ZnSe as a function of frequency, in darkness and under 525nm monochromatic illumination. The data were taken at 185K.

[The ZnSe sample used here is not the same as that discussed in earlier chapters (ZnSe1 S1) , although the two are from the same source material.]

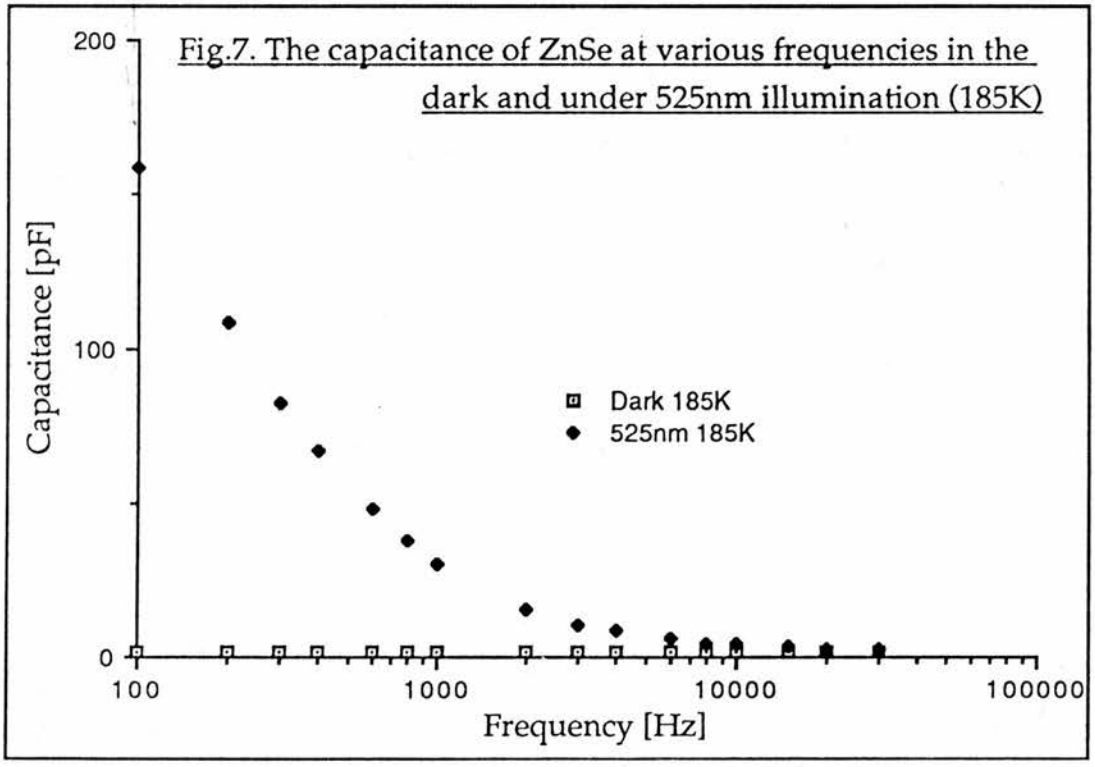

Fig.7. The capacitance of ZnSe at various frequencies in the dark and under 525nm illumination (185K)

The two curves overleaf (Figs. 8&9) show the variation of the difference capacitance of ZnSe with frequency and temperature. Two separate plots are provided for clarity. Once again the difference capacitance is defined as,

$$C_{(Diff.)} = C_{(light)} - C_{(Dark)},$$

$C_{(light)}$ in this case corresponds to data taken under 525nm illumination. In the case of the ZnSe material the capacitance change only obeys a power law at higher frequencies. The dispersion parameter "s" must thus be determined from the high frequency asymptotes.

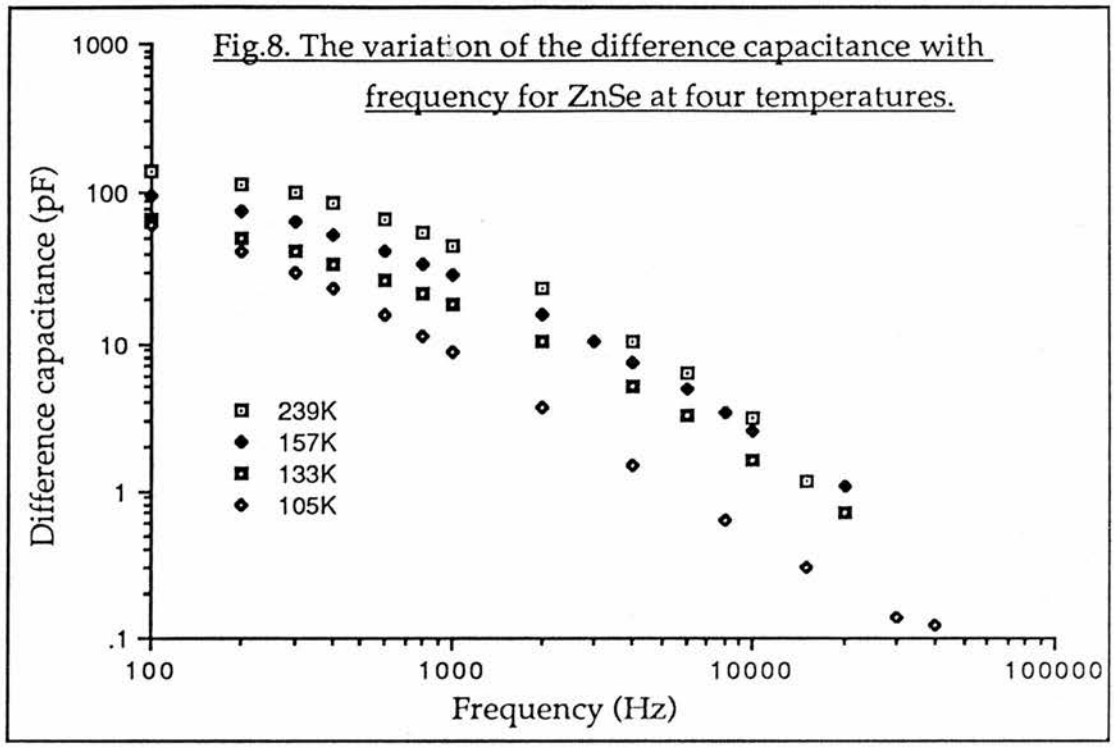

Fig.8. The variation of the difference capacitance with frequency for ZnSe at four temperatures.

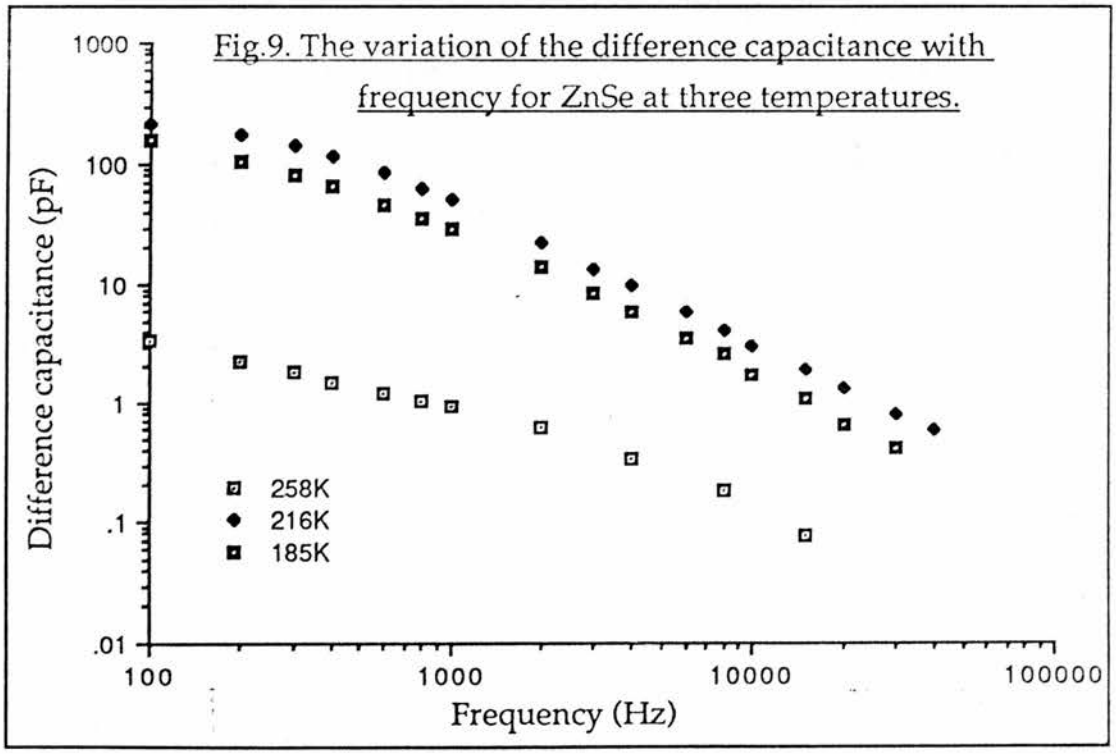

Fig.9. The variation of the difference capacitance with frequency for ZnSe at three temperatures.

The graph below (Fig. 10) shows the variation of the dispersion parameter "s" with temperature for the ZnSe sample. (Data from asymptotic fits to Figs. 8&9.)

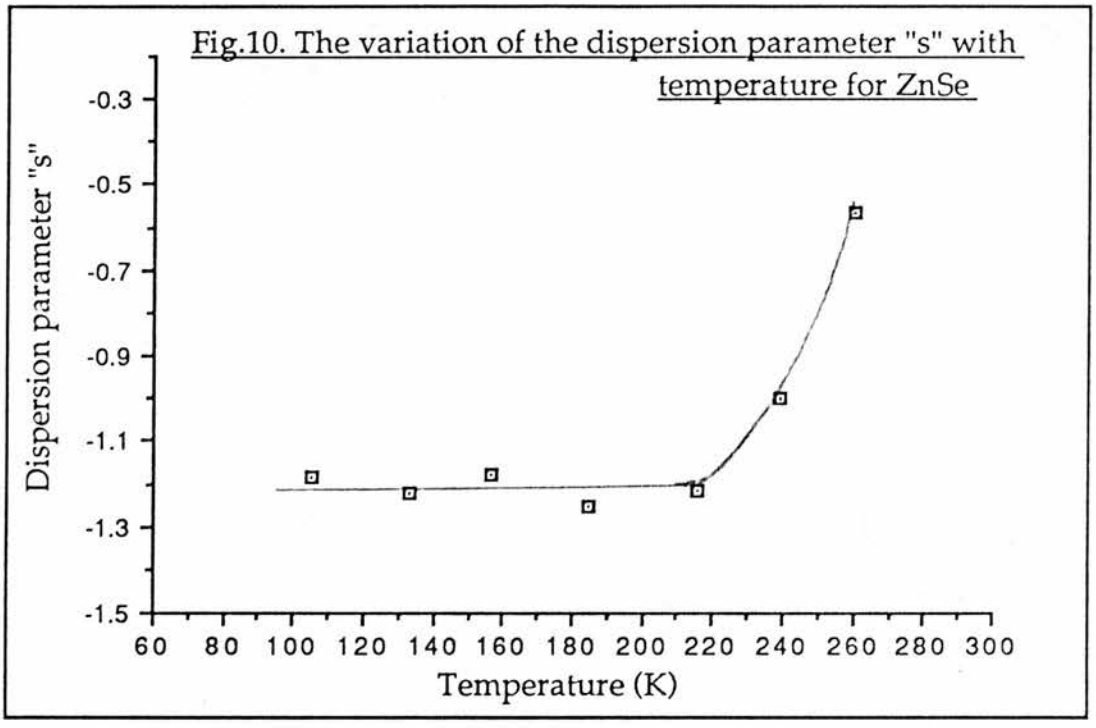

(3.3) InP:Fe

The graph below (fig. 11) shows the variation of the dark capacitance of the InP:Fe sample with frequency and temperature. The geometric capacitance of the structure was estimated at ~30pF. The 163K lower temperature limit was set by contact problems.

Fig.11. The variation of the capacitance of the InP:Fe sample with frequency at six temperatures.

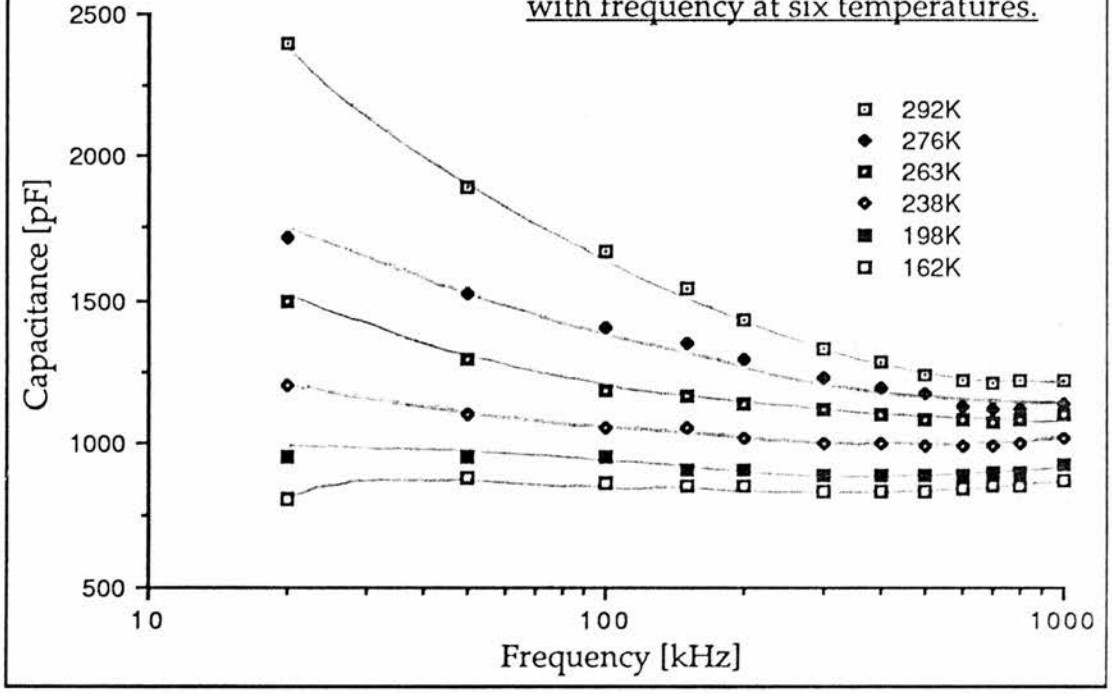

Difference capacitance as we have previously defined it, is meaningless for the InP:Fe samples since the dark capacitance is dispersive. However, the dispersion levels out above 500kHz and so the value of the capacitance at 500kHz was taken as a non-dispersive limit, in order to produce a log/log plot for this data. The result of such a plot for the room temperature data is shown in Fig.12 (below).

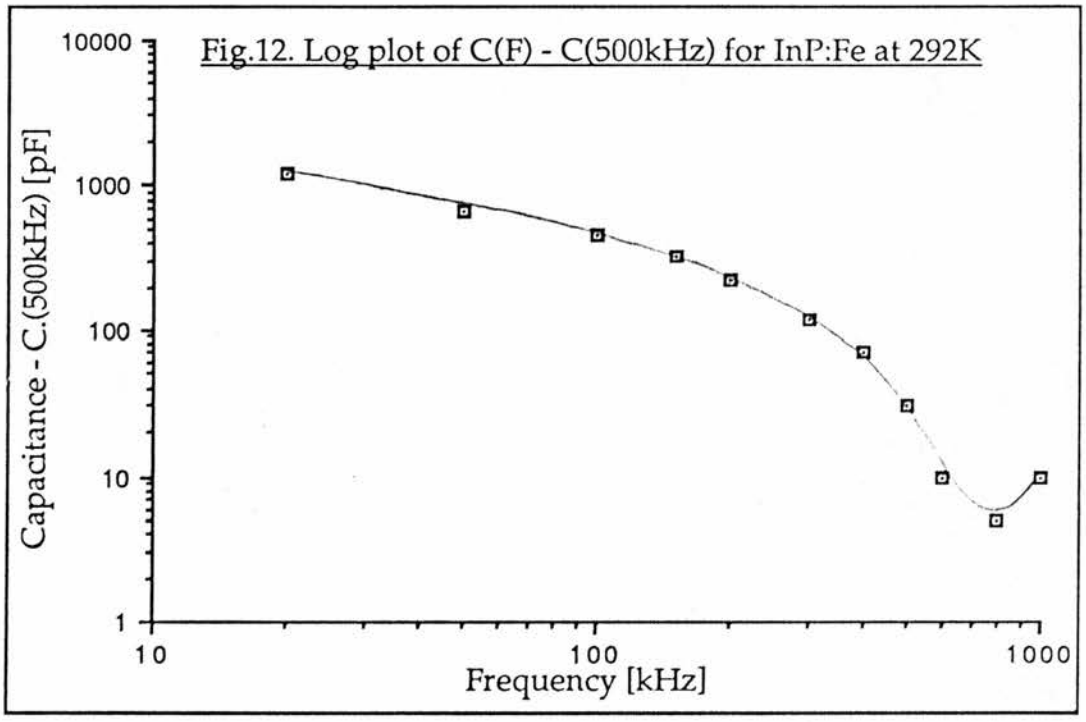

Fig.13 (below) shows a capacitance^{-2} voltage plot for the InP;Fe sample. The sample has two roughly equal sized contacts of the same metal, and so definition of a bias direction is some-what arbitrary. The upper voltage limit is set by excessive current flow (the diode contacts are far from ideal).

The straight line represents an asymptotic $C^{-2} \propto V$ relation from which one can deduce an ionised donor density of $7.5 \times 10^{14} cm^{-3}$ at 163K.

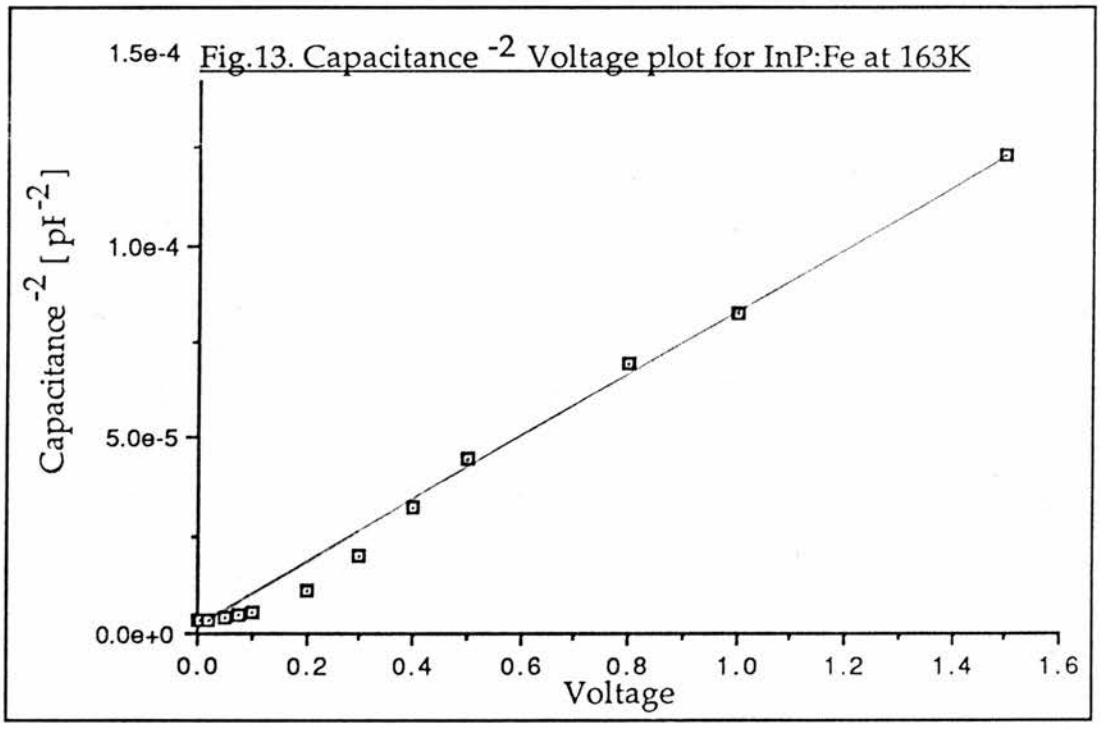

The graph below (Fig.14) shows the variation of the dark capacitance of the InP:Fe sample with temperature. (The contacts were changed to aluminium for this experiment).

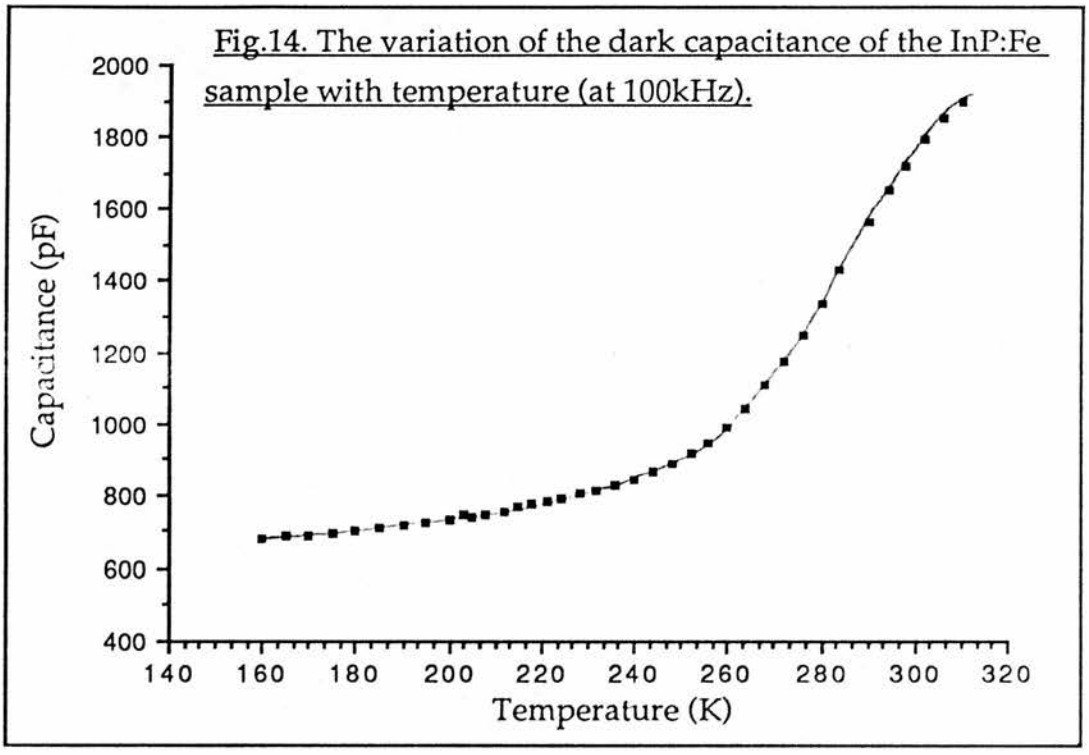

Fig.14. The variation of the dark capacitance of the InP:Fe sample with temperature (at 100kHz).

The graph below (Fig.15) shows the variation of the dark capacitance of the GaP:Co sample with frequency. The data were taken at 105K (the low temperature limit of the cryogenic apparatus.)

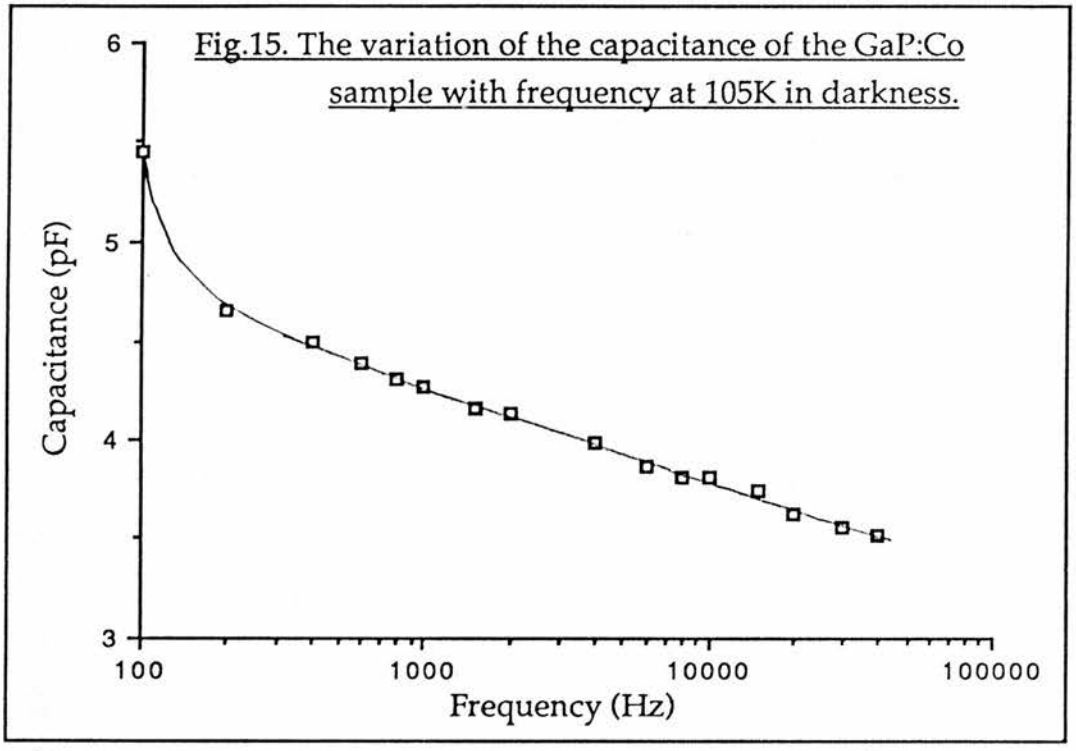

Fig.15. The variation of the capacitance of the GaP:Co sample with frequency at 105K in darkness.

Fig.16 (below) shows the variation of the dark capacitance of the GaP:Co sample at 100kHz with temperature.

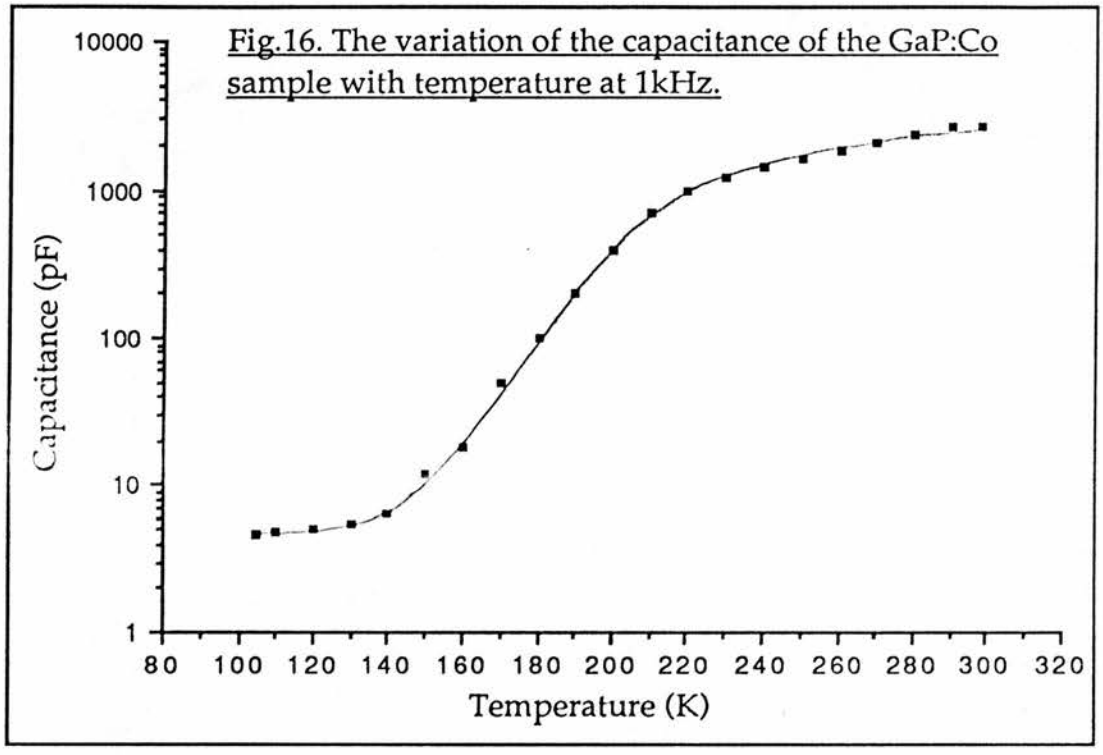

Fig.16. The variation of the capacitance of the GaP:Co sample with temperature at 1kHz.

(5) Discussion.

Jonscher has suggested that dielectric dispersion is a phenomena which is common to most materials (see for example[82]), and has, with reference to the earlier work of Cole & Cole[85], proposed a universal dielectric dispersion law of the form,

$$\varepsilon'' \propto \omega^{(n-1)}.$$

He is reluctant to accept specific models which only relate to one class of materials, such as that discussed by Pollak & Geballe[77] for silicon, on the grounds that similar results can be obtained with many other types of dielectric. To some extent his scepticism may be justified, however in the case of the work of Pollak & Geballe, there is evidence other than the observed dispersion to support their ideas. In undoped silicon dielectrics Pollak & Geballe have observed a purely reactive impedance with no dispersion. The fact that the introduction of impurities leads to dispersion being observed, particularly at temperatures where none of these levels are ionised, is strong evidence to associate the dispersion with the impurity levels. Also, in the case of our GaAs:Cr & ZnSe work, the conductivity only becomes dispersive when the sample is illuminated with light of sufficient energy to empty some of the deep levels. Once again it is hard to imagine why this should be so if the idea of impurity hopping leading to dispersion is fundamentally incorrect. This being the case it is unlikely that the many theoretical models based on such experimental observations should all be misconceived.

Jonscher has reviewed a large number of reports of dielectric dispersion from the literature[82]. From this he has demonstrated that in many diversely different materials (such as liquids and powders) a similar dispersion to that in partially compensated semiconductors, does indeed occur. Jonscher himself proposes that some form of hopping process is responsible in all cases, and that screening and electron-electron interaction are responsible for any observed differences[80[. Indeed, many of the fundamental ideas about localised electrons and hopping are not confined to semiconductors. Detailed theories aside one might imagine that the dispersion observed in other materials may well be due to some form of hopping process. If a "universal" theory for such processes were to be produced it need not necessarily contradict existing work for semiconductors. It seems unreasonable to totally dismiss all the current models of hopping conduction solely on the grounds that similar results can be observed in materials to which these theories cannot be directly applied. To draw analogy from another branch of physics, one can construct a low pass filter from either capacitors or inductors, and both may give identical amplitude response. However the physical process occurring in each system are quite different, one would not propose a rethink of classical electromagnetism on the basis of this observation. In defence of the ideas of Jonscher, one cannot ignore the wide spread occurrence of dispersive conductance. A more rigorous investigation of such phenomena might prove interesting and useful.

Much of the work done on hopping conduction to date has been

concerned with shallow donors in partially compensated n-type material. The presence of the deep acceptors leads to a number of the donors being unoccupied. Electrons may thus hop from adjacent donors into these empty states. The deep acceptors produce perturbation of the nearest donor levels as is illustrated by the diagram (a) overleaf (Mott-Conwell, see[77]). This can result in a threshold energy for some of the hopping processes. In such a system an electron may only hop with phonon assistance. However if the material is heated too much the donors ionise and carrier movement within the conduction band swamps any observable hopping.

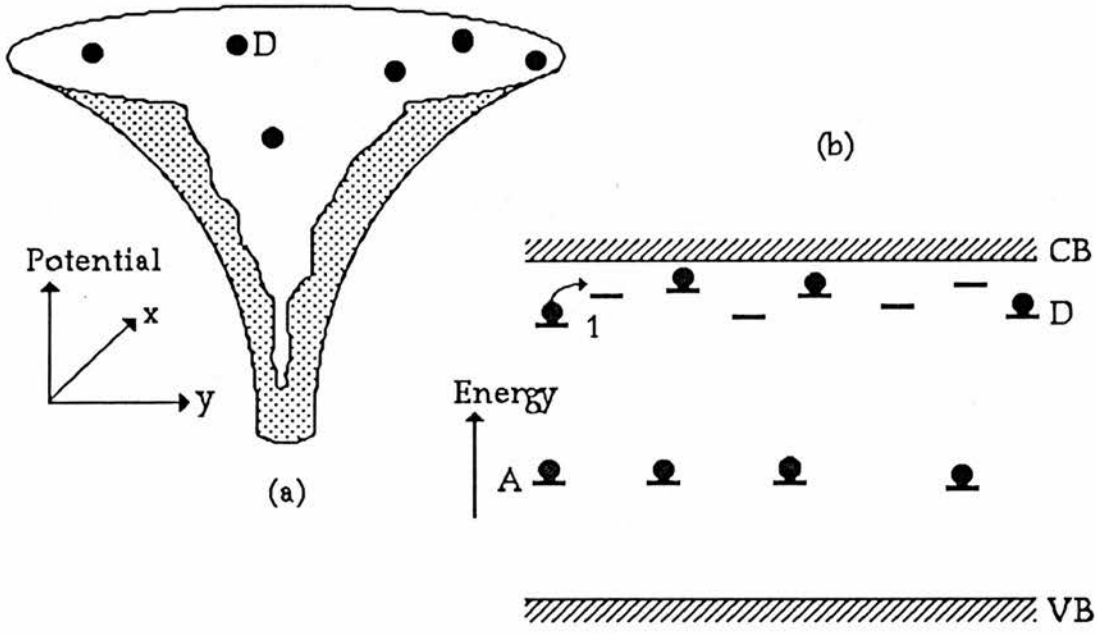

The diagram above (b) illustrates thermally assisted shallow level hopping. Such hopping can be simply between adjacent states or continue spatially through the lattice leading to DC conductivity. Shallow level

hopping has been studied previously in partially compensated GaAs, Kahlert[78] and semi-insulating GaAs, Jonscher & Pickup[87]. However, the GaAs:Cr samples used in the work reported here are almost completely compensated so that they are insulating. No electrons remain trapped on donors at room temperature, so that hopping between the shallow levels is impossible. If $N_A=N_D$ all the acceptor states are full since these are deep (~0.6eV). There are thus no empty states for an electron on an acceptor to hop to. The diagram below illustrates the occupancy of the levels in the dark.

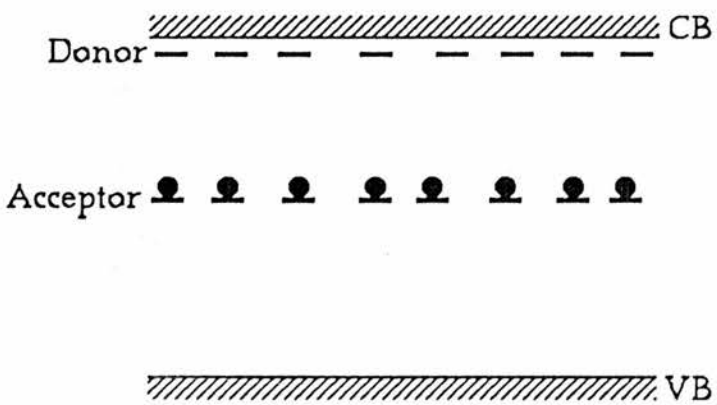

[In general the wave function of an electron on a shallow level is less spatially confined than that for an electron on a deep centre. In the most simple view, the probability of a hopping event is proportional to the overlap of the wave functions of neighbouring states, and as such is much smaller for a pair of deep centres than a pair of shallow ones of the same spatial separation.]

In darkness all the acceptor states are occupied and so, as would be expected from this model, we observe no significant dispersion. From the

sample geometry a value of the dielectric constant for GaAs of 13.1 was calculated (cf. 12 from tables). The agreement is sufficiently good for us to have confidence in treating the darkened sample as a normal dielectric.

When the sample is illuminated with light of greater energy than E1(see diagram below), some deep levels are emptied and thus hopping becomes possible and consequently dispersion is seen. The diagram below illustrates the process involved.

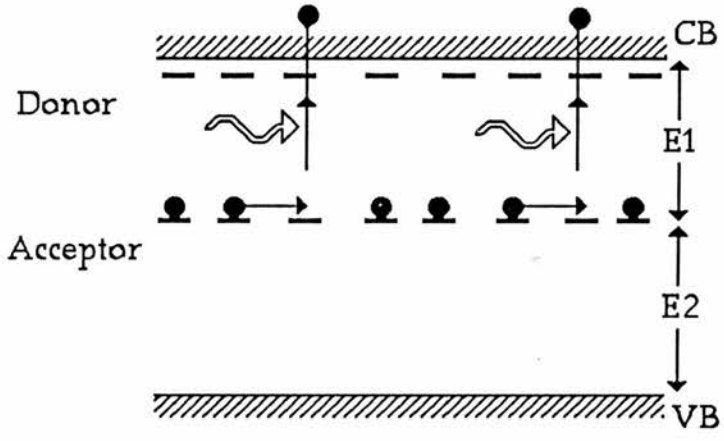

The general form of the observed dispersion is illustrated by Fig.1(Results 3.1). The magnitude of this light induced dispersion at any given frequency, varies with photon energy as can be seen in Fig.6. At ~0.64eV the deep acceptors begin to empty and the light capacitance increases considerably. At ~ 0.85eV the complimentary valence band centre transition begins. This results in the refilling of the centres and the quenching of the hopping. The diagram overleaf illustrates this process.

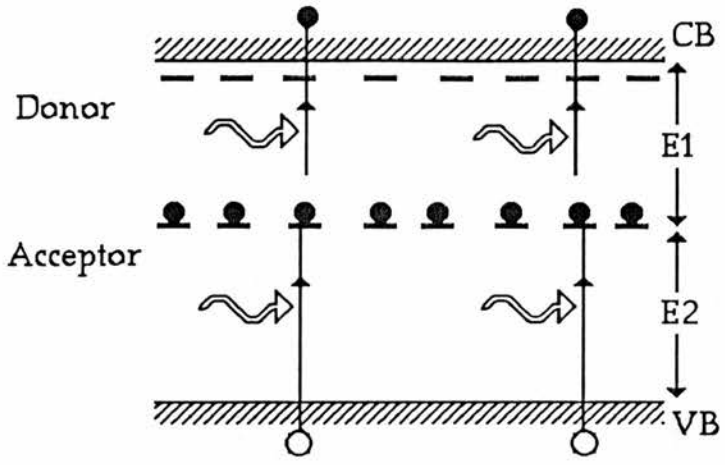

It is interesting to note the similarity between our hopping conductivity spectrum and the GaAs photoconductivity spectra reported by Broom[86]. From our results (Fig.6), the cumulative energy of the two transitions adds up to a little less than the energy gap. This is simply a consequence of the wide bandwidth of the monochromator. The rise at ~1.35eV represents the fundamental absorption edge, once again shifted a little by the monochromator bandwidth. At photon energies above band gap great numbers of electron hole pairs are created. Broom[86] has pointed out that occupied chromium centres in GaAs are efficient hole traps. The capture cross-section of such traps for holes is greater than that for electrons, and consequently some of the acceptor levels are empty. We believe that this depopulation of the deep centres leads to a renewal of the hopping process.

The log/log plots of difference capacitance against frequency for GaAs:Cr (Figs.2&3) show the power law nature of the dispersion. All these plots follow the relation,

$$C_{(Light)} - C_{(Dark)} = A\omega^{s},$$

where A is a constant. For our GaAs:Cr samples the dispersion parameter "s" is approximately linearly temperature dependent over the range 105 to 300K, and takes values from -0.65 to -1.1.

In terms of Jonscher's "universal law",

$$\varepsilon'' \propto \omega^{(n-1)},$$

the corresponding range of "n" would be $0.35 < n < -0.1$. Jonscher claims that hoping processes yield values of "n" in the range $0.6 < n < 0.9$ whilst values close to unity are due to "lattice" effects. In a sense this seems strange since a dielectric with "n" close to unity is essentially non-dispersive and as such requires no special treatment. The values of "n" for deep level hopping in GaAs:Cr are considerably lower than those quoted by Jonscher for a hopping process, yet we have evidence to associate the process with the deep levels.

Returning to the temperature dependence, the two GaAs:Cr samples were found to obey the following relations,

S1, $\quad s = -1.40 + 2.54\times10^{-3}T \quad (\pm1.0\%)$

S2, $\quad s = -1.95 + 2.53\times10^{-3}T \quad (\pm0.5\%)$

The difference in the constants (1.4 & 1.95) probably results from differences in the concentrations of the levels in the two samples. The variation with temperature is however, very similar for the two. The value of the dispersion parameter decreases with decreasing temperature, the overall difference capacitance also decreases. That is to say, in terms of the power law,

$$C = A\omega^s,$$

"A" decreases with decreasing temperature where as "s" increases. The reduction of the light capacitance with decreasing temperature is likely to be the result of the existence of a thermal threshold for hopping transitions, analogous to that discussed for shallow level systems. In effect an increase in the value of "s" as the temperature decreases implies that the reduced phonon assistance has more effect on the higher frequency conductivity than the low.

Turning attention towards the ZnSe sample, the capacitance of this material became very dispersive when the sample was illuminated with 525nm light. In ZnSe the results are much more difficult to interpret than in GaAs:Cr because of the large number of defect related levels that are almost always present in II-VI materials. Unlike the other samples studied the ZnSe is not deliberately doped with a deep level and yet one observes dispersion under illumination. Other work we have performed on ZnS and to some extent ZnSe has led us to believe that these materials do in fact contain large concentrations of deep neutral centres or complexes (See chapters 3&4), which may also be responsible for the dispersive capacitance. 525nm light has photon energy of well above half the band gap and yet unlike the GaAs:Cr sample, the dispersion is still present. Even though transitions into and out of the centre are both present, differences in the photoionisation cross-sections for the two transitions may result in some proportion of the centres being empty in equilibrium. If there is a very large concentration of these centres, even a small

proportion may represent a significant number of empty states and so hopping related dispersion might still be observed. If these centres lie below mid gap (as is the case in ZnS, and possibly also ZnSe) an experiment identical to that performed on GaAs:Cr, is not possible on ZnSe.

Below 220K the dispersion parameter "s" is not strongly temperature dependent. The light capacitance does however increase with increasing temperature indicating that once again phonon assistance is necessary for the transitions. Above 200K the dispersion parameter decreases rapidly. Mudhar[83], working on hopping in ZnSe at higher temperatures has observed a linearly temperature dependent dispersion parameter over the range 280K to 340K. In the absence of more detailed knowledge of the nature of the centres present in the ZnSe sample it is difficult to substantiate any specific models for the temperature dependence of the dispersion parameter.

Both the GaP:Co and the InP:Fe samples were different to the GaAs:Cr in that they were not completely compensated. The presence of a large number of uncompensated ionised donors or acceptors leads to the formation of Schottky barriers at the metal semiconductor interface. The resulting depletion regions are usually very much smaller than the sample thickness and have very much greater resistance than the bulk material. The sample thus behaves as two large capacitors in series with a comparatively small bulk resistance. The capacitance of the depletion region varies according to the relation,

$$1/C^2 = 2 (N_d e \varepsilon_o \varepsilon_s A^2)^{-1}(V_{bi} + V_a).$$

where A is the contact area, V_{bi} is the built in barrier potential, V_a is the applied voltage and the other symbols have their usual meanings. The diode behaviour of such a sample means that as a DC bias is applied one contact is effectively forward biased and low resistance, whilst the other is under reverse bias and has a high resistance. At higher voltages almost all the ohmic drop is across the reverse biased contact. Furthermore, the reverse biased depletion region will be extended whilst the forward biased one will collapse. The combination of the two effects leads to a linear capacitance^{-2} voltage plot at higher voltages as can be seen in Fig. 13. The ionised donor density for the InP:Fe sample was calculated from this plot and found to be $7.5 \times 10^{14} cm^{-3}$ at 163K. This value can only be viewed as a rough guide, since the contacts were not ideally suited to this type of experiment.

It is interesting that the dark capacitance of the sample exhibited considerable low frequency dispersion at room temperature. If the equivalent circuit of the sample contains capacitance and resistance in series, the equivalent parallel capacitance (which the bridge measures) is not necessarily an accurate indication of the junction capacitance. Conversion to series equivalent values was made using the relations,

$$C_s = C_p + (\omega^2 C_p R_p^2)^{-1}$$

$$R_s = R_p (1 - \omega^2 C_p^2 R_p^2)^{-1}$$ After[84]

The capacitance was still found to be highly dispersive after this conversion, so an alternative explanation is required. The dispersion does not follow a power law. One possible explanation is that surface trap states are present at the interface and that the polarisation of these states results in dispersion.

Thermal contraction damage to the contacts prevented measurements on this sample at temperatures below ~160K. From the capacitance temperature plot (Fig.14) one can see that carrier freeze out is unlikely to occur above 105K (the cryogenic limit of our system) and so hopping conduction in the bulk material is unobservable in this sample.

The GaP:Co sample does have a capacitance close to the expected geometric value at 105K indicating that sufficient carrier freeze out has occurred to remove the Schottky depletion regions. However in this case the dark capacitance is dispersive and so it was also impossible to perform good deep level hopping experiments on this sample.

(6) Concluding remarks.

We have shown that the capacitance of a parallel plate capacitor based around a GaAs:Cr dielectric is not frequency dependent (in the range 10^2 to 10^4Hz) in darkness. However, when illuminated with 0.7eV light a strong dispersion appears. This dispersion was found to obey the power law,

$$C_{(light)} - C_{(Dark)} = A\omega^s$$

where A and s are constants and ω is the angular frequency. Such dispersive behaviour is characteristic of carrier hopping processes and we believe such a mechanism operates in this case. The photon energy threshold for the dispersion was ~0.65eV, and by 0.9eV the effect was quenched. We see this as evidence that the hopping is taking place between deep centres rather than shallow ones because of consistency with the following model. In the dark all the deep centres are full and so hopping between them is not possible. With 0.65eV light some centres are emptied and so we observe dispersion. Quenching may occur when the >0.9eV light causes the centres to be refilled by electrons from the valence band.

We have seen a similar light induced dielectric dispersion effect in ZnSe, although the nature of the deep centres in this material has made interpretation of these results more difficult than for GaAs:Cr.

In both GaAs:Cr and ZnSe the overall magnitude of the dispersion decreases with decreasing temperature, this is also consistent with a phonon assisted hopping process.

The GaP:Co and InP:Fe samples at our disposal were found to be unsuitable for our photocapacitance/frequency measurements. We have thus been unable to

derive information about these materials by this method.

Chapter 8

Conclusion.

(1) Conclusion.

An overview of the work contained in this thesis can by obtained by reading the conclusions of the individual chapters in sequence, Pages, 55, 109 ,158 ,208, 231 & 272. Rather than simply repeating these in this final chapter, we wish to consider the wider implications of some of the work we have done and its relation to operational devices.

We have demonstrated the feasibility of a frequency domain phosphor based temperature sensor. We believe with a little refinement a commercial system could be manufactured and are currently exploring this possibility with industrial companies.

We have shown that in insulating GaAs:Cr and ZnSe impurity band conduction based on deep centres can be a significant effect, despite the confined wave function of an electron on such a centre. This is very important since GaAs is becoming increasingly popular in device manufacture. Previous workers have shown that carrier hopping between the chromium centres leads to a conduction mechanism in partially compensated material[78][87]. Complete compensation of n-type GaAs with chromium leads to highly insulating material in which there are no empty deep states for carriers to hop in to. We have shown that if such insulating GaAs is exposed to infrared light, the resulting optical ionisation of the centres renews the hopping effect. As interest in ZnSe as a material for luminescent devices increases, the impurity band conduction mechanism could have significant implications. It would be interesting to produce some fully compensated InP:Fe and GaP:Co samples

so that similar work might be carried out on these materials.

The assumption that band-to-band impact ionisation and avalanche occurs at the operating fields of Inoguchi[3] type luminescent devices has often been made[5]. By measuring the threshold field for this process in ZnS diodes we have confirmed that the process will most definitely occur. To our knowledge this is the first time a determination of the band-to-band ionisation threshold in ZnS has been reported. Our measurements on evaporated thin films confirm that the threshold field in such devices is of the same order as in diodes, although any quotation of an electric field value within a polycrystalline film must of course be treated with care.

By measuring the photocurrent in a reverse biased Schottky diode we have also shown that a two stage impact ionisation mechanism based on a deep impurity operates in ZnS. (Livingstone[26][35] has shown that a similar mechanism operates in ZnSe). Photocapacitance studies have led us to believe that a neutral centre ~2eV below the conduction band is related to this process. (Apart from this comparatively little work has been done on two stage impurity impact ionisation.) Since the deep impurities associated with the impact ionisation mechanism are ~2eV below the conduction band, any electrons which ionise this level must be very energetic. Consequently such a process is useful as a probe of the hot electron behaviour, and also has considerable device potential. This is an area in which we hope there will be development in the future.

We have measured the variation of the quantum efficiency of the

manganese luminescent centre with electric field in the same diode as our photocurrent measurements. Both processes were found to exhibit a similar variation with electric field. Rigby and Allen[10] have shown that at slightly lower fields than those at which band-to-band impact ionisation occurs, most of the electrons have experienced runaway from the Γ_1 minima and occupy the upper valleys of the conduction band. We have performed photocurrent measurements on a twin diode to that which Rigby and Allen used to measure the hot electron transition luminescence quantum efficiency, and once again found a correlation between the two processes. We have thus been able to produce further evidence to support the idea that electrons transfer to the upper valleys of the conduction band at high fields.

Since band-to-band impact ionisation occurs in Inoguchi devices, some of the electrons must have undergone a second runaway out of the X_1,X_3 & L_1 valleys. We have shown that the band-to-band ionisation in ZnS fits the "lucky electron" model of Shockley[17]. This being the case it is probable that the majority of electrons still occupy the upper valleys of the conduction band in these devices. Electrons in such valleys have comparatively low velocity despite their high energy.

Since multiplication factors of >2 can be achieved within the Inoguchi devices the number of free holes* will be almost equal to the number

* We have shown that it is possible to maintain a steady avalanche in ZnS, this could only be possible if free holes are not trapped at high fields. The photocapacitance work of Zheng[12] also illustrates this.

of free electrons. This leads to the rather surprising conclusion that almost half of the current in Inoguchi devices may be carried by holes.

There are no valleys in the valence band and thus, in contrast to the electrons, the holes will have high velocity. Even if such holes are able to gain sufficient energy to excite a luminescent centre, they are less likely to do so than the electrons because of their higher velocity. It is, however, possible that the free holes make some contribution to the manganese excitation.

If, as we believe, the majority of the electrons do accumulate in the upper valleys of the conduction band, the resulting high energy and low velocity might strongly favour impact excitation of a luminescent centre. The precise energy difference between the X_3 minima and the Γ_1 minima is not known. However, most calculations yield a value around 2eV*. This could present an obstacle to blue light emission via an impact excitation process for two reasons. Firstly, if the majority of the electrons do still reside in the X_1,X_3 and L_1 valleys they may be insufficiently energetic to excite a blue centre. Secondly, the electrons which leave the X_3 valley might be expected to have high velocity and consequently would be considerably less likely to excite a luminescent centre.

Impact excitation mechanisms are generally inefficient. Even if it were possible to produce a blue lamp in this way, it is worth while considering

* One of the few pieces of direct experimental evidence for the energy difference yields a value of approximately 3eV[10]. It is possible that a 3eV electron might excite a blue centre.

alternatives on this basis alone.

We believe that the way forward for blue emitting ZnS devices may lie with electron hole recombination excitation rather than electron impact excitation. We have shown that hole trapping is not an efficient process at high fields and thus such recombination luminescence might only be achieved in low field devices. We have proposed a ZnS electroluminescent device which has an MIS structure. Impact ionisation in the insulating layer produces holes which are injected into an n-type substrate which contains a luminescent centre. Thus the high field hole generation process and the low field recombination occur in adjacent but separate regions. Experiments that we have performed on prototypes have led us to believe that the key to efficient operation of such a device lies in the appropriate choice of a luminescent centre and the elimination of non radiative recombination mechanisms. We believe that a durable device could be made which employs avalanche breakdown (band-to-band or impurity based) as hole generation mechanism because band-to-band impact ionisation occurs in Inoguchi type devices and these have considerable lifetimes. Solid state violet emitting devices, along the lines of our proposal which utilise the tellurium singlet centre as a hole trap, could in principle be manufactured today. It is, however, important not to underestimate the quality of fabrication that would be required for such a device, and to realise that sophisticated growth techniques would be necessary. Looking further into the future, in principle there is no reason why our devices could not operate AC, perhaps in the form of a two layer

Inoguchi device. That is, n-type ZnS containing a suitable luminescent centre could be deposited on the back of an insulating ZnS film and the two encapsulated in an insulator. This might utilise the existing developments in fabrication techniques for such devices whilst avoiding the intrinsic problems associated with electron impact based blue emitting ZnS devices.

Tellurium forms an isoelectronic hole trap in ZnS[13] which leads to a violet photoluminescence emission band. Unfortunately this emission is quenched at room temperature. However, in heavily doped ZnS:Te, a blue room temperature luminescence band has been attributed to tellurium doublet centres[13][63][64]. We had hoped that such a centre would form a suitable hole trap for the above described MIS devices. Our photoluminescence studies of such material produced almost identical results to those on our undoped material (presumed to exhibit self-activated emission). On the basis of these and other experiments we believe that the blue luminescence band in heavily doped material may simply be due to the self-activated centre. The lattice stress associated with the introduction of the large tellurium atoms may lead to defect formation and thus enhancement of this emission at high tellurium concentrations. We have been unable to find any experimental evidence in the literature to contradict this idea, or to rigorously support the doublet model. An analogous situation has occurred in the past with the manganese centre in ZnS. The non-exponential decay of the manganese centre has often been ascribed to contributions from doublet and triplet centres (see for

example[88]). Although doublets do sometimes produce emission[89], they are not always the cause of non exponential decays in manganese doped ZnS[90]. An investigation of the origins of the photoluminescence emission peaks of ZnS:Te samples of differing tellurium concentration would provide an interesting topic for future work.

In both ZnS:Te and nominally undoped material we have observed an exponential build up with time of the photoluminescence emission. The emission can take of the order of a minute to reach full visual brightness. We have investigated this phenomena, and proposed a model involving the competitive trapping (by non radiative centres) of electrons excited from luminescent centres. We hope that in the future the species and origin of these centres may be determined, since there are considerable implications for electroluminescence.

As a result of the work that we have done, we have been able to add to the existing knowledge about luminescent processes in ZnS. We hope that this, coupled with other work in this field will lead towards a more scientifically based design of ZnS electroluminescence devices. Many current ZnS devices have been "stumbled upon" rather than designed, and yet they prove effective in operation. If we are ultimately able to fully understand all the luminescent process in this material the resulting new generation of devices might revolutionise display lighting.

References

References.

[1] Derry T.K. & Williams T.I. (1960) "A short history of technology" Oxford Uni. Press

[2] Destriau G. (1936) J. chim. Physique **33** 587

[3] Inoguchi T., Takeda M., Kakihara Y., Nakata Y. &Yoshida M. (1974) SID International Symposium Digest. **86**

[4] Smith D.H. (1981) J. Lum. **23** 209

[5] Mach R. & Müller G.O. (1982) Phys. Stat. Sol. (a) **69** 11

[6] Thompson T.D. & Allen J.W. (1987) J. Phys. C: Solid State Phys. **20** L499

[7] Livingstone A.W. & Allen J.W. (1970) J. Phys. C: Solid State Phys. **3** 2468

[8] Heiblum M., Nathan M.I., Thomas D.C & Knoedler C.M. (1985) Phys. Rev. Lett. **55** 2200

[9] Wang C.S. & Klein B.M. (1981) Phys. Rev. B **24** 3393

[10] Rigby N.E. & Allen J.W. (1988) J. Phys. C: Solid State Phys. **21** 3483

[11] Bryant F.J., Hagston W.E. & Swift M.J.R. (1988) J. Lum. **40** & **41** 767

[12] Zheng J. To be published.

[13] Iseler G.W. & Strauss A.J. (1970) J. Lum. **3** 1

[14] Rigby N.E.,Thompson T.D. & Allen J.W. (1988) J. Phys. C: Solid State Phys. **21** 3295

[15] Moll J.L. (1964) "Physics of Semiconductors." Mc Graw Hill

[16] Wolff P.A. (1954) Phys. Rev. **95** 1415

[17] Shockley W. (1961) Sol. State Elect. **2** 35

[18] Baraff G.A. (1962) Phys. Rev. **128** 2507

[19] Katayama H., Oda S. & Kukimoto H. (1975) Appl. Phys. Lett. **27** 697

[20] Lukyanchikova N.B., Pavelko T.M. & Pekar G.S. (1981) Phys. Stat. Sol. (a) **66** 749

[21] Cowley A.M. (1966) J.Appl.Phys. **37** 3024

[22] Goodman A.M. (1963) J.Appl.Phys. **34** 329

[23] Horvath Z.J. (1988) Proc. 19th Int. Conf. on Phys. of Semicond. Warsaw. (In press)

[24] Aven M. & Mead C.A. (1965) Appl. Phys. Lett. **7** 8

[25] Kukimoto H., Shionoya S., Koda T. & Hioki R. (1968) J.Phys. Chem. Solids **29** 935

[26] Livingstone A.W. & Allen J.W. (1973) J. Phys. C: Solid State Phys. **6** 3491

[27] Petroff M.D., Stapelbroek M.G. & Kieinhans W.A. (1987) Appl. Phys. Lett. **51** 406

[28] Müller G.O. (1984) Phys. Stat. Sol. (a) **81** 597

[29] Theis D. (1981) Optoelectronic materials and devices. Proc. 3rd international school cetniewv P.W.N. Polish scientific publishers Warsaw 1983

[30] Howard W.E. (1981) J. Lum. **23** 155

[31] Solomon P. & Klien N. (1975) Solid State Comm. **17** 1397

[32] Andreev I.A., Mikhailova M.P., Somonov A.N. ,SlobodchikovS.V. , Stus N.M. & Filaretova G.M. (1984) Soviet Phys. Semi. **18** 338

[33] Turvey K. & Allen J.W. (1973) J. Phys. C:Solid State Phys. **6** 2887

[34] Gordon N.T. (1981) IEEE Transactions on Electron Devices. ED-28 434

[35] Livingstone A.W. (1979) Ph.D. Thesis "Electroluminescence and switching phenomena in ZnSe Schottky diodes." University of St.Andrews.

[36] Fornell J.O., Grimmeiss H.G., Mach R. & Müller G.O. (1988) Semicond. Sci. & Tech. **3** 511

[37] Bryant F.J., Hagston W.G. & Krier A. (1986) J. Phys. C: Solid State Phys. **19** L375

[38] Jiaqi Y.U., Tianren Z.H.A.O. & Wenlian L.I. (1985) J. Lum. **33** 427

[39] Grimmeiss H. G. & Kullendorff N. J. (1980) Appl. Phys. **51** 5852

[40] Brotherton S.D. (1976) Solid State Elect. **19** 341

[41] Stratton R. (1958) Proc. R. Soc. A **246** 4061

[42] Rode D.L. (1970) Phys. Rev. B **2** 4036

[43] Rigby N.E. (1987) Ph.D. Thesis "Electroluminescence by hot electrons in doped and undoped ZnS." University of St.Andrews.

[44] Allen J.W. (1986) J. Phys. C: Solid State Phys. **19** 6287

[45] Krupka D.C. (1972) J. Appl. Phys. **43** 476

[46] Zhong G.Z. & Bryant F.J. (1980) J. Phys. C: Solid State Phys. **13** 4797

[47] Krier A. & Bryant F.J. (1984) Phys. Stat. Sol. (a) **83** 315

[48] Zhong G.Z. & Bryant F.J. (1981) J. Phys. C: Solid State Phys. **14** 2175

[49] Budhudu S., Hagston W.E., Swift M.J.R. & Waring A.J. (1988) J. Phys. C: Solid State Phys. **21** L725

[50] Bryant F.J., Hagston W.E. & Krier A. (1986) Phys. Stat. Sol. (a) **94** 701

[51] Zhong G.Z. & Bryant F.J. (1981) J. Lum. **24&25** 909

[52] Kahng D. (1968) Appl. Phys. Lett. **13** 210

[53] Bala W., Bukaluk A. & Siuda R. (1985) Appl. Phys. A **37** 231

[54] Fan X.W. & Woods J. (1981) J. Phys. C: Solid State Phys. **14** 1863

[55] Watt D.E. (1988) Stopping cross-sections, mass stopping powers and ranges in 30 elements for α particles (1keV to 100MeV). International commission on radiation units and measurements, Maryland, USA.

[56] Watkins G.D. (1977) Inst. Phys. Conf. Series **31** 95

[57] Ryall M.D. & Allen J.W. (1973) J. Phys. Chem. Solids 34 2137

[58] Lawther C. & Woods J. (1977) Phys. Stat. Sol. (a) **44** 693

[59] Fan X.W., Zhang J.Y., Zhang Z.S., Wang S.Y., Lu A.D., Li W.Z., Jiang J.X. & Sun Y.W. (1984) J. Lum. **31 & 32** 957

[60] Livingstone A.W., Turvey K. & Allen J.W. (1973) Solid State Elect. **16** 351

[61] Allen J.W. J. Phys. C: Solid State Phys. (1971) **4** 1936

[62] Cuthbert J.D. & Thomas D.G. (1968) J. Appl. Phys. **39** 1573

[63] Heimbrodt W. & Goede O. (1986) Phys. Stat. Sol. (b) **135** 795

[64] Fukushima T. & Shionoya S. (1973) Jpn. J. App. Phys. **12** 549

[65] Leverenz H.W. (1950) "An Introduction to Luminescence of Solids" Wiley, New York

[66] Abdel-Kader A., Bryant F.J. & Hogg J.H.C. (1984) Phys. Stat. Sol. (a) **81** 333

[67] Koda T. & Shionoya S. (1964) Phys. Rev. **136** 541

[68] Era K., Shionoya S. & Washizawa Y. (1968) J. Phys. Chem. Sol. **29** 1827

[69] Era K., Shionoya S. & Washizawa Y. (1968) J. Phys. Chem. Sol. **29** 1843

[70] Dowell L. J., Gillies G.T., Allison S.W. & Cates M.R. Martin Marietta Energy Systems.

[71] Wickersheim K.A., Heinemann S.O., Tran H.N. & Sun M.H. (1985) ISA Paper #85-0072

[72] Parker A.D. (1986) Unpublished

[73] Radio Spares data library (1983) Sheet 2983

[74] Austin I.G. & Mott N.F. (1969) Adv. Phys. **18** 41

[75] Scher H. & Lax M. (1973) Phys. Rev. B **7** 4491

[76] Scher H. & Lax M. (1973) Phys. Rev. B **7** 4502

[77] Pollak M. & Geballe T.H. (1961) Phys. Rev. **122** 1742

[78] Kahlert. H. (1975) J. Phys. C: Solid State Phys. **9** 491

[79] Rentzsch R., Shlimak I.S. & Berger H. (1979) Phys. Stat. Sol. (a) 54 487

[80] Jonscher A.K. (1977) Phys. Stat. Sol. (b) 84 159

[81] Jonscher A.K. (1978) Phil. Mag. B **38** 587

[82] Jonscher A.K. (1977) Phys. Stat. Sol. (b) **83** 585

[83] Mudhar P.S. (1968) Ph.D. Thesis "Photocapacitance, photoconductivity and AC conductivity of semiconductors containing deep impurities."University of St.Andrews.

[84] Wayne Kerr 601 Radio frequency capacitance bridge handbook.

[85] Cole K.S. & Cole R.H. (1941) J. Chem. Phys. **9** 341

[86] Broom R.F. (1967) J. Appl. Phys. **38** 3483

[87] Jonscher A. K. & Pickup C. (1985) J. Phys. C: Solid State Phys. **18** L343

[88] Vlasenko N.A., Zynio S.A. & Kopytko Yu.V. (1975) Phys. Stat. Sol. (a) **29** 671

[89] Busse W., Gumlich H.-E., Messner B. & Thesis. D (1976) J. Lum. **12** & **13** 693

[90] Rigby N.E. & Allen J.W. (1988) J. Lum. **42** 143